CHARACTERISATION OF MOLECULAR MATERIALS FOR ELECTRONIC DEVICES

A thesis presented by
Justin Thomas Shepherd
to the University of Abertay Dundee
(collaborating establishment: Electronic Materials Centre, University of Wales)
in partial fulfilment of the requirements
for the degree of Doctor of Philosophy
February 1998

I certify that this thesis is the true and accurate version of the thesis approved by the examiners.

Signed [redacted] Date 18th June 1998

(Director of Studies)

For my wife

Declaration

I declare that while registered as a candidate for the degree for which this thesis is presented I have not been a candidate for any other award. I further declare that except where stated the work contained in this thesis is original and was performed by the author.

Signed 

Justin Shepherd

Advanced Studies

In addition to the original research reported in this thesis the author followed a program of postgraduate study. This program included attendance at the relevant lectures of the M.Sc. course on the Physics and Technology of Amorphous Electronic Materials held at Dundee University during 1994-95. In addition the author attended the Chelsea Meeting on Amorphous and Organic Semiconductors in 1995, 1996 and 1997; with a paper presentation at the 1996 meeting, and contribution to another in 1997.

Acknowledgements

I would like to thank my supervisors Dr Steve Reynolds and Dr Charlie Main for their constant interest, encouragement and friendship throughout the course of this work. I would also like to express my gratitude to my external supervisor, Professor Joe Marshall and to Dr John Maud for their helpful advice and guidance.

Further thanks are due to the following:

Members of the technical staff for their assistance during this study.
Dr Rudi Brüggemann for his hospitality and advice on my visit to Oldenburg.
Nick Cook and Hendrik Zollondz for their friendship and beer drinking abilities.

Finally, I would like to thank my wife, Tracy, without whom this thesis would not have been possible.

Characterisation of Molecular Materials for Electronic Devices

Justin Shepherd

Characterisation of thin films of conjugated oligomers deposited by thermal evaporation and pulsed laser ablation has been carried out through measurements of the optical absorption, dark conductivity and photoconductivity of samples with coplanar and sandwich geometries. The dark conductivity was measured as a function of field and temperature. The photoconductivity was measured with steady state optical excitation, and transient excitation as a function of temperature, field, excitation intensity and excitation energy. It was found that in most experiments all oligomers yielded similar results, suggesting that the specific chemical structure of the oligomers is relatively unimportant in determining the electrical properties of the thin films.

Experimental results have been interpreted using computer simulation techniques and current transport models for organic semiconductors. It is found that the multiple trapping and disorder limited hopping models are not applicable to these materials; and a trap-controlled hopping mechanism is suggested as appropriate.

An apparent density of states for the oligomers has been obtained using the transient photocurrent (TPC) decays and a multiple trapping analysis. Qualitatively, the TPC decays are of a form that suggest a flat density of states at high energies with an exponential at deeper energies. The DOS was also determined quantitatively using a Fourier transform (FT) technique. This resulted in a density of states similar to that predicted qualitatively. Transport in such a density of states is suggested to occur by carriers directly "hopping down" in the flat region of the DOS, followed by trap-controlled hopping in the exponential region.

The validity of the Fourier transform technique in systems not exhibiting multiple trapping is discussed and evaluated using computer simulation. It is concluded that the FT technique must be valid for trap-controlled hopping. Thus the form of the obtained DOS for the oligomers is correct, although the magnitude and energy scale can not be considered to be accurate, in either the "hopping down" regime or the trap-controlled hopping regime. An attempt to escape frequency of approximately 10^8 s^{-1} is predicted by fitting DOS plots at different temperatures.

Measurements of the effect of oxygen absorption and the slow relaxation of the steady state photocurrent have also been performed, as these effects are found to be characteristic of the oligomers. Oxygen absorption appears to lead to carrier generation and was found to be more important in sandwich samples. This is attributed to oxygen absorption at the electrode-oligomer interface leading to carrier injection. The slow relaxation of the steady state photocurrent could not be explained using previously developed models. It is tentatively suggested that the effect may be due to very deep trapping of holes.

List of Symbols

a	lattice constant
$A_{c,g}$	electron affinity (crystalline, gaseous)
A	conduction cross-section
B	bandwidth
C_t, C_R	trapping, recombination coefficients
d	film thickness
D	diffusion coefficient
e	electronic charge
$e_{p,n}$	hole, electron emission probability
E	field strength
F	photon flux
$g(\varepsilon)$	density of states distribution function
G_0, ΔG	thermal equilibrium and steady state photogeneration rates
i_d, i_{pc}, i_{SCL},δi_{pc}	dark, photo- and space charge limited currents, transient photocurrent
$I_{c,g}$	ionisation energy (crystalline, gaseous)
J	overlap integral
k	wave vector
k_B	Boltzmann constant
L	mean free path
L_D	diffusion length
L_{gap}	electrode gap
n_{tr}, Δn_r	Thermally, optically generated recombination centre density
N_c	effective conduction band density of states
N_t	trap density
N_e	injected carrier density
p_0, Δp	thermal equilibrium, excess photogenerated hole density
$\bar{p}$	e_p/C_t
P^+,P^-	polarisation energy
r_c	Coulomb radius
r_{th}	thermalisation radius
R	recombination rate

R_{ij}	intersite separation
S	capture cross-section
t_{tr}	carrier transit time
T	absolute temperature
T_0	exponential DOS width in temperature units
T_1	temperature at which mobility field dependence vanishes
U_{cp}	Coulombic binding energy
v	thermal carrier velocity
V_0	disorder potential
V_t	ohmic-space charge limited current transition voltage
W	hopping energy
z	co-ordination number

α	absorption coefficient
α_d	dispersion parameter
α'	hopping asymmetry barrier
α_{loc}	inverse wavefunction decay length
α_{pol}	polarisability
β	Poole-Frenkel coefficient
ε_∞	equilibration energy ($=\sigma_g^2/k_BT$)
ε_g	band gap
ε_ω	thermalisation energy ($= k_BT \ln(\upsilon/\omega)$)
ε_d	thermalisation energy ($= k_BT \ln(\upsilon t)$)
ε_f	thermal equilibrium Fermi level
ε_{fp}, ε_{fp}^t	hole quasi Fermi level, trap quasi Fermi level
ε_0	vacuum permittivity
ε_r	relative dielectric constant
ε_t	transport energy
ε_p	polaron binding energy
$\Delta\varepsilon_\sigma$	activation energy
$\Delta\varepsilon_0$	zero field activation energy
$\phi(\omega)$	MPC phase shift
φ_B	barrier height

φ_m	metal work function
γ	photoconductivity index
η	quantum efficiency
λ	wavelength
μ_0, μ_d	free carrier mobility, drift mobility
θ	ratio of free to trapped charge
σ_g	gaussian width
$\hat{\sigma}$	gaussian disorder parameter ($= \sigma_g/k_BT$)
σ_d, σ_{pc}, σ_0	dark conductivity, photoconductivity, conductivity prefactor
τ_r	carrier lifetime
τ_{rel}	dielectric relaxation time
υ_{ij}	average hop frequency between sites i and j
υ_0	attempt to escape frequency
υ_{el}, υ_{ph}	electron, phonon hop frequencies
ω	angular frequency

Contents

1. Introduction to organic solids

1.1 Historical Perspective

The electronic properties of organic solids have been studied for almost one hundred years. Photoconductivity in an organic solid was first observed in crystalline anthracene in 1906 (see Inokuchi and Maruyama, 1978, for a review). However, after this finding relatively little work was performed on molecular crystals until interest was renewed in the 1950s following the work on "organic semiconductors" by Inokuchi (1954), and the important measurements of carrier drift mobility in crystalline anthracene by LeBlanc (1960) and Kepler (1960). Much work has been carried out on molecular crystals since these early pioneering studies and charge generation and transport are now quite well understood in such materials.

The understanding of the electronic properties of organic solids can be contrasted with that of the inorganic semiconductors. After the development of adequate theories to explain the electronic properties of crystalline inorganic semiconductors many workers became interested in non-crystalline or amorphous materials, *e.g.* chalcogenides and amorphous silicon (a-Si). Amorphous materials, as well as being interesting on a purely scientific basis, were soon found to display some inherent advantages over their crystalline counterparts when used in device applications. A major advantage is the ease with which many amorphous materials can be deposited over large areas by, for example, spin coating or thermal evaporation. This has resulted in vigorous research into the use of amorphous materials for applications such as solar cells were large area deposition is essential.

A similar transition from crystalline to amorphous has occurred with organic materials, although progress has lagged behind in this case due to the inapplicability of standard band theory to many molecular crystals. Advancement in this field has perhaps also been impeded due to a lack of appropriate applications for such materials; they definitely cannot compete with their corresponding inorganic counterparts for most device applications. At the present time organic materials have found large scale commercial application in relatively few areas, the most notable being photoconductors for electrophotography and laser printers, and liquid crystals for displays.

In-depth experimental studies of disordered and amorphous organic solids began in the late 1960s. Most interest was in polymeric materials, although amorphous and polycrystalline forms of well studied molecular crystals (for example tetracene, pentacene *etc.*) were also investigated (Maruyama and Bässler, 1981). Over the last twenty years or so interest in organic materials has centred around two main classes of materials; the so-called conducting polymers, and molecularly doped polymers (MDPs) which are solid solutions of active transport molecules in an inert polymer binder.

Interest in the pi-conjugated, conducting polymers, such as poly(acetylene), was mainly due to the discovery in 1977 that they could be "doped" to high levels of conductivity (Chiang *et al.*, 1977). Since this finding a great deal of effort has gone into the clarification of the transport properties and photoexcitations of such materials in the doped and undoped form. Polyacetylene can now be doped to exhibit conductivities of the order of that of copper (Heeger, 1993), and doped conjugated polymers in general are now employed in a range of mostly low-tech applications, *e.g.* corrosion preventative, antistatic and conductive coatings; capacitor electrolytes and rechargeable batteries and electrodes, to name but a few.

The interest in molecularly doped polymers is due mainly to their application in large area electrophotographic receptors. However, from a scientific viewpoint, they are also ideal systems for investigating hopping transport. Several different transport models have been developed to explain the temperature, field and concentration dependence of the mobility in such systems. The behaviour of the mobility is found to be common to MDPs with diverse transport species, and is also observed in sigma and pi conjugated polymers. Two main theories have emerged which attempt to explain charge transport in such materials, these are the disorder limited hopping theory and polaron theory. It has become evident in recent years that while the disorder limited hopping theory provides a more convincing fit to the experimental data, the formation of polarons cannot be neglected. These transport models will be discussed in detail in § 4.4.

1.2 Recent Advances

In the 1990s applications for conjugated polymers, and more recently conjugated oligomers, have begun to show great promise for the future. The two most widely investigated applications are organic light emitting diodes (OLEDs), and field effect transistors (FETs).

Conjugated polymer electroluminescence was first observed in poly(phenylenevinylene) (PPV) by Burroughs *et al.* in 1990 using a simple charge injection device structure (Burroughs *et al.*, 1990). Since this initial discovery rapid improvements in electroluminescence efficiency have occurred through the use of heterostructure devices and improved materials, although these are still generally PPV based. OLEDs are now available which emit colours throughout the visible spectrum. Different colours are achievable by changing the polymer band gap which can be controlled by chemical modification of the polymer backbone. Devices have also been developed which emit polarised light (Hagler *et al.*, 1991). At the present time the efficiency of OLED devices is comparable to that of commercial LEDs, and several specialised companies have been set up to exploit this new technology, *e.g.* Uniax, Cambridge Display Technologly.

Burroughs *et al.* (1988) also initiated interest in field effect transistors with active organic layers. They fabricated a metal-insulator-semiconductor field effect transistor (MISFET) using poly(acetylene), and used this device to investigate the nature of the charge carriers in the polymer. This initial work was built upon by Horowitz *et al.* (1990) who have used oligomers of thiophene as the active semiconducting layer, after finding that poly(thiophene) exhibited a very low field effect mobility. Using α-sexithiophene they have demonstrated field effect mobilities in the range 0.1-1 $cm^2\ V^{-1}\ s^{-1}$ by optimising the MISFET structure and the purity of the oligomer thin film. Field effect mobilities of this magnitude are comparable with those exhibited by similar a-Si:H devices. It is hoped that eventually organic LEDs and FETs will be developed to such a level that they can be used in "all organic" large area flat panel displays. The advantages such displays would have over competing technology, such as field emission or liquid crystal displays, are the freedom of design, flexibility and low cost of plastics.

1.3 Work carried out in this study

The primary purpose of this work was to obtain a range of information on the electronic properties of thin films of oligomeric materials. Specifically, we were interested in issues such as the charge transport mechanism, the form of the density of states and the nature of the charge carriers and their generation. Four oligomers were chosen for investigation. Three of these were oligomers of poly(thienylenevinylene) with slightly different chemical groups attached to the oligomer backbone. It was anticipated that characterisation of these materials would lead to information on the effects of different substituents on the electronic properties of the oligomer. The other oligomer chosen for study was pentacene, which is an aromatic hydrocarbon consisting of five linearly bonded benzene rings. Pentacene was chosen because it has been well studied in its crystalline and amorphous form by other workers, and is widely available (see § 5.1 for chemical structures).

The field of electronically-active organic materials is a very wide-ranging one, and as a consequence of this charge transport is only well understood in a small number of systems, *e.g.* molecularly doped polymers. The charge transport mechanism in oligomeric materials has not been studied in detail and thus initially we were presented with materials about which we knew very little. Due to this lack of solid experimental information on the chosen oligomers it was decided that a wide ranging characterisation of the electronic behaviour was necessary. This information was obtained by studying thermally evaporated and laser ablated thin films of the oligomers, in coplanar and sandwich geometry, using a range of steady state and transient photoconductivity techniques. The dark current was also examined as a function of field and temperature. Computer simulations were used to aid in the analysis of the experimental results.

The main objectives pursued in the course of this work were :

- Experimental investigation of electronic conduction processes in a range of organic thin films as a function of chemical structure, preparation and sample geometry.
- Assessment of proposed models of electronic conduction in such materials, by analytical methods and computer modelling.
- Assessment of the potential of such materials for device applications.

2. Molecular crystals

2.1 Electronic structure

An ideal crystal is defined as a substance consisting of atoms or molecules arranged in a pattern that repeats periodically in three dimensions to infinite extent. An equivalent way of stating this is to say that crystals possess long range order. The existence of long range order in a material also means that short range order will be present, which means that for any atom or molecule the immediate surroundings, such as the number of nearest neighbours and their distances are identical for any arbitrary lattice position. Therefore the existence of long range order in a material implies the existence of short range order and therefore crystallinity; however a material may possess short range order without having long range order. In reality ideal crystals do not exist as all real samples have boundaries where periodicity must end, and they also contain a certain number of unavoidable defects.

Molecular crystals are periodic arrangements of covalently bonded molecules held together by relatively weak van der Waals bonds. This distinguishes them from inorganic crystals such as c-Si which consist of silicon atoms held together by covalent bonds. The covalent bonding in inorganic crystals leads to relatively wide bands ($B \sim 5$-10 eV, where B is the bandwidth) due to strong overlap of wavefunctions on neighbouring atoms. However, the inter-molecular bonds in molecular solids are much weaker than the covalent bonds which hold the constituent molecules together, and this leads to very narrow energy bands, $B \sim k_B T$. The narrow bands in turn cause the carrier effective mass to become large, decreasing the mobility and hence the carrier mean free path (for example, a bandwidth of 0.01 eV leads to an effective mass of about 400 times m_e) The low mobilities and mean free paths observed in molecular crystals have cast doubt on the validity of applying band theory to these materials, however it has been used successfully to make predictions of charge carrier mobilities (Gutmann and Lyons, 1981). In this section we will assume coherent band transport and investigate the effects of disorder on the band structure.

2.2 Effects of disorder

As the amount of disorder in a crystalline solid is increased the amount of scattering also increases due to more and more atoms or molecules being displaced from their periodic positions. The crystal is said to have lost its long range order, although it may retain short range order. As disorder and scattering increase the carrier mean free path, L decreases, and if the disorder is strong enough the uncertainty Δk in the wave vector, k may become comparable with the magnitude of k, *i.e.* $\Delta k/k \sim 1$ so that k is no longer a valid quantum number. As $\Delta k/k$ approaches unity the mean free path decreases until it reaches the limiting condition, $L \sim a$ (the Ioffe-Regel limit), where a is the lattice constant. At this point the carrier wavefunction loses phase coherence on moving from site to site, and consequently coherent band transport must be abandoned. The non-validity of band theory means that the familiar concepts used to describe crystalline semiconductors are no longer applicable to disordered solids, for example bands can no longer be explained with ε-k diagrams, Brillouin zones no longer exist; and other concepts such as carrier effective mass are inappropriate for amorphous materials. However, disorder has only a small (but important) effect on the density of states distribution and this is therefore conserved in the amorphous state. If disorder is increased beyond the Ioffe-Regel limit the carrier wavefunctions can become spatially isolated or "localised". Localised states are characteristic of amorphous materials and are largely responsible for their charge transport properties.

2.2.1 Anderson localisation

The first paper to provide a model for localisation was that of Anderson (Anderson, 1958). The model is based on the tight-binding approximation which is applicable to weakly overlapping wavefunctions (see Mott and Davis, 1979). It investigates the effects of increasing energetic (diagonal) disorder on an initially perfect crystalline lattice, (the model does not deal with spatial (off-diagonal) disorder). The ideal crystal is represented by an array of potential wells of equal depth.

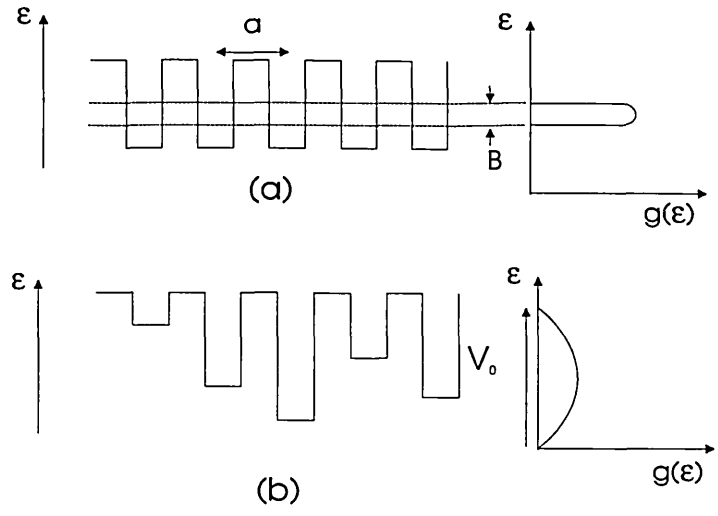

Fig. 2.1 (a) Potential wells for an ideal crystal (b) Potentials wells with fluctuations due to disorder. The DOS is also shown.

Increasing disorder is simulated by allowing the well depth to vary randomly by an amount V_0. This has the effect of broadening the DOS as shown in fig. 2.1.

The ratio between the average site separation and the mean free path can be given by,

$$\frac{a}{L} = \left(\frac{z^2}{8\pi}\right).\left(\frac{V_0}{B}\right)^2 \tag{2.1}$$

where the bandwidth, B is related to the overlap integral, J by,

$$B = 2zJ \tag{2.2}$$

and z is the co-ordination number. It can be seen that an increase in V_0 leads to a decrease in L, and at the Ioffe-Regel limit we obtain,

$$\frac{V_0}{B} \geq \sqrt{\frac{8\pi}{z^2}} \approx 0.6 \qquad \text{(for z = 6)} \tag{2.3}$$

The transition from delocalised to localised states (Anderson localisation) occurs when V_0/B attains a critical value of ~2. After Anderson localisation has occurred the average conductivity $<\sigma>$ at T = 0 K becomes zero because the states are too widely spaced energetically for tunnelling to occur without thermal assistance.

2.2.2 Anderson localisation in wide band semiconductors

It was stated in § 2.2.1 that the Anderson model applies to narrow, tight binding bands. When it is applied to inorganic semiconductors with wide bands, such as silicon, the disorder potential V_0 must be very large to cause localisation of the entire band. In materials such as this it is generally found that the critical value V_0/B for complete localisation of the band is not attained, consequently only part of the band becomes localised, fig. 2.2. If V_0 is constant throughout the band the critical value for localisation depends on the overlap, J. Thus where the DOS, and therefore J is small, (as at the extremities of the band in fig. 2.2), localisation will occur, whereas the rest of the band will remain delocalised. In a-Si these regions of localised states are known as band tails, and are separated from the extended states by a "mobility edge", so-called because the mobility increases rapidly in moving from localised to delocalised states. The band tails in a-Si have a profound effect on the carrier transport mechanism (see § 4.1.).

2.2.3 Effects of disorder in narrow band molecular solids

As outlined above, if coherent band transport is assumed the Anderson model leads to complete localisation of carriers in the bands of molecular crystals. A further model seeking to incorporate the effects of disorder specifically in molecular crystals, has been proposed by Silinsh (Silinsh, 1970). This model describes the effect of random fluctuations in intermolecular separation on the distribution of site energies, (cf. the Anderson model which ignores off-diagonal disorder).

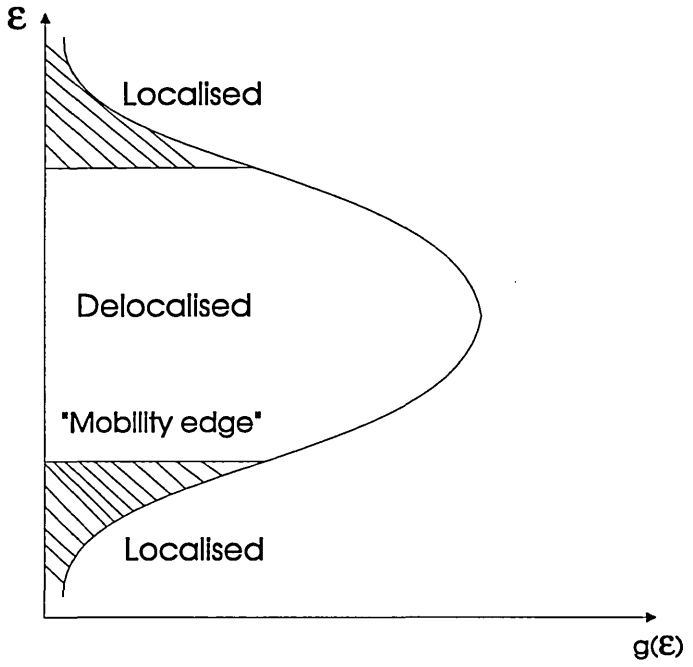

Fig. 2.2 Localised band tails, extended states and the mobility edge in a wide band amorphous semiconductor.

Of central importance in this model is a quantity known as the polarisation energy (P), which is defined by the following two equations,

$$I_c = I_g - P^+ \tag{2.4}$$

and

$$A_c = A_g + P^- \tag{2.5}$$

where I_c and A_c are the crystalline ionisation energy and electron affinity respectively; and I_g and A_g are the values of these quantities in the gas phase. P^+ and P^- are the polarisation energies of positive and negative excess charges inside the solid, respectively. The polarisation energy is mainly caused by electrostatic stabilisation of photoinduced molecular ions, due to fast electric polarisation of surrounding molecules in the solid. Due to the narrowness of the bands in molecular solids, the values I_c and A_c give, respectively, the position of the valence and conduction bands in the crystal (fig.2.3).

In the point charge approximation the polarisation energy P_i of a charge located on a molecule i is,

$$P_i = \sum_{i \neq j} \frac{e^2 \alpha_{pol}}{2R_{ij}^4} \tag{2.6}$$

where α_{pol} is the polarisability of the surrounding, neutral molecules. For pentacene the polarisation energy P^+ evaluates to ~ 1.7 eV.

It can be seen above that the polarisation energy depends on the intermolecular separation, R_{ij}. If R_{ij} varies by a small amount, ΔR_{ij} then this should result in relative fluctuations in the polarisation energy,

$$\frac{\Delta P}{P_i} = 4 \sum_{i \neq j} \frac{\Delta R_{ij}}{R_{ij}} \tag{2.7}$$

If the fluctuations in distance are random then the distribution function for the polarisation energy is predicted to be a gaussian, whose width is given by the rms standard deviation of P,

$$\sigma_g = <\Delta P> = 4P \left(\left\langle \left(\sum_{i \neq j} \frac{\Delta R_{ij}}{R_{ij}} \right)^2 \right\rangle \right)^{\frac{1}{2}} \tag{2.8}$$

or

$$\sigma_g = 4P \left\langle \frac{\Delta R}{R} \right\rangle \tag{2.9}$$

where $<\Delta R/R>$ is the average fluctuation of the intermolecular distance. For a bandwidth of 0.01 eV and a polarisation energy of 1.5 eV, σ_g exceeds the width of the transport bands in the crystal if $<\Delta R/R> > 10^{-3}$. Thus the overall effect of disorder is to split the valence and conduction bands into gaussian distributions of localised states centered around the band energies in the crystal, *i.e.*

$$g(\varepsilon)d\varepsilon = \frac{g_{tot}}{\left(2\pi\sigma_g\right)^{\frac{1}{2}}}\exp\left(\frac{-\varepsilon_0^2}{2\sigma_g^2}\right)d\varepsilon \tag{2.10}$$

where g_{tot} is the total density of states, which equals the molecular density (Bässler, 1981).

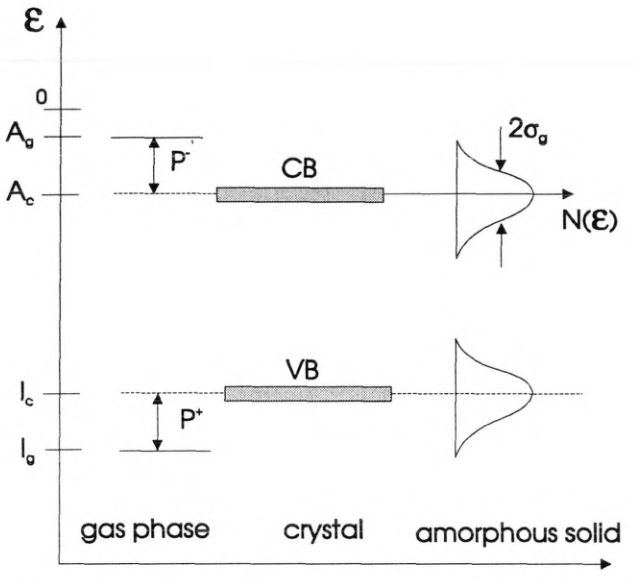

Fig.2.3 Energy level spectrum of ionic states in molecular solids.

3. Disordered organic solids

In this work we will be concerned with disordered, organic, molecular solids, and thus when we discuss "organic solids" we will assume that they are molecular and disordered. If we are referring to crystalline or non-molecular solids this will be specifically stated in the text. Discussion of the properties of inorganic semiconductors and molecular crystals will also be included when necessary or appropriate.

The field of organic solids is a very varied one, ranging from solids consisting of small molecules, through polymers, to systems containing more than one type of molecule; or molecules dissolved in an inert binder. In the next section we will discuss the so-called conjugated conducting polymers. These have generated a lot of research interest since it was discovered in 1977 that they could be chemically "doped" to give very high values of conductivity (Chiang *et al.*, 1977), *e.g.* for stretch-aligned poly(acetylene) approaching that of copper. Although we do not explicitly look at polymers in this work the theory developed provides a basis for understanding the electrical properties of oligomers, and introduces some novel concepts, such as solitons and polarons. We will not discuss chemical doping of conjugated polymers in this work.

Finally in this chapter we will briefly discuss some other types of molecular materials that have been studied.

3.1 Conjugated conducting polymers

Polymers are long-chain, quasi one-dimensional molecules which are formed from smaller molecular units known as *monomers*, so for example poly(ethylene) (PE) is formed from a very large number (n) of ethylene molecules (fig. 3.1). Note that the polymerisation of double-bonded ethylene results in a polymer which is only sigma bonded.

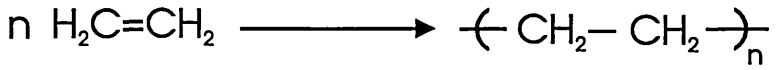

Fig. 3.1 Addition polymerisation of ethylene to form poly(ethylene).

The simplest conjugated polymer is poly(acetylene) (PA) which is formed from triple-bonded acetylene. Our discussions in this section will be mainly based on the trans isomer of this material. Trans Poly(acetylene) can be pictured as deriving from poly(ethylene) (fig. 3.2 (a)). If we remove one hydrogen atom per carbon from PE we are left with one pi electron on each monomer (fig. 3.2 (b)). These pi electrons are now free to form pi bonds and this results in the bond alternated (dimerised) PA chain (fig. 3.2 (c)).

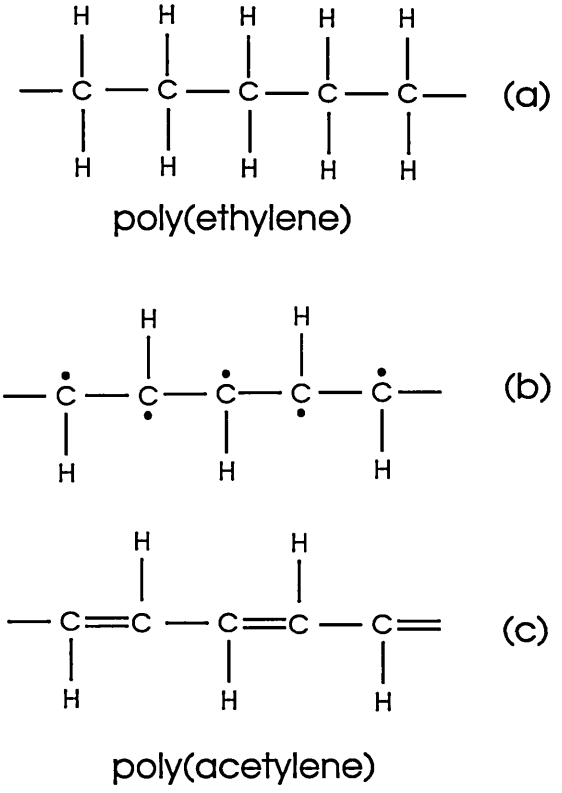

Fig. 3.2 Schematic diagram showing how poly(acetylene) can be formed from poly(ethylene) by removing one hydrogen atom per carbon.

Poly(acetylene) was first produced in 1956 and was found to be a black, semicrystalline, intractable powder (Natta *et al.*, 1956). It was also shown to be semiconducting, not metallic as had been assumed due to energy gap narrowing with increasing degree of conjugation (fig. 3.3). Subsequent improved syntheses produced a more tractable form of poly(acetylene), but it was still found to be a semiconductor (Ito, Shirakawa and Ikeda. 1974), with a band gap of ~1.4 eV. Two theoretical approaches

can be taken to explain the formation of a gap, with either electron-phonon interaction or electron correlation as the dominant mechanism.

If the gap is the result of electron-phonon interaction Peierls' argument can be used to explain why poly(acetylene) does not exhibit metallic properties. If all the carbon atoms are equally spaced with distance a, the first Brillouin zone is defined by $-\pi/a < k < \pi/a$. With one electron per carbon atom as in PA the band would be half filled and the chain would be metallic. However, a periodic distortion of the chain will reduce the Brillouin zone to $-\pi/(na) < k < \pi/(na)$, where n is the number of atoms in the new unit cell.

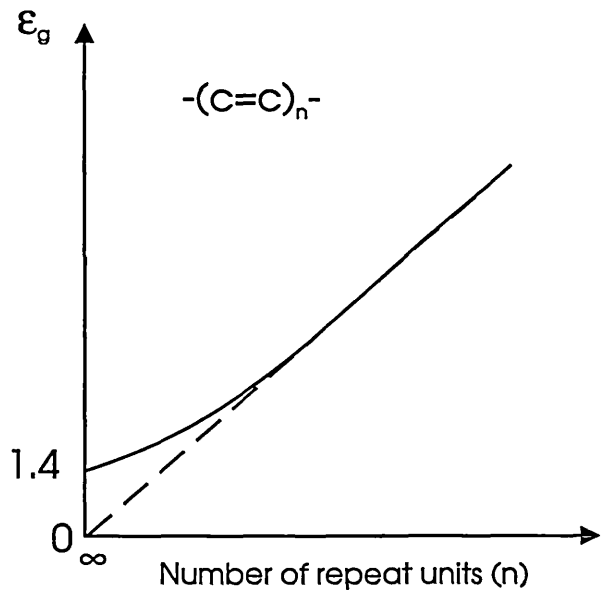

Fig. 3.3 Variation of band gap with degree of polymerisation for poly(acetylene).

The effect of the distortion is to open up a gap at the Brillouin zone boundaries, and if only states below the gap are occupied there is a reduction in the total energy and thus the distorted state will be more favourable. This argument forms the basis of the model of Su, Schrieffer and Heeger (SSH) (1979).

The lengths of the bonds in PA have been measured by X-ray diffraction (Vannoni and Clarke, 1983) and NMR techniques (Fincher *et al.*, 1982) and have been found to be 144 pm (single) and 135 pm (double) thus supporting electron-phonon interaction as the cause of the band gap.

The SSH model neglects completely the coulomb repulsion for an electron that is transferred to a site that is already occupied, these are taken into account simply by

adjusting the parameters of the Hamiltonian. In the simple Hubbard model, this electron correlation is taken into account but electron-phonon interaction is assumed to be negligible (Hubbard, 1963). This model also yields a gap in the absence of the Peierls distortion (see Kiess, 1992, for a comparison of SSH and Hubbard theory). In general it is the SSH model which is more widely applied to conjugated polymers because electron-phonon interaction is believed to be fundamental to transport in these materials. We shall discuss some of the predictions of this model below. It should be noted that the above models are based on perfect PA chains and do not take disorder into account. Increased disorder will have a profound effect on these quasi 1-D polymers.

3.1.1 Charge carriers in conjugated polymers

The SSH model assumes that charge carrier generation occurs via a direct band-to-band transition. However excitation across the gap does not produce free electrons and holes at the band edges as in inorganic semiconductors. The physical reason for this is associated with strong electron-phonon interaction, and thus charge carriers are strongly coupled to the polymer backbone. The nature of the charge carriers in conjugated polymers depends on the degeneracy of the ground state. Trans poly(acetylene) is one of only a few conjugated polymers with a degenerate ground state *i.e.* both possible forms of PA, formed by interchanging the double and single bonds, have the same energy. In contrast if the double and single bonds are swapped in poly(p-phenylene), PPP or cis poly(acetylene) we obtain a structure of higher energy; these polymers have non-degenerate ground states. For example, in PPP the quinoid (Q) form has a higher energy than the benzenoid (A) form (fig. 3.4).

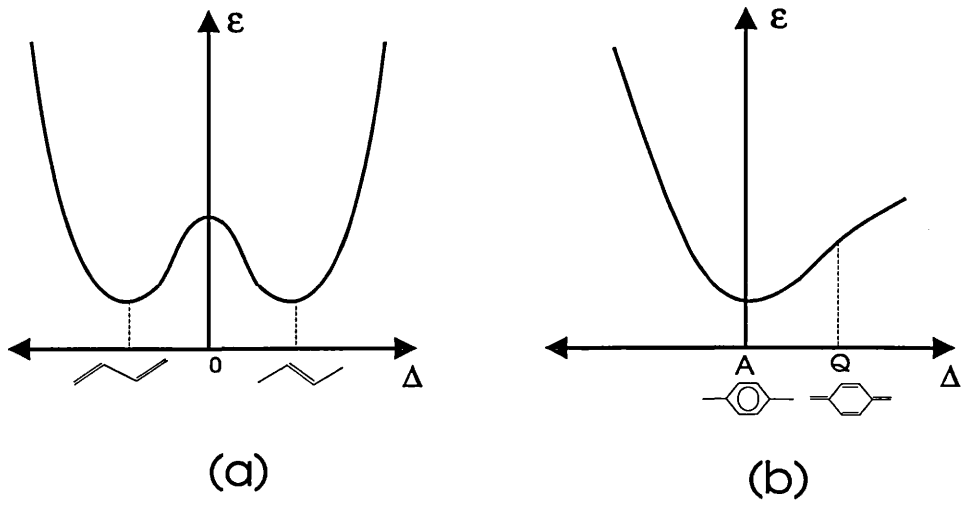

Fig. 3.4 Ground state energy as a function of the configuration co-ordinate (Δ) for a system with a degenerate ground state (a) and a single ground state (b).

Su and Schrieffer have performed a numerical integration of the SSH Hamiltonian to investigate the response of a trans-PA chain to the creation of an electron-hole pair (Su and Schrieffer, 1980). They found that the system relaxes in a time of the order of 10^{-13} s yielding spinless charged solitons either $\overline{S}^{+} - S^{-}$ or $\overline{S}^{-} - S^{+}$. In PA a soliton can be schematically represented as in fig. 3.5 it can be seen that the soliton separates degenerate ground state structures. Fig. 3.5 shows a soliton localised on one carbon atom, but in reality the transition between the two different phases and thus the soliton is spread out over several carbon atoms. In the electronic level spectrum of the chain the two soliton states lie at mid-gap. In trans-PA the quantum efficiency for free carrier (charged soliton) generation is low due to fast geminate recombination.

In non-degenerate polymers photoexcitation leads to a bound soliton-antisoliton pair. The $\overline{S} - S$ pair is bound because it is too energetically costly to have a large segment of the high energy isomer (*e.g.* the quinoid form of PPV) between the two charged solitons. Instead, the pair reaches an equilibrium separation determined by the energy difference between the two degenerate forms: a large difference leads to strong confinement. In this case the energy levels are only slightly displaced from the band edges.

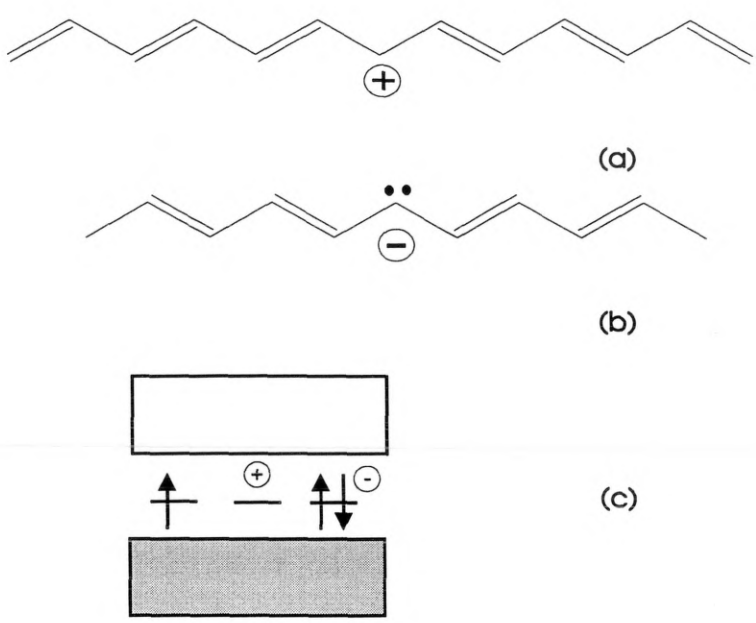

Fig. 3.5 Schematic structures showing (a) positive and (b) negative solitons. Part (c) shows the energy levels and possible charge states for solitons.

It is important to note that the bound $\overline{S} - S$ pair cannot be termed a soliton exciton because the binding is due to electron-phonon coupling in one dimension and not coulombic forces. In cis-PA the lifetime of the bound solitons is expected to be less than 10^{-7} s. Thus charge carrier generation on a single chain is unique to degenerate ground state structures, such as trans-PA.

Su and Schrieffer also investigated the effect of adding a single electron or hole to a neutral trans-PA chain. This situation describes what happens when excitation produces an electron-hole pair on different chains. They found that positive and negative polarons (P^+ and P^-) situated on different chains are formed in this case. In PA polarons can be thought of as a bound charged and neutral soliton.

For example, the negative polaron, formed on the chain the electron is transferred to, can be thought of as a bound negative and neutral soliton. In this case they are bound because the state that breaks away from the valence band is doubly occupied compared to the conduction band state which is singly occupied. Thus as the distortion proceeds the overall energy will rise. In trans-PA polarons are inherently unstable quasi-particles; if two polarons meet (say a pair of P^-s) they will decay to form a $\overline{S}^- - S^-$ pair.

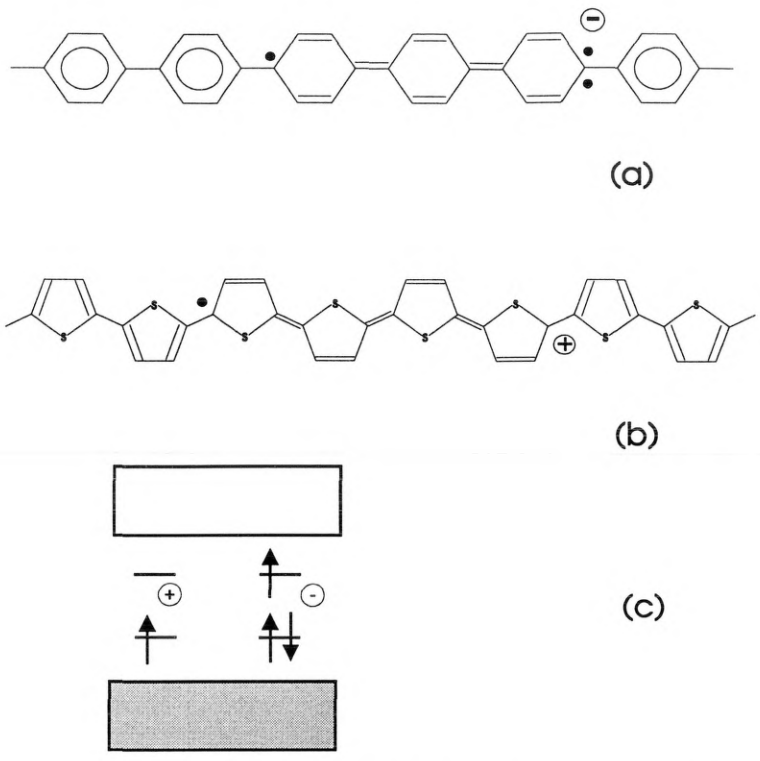

Fig.3.6 Schematic structures showing (a) negative and (b) positive polarons in poly(phenylene), PPP and poly(thiophene), PT respectively. Part (c) shows polaron charge states and energy levels in the gap.

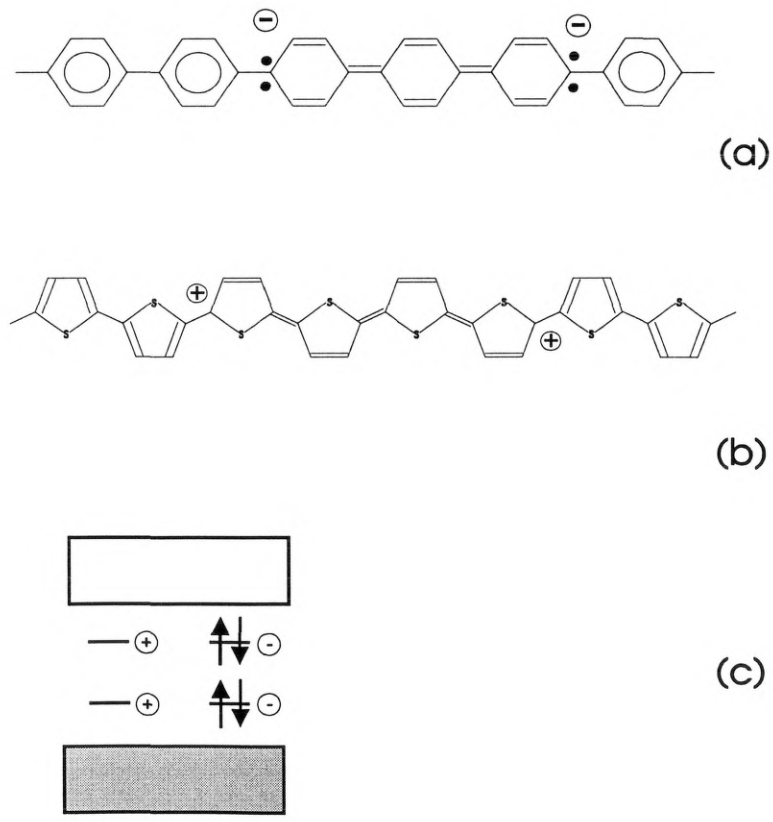

Fig. 3.7 Schematic structures depicting (a) negative and (b) positive bipolarons in PPP and PT respectively. Part (c) shows bipolaron charge states and energy levels in the gap.

In non-degenerate polymers polarons are the only stable charged excitations (fig 3.6). A final type of quasi particle that can be formed is known as the bipolaron. Bipolarons are formed in non-degenerate polymers from two similarly charged polarons, *i.e.* $P^+ + P^+ \rightarrow BP^{2+}$ or $P^- + P^- \rightarrow BP^{2-}$ and thus will be present when the polaron density is high (fig. 3.7).

3.2 MDPs and other organic photoconductors

The conjugated polymers discussed in § 3.1 can be considered as a sub-group of the family of photoconductive, organic solids in general. The range of materials in this field can be roughly divided into four groups:

1. **Solid solutions of active molecules in an inert polymer.** These are the so-called molecularly doped polymers or MDPs of the section heading. We can consider the limiting extension of these materials as a solid consisting of pure active molecules; which are the materials studied in this work. MDPs are perhaps the most widely studied of all the materials mentioned here after the conjugated polymers. This is due to the fact that the intermolecular separation can be controlled by varying the concentration of the active molecule, and thus the effect of the intermolecular separation on carrier transport can be assessed. Transport in MDPs occurs by hopping between the active molecules, they are thus ideal systems for studying hopping transport, because the combined effects of temperature, field and intermolecular separation can be studied (Mort and Pfister, 1982). MDPs are now commonly used as the charge transport layer in multi-layer electrophotographic receptors.

2. **Polymers with active side groups.** The archetypal example of this group of materials is poly(vinylcarbazole). In these polymers the σ-bonded polymer backbone is electrically inactive, and transport proceeds by thermally activated hopping between the active carbazole pendant groups (Gill, 1972).

3. **Polymers with active groups in the chain.** In polymers such as these transport will proceed by a similar process as in 2 above *i.e.* carriers will hop between the active groups incorporated into the chain.

4. **Polymers with a transport active chain.** This group contains the conjugated polymers discussed in § 3.1. Band transport occurs in these polymers, however hopping transport can dominate if the material becomes sufficiently disordered, inter- and intrachain hopping then occurs between conjugated segements of the chain (Gailberger and Bässler, 1991). Also contained in this group are transport active σ-bonded polymers such as aryl and alky substituted polysilylenes and polygermylenes. Carrier transport is believed to occur by hopping between all *trans* domains of the chain (of length 15-30 repeat units) which are separated by disordered sections, again inter- or intrachain hops can occur (Abkowitz *et al.*, 1990).

4. Electrical properties of molecular materials

We begin this chapter with a discussion of basic electronic transport in a typical amorphous semiconductor. Steady state and transient photoconductivity are then reviewed, and it is shown how these techniques can be used to obtain information on the density of states. We conclude this chapter with a discussion of the main models put forward to explain charge transport in organic semiconductors.

4.1 Electronic transport in amorphous semiconductors

In this section we will discuss electrical transport in a hypothetical amorphous semiconductor with a schematic density of states distribution as shown in fig. 4.1. The concepts laid out here are quite general and, depending on the nature of the electronic states, should be applicable to amorphous molecular solids, (Note that this DOS distribution is assumed to consists of both extended and localised states, which might not exist simultaneously in disordered molecular solids).

The electrical conductivity σ of an electronic material is determined by the number of free carriers at a particular energy $n(\varepsilon)$, and their mobility $\mu(\varepsilon)$. For an arbitrary DOS distribution the number of carriers per unit energy is given by the product of the density of states $g(\varepsilon)$, and the Fermi-Dirac occupation function $f(\varepsilon)$. Thus in the dark the total conductivity can be written as

$$\sigma = e\int_0^\infty g(\varepsilon)\,\mu(\varepsilon)f(\varepsilon)d\varepsilon \tag{4.1}$$

where

$$f(\varepsilon) = \frac{1}{1+\exp\left[\dfrac{\varepsilon-\varepsilon_f}{k_B T}\right]} \tag{4.2}$$

The magnitude of the mobility is determined by the specific conduction mechanism operating at a certain energy. There are two main conduction mechanisms which are generally observed in amorphous materials and these are discussed below.

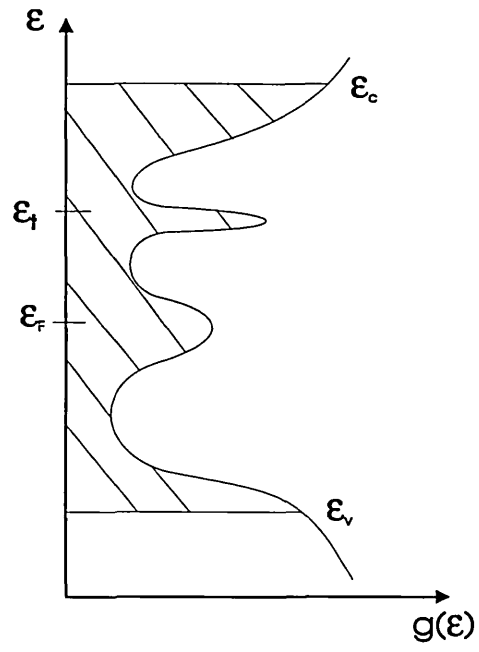

Fig. 4.1 Density of states, definitions in text.

4.1.1 Extended state conduction

Extended state conduction occurs for electrons at energies above ε_c , and for holes below ε_v. In these regions the electron mean free path is comparable to the inter-atomic distance, and consequently transport cannot be assumed to be band motion with occasional scattering. Instead extended state conduction is pictured as diffusive (Brownian) motion occurring without thermal activation, with a mobility given by

$$\mu = \left(\frac{ea^2}{6k_BT}\right)\nu_{el} \tag{4.3}$$

where ν_{el} is the electron hop frequency and a is the average inter-atomic separation.

At high temperatures the conductivity is dominated by carriers thermally activated to extended states above ε_c or below ε_v. Under these conditions the conductivity can be written

$$\sigma = \sigma_0 \exp\left[\frac{-(\varepsilon_c - \varepsilon_f)_0}{k_B T}\right] \tag{4.4}$$

with

$$\sigma_0 = eg(\varepsilon_c)k_B T\mu_c \exp\left(\frac{\delta}{k_B}\right) \tag{4.5}$$

where $\exp(\delta/k_B)$ accounts for band gap reduction with increasing temperature and ε_0 is the bad gap at T = 0 K, ($\varepsilon_c - \varepsilon_f = \varepsilon_0 - \delta.T$). Thus a graph of ln σ vs. 1/T should be a straight line with a slope of $(\varepsilon_c - \varepsilon_f)_0$ and y-axis intercept of σ_0.

4.1.2 Localised state conduction

Conduction through localised states such as band tails or defect states requires thermal activation and occurs via interaction with phonons. This phonon-assisted tunnelling process is known as "hopping" and the resulting mobility at energy ε_t is given by

$$\mu_H = \left(\frac{eR_{ij}^2}{6k_B T}\right)\nu_{ph} \exp(-2\alpha_{loc}R_{ij}) \exp(-W / k_B T) \tag{4.6}$$

The mobility for hopping transport in localised states is reduced from that in extended states by two terms, $\nu_{ph} \exp(-W/k_B T)$ and $\exp(-2\ \alpha_{loc}\ R_{ij})$. The first term is the product of a phonon "attempt to escape" frequency ν_{ph}, and the probability that an electron will gain an energy W, to hop to a nearby site. The latter term represents the overlap of the wavefunctions on neighbouring sites, where α_{loc} is the inverse wavefunction decay length (see fig. 4.2).

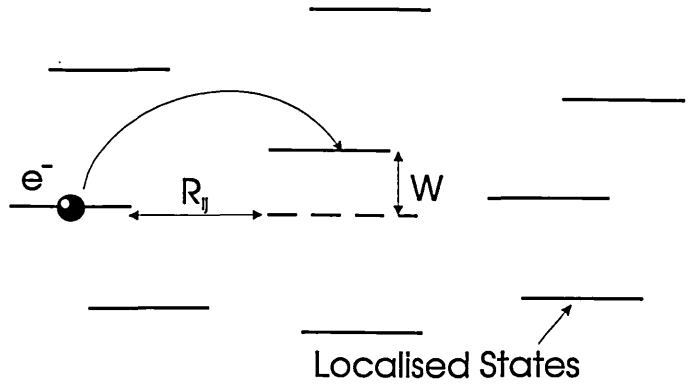

Fig. 4.2 Thermally activated hopping in localised states

The magnitude of the hopping mobility is generally at least two orders of magnitude less than that in extended states, and for this reason the energy at which localisation begins is known as the "mobility edge" (ε_c or ε_v). The conductivity associated with hopping in localised states at ε_t is

$$\sigma_H = \sigma_1 \exp\left[\frac{-(\varepsilon_t - \varepsilon_f)_0 + W}{k_B T}\right] \tag{4.7}$$

with

$$\sigma_1 = eg(\varepsilon_t)\mu_a \exp\left[\frac{\delta}{k_B}\right] \tag{4.8}$$

It can be seen that the activation energy for hopping is reduced from $(\varepsilon_c - \varepsilon_f)_0$ to $(\varepsilon_t - \varepsilon_f)_0 + W$. This process of "band-tail hopping" at ε_t can become the dominant transport mechanism at lower temperatures where the number of carriers thermally activated to extended states is reduced.

At even lower temperatures the occupation probability of states at ε_t drops, resulting in a smaller contribution to the total conductivity from ε_t. Under these conditions the dominant conduction path can switch from band tail hopping at ε_t to nearest-neighbour (Miller-Abrahams) hopping at the Fermi level, where the conductivity can be written in the form

$$\sigma = \sigma_2 \exp\left(\frac{-W_2}{k_B T}\right) \tag{4.9}$$

with

$$\sigma_2 = eg(\varepsilon_f)\mu_f \tag{4.10}$$

At still lower temperatures, due to the low number of phonons present, it may become energetically favourable for the carriers to hop large distances to find a site close enough in energy ($\sim k_B T$) to the initial site. This mechanism is known as variable range hopping and is due to competition between the overlap and energy factors in equation 4.6.

4.2 Photoconductivity

When a photoconductive material is kept under conditions of thermal equilibrium (*i.e.* in the dark at a fixed temperature) free carriers are generated at a constant rate G_o, which is identical to the rate at which they recombine, R. This is due to the *principle of detailed balance* which states that the forward and reverse directions of any process must balance at equilibrium. If the sample is then exposed to light of photon energy greater than the band gap excess carriers will be produced at a rate ΔG. The photogeneration rate is determined by the quantum efficiency for carrier generation, η (see § 4.2.1) and the volume photon absorption rate, given by the product of the photon flux, F and the absorption coefficient, α,

$$\Delta G = \eta (\alpha F) \tag{4.11}$$

If the illumination is constant with time a new quasi-equilibrium is set up, where the steady-state photocurrent σ_{pc}, is the difference between the dark conductivity σ_d and the total conductivity under illumination, σ, *i.e.*

$$\sigma_{pc} = \sigma - \sigma_d \tag{4.12}$$

or in other words the total conductivity under illumination is the sum of the dark conductivity and the photoconductivity (see fig. 4.3).

After excitation carriers are free to take part in electronic transport until trapping or recombination occurs.

In this section we will examine some general aspects of photoconductivity in amorphous materials and assess their applicability to organic photoconductors.

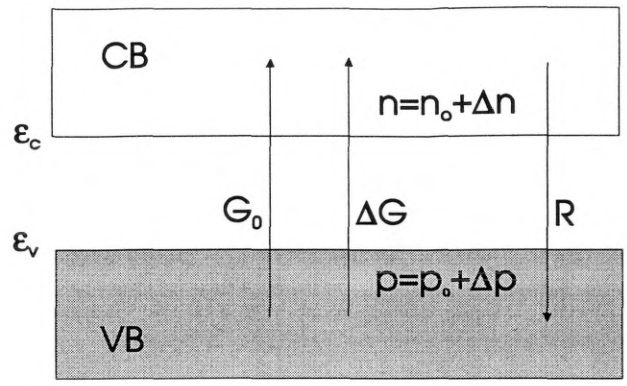

Fig. 4.3 Thermal and optical generation, and recombination of carriers in an intrinsic semiconductor.

4.2.1 Excess carrier generation

In this section we will consider carrier generation as a result of the absorption of light only, although other mechanisms are possible (*e.g.* carrier injection from electrodes). In general, the photocarrier generation in organic solids results from one or more of the following processes:

1) *Processes involving the dissociation of excitons* :

a) exciton dissociation at electrode/semiconductor interfaces;

b) exciton dissociation due to the interaction of excitons and trapped carriers;

c) autoionization processes;

d) exciton dissociation at impurity or defect sites.

2) *Non-excitonic processes* :

e) direct band-to-band transitions;

f) direct excitation of trapped carriers into the conduction or valence bands.

Processes (e) and (f) are illustrated in fig. 4.4 along with intraband excitation which does not produce free carriers (process g).

4.2.2 Excitons

An exciton is a coulombically bound electron-hole pair, and constitutes a neutral excited state of a solid. Excitons can be considered as quasi particles and are able to move diffusively through a material and transport energy; they do not transport a net charge because they are electrically neutral. It is shown in fig.4.4 that process (e) produces an electron-hole pair when the photon energy is greater than the band gap, *i.e.* $h\nu > \varepsilon_g$ In the formation of excitons this threshold is lowered by an amount which represents the exciton binding energy. Thus exciton formation in a solid should result in the appearance of structure below the band gap in the absorption spectrum, and this is indeed the case in disordered and crystalline molecular solids, although not in disordered inorganic semiconductors.

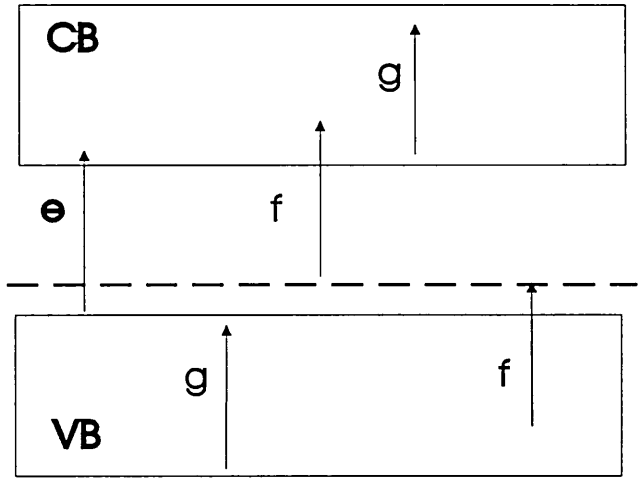

Fig. 4.4 Possible electron transitions for a photoconductor with a discrete defect level

There are two limiting types of excitons, known as Frenkel and Wannier excitons (fig. 4.5). Frenkel excitons are described by the tight-binding approximation and are thus small and spatially localised, whereas Wannier excitons are weakly bound, with a electron-hole separation large compared to the average intersite separation. Frenkel excitons can be pictured as an excited state of a molecule, in which an electron has been excited to a higher energy orbital, leaving a hole in the original (ground state) orbital. Wannier excitons occur when interaction between molecules is strong due to close packing, resulting in a reduction in the coulombic interaction between the electron and hole which can consequently become widely separated. The binding energies of

excitons are typically of the order of meVs: for example the exciton binding energy in crystalline silicon is quoted as 14.7 meV, whereas that for KCl is 400 meV (see Burns, 1985).

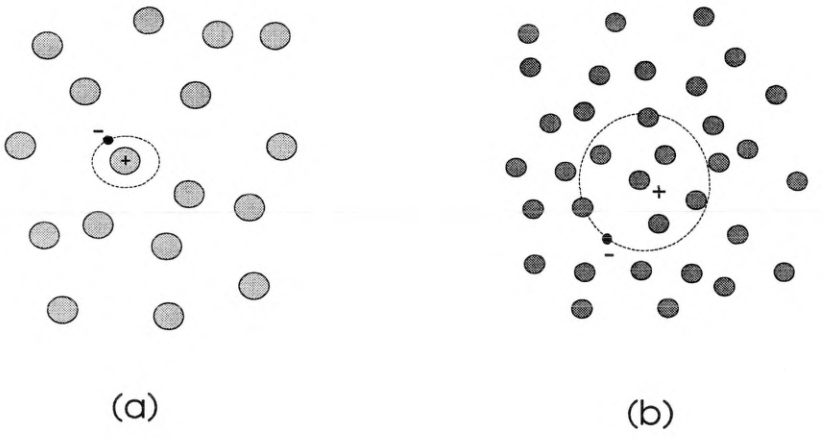

Fig. 4.5 Schematic illustration of (a) the Frenkel exciton, and (b) the Wannier exciton.

In molecular solids the covalent binding of atoms within a molecule is much stronger than the van der Waals binding between molecules, and due to this the properties of the individual molecules are preserved in the solid (cf. Si). This is indicated by the fact that the absorption lines of an isolated molecule appear also in the solid state with only slight shifts in frequency. On this basis, excitons in molecular solids are likely to be of the Frenkel type.

Depending on the excitation energy excitons can be created in either the singlet (S) or the triplet (T) state. Triplet excitons are formed when illumination results in an excited state in which the two highest energy electrons have parallel spins, singlet excitons are formed when the excited electron has an anti-parallel spin to the highest energy unexcited electron. Pauli's exclusion principle tells us that electrons with parallel spins are in a lower energy state than those with anti-parallel spins (cf. Hund's rule), due to *spin correlation*. Spin correlation causes electrons with parallel spins to behave as if they have a tendency to stay well apart, and hence they repel each other less. The effect of spin correlation is to allow the atom to shrink slightly, so the electron-nucleus interaction is improved when the spins are parallel. Thus the first triplet exciton of a molecule (T_1) is generally lower in energy than the singlet (S_1). Higher energy photons will produce higher energy excitons *e.g.* S_2, S_3....T_2, T_3.....*etc.*

Excitons are ultimately unstable with respect to recombination in which the electron drops into the hole producing either a photon or phonons. Fluorescence and phosphorescence result from the radiative recombination of singlet and triplet excitons respectively, excitons can also recombine without the emission of photons As well as recombining excitons can also be made to dissociate into electron-hole pairs as long as the binding energy can be overcome. Some of the processes by which excitons can dissociate were given above, these processes normally resulting in creation of one type of carrier (say holes), and capture of the other type (say electrons), *i.e.* they are extrinsic processes. Exciton dissociation, (not band-to-band excitation), is believed to be the one of the main routes to charge carrier production in molecular crystals and has also been applied to disordered organic solids. Charge carrier generation by exciton dissociation generally occurs when the exciting energy is low. For example, in pentacene crystals, in the energy range from 1.4 to 2.2 eV charge carrier generation occurs through the interaction of triplet excitons with trapped holes (Silinsh, 1974). At higher excitation energies intrinsic carrier production can occur. In molecular solids this is believed to occur via the *autoionization* (AI) mechanism. This was demonstrated in the late 1960s by Geacintov and Pope (1967) for polyene crystals; they showed that the conventional semiconductor band-to-band transition was not valid in this case. The AI mechanism occurs when an electron is excited to a metastable state (A) which lies above the band gap ε_g, this state can then spontaneously decay yielding free charge carriers, *i.e.*

$$S_0 + h\nu \rightarrow A \rightarrow e + h \qquad (4.13)$$

where S_0 is the singlet ground state (see fig. 4.6). This process competes with internal conversion back to S_1, the first singlet excited state,

$$S_0 + h\nu \rightarrow A \rightarrow S_1 + \text{phonons} \qquad (4.14)$$

Later, studies carried out on anthracene crystals (Batt *et al.*, 1968; Chance and Braun, 1976; Kato and Braun, 1980) indicated that the AI mechanism could not fully explain the carrier generation process, and this led to the development of a multi-step photogeneration model (Silinsh *et al.*, 1982) which will be discussed below.

The first stage is photon absorption and formation of a Frenkel exciton (fig. 4.6 (a)). This is followed by autoionization of the exciton, creating a positive parent

molecule and a "hot" electron (not an e-h pair) with excess kinetic energy, ε_k depending on the photon energy.

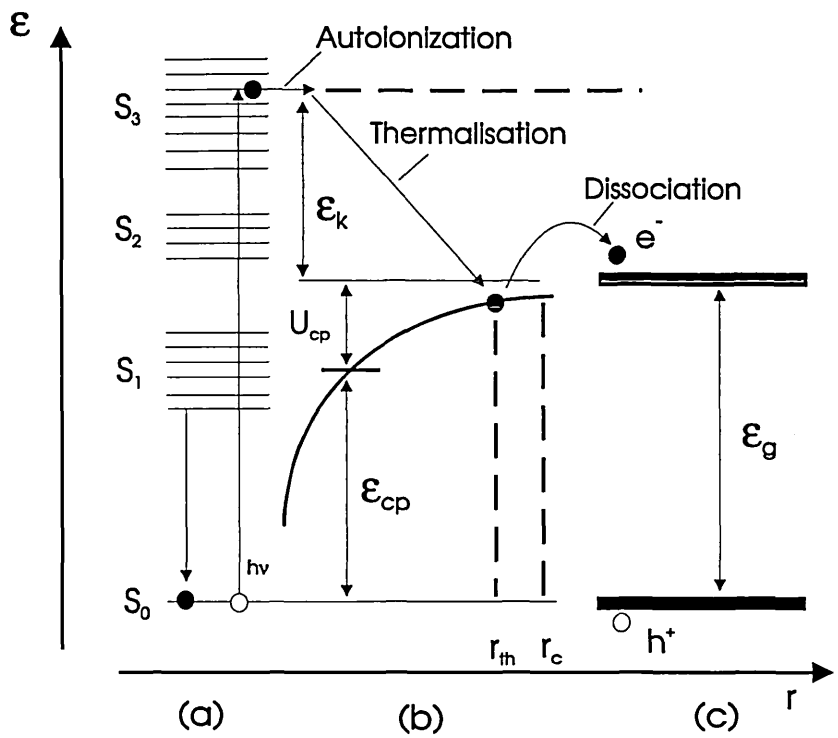

Fig. 4.6 Multi-step photogeneration process appropriate for molecular solids.

In the third stage, the hot, quasi-free electron loses excess energy by fast, inelastic scattering, and becomes thermalised at a mean thermalisation length, r_{th} inside the critical coulomb radius, r_c ($r_{th} < r_c$), thus forming an intermediate charge pair (CP) state of bound carriers (fig.4.6 (b), where ε_{cp} is the energy of the charge pair state and U_{cp} is the coulomb binding energy). In the final stage free carriers are created by dissociation of the CP state (fig. 4.6 (c)). This final step can be described by the Onsager model which predicts the probability of thermal dissociation of a bound charge pair under the influence of the combined coulombic and applied fields (Onsager, 1938). The Onsager equation is

$$\frac{df}{dt} = \frac{k_B T}{e} \mu . \nabla . \left[\exp\left(\frac{-U(r)}{k_B T} \right) grad . f \exp\left(\frac{U(r)}{k_B T} \right) \right] \qquad (4.15)$$

where f is a probability function, μ is the electron mobility, and U(r) is the coulombic potential modified by the applied field, and is given by

$$U(r) = -\left(\frac{e^2}{4\pi.\varepsilon_r.\varepsilon_0 r_{th}}\right) - qEr_{th}\cos\theta \qquad (4.16)$$

The Onsager equation as given above cannot be solved analytically, but numerical solutions can be obtained with r_{th} as an adjustable parameter. The overall field dependence of photogeneration is governed by the efficiency of the dissociation step.

A one-dimensional version of eq. 4.15 is also possible and has been applied to poly(diacetylene), and other conjugated polymers due to their 1-D nature (Gailberger and Bässler, 1991).

4.2.3 Steady state photoconductivity

In this section we will begin by discussing photoconductivity in the simple case of a trap-free semiconductor illuminated with constant, super-bandgap light, as shown in fig. 4.3, and then expand our discussion to include localised states in the gap (we assume electron carriers for simplicity). The illumination generates excess electron-hole pairs at a rate ΔG, which then transport charge until they are trapped or recombine. The mean time an excess electron spends in extended states, before recombination, is known as the electron lifetime, τ_r. Under steady state conditions the generation and recombination rates are equal due to detailed balance, so

$$\Delta G = \frac{\Delta n}{\tau_r} \qquad (4.17)$$

From above it can be seen that a measurement of the steady state photoconductivity, $\sigma_{pc} = n\, e\, \mu$ reflects the product $\mu\tau_r$.

The rate of change of free electron and hole concentrations is given by

$$\frac{dn}{dt} = \frac{dp}{dt} = G_0 + \Delta G - R \qquad (4.18)$$

The recombination rate, R is given by

$$R = (n_0 + \Delta n)(p_0 + \Delta p)C_R \tag{4.19}$$

where C_R is the capture coefficient for capture of a free hole by a free electron and is determined by the product of the carrier thermal velocity, v and the band-to-band capture cross section, S

$$C_R = vS \tag{4.20}$$

The capture coefficient represents the probability of electron-hole recombination per unit time. The dark generation rate G_0 is given by $n_0 p_0 C_R$. The material is neutral and trap free so the number of electrons and holes balance *i.e.* n = p and $n_0 = p_0$ so $\Delta n = \Delta p$. Substituting into 4.19 gives

$$\Delta G = (2n_0 \Delta n + \Delta n^2)C_R \tag{4.21}$$

This equation exhibits two regimes depending on the magnitude of the generation rate (proportional to photon flux, F).

Under conditions of low light the thermal generation rate is much greater than the excess carrier generation rate, $G_0 >> \Delta G$ and thus $n_0 >> \Delta n$. The excess electrons recombine with the large, fixed density of thermally generated holes, so 4.21 becomes

$$\Delta G = 2\Delta n n_0 C_R \tag{4.22}$$

In this regime the photoconductivity is proportional to the generation rate and the lifetime is constant. This process is known as *monomolecular* recombination (MR) because the recombination rate depends on the excess density of only one type of carrier. When the generation rate is high we have $\Delta G >> G_0$ and $\Delta n >> n_0$ yielding

$$\Delta n = \left(\frac{\Delta G}{C_R}\right)^{\frac{1}{2}} \tag{4.23}$$

Here the photocurrent varies as the square root of the excess generation because the recombination rate depends on the densities of both recombining species (fig.4.7). This is known as *bimolecular* recombination (BR) and results in a carrier lifetime which decreases as the excess carrier density increases.

In reality, band-to-band recombination of free electrons and holes in amorphous semiconductors is a very unlikely process. This is due in part to the small capture cross section (and thus capture coefficient) for this process (typically $S \sim 10^{-20}$ cm^2), but it is more usually the case that band-to-band recombination is swamped by recombination occurring via localised states in the gap. In the case of crystalline semiconductors with no gap states band-to-band recombination of free electrons and holes can be the main recombination mechanism, however. Gap state mediated (Shockley-Read) recombination occurs in two steps, electron capture by a localised state in the gap, followed by hole capture from the valence band (Shockley and Read, 1952).

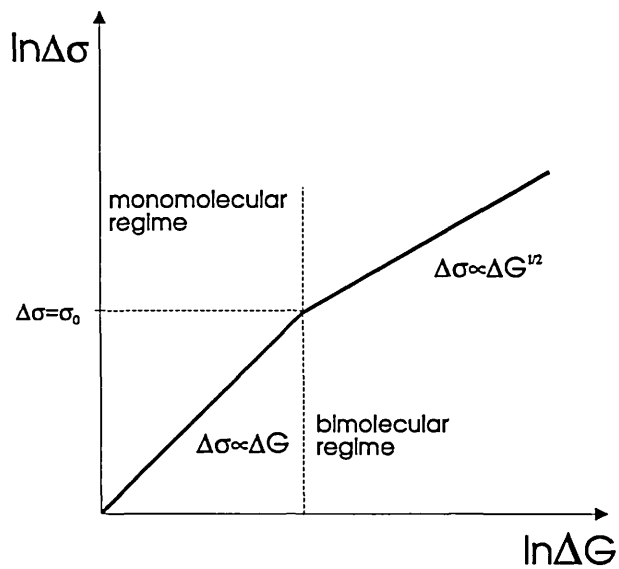

Fig.4.7 Effect of generation rate on recombination: monomolecular and bimolecular recombination regimes.

Shockley and Read derived the occupation statistics in the non-equilibrium, steady state by considering all possible electron and hole transitions that can occur via a given set of localised states (fig. 4.8). In the steady state the rate of change of free and trapped electrons is zero, therefore the four transitions shown in fig.4.8 must balance, *i.e.* A+D = B+C, (A and B are electron capture and release, and C and D are hole capture and release respectively).

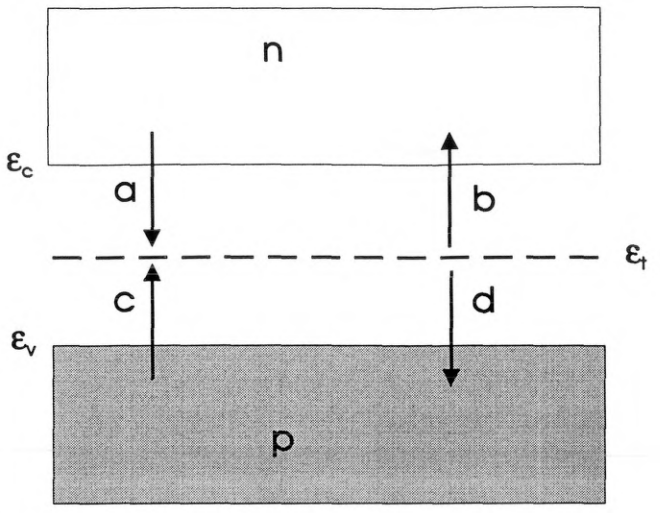

Fig. 4.8 Possible electron and hole transitions from a discrete localised state.

Writing this in terms of the capture and release rates at ε_t we have,

$$\frac{dn_t}{dt} = A - B - C + D = 0 \tag{4.24}$$

or

$$0 = nC_n N_t\left[1 - f(\varepsilon_t)\right] - e_n N_t f(\varepsilon_t) - pC_p N_t f(\varepsilon_t) + e_p N_t\left[1 - f(\varepsilon_t)\right] \tag{4.25}$$

where N_t is the trap density and e_n is the electron emission probability given by

$$e_n = \upsilon \exp\left(\frac{-(\varepsilon_c - \varepsilon_t)}{k_B T}\right) \tag{4.26}$$

In 4.26 υ is the attempt-to-escape frequency which is the product of the electron capture cross section and the effective density of states in the conduction band, $\upsilon = C_n N_c$.

Equation 4.25 can be manipulated to yield the overall Shockley-Read statistic, which is

$$f(\varepsilon_t) = \frac{nC_n + \overline{p}C_p}{nC_n + \overline{n}C_n + pC_p + \overline{p}C_p} \tag{4.27}$$

where $\overline{n}\,C_n = e_n$ and $\overline{p}\,C_p = e_p$. Note that this expression does not depend on the trap density at ε_t, *i.e.* it is independent of N_t. Due to this it can be applied to arbitrary distributions of states as was shown by Simmons and Taylor (Simmons and Taylor, 1972).

States close in energy to the bands act as traps and immobilise carriers for a certain period of time (depending on their depth) before releasing them to their respective bands, whereas states deep in the gap act as recombination centres because thermal re-emission to the band is unlikely. The Shockley-Read statistic enables us to determine whether a gap state is acting as a trap or a recombination centre. For traps the electron release rate is much greater than the hole capture rate, *i.e.* $\overline{n}\,C_n >> pC_p$ so 4.27 becomes

$$f(\varepsilon_t) \approx \frac{n}{\overline{n}} = \frac{n}{N_c \exp\left(\frac{-(\varepsilon_c - \varepsilon_t)}{k_B T}\right)} \tag{4.28}$$

so the occupancy at ε_t is related to that at ε_c by a Boltzmann ratio and is thus temperature dependent.

For recombination centres the capture rates are much larger than the release rates (far from bands) and eq. 4.27 becomes

$$f(\varepsilon_t) \approx \frac{nC_n}{nC_n + pC_p} \tag{4.29}$$

It can be seen that thermal communication with the conduction band is lost and thus the occupancy becomes constant ($f(\varepsilon_t) = 0.5$ if $C_n = C_p$). Note that in these approximations we have assumed that the capture coefficients are independent of energy. Figure 4.9 shows the form of the occupation in a semiconductor with a continuous distribution of localised states in the gap.

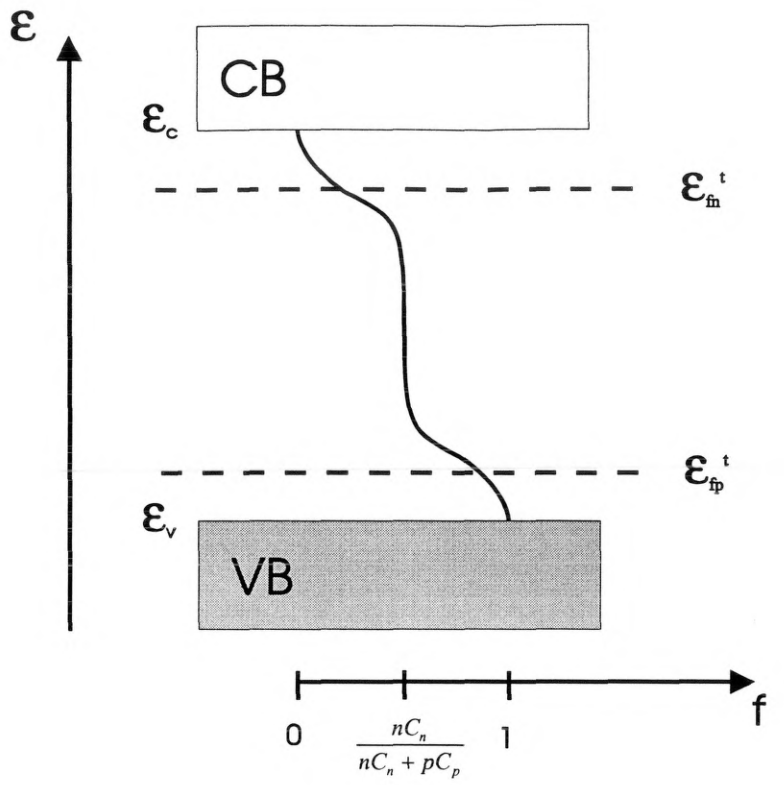

Fig. 4.9 Simmons-Taylor occupation function for a semiconductor with a continuous gap state distribution.

Under external excitation the density of free carriers is much greater than in thermal equilibrium, thus we can no longer use the relation

$$n_0 = N_c \exp\left(\frac{-(\varepsilon_c - \varepsilon_f)}{k_B T}\right) \tag{4.30}$$

where ε_f is the thermal equilibrium, or dark Fermi level. In the steady state we rewrite 4.30 as

$$n = N_c \exp\left(\frac{-(\varepsilon_c - \varepsilon_{fn})}{k_B T}\right) \tag{4.31}$$

where ε_{fn} is the electron quasi-Fermi level (QFL), and is defined in accordance with the above equation (a similar equation can be written for holes). Thus when a semiconductor is illuminated, the dark Fermi level splits into two QFLs which move

towards the band edges with increasing excitation intensity. Note that since n is not necessarily equal to p in the steady state the QFLs need not be split equidistant from their respective band edges. The quasi-Fermi levels may also be expected to describe the occupation of traps in thermal equilibrium with the bands.

The occupation of traps is more appropriately described using the so-called trap quasi-Fermi level ε_{fn}^{t}, first used by Simmons and Taylor (1972). The occupation at ε_{fn}^{t} is half that of eq. 4.29, and it thus marks the transition between recombination centres and traps The trap quasi-Fermi level is situated above ε_{fn}, (but only slightly so in n-type semiconductors), and it behaves similarly under illumination. Thus as the light intensity is increased ε_{fn}^{t} and ε_{fp}^{t} move towards their respective bands signifying the conversion of traps into recombination centres.

The conversion of traps to recombination centres forms the basis of a model developed by Rose to explain the commonly observed phenomenon of a photocurrent excitation dependence γ intermediate between that of monomolecular and bimolecular recombination (Rose, 1963), *i.e.* $i_{pc} \propto \Delta G^{\gamma}$, $0.5<\gamma<1.0$. The deviation from the normal MR or BR regimes is caused by the gap states and the resulting value of γ will depend on the particular distribution of these states. In his model Rose assumed an n-type semiconductor with an exponential density of states described by

$$g(\varepsilon_t) = g_0 \exp\left(\frac{-(\varepsilon_c - \varepsilon_t)}{k_B T_0}\right) \tag{4.32}$$

where $k_B T_0$ determines how rapidly the DOS changes with energy (*i.e.* the "width" of the tail), and g_0 is the extrapolation of $g(\varepsilon)$ to ε_c. As the excitation is increased traps are converted to recombination centres causing the electron lifetime τ_n to decrease. Rose found that for an exponential DOS $\gamma = T_0/(T_0 + T)$ as long as $0 < T < T_0$. Exponents between 0.5 and 1.0 can be explained by a continuous density of states.

4.2.4 Photocurrent relaxation from steady state

A slow relaxation of the steady state photocurrent after the removal of excitation or "persistent photocurrent" (PPC) has been observed in many disordered materials (Lee, Yu and Heeger, 1993; Akashi *et al.*, 1995)). The existence of PPC in a material suggests that charge is being stored (for example by being very deeply trapped) or that

recombination of carriers is severely inhibited. Persistent photocurrents observed in poly(p-phenylenevinylene) (PPV) have been fitted with a stretched exponential function. They have been found to be essentially temperature independent and only slightly dependent on excitation intensity (Lee, Yu and Heeger, 1993). By studying the spectral dependence of the photocurrent using DeVore's model (1956) the aforementioned authors obtained good agreement between theory and experiment and demonstrated that surface recombination was of prime importance in PPV. They attributed the persistent photocurrent to the slow dispersive diffusion of bulk generated bipolarons (which are the lowest energy excitation in the bulk, and are energetically inhibited from recombining there) to the surface. Reduced dielectric screening near the surface allows polarons to become the lowest energy excitation in this region. Polaron transport and recombination can then occur at the surface.

Persistent photocurrents observed in poly(3-alkylthiophene)s doped with C_{60} have been observed to depend on the illumination period and the concentration of C_{60}, and have also been shown to exhibit a unique temperature dependence (Akashi *et al.*, 1995, Yoshino *et al.*, 1994). In these systems photoexcitation is believed to lead to the formation of a hole polaron on the polymer chain and an electron polaron on the C_{60} molecule. Stabilisation of the electron polaron on the C_{60} due to charge rearrangement, as well as further stabilisation to the bipolaron state is believed to reduce interaction with the hole polaron on the polymer chain, and thus inhibit recombination.

4.2.5 Transient photoconductivity

Transient photoconductivity techniques are those in which a photoconductor is excited into a state far from equilibrium by the action of a short pulse of illumination. Analysis of the photocurrent decay can then provide information on the carrier mobility and the density of localised states. The two transient techniques discussed in this work are the time of flight technique (TOF) technique and the transient photocurrent decay technique (TPC), although only TPC has been successfully carried out. The main difference between time of flight and TPC is caused by the type of electrodes used and their geometry. In TPC, coplanar, ohmic electrodes are used, making this a secondary photocurrent technique; whereas in TOF blocking electrodes are used in a sandwich configuration, making this a primary photocurrent technique. TPC may also be

performed with a background steady state illumination which is referred to as optical bias. Figure 4.10 shows the basic set-ups for the TOF and TPC experiments and includes schematic current decays for each.

The TOF technique has been more widely utilised than TPC to characterise both inorganic and organic amorphous semiconductors, and this is mainly because it provides a simple method for obtaining the carrier (drift) mobility, μ_d. In a typical TOF experiment the sample is illuminated with a short flash of highly absorbed light and consequently electron-hole pairs are produced close to the illuminated electrode. In the normal, small signal case the total injected charge Q must not exceed CV_b where C is the capacitance of the sample and V_b is the applied voltage. If the illuminated electrode is positive electrons will be removed effectively instantaneously whereas the holes will drift in the applied field towards the negative (extraction) electrode. The contacts in the TOF experiment are "blocking", that is to say they do not inject carriers into the sample, and thus the only current measured in the external apparatus is due to the drifting holes. When the drifting carriers reach the extraction electrode they are removed and the current drops to zero. The experiment can also be carried out with the illuminated electrode negative in order to study electron transport. The TOF technique is only useful for low conductivity material such that the transit time t_{tr} is much less than the dielectric relaxation time τ_{rel} which is given by

$$\tau_{rel} = \sigma/(\varepsilon_r\varepsilon_0) \tag{4.33}$$

For experimental transients unaffected by recombination we also require that the recombination time, t_r is longer than the transit time, *i.e.* $t_r > t_{tr}$.

In crystalline samples with no traps the current decay obtained from a TOF experiment is constant, after a rapid initial drop due to thermalisation, until the carriers are extracted at the back electrode (fig. 4.11). The current does not drop immediately to zero after the transit time because the carriers assume a gaussian distribution of velocities due to diffusion and thus also have a gaussian spatial distribution. Decays of this type are therefore known as *gaussian* or *conventionally dispersive.*

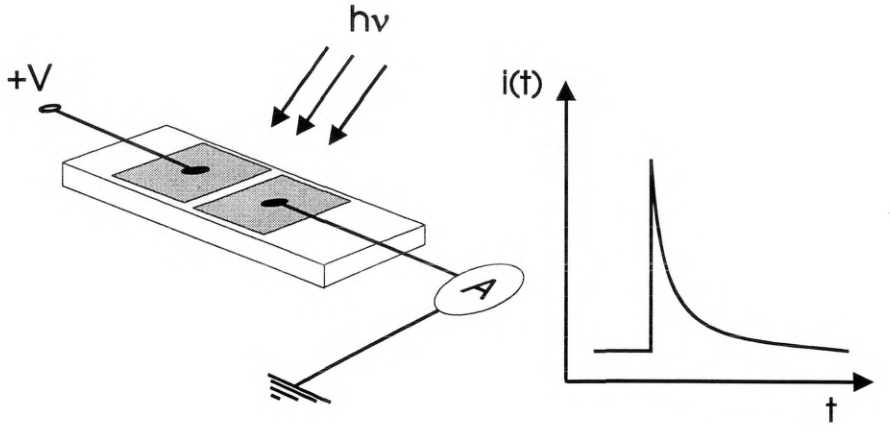

(a)

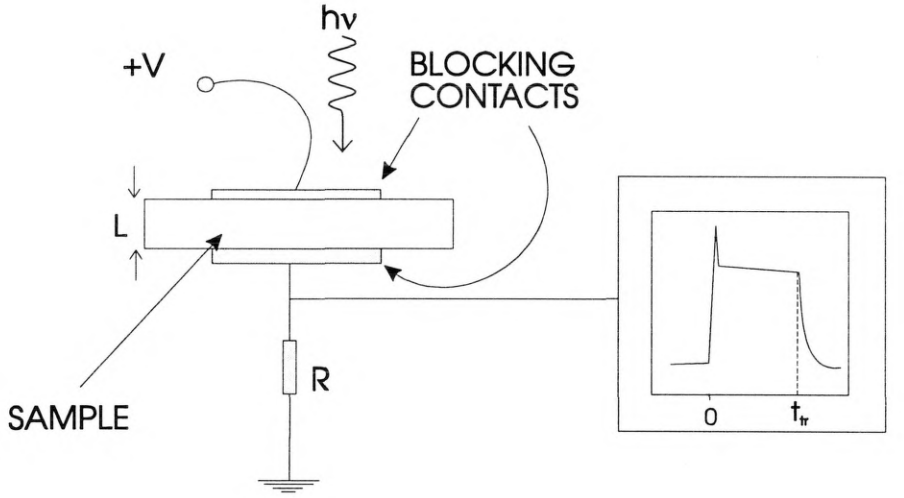

(b)

Fig. 4.10 Experimental setups for (a) transient photocurrent decay (TPC) and, (b) time of flight (TOF)

The experimentally determined transit time of carriers through the sample is taken to be the time at which the current has dropped to 50% of its plateau value, and is related to the average drift mobility by

$$\mu_d = \frac{L}{t_{tr} E} \tag{4.34}$$

where L is the film thickness and E the electric field.

In amorphous materials the TOF lineshapes are very different to those of gaussian transport and assume an almost featureless decay with no observable extraction

feature. However if the current decay is plotted on double logarithmic axes two power law slopes are obtained and an extraction feature is recovered. In these *anomalously dispersive* decays the actual value of t_{tr} can be measured in several ways, although the most popular is usually where the extrapolated power law sections intersect (see for example Pautmeier, Richert and Bässler, 1991). Equation 4.34 above is still valid for decays of this type but it is now found that the transit time is not linearly proportional to L or E as in gaussian transport. The nonlinearity is caused by a broad distribution of individual carrier transit times (much broader than in gaussian transport), due to either interaction with a continuous trap distribution in materials with an extended band of states (multiple trapping) or a distribution of hopping site energy (not separation, as originally suggested by Scher and Montroll (Scher and Montroll, 1975)) in materials containing localised states only (multiple hopping). Thus when traversing the sample some carriers may pass through almost unhindered whereas others may be deeply trapped resulting in a much longer transit time. This results in the peak in the injected carrier density remaining near to the top electrode and being gradually "smeared out" towards the extraction electrode.

A TOF decay can be thought of as a unipolar TPC decay with the steeper power law decay after extraction representing monomolecular recombination, thus it is often possible to interpret TOF and TPC in a similar manner, as long as the important differences are borne in mind.

In the next section we will discuss some models put forward to explain anomalously dispersive transport in amorphous (inorganic) semiconductors, they are based on the multiple trapping model which will be outlined first.

4.2.6 Multiple trapping

In inorganic amorphous semiconductors both TOF and TPC current decays are usually interpreted in terms of the multiple trapping model. Conduction by the multiple trapping mechanism begins with carriers being excited to band states above the mobility gap, followed by rapid thermalisation of carriers to the band edges. Transport then

proceeds at the band edge producing an electric current until the carrier reaches a trapping state and becomes immobilised. At some later point (depending on the energy depth of the trap) the carrier will be thermally re-excited to the band where it can again contribute to the electric current until it is retrapped. This capture-release cycle will in general occur many times before the carrier recombines (fig. 4.11).

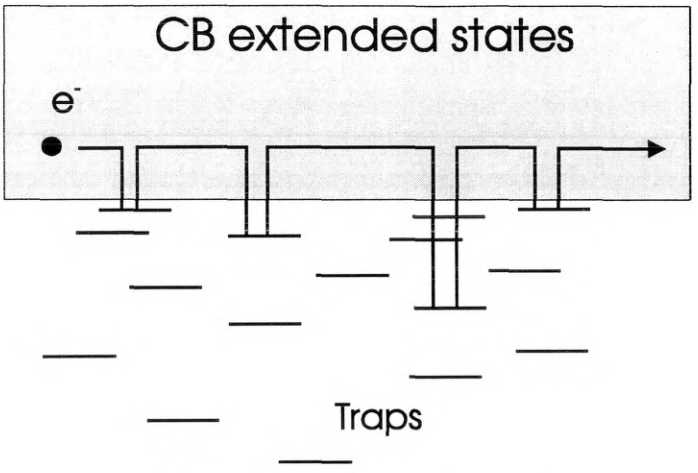

Fig. 4.11 Multiple trapping conduction mechanism.

Experimental evidence for a-Si:H fits very well with the predictions of multiple trapping and there is now little doubt that this is the correct transport mechanism in this case, except perhaps at low temperatures where band tail hopping may become dominant (Monroe, 1985). Whether the MT model is applicable to organic semiconductors in which the existence of a delocalised band is uncertain has not yet been determined, although some authors have employed it in interpretation of results (Meyer *et al.*, 1995).

An analogous transport mechanism to multiple trapping can occur in the absence of a band of extended states and is termed trap-controlled hopping. In this case transport of charge occurs by hopping between localised states at a critical energy (ε_t) in the gap, in effect this is what replaces the band in multiple trapping. The critical energy at a particular temperature is determined by competition between the overlap term and the Boltzmann factor in eq. 4.50. Trapping of carriers again occurs, this time in traps below ε_t with release times (to ε_t) that are considerably longer than those for hopping at the critical energy (fig. 4.12). Trap-controlled hopping may explain why multiple trapping models often fit with data obtained from organic materials which are not expected to contain an extended band of states.

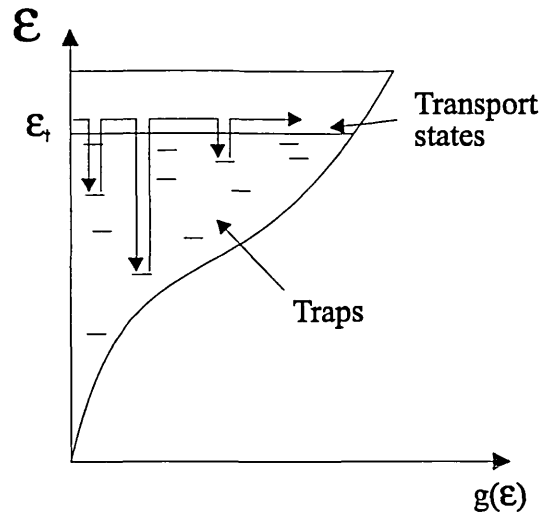

Fig. 4.12 Trap-controlled hopping scenario.

A simple model explaining the main features of dispersive transport was put forward separately by Tiedje and Rose and Orenstein, Kastner and Vanninov and is generally referred to as the TROK model (Tiedje and Rose, 1980; Orenstein, Kastner and Vanninov, 1982). The model assumes multiple trapping in a continuous density of localised states but may also be applicable to trap-controlled hopping (Monroe, 1985; Silver, Schönherr and Bässler, 1982). The model begins with a pulsed carrier density N_e, (we will assume electrons), being rapidly trapped by localised states in the gap, the trapped electron distribution reflecting the DOS (the capture cross section is assumed to be the same for all states). After a short period of time carriers immobilised in shallow traps will be released and come into thermal equilibrium with the band, whereas deeply trapped carriers will remain localised.

Thus at a particular time after trapping the thermalising carriers can be separated into two groups:

(i) carriers in thermal equilibrium with extended states, and
(ii) carriers too deep to have been released within the measurement time

The energy level separating these two groups known as the *thermalisation energy* (ε_c-ε_d) was first introduced by Arkhipov and Rudenko, and is defined as

$$e_n(\varepsilon_d).t = 1 \tag{4.35}$$

where $e_n(\varepsilon_d)$ is the electron release rate at energy ε_d. In other words at energy ε_d traps have on average released carriers only once at time t (Arkhipov and Rudenko, 1979). In DOS distributions that decrease uniformly from the band edge (*e.g.* exponential) the electrons will thermalise in the form of a packet with a peak at ε_d (fig. 4.13) which moves down at a rate given by

$$\varepsilon_d = k_B T \ln(\upsilon t) \tag{4.36}$$

As time proceeds it can be seen that the thermalisation energy will move deeper into the gap releasing trapped charge which will be subsequently recaptured in deep traps below ε_d. Thus states above ε_d have an occupation in a Boltzmann ratio with the extended states, whereas those below ε_d have a constant occupation, increasing with time. Orenstein *et al.* (1982) applied the TROK model to an exponential DOS. For low N_e and free electron recombination with trapped holes they obtained a two region decay of the transient photocurrent, δi_{pc}:

$$\delta i_{pc} = t^{-\left(1-\alpha_d\right)} \qquad \text{for } t<t_{tr} \tag{4.37}$$

$$\delta i_{pc} = t^{-\left(1+\alpha_d\right)} \qquad \text{for } t>t_{tr} \tag{4.38}$$

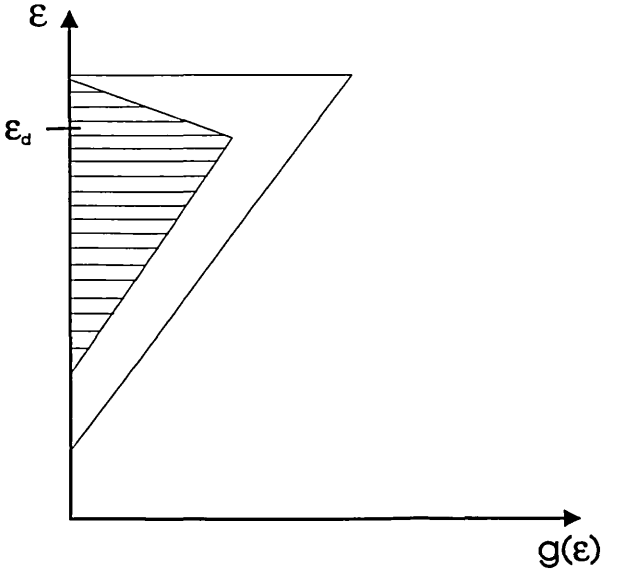

Fig. 4.13 Electron thermalisation in an exponential conduction band tail.

4.3 Methods for DOS retrieval

In a transient photoconductivity experiment on an amorphous material the current decreases with time before recombination due to interaction between the injected carriers and the trap distribution. If there are no traps in the gap the current will be constant until recombination. It can thus be seen that the transient photocurrent decay contains information on the density of states in the gap. It is this relation between the transient photocurrent and the DOS which has led to the development of DOS spectroscopies using the TPC and TOF techniques. Whereas the TOF technique has mainly been used for the calculation of the drift mobility and its temperature and field dependence the TPC method has become popular in situations where it is desired to study the decay of the photocurrent to long times, or to observe recombination without the limitation of a transit time extraction feature. Therefore it is usually the TPC experiment that is used when it is required to obtain the DOS of a particular material, although the analyses explained in the next few sections are generally applicable to TOF data also. It should also be borne in mind that the following techniques assume a multiple trapping transport model.

4.3.1 From TPC i(t) data

The TROK model shows in a simple way the relation between the transient photocurrent decay i(t) and the density of states at the thermalisation energy $g(\varepsilon_d)$ *i.e.* $g(\varepsilon_d) \propto (i(t).t)^{-1}$ where $\varepsilon_d = k_B T \ln(\upsilon t)$ (see, for example, Marshall, 1989). As was stated in § 4.2.6 an exponential density of states yields a transient current consisting of two power law decays, the transition occurring at the recombination time τ_r, after which the current decays more rapidly. The above method will work in this case because the peak of the carrier density is at the thermalisation energy at all times during the decay, and it is thus these states which control the current. However, if the DOS consists of an exponential with a bump of states at a deeper energy it can be demonstrated that the above method of extracting the DOS will not work. In this case the peak in the carrier density (which the TROK model assumes is at ε_d) will shift from ε_d in the exponential, to the bump in the DOS. The thermalisation energy will thus be shallower than the peak

in the carrier density, *i.e.* states in the bump are controlling the current, not those at ε_d. So it can be seen that a structured DOS will cause this "single time-point" DOS retrieval method to fail. The TROK method is a single time-point method because it attempts to calculate a $g(\varepsilon)$ point from a single i(t) point. The above example shows that single time-point methods do not work if the DOS has considerable structure because they ignore the effect of other states on the current decay. Marshall and Main showed this to be the case in a DOS consisting of three discrete levels (Marshall and Main, 1983). Using the above method they calculated the DOS from a simulated current decay: the reconstructed DOS gave incorrect values for the density of the trapping levels and placed them at the wrong energies. The reason for these errors is the TROK model assumption that the thermalisation energy is at ε_d.

The realisation that the TROK model will not give reliable results if the material studied has a structured density of states led some workers to develop so-called "multi time-point" methods for DOS retrieval. In these analyses more than a single i(t) point is used to calculate a single $g(\varepsilon)$ point, and thus the effect of states at more than one energy in the DOS should be accounted for in the reconstructed DOS. Among these methods are those developed by Michiel, Marshall and Adriaenssens (1983) and Michiel and Adriaenssens (1985). We will not discuss these methods here, suffice to say that they work well but are complicated and at the time they were developed suffered from being computationally intensive. Since the development of these methods simpler DOS retrieval techniques have become available (as will be discussed in § 4.3.3), and thus the above methods have not gained popularity with the advent of more powerful, cheap computers.

A further multi time-point method is that of Marshall, Berkin and Main which uses TOF data TO probe the DOS (Marshall, Berkin and Main, 1987). The method works by measuring the drift mobility at a variety of temperatures at a fixed field. The mobility activation energy can then be obtained which identifies the depth of the traps controlling the mobility at that field. If the field is now varied the dependence of the mobility activation energy on field, $\Delta\varepsilon_\mu(E)$ can be determined. The density of states is proportional to $[d\Delta\varepsilon_\mu(E)/dE]^{-1}$. This method works well but is experimentally time consuming as many TOF decays are needed to obtain $\Delta\varepsilon_\mu$ at a particular field, and the activation energies at a variety of fields are required to form an overall picture of the energy dependence of the DOS.

4.3.2 From MPC $\phi(\omega)$ data

The modulated photoconductivity (MPC) experiment is equivalent to a TPC experiment in the frequency domain and can provide complementary data to TPC, however the main utility of MPC in this context is that a single MPC data point $(I_\omega,\phi_\omega,\omega)$ does give a correct DOS point, *i.e.* the single point method works for MPC.

In the MPC experiment the specimen, which may be in coplanar or sandwich configuration, is illuminated with light of an appropriate wavelength, the intensity of which is modulated with a sine wave. The generation rate can therefore be represented as a steady state term G_{ss} and an alternating component of angular frequency ω and amplitude G_ω (fig.4.14). The response to sinusoidal excitation is a sinusoidal photocurrent which is phase shifted by a frequency dependent angle $\phi_\omega(\omega)$ with respect to the generation and has a complex amplitude $I_\omega(\omega)$ which is also a function of frequency. In a typical MPC experiment the complex photocurrent spectrum $(I_\omega,\phi_\omega,\omega)$ is measured with a lock-in amplifier over a range of frequencies (typically 1-10^5 Hz).

A full analysis of the solution to the multiple trapping equations in the frequency domain is not appropriate here, more information may be found in the papers by Oheda and Brüggemann *et al.*(Oheda, 1981; Brüggemann *et al.*, 1990).

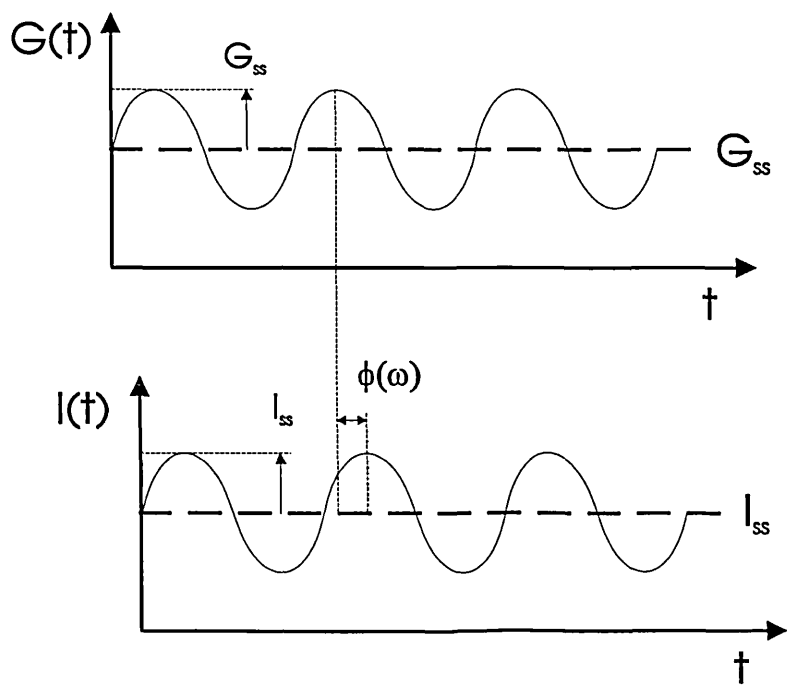

Fig. 4.14 Generation rate and resulting photocurrent in the MPC experiment.

The important result is that solution of the said equations leads to a full analytical solution and a similar expression to that obtained in the TROK model is obtained which can be expressed in the frequency domain as

$$\varepsilon_{\omega} = k_B T \ln(\upsilon / \omega) \tag{4.39}$$

However in this case the definition for ε_{ω} is obtained without making any assumption about the shape of the DOS. With some approximations the working equation for determining the DOS from the experimental data is

$$g(\varepsilon_w) = \frac{2}{\pi k T C_n}\left\{\frac{G_{\omega} e \mu_0 EA}{I_{\omega}} \sin\phi - \omega\right\} \tag{4.40}$$

where A is the conduction cross-section (coplanar geometry), μ_0 is the free carrier mobility and φ is the phase shift (Brüggemann *et al.*, 1990).

4.3.3 TPC-MPC Fourier transform method

It would appear that the MPC experiment should provide a satisfactory method for DOS spectroscopy, however its use has been limited because the energy range that it can probe is limited; there are two reasons for this. The first is that due to the steady state generation rate G_{ss} the quasi-Fermi levels are split. This limits the energy range which can be probed because the MPC experiment cannot "see" states below ε_{fn} (or ε_{fp}). This is not the case in a TPC experiment, which does not lead to splitting of the quasi-Fermi levels and can therefore probe states down to the Fermi level. The second reason is experimental and is associated primarily with electromagnetic coupling which constrains the upper frequency limit (and thus energy range) that can be covered. In MPC frequencies of ~1-10^5 Hz can be probed which corresponds to the time range ~1.6μs-0.16s; in TPC the accessible time range is considerably better at ~ 10^{-9}-10s (at 300 K this corresponds to TPC having about twice the energy range of MPC (using υ = 10^{12} s^{-1})).

Thus it would appear that some means of combining the TPC experiment and MPC analysis would lead to a solution of the above problems. This issue has been addressed by workers at the University of Abertay Dundee, and a coupling of the TPC and MPC experiments using a Fourier transform (FT) method has been successfully developed (Main *et al.*, 1992). The FT method converts time-domain TPC i(t) data into frequency-domain $I(\omega)$, $\phi(\omega)$ data via a numerical discrete Fourier transform. The density of states can then be obtained from an MPC analysis of the data. The TPC-MPC transform method is thus a multi point method. A detailed description of the Fourier transform method is given by Webb (Webb, 1994). The strengths of the technique have been well tested using computer simulated and experimental data (Main *et al.*, 1993) and is found to be accurate, and applicable to anomalous or conventionally dispersive transport. It is also valid in the pre- or post-recombination (transit) regions of the decay.

The FT method is generally applicable to amorphous semiconductors, however several circumstances can distort the computation of the transform. The most serious of these is a possible lack of short time TPC data which, if missing from the summation in the numerical integration in the transform can lead to a significantly incorrect DOS (see Webb, 1994)). It should also be remembered that the Fourier transform is only valid if the system response is linear. The FT method will be used on experimental results in this work and its applicability to materials which transport charge by mechanisms other than multiple trapping will be assessed.

4.4 Charge transport in organic materials

As was discussed in § 2.2.3, the introduction of disorder to a molecular crystal can cause the entire band to become localised. Due to this the description of extended state conduction given in § 4.1.1 is likely to be inappropriate for organic materials. (A possible exception to this is the conjugated polymers which have wide bands (trans-PA, B~10eV) and may be subject to localisation of states in the band tails only).

Charge transport in organic solids is generally believed to occur through localised states by thermally activated processes *i.e.* by hopping, and this assumption is supported by the very low conductivities and mobilities reported for materials of this type. Charge transport characterisation studies on organic materials have been carried out almost exclusively using the TOF technique to determine the temperature and field dependence of the drift mobility, and a recurrent pattern of features has been recovered on a diverse range of materials. For example similar behaviour has been observed in the broad class of molecularly doped polymers (Schein, Glatz and Scott, 1990; Borsenberger, 1990; Peled and Schein, 1988), main chain polymers such as poly(silanes) (Abkowitz and Stolka, 1988) or poly(phenylenevinylenes) (Gailberger and Bässler, 1991) and polymers with active side groups such as poly(vinylcarbazole) (Gill, 1972).

The typical recurrent features of transport in these materials include the following: (i) an activated behaviour of the carrier mobility, the activation energy from Arrenhius' equation being in the range ~ 0.4-0.6 eV; (ii) a field dependence of the mobility resembling the Poole-Frenkel law, *i.e.* $\ln \mu \propto \beta E^{1/2}$ over certain field ranges; (iii) a deviation of the magnitude of β and its temperature dependence from that predicted by the Poole-Frenkel theory; (iv) a sign reversal of β above a certain temperature, *e.g.* ~ 408 K in poly(methylphenylsilylene) and ~ 294 K in poly(di-n-butylgermylene) (Abkowitz, Bässler and Stolka, 1991); (v) non Poole-Frenkel field dependence at low fields; (vi) TOF tails which are broader than those expected from solely conventional (thermal) diffusion; (vii) a transition to dispersive transport at low temperatures.

The recurrence of the above features in different materials suggests that these are *intrinsic* material properties rather than impurity related as it is hard to see how such chemically diverse systems could contain approximately the same density of traps

having a similar depth relative to the transport states, and also account for the fact that they must be charged when empty to conform to Poole-Frenkel behaviour.

In the next section we will discuss some of the basic concepts of hopping transport and examine some of the phenomenological models put forward to explain the dependence of the mobility on temperature, field and site separation; we will then describe in more detail two transport models developed to explain the pattern of features described above.

4.4.1 Hopping in organic solids

The observed magnitude of the mobilities in organic solids such as molecularly doped polymers and single component organic glasses are typically in the range 10^{-4}-10^{-9} $cm^2\ V^{-1}\ s^{-1}$ which is much too small for band transport. For comparison the mobility in crystalline organics is expected to be ~ 1 $cm^2\ V^{-1}\ s^{-1}$ whereas in crystalline inorganic semiconductors or metals μ is in the range ~ 10 - 10^3 $cm^2\ V^{-1}\ s^{-1}$. For hopping transport the magnitude of the mobility is determined by the hop rate between molecules, which itself is a function of the average intermolecular separation, a, the temperature, T and the applied field, E. The majority of the work discussed subsequently has been carried out on MDPs because in these materials the intermolecular separation is controllable. In the simplest case of isoenergetic hopping sites at zero applied field the mobility can be written as

$$\mu = \mu_0 a^2 \exp[-2\alpha_{loc} a] \tag{4.41}$$

where $\exp[-2\alpha_{loc}a]$ represents the wavefunction overlap, α_{loc} is the inverse wavefunction decay length and $\mu_0 = e\upsilon_0/6k_BT$, υ_0 being the attempt to escape frequency. Thus f_1 and μ should depend solely on intersite separation if α_{loc} is the same for all molecules, μ_0 is independent of field and intersite separation and only weakly temperature dependent. However, it has also been shown that α_{loc} can be temperature dependent (Pfister, 1977).

If we now allow the molecules to have a distribution of energies *i.e.* we introduce diagonal disorder, then for some hops the carrier must gain an amount of energy $\Delta\varepsilon_\sigma$, which is equal to the energy difference of the initial and final sites. The

hopping probability is then proportional to the Boltzmann factor $\exp(-\Delta\varepsilon_\sigma/k_BT)$, where $\Delta\varepsilon_\sigma$ is the activation energy. In many organic solids it is found that the activation energy is not constant but depends on the intermolecular separation (Pfister, 1977), and some authors have suggested a T^{-2} dependence for the mobility, rather than the familiar Arrhenius form, 1/T (see § 4.4.2). Thus the expression for the mobility can now be written as

$$\mu = \mu_0 a^2 \exp[-2\alpha_{loc} a]\exp[-\Delta\varepsilon_\sigma / k_B T] \tag{4.42}$$

The final variable we have to consider is the applied field and its effect on the hopping mobility. It is well known that the application of an external field shifts energy levels into closer coincidence by an amount eEa, thus an applied field will lower the activation energy by an amount

$$\Delta\varepsilon_\sigma = \Delta\varepsilon_0 - eEa \tag{4.43}$$

where $\Delta\varepsilon_0$ is the zero-field activation energy. Thus the field dependence of the mobility should be given by

$$\mu \propto \exp(-eEa / k_B T) \tag{4.44}$$

Bässler suggested a similar field dependence on the basis of Monte Carlo simulations and used it to fit data taken by other authors (Bässler, 1984), more recent simulation work however, has shown that an $E^{1/2}$ dependence is a more accurate fit to the data (see for example Bässler, 1993).

The hopping rate in the reverse direction with respect to the field can be taken into account by subtracting it from the hopping rate in the forward direction, and leads to the following result

$$\mu \propto \{\exp(eEa / 2k_B T) - \exp[-(eEa / 2k_B T)]\} / E \tag{4.45}$$

or

$$\mu \propto [\sinh(eEa / 2k_B T)] / E \tag{4.46}$$

This type of field dependence has been suggested by Bagley (Bagley, 1970) and is also expected to describe the field dependence of small polaron hopping (Emin, 1973). Facci and Stolka have dealt with the case of an asymmetric barrier to hopping in forward and reverse directions by introducing a parameter α' with a value between 0 and 1 (Facci and Stolka, 1986), giving

$$\mu \propto \{\exp(\alpha' eEa / 2k_B T) - \exp[-(1-\alpha')eEa / 2k_B T]\} / E \tag{4.47}$$

More recent work on the field dependence of the mobility in MDPs has shown that the only function that adequately describes the experimental data is $\ln \mu \propto E^{1/2}$ (Schein *et al.*, 1989). If a potential energy with a r^{-n} dependence (where r is the distance from the centre, and n is a integer) is employed instead of the square well potential that is implicitly assumed in the above equations, it can be shown that the field dependence of the mobility becomes $E^{n/n+1}$, thus for n = 1, as in a Coulomb potential, the field dependence is $E^{1/2}$ (Schein *et al.*, 1989).

There have been numerous observation of this type of field dependence in the literature, the first of which was that of Gill, taken on trinitrofluorenone-poly(vinylcarbazole), PVK-TNF (Gill, 1972), other authors have also used this function to fit data (Pfister, 1977; Santos Lemus and Hirsch, 1986; Abkowitz *et al.*, 1987; Schein *et al.*, 1986). It is experimentally found that the field dependence of the mobility is itself dependent on temperature and therefore also dependent on the intersite separation. Thus we can now write our general equation for the mobility as

$$\mu = \mu_0 a^2 \exp[-2\alpha_{loc} a]\exp[-\Delta\varepsilon_\sigma / k_B T]\exp[-eEa / k_B T] \tag{4.48}$$

It can be seen from the equation above that the dependence of the mobility on the variables a, T and E is not simple and further that the effects of the variables are interconnected (Mack *et al.*, 1989).

Several empirical equations have been developed to describe experimentally obtained hole mobility data, the first of these was due to Gill

$$\mu = \mu_1 \exp\left[-\frac{(\Delta\varepsilon_0 - \beta E^{1/2})}{k_B T_{eff}}\right] \tag{4.49}$$

where β is a constant, $T_{eff} = 1/T - 1/T_1$ (and $\mu = \mu_1$ when $T = T_1$) and $\Delta\varepsilon_0$ is the zero field activation energy (Gill, 1972). T_1 is the temperature at which the field dependence of the mobility vanishes, *i.e.* where ln μ vs. $E^{1/2}$ curves intercept. The $E^{1/2}$ field dependence of the above equation was initially taken as evidence for the Poole-Frenkel mechanism of barrier lowering, indeed experimentally derived values of β fit very well with the value expected by the Poole-Frenkel theory. This has since been disregarded as an explanation because the PF mechanism necessitates the existence of charged trapping states at each hopping centre which has never been observed in materials such as MDPs. A further problem is that the distance to the peak of the potential, r_p after barrier lowering is predicted by the PF theory to be about an order of magnitude larger than the average intersite separation, and thus the carrier will not be free of the coulomb potential after a single hop.

A final and important problem with eq. 4.49 is the T_1 parameter, where the field dependence of the mobility vanishes. There have been few suggestions in the literature as to the physical meaning of this term and such a parameter is not predicted by any hopping theory. It should also be noted that at temperatures above T_1 the mobility is predicted to decrease with increasing field, contrary to the prediction of an increased field bringing energy levels into closer coincidence. Some worker suggested that T_1 is associated with the glass transition temperature (Fujino *et al.*, 1984). However it has been shown that the temperature dependencies of T_g and T_1 are dissimilar, which suggests that T_1 is not associated with rheological properties (Schein, 1990). Hirsch suggested that the existence of T_1 is caused by a temperature dependent dielectric constant, Schein has also shown that this is inconsistent with experimental data. A decrease of mobility with field was first observed experimentally in the pyrazoline compound DEASP in polycarbonate by Peled and Schein (1988). They observed that T_1 decreases with increasing intermolecular separation whereas T_g increases, and thus found it possible to produce samples where $T_g > T_1$ at low concentrations of DEASP. In the temperature range where $T_g > T > T_1$ they found that the mobility decreased with increasing field as predicted by Gill's equation.

Other phenomenological equations have been suggested by Pfister, and Schein and Mack, however these are in general just convenient variations on Gill's equation and do not lead to any greater physical insight of the hopping mechanism, in particular neither explain the origin of the T_1 parameter (Pfister, 1977; Schein and Mack, 1988).

The need for a hopping model that can describe the experimental data and relate the observed parameters to physical aspects of the studied material has led to the development of two main theories for MDPs: the disorder limited hopping model and the polaron model, which will now be discussed.

4.4.2 Disorder-limited hopping

This model has been developed by the Marburg group of Bässler *et al.* and assumes that the disorder inherent in experimental samples is responsible for the recurrent pattern of features mentioned in § 4.4, in particular the activation energy of the mobility. The disorder limited hopping (DLH) scenario uses as its basis the model of Silinsh discussed in § 2.2.3 which predicts that the introduction of disorder to molecular crystals leads to localisation of the whole band. Transport then proceeds by hopping between the constituent sites in the resulting gaussian DOS.

A key parameter of the DLH model is the width of the DOS, σ_g. Recent work has shown that the value of σ_g is influenced by the dipole moment of the transport molecule. These so-called dipolar disorder models are based on the argument that a random distribution of permanent dipoles generates fluctuations in electrostatic potential that add to local variations resulting from van der Waals interactions. The total width of the DOS may then be considered to be determined by a dipolar component and a van der Waals component (Borsenberger and Bässler, 1991; Young, 1995). The main predictions of the dipolar disorder models are that the dipolar component increases with increasing dipole moment and concentration of the polar species (Borsenberger *et al.*, 1996).

Evidence for a gaussian DOS comes from the inhomogeneously broadened absorption profiles of disordered, vapour-deposited polyacenes such as tetracene and pentacene (Jankowiak, Rockwitz and Bässler, 1983). In the disordered state the k-selection rule for optical transitions is relaxed and thus optical absorption maps the (exciton) density of states. In disordered tetracene and pentacene the absorption profiles for the lowest excited singlet states are gaussian and the inhomogeneous broadening of these profiles compared to those in the respective crystals reflects the positional disorder in the neighbourhood of an excited molecule. Although optical absorption only probes the distribution of exciton states the states for charge carriers must have a similar DOS

because the van der Waals energies of Frenkel excitons and charge carriers have a similar physical origin.

The predictions of the disorder limited hopping (DLH) model have been determined almost entirely by computer simulation which will be discussed in § 5.1, although some analytical work has been done using the effective medium approach (EMA), which for finite temperature describes very well the hopping process in organic solids (Grünewald *et al.*, 1984; Movaghar *et al.*, 1986).

The hopping rate of a carrier in this model is of the Miller-Abrahams type and is activated for hops up in energy ($\varepsilon_j > \varepsilon_i$) and constant for hops down in energy ($\varepsilon_j < \varepsilon_i$)

$$\upsilon_{ij} = \upsilon_0 \exp\left(-2\alpha_{loc} a \frac{R_{ij}}{a}\right) \exp\left(\frac{\varepsilon_j - \varepsilon_i}{k_B T}\right) \qquad \text{for } \varepsilon_j > \varepsilon_i \qquad (4.50)$$

$$\upsilon_{ij} = \upsilon_0 \exp\left(-2\alpha_{loc} a \frac{R_{ij}}{a}\right) \qquad \text{for } \varepsilon_j < \varepsilon_i \qquad (4.51)$$

where a is the average intersite distance and υ_0 is the attempt to escape frequency. In the case of an applied field the site energies include the electrostatic energy term eEΔx where Δx is the site separation in the field direction.

A carrier introduced at an arbitrary energy within a gaussian DOS will execute a random walk according to the above hopping rates and will relax into the tail of the gaussian. Hopping relaxation in an exponential DOS has been shown to lead to dispersive transport on a macroscopic time scale (Silver, Schönherr and Bässler, 1982), however relaxation in a gaussian DOS ceases after a temperature-dependent time interval at an energy $\langle\varepsilon\rangle$, indicating the attainment of dynamic equilibrium. This is due to the more rapid dilution of the state density with energy in the tail of the gaussian distribution. The equilibration energy $\langle\varepsilon_\infty\rangle$ of a carrier at zero electric field can be calculated analytically using EMA (Ries *et al.*, 1988) and is given by

$$\langle\varepsilon_\infty\rangle = \lim_{t\to\infty} \langle\varepsilon(t)\rangle = \frac{\int_{-\infty}^{+\infty} \rho(\varepsilon)\varepsilon \exp(-\varepsilon / k_B T) d\varepsilon}{\int_{-\infty}^{+\infty} \rho(\varepsilon) \exp(-\varepsilon / k_B T) d\varepsilon} = -\frac{\sigma_g^{\,2}}{kT} = -\sigma_g \hat{\sigma} \qquad (4.52)$$

where $\rho(\varepsilon)$ characterises the DOS, σ_g is the width of the gaussian distribution and $\hat{\sigma} = \sigma_g/k_BT$. Note that $\langle\varepsilon_\infty\rangle$ is independent of the presence of off-diagonal disorder. Relaxation of a non-interacting packet of carriers in a gaussian DOS has been simulated by Pautmeier, Richert and Bässler and it was found that in the long-time limit $\langle\varepsilon_\infty\rangle = -\sigma_g \hat{\sigma}$ and the shape of the occupational DOS (DOS^{occ}) becomes gaussian and acquires a width σ_g (*i.e.* the same as the DOS) indicating that dynamic equilibrium has been established (Pautmeier, Richert and Bässler, 1989).

Fig. 4.15 shows a Monte Carlo simulation of the time dependence of the average carrier energy parametric in temperature. It can be seen that $\langle\varepsilon(t)\rangle$ relaxes approximately logarithmically with time as predicted by the EMA result (Ries *et al.*, 1988). As the temperature is lowered relaxation is slowed down, and as $T\rightarrow 0$ the carriers may become "frozen in" as thermally activated hops which allow the carriers access to additional sites for relaxation are eliminated.

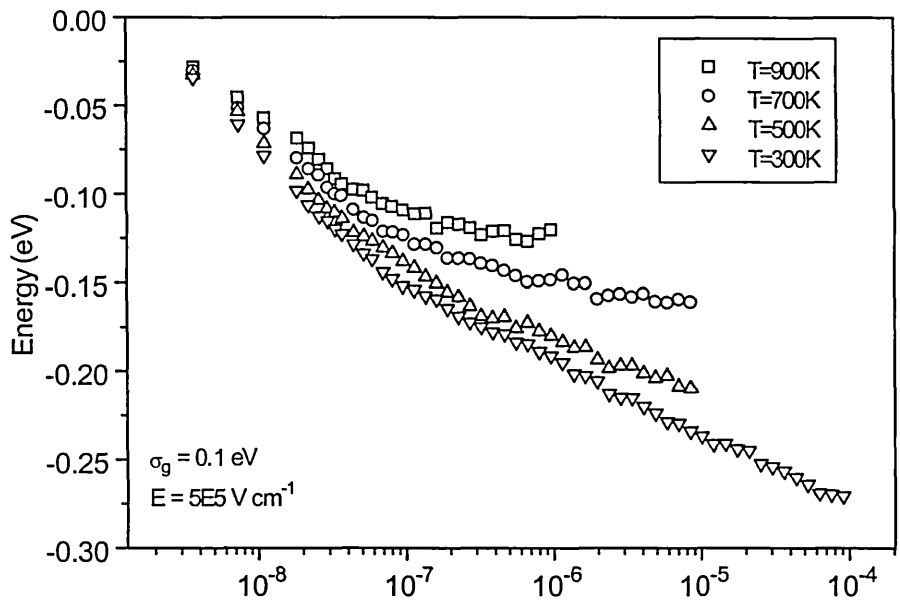

Fig. 4.15 MC simulation of the relaxation of the mean carrier energy in a gaussian DOS.

The DLH model predicts a non-Arrhenius-type temperature dependence of the carrier mobility. This can be demonstrated if we consider a material in which carriers have relaxed to $\langle\varepsilon_\infty\rangle$. If the gaussian width is 0.1 eV at 295 K ($\hat{\sigma} = 4$) which is typical for many materials, the fractional DOS for $\varepsilon < \langle\varepsilon_\infty\rangle$ is

$$\int_{-\infty}^{-4\sigma_g} \rho(\varepsilon)d\varepsilon \approx 3\times 10^{-5} \tag{4.53}$$

thus a carrier located at $\varepsilon = \langle\varepsilon_\infty\rangle$ can on average only continue its motion after thermal excitation higher into the DOS. If we assume that all the carriers are located at $\langle\varepsilon_\infty\rangle$ and the transport energy is located at the centre of the gaussian ($\varepsilon = 0$) the activation energy will be $\sigma_g \hat{\sigma}$ and the temperature dependence of the mobility should be

$$\mu(T) = \mu_0 \exp\left(-\left(\frac{\hat{\sigma}\sigma_g}{k_B T}\right)\right) \tag{4.54}$$

or

$$\mu(T) = \mu_0 \exp\left(-\left(\frac{\sigma_g}{k_B T}\right)^2\right) \tag{4.55}$$

Monte Carlo and EMA studies show that the above non-Arrhenius behaviour is correct, the working equation differing from above by a factor of 2/3 in the exponent

$$\mu(T) = \mu_0 \exp\left(-\left(\frac{2}{3}\hat{\sigma}\right)^2\right) \tag{4.56}$$

The exponent accounts for the statistics of both the occupational energies and the barrier heights. Thus in the zero field limit plotting ln μ vs T^{-2} should yield a straight line of slope $2\sigma_g/3k_B$ from which the gaussian width of the DOS can be obtained (in some cases $2\sigma_g/3k_B$ is written as T_0 *i.e.* the gaussian width in temperature units). Experimental data plotted vs. T^{-2} is generally found to give a better fit than if plotted in the conventional Arrhenius manner, however the better fit is sometimes difficult to justify when the temperature range covered becomes small. The application of equation 4.56 to experimental data is further justified by the magnitude obtained for the mobility pre-factor. Plotting the data against T^{-1} yields μ_0 values which are too large for non-

crystalline molecular solids, of the order of 10 $cm^2\ V^{-1}\ s^{-1}$, whereas plotting against T^{-2} yields values between 10^{-2} - $10^{-1}\ cm^2\ V^{-1}\ s^{-1}$ which are more realistic for such materials.

Equation 4.56 implies thermally activated transport, the activation energy being given by

$$\Delta\varepsilon_{\sigma} = \frac{4}{9}\frac{\sigma_g^{\ 2}}{k_B T} \tag{4.57}$$

Note that the apparent activation energy is temperature dependent and if derived from a Arrhenius plot is twice $\Delta\varepsilon_{\sigma}$. Combining the energy of the centre of the occupational density of states $\langle\varepsilon_{\infty}\rangle$ and the above activation energy implies the existence of a "transport energy" at

$$\varepsilon_t = \frac{4}{9}\frac{\sigma_g^{\ 2}}{k_B T} - \frac{\sigma_g^{\ 2}}{k_B T} \tag{4.58}$$

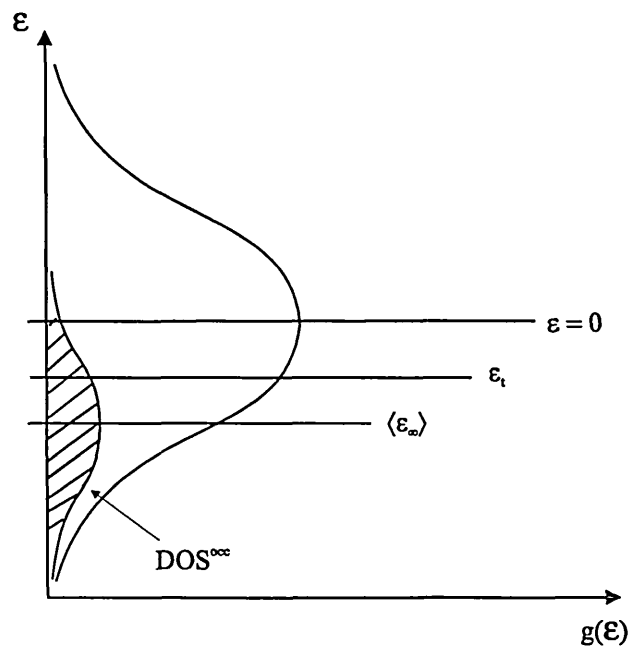

Fig. 4.16 Occupational density of states (DOS^{occ}) for carriers hopping in a gaussian DOS after dynamic equilibrium has been obtained, also shown is the predicted transport energy.

with respect to the centre of the gaussian DOS *i.e.* $\varepsilon = 0$ (fig. 4.16).

The validity of the transport energy concept in an exponential DOS has been demonstrated by Monroe who showed that the transport energy ε_t is given by

$$\varepsilon_t = -3k_B T_0 \ln \frac{3k_B T_0 (4\pi/3)^{1/3}}{2\alpha_{loc} akT} \tag{4.59}$$

The transport energy is the mean energy of the sites to which a carrier hops with maximum rate. Note that ε_t depends on temperature and overlap (Monroe, 1985).

Hartenstein and Bässler have investigated the concept of a transport energy in a gaussian DOS (Hartenstein and Bässler, 1995). Using Monte Carlo simulations they determined the energy of the sites most frequently visited by the hopping carriers and found that the apparent transport energy decreases with temperature. This is in agreement with equation 4.59 and Monroe's reasoning that the carriers will optimise their hop rates through a trade-off between activated and long distance jumps. However more detailed analysis of the results led the authors to conclude that neither the activation energy nor the computed values of ε_t reflected the exact energy level to which carriers are raised to continue their motion. The evidence for this was provided by simulations which showed that ε_t was virtually independent of intersite coupling, rather than inversely proportional to it as predicted by equation 4.59. The authors went on to suggest that the inconsistencies were due to oscillation of carriers between nearest neighbour sites at ε_∞ in the case where one of the sites lies lower in energy than the others, thus making the rate for this hop far greater than that for excitation to ε_t. This oscillation affects the carrier transit time and thus the mobility, and since all hops contribute to the temperature dependence of transport the ensemble averaged activation energy will be lower than the energy needed by a carrier to execute a "transport" jump and it must decrease with decreasing temperature because oscillatory motions gain importance.

Thus the decrease of ε_t upon lowering the temperature is not a reflection of the mean jump distance as implied by the concept of variable range hopping but of the growing importance of oscillatory motions of a carrier. A related situation was noted by Marshall, however in this case the carrier oscillates because two sites are very close

together spatially, thus in this case the greatly increased transition rate is due to the overlap term in eq. 4.50 (Marshall, 1979).

Monte Carlo simulations of the DLH model have shown that the Poole-Frenkel-like field dependence observed in organic materials *i.e.* $\ln \mu \propto \beta E^{1/2}$ is simply a consequence of the hopping motion of carriers in a gaussian DOS, albeit within a certain field range. At low fields the simulated mobility is found to be effectively independent of field, however at higher fields the mobility assumes the $\beta E^{1/2}$ form. The value of β decreases with increasing temperature (decreasing disorder) and changes sign above a certain temperature, thus the DLH theory accounts for the T_1 parameter where the field dependence of the mobility disappears (see § 4.4.1). The decrease of μ with E at vanishing disorder (high T) shows that the drift velocity has saturated because hopping in an isoenergetic hopping system is not affected by the field strength. This yields a mobility with a E^{-1} field dependence. Further evidence for the $\mu(E)$ behaviour resulting from hopping motion is the analytical theory developed by Movaghar *et al.* who showed that the field dependence in pure hopping systems follows a $\ln \mu \propto \beta E^n$ law with $0 < n < 0.5$, the exact value of n being determined by the shape of the DOS (Movaghar *et al.*, 1990).

The effect of off-diagonal disorder on the $\mu(E)$ relation described above has also been investigated and is found to change the $\mu(E)$ pattern in a characteristic way (Pautmeier *et al.*, 1988; Pautmeier, Richert and Bässler, 1990, Borsenberger *et al.*, 1991). Increasing off-diagonal disorder, Σ in an isoenergetic hopping system (*i.e.* $\sigma_g = 0$, where $\ln \mu \propto E^{-1}$) enhances the magnitude of the mobility and causes it to decrease more rapidly with field. This has been ascribed to increased positional disorder opening up "fast" channels for carrier transport, which may involve jumps against the field. As the field is increased these detour routes are cut off, and therefore the mobility must decrease faster with field as compared to a system devoid of any disorder.

Simulations which involve both diagonal and off-diagonal disorder yield $\mu(E)$ relationships which qualitatively agree with experimental data. At low fields the experimental mobility consistently decreases with field at different temperatures, at higher fields the $\ln \mu \propto \beta E^{1/2}$ dependence is observed with β decreasing with increasing temperature and eventually changing sign (see, for example, the data of Borsenberger *et al.*, 1991). The decrease of the mobility at low fields can be ascribed to off-diagonal disorder opening up fast detour routes for charge carriers as described above, it is

effectively independent of temperature because it is not controlled by the energy distribution of hopping sites. At higher fields barrier lowering becomes important and competes with the field-induced quenching of detour routes a carrier may follow, causing the Poole-Frenkel like field dependence. Thus it is competition between diagonal and off-diagonal disorder which causes the disappearance of the mobility field dependence (and thus accounts for T_1).

Analysis of the slope parameter, β has led to the development of a universal law describing the dependence of the mobility (in the high field, $\ln \mu \propto \beta E^{1/2}$ region) on temperature (diagonal disorder), field and off-diagonal disorder,

$$\mu(\hat{\sigma},\Sigma,E) = \mu_0 \exp(-(\tfrac{2}{3}\hat{\sigma})^2)\begin{cases} \exp C(\hat{\sigma}^2 - \Sigma^2)E^{1/2}; \ldots\ldots \Sigma \geq 1.5 \\ \exp C(\hat{\sigma}^2 - 2.25)E^{1/2}; \ldots\ldots \Sigma < 1.5 \end{cases} \quad (4.60)$$

where $C = d\beta/d\hat{\sigma}^2 = 2.9 \times 10^{-4}$ $(cm/Vs)^{1/2}$ (Borsenberger, Pautmeier and Bässler, 1991). Thus experimental data obtained on the temperature and field dependence of the mobility can be analysed using eq. 4.60 to obtain information on the degree of diagonal and off-diagonal disorder present within an experimental sample.

A further success of the DLH model is in the explanation of the dispersive to non-dispersive transition (D $\rightarrow$ ND) which is seen to occur in many organic solids as the temperature is increased. Fig 4.17 shows simulated TOF decays at different temperatures. It can be seen that the signals become increasingly dispersive as the temperature is lowered. In this case the D $\rightarrow$ ND transition occurs if the carrier relaxation time is shorter than the carrier transit time t_{tr} across the sample. It was found that the relaxation time of hopping carriers increases more rapidly with $\hat{\sigma}$ than the carrier transit time and thus as the temperature is lowered there must occur a critical value of disorder at which transport becomes dispersive $\hat{\sigma}_c$. The critical disorder parameter was found by Pautmeier *et al.* to be given by the relationship

$$\hat{\sigma} = 1.22\left[\ln\left(\frac{6k_BTd}{ea^2E}\right)\right]^{1/2} \quad (4.61)$$

where d is the sample thickness and a is the average intersite separation (Pautmeier, Richert and Bässler, 1989). The concept of hopping in a gaussian DOS thus implies a ND → D transition when the temperature is raised above

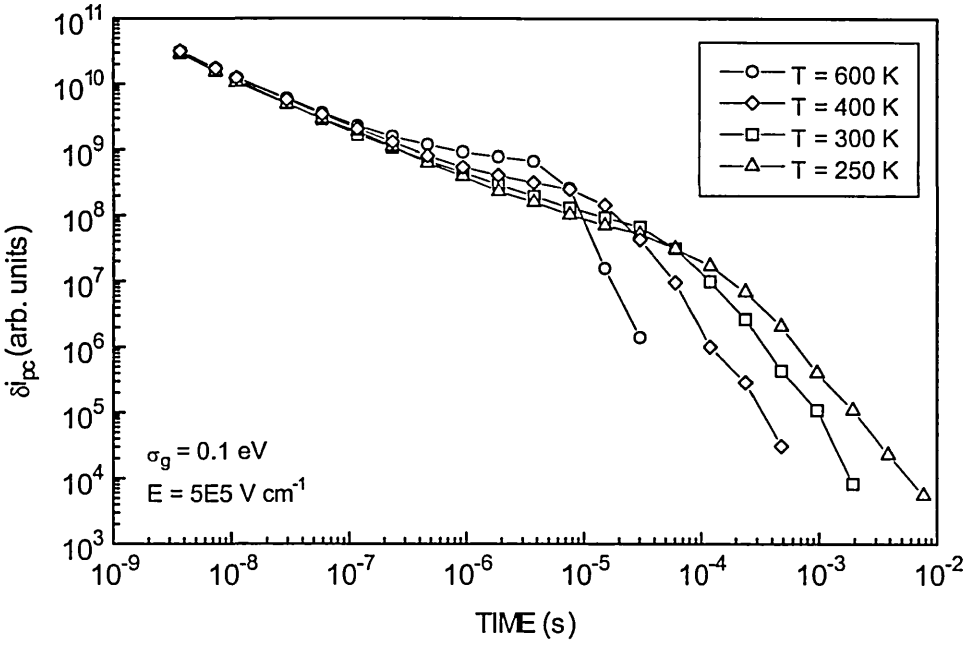

Fig. 4.17 Simulated TOF decays for hopping in a gaussian DOS, parametric in temperature.

$$T_c = \frac{\sigma_g}{4.4k_B} \tag{4.62}$$

The DLH model has also been applied to the problem found experimentally of anomalously broad tails in TOF signals (Yuh and Stolka, 1988). The spreading of the TOF signals can be accounted for by defining a diffusivity that consists of an ordinary thermal term D_0 and a field and disorder dependent contribution $D_f(\hat{\sigma}, E)$ (Pautmeier, Richert and Bässler, 1991).

Diffusive broadening of a sheet of charge carriers drifting under the action of a bias field follows Einstein's law relating diffusivity and mobility provided that the field is small, *i.e.* $eEa/2k_BT << 1$ and the system is homogeneous. In a homogeneous system the hopping rate will be a well defined quantity, however this assumption is violated in a diagonally (or off-diagonally) disordered medium. It was shown earlier that carriers hopping in a gaussian DOS settle in the long time limit to an energy σ_g^2 / k_BT below the

centre of the DOS, the variance of the occupational DOS being identical to the width of the DOS itself. The distribution of jump rates will vary throughout the DOS^{occ} being lower than average for carriers localised in the low energy tail of the distribution and higher than average for those in the high energy tail. It is this distribution of hop rates which, if subject to an applied field, causes the non-thermal spatial spreading of the carrier packet. A similar effect to this was observed by Rudenko and Arkhipov when analysing transport of carriers via a multiple trapping mechanism in a gaussian distribution of traps (Rudenko and Arkhipov, 1982).

A recent review of the main points of the DLH theory can be found in Bässler's 1993 paper (Bässler, 1993).

4.4.3 Small polaron hopping

We have already discussed the formation of polarons in § 3.1.1 for the case of conjugated polymers. However, polaron formation is not restricted to these materials (although polaron formation is favoured in low dimensional systems such as quasi-1-D polymers), nor is it restricted to polar materials (in which polarons were first discovered) from which polarons take their name.

Polarons have been suggested as being possible charge carriers in organic materials in keeping with the low intrinsic mobilities observed in such systems. In the band model the effects of electron-phonon interaction are expected to be minimal because the carrier's wavefunction is represented by a Bloch wave and is delocalised throughout the solid. Thus the carrier's charge can also be regarded as being smeared out over the entire solid and does not have a significant effect on the positions of the lattice atoms. If transport proceeds by hopping, however the mobility will be low and thus the effective mass high. Under these circumstances the carrier (as seen by nearby atoms) behaves like a point charge and due to its slow motion the effect on adjacent atoms can be significant, displacing them from their equilibrium positions (fig. 4.18). If the deformation of neighbouring atoms is sufficiently strong the carrier may become self-trapped *i.e.* it lies at the bottom of a potential well formed as a result of its presence. This coupled unit of the carrier and the concomitant distortion is known as a *polaron*. If the carrier is essentially confined to a single site it is referred to as a *small polaron*.

At low temperatures polarons can move between sites without thermal activation, and this corresponds to polaron band motion. However, as a result of the very narrow width of the polaron band (~10^{-4} - 10^{-5} eV) at all reasonable temperatures polarons can be considered as moving by hopping between neighbouring sites. Furthermore, in disordered materials the hopping regime is likely to be the only operative transport mechanism for polarons as the random fluctuations in site energy are likely to be much greater than the polaron bandwidth. These predictions on the nature and transport of polarons have mostly resulted from the work of Holstein and Emin using the molecular crystal model, which considers a single excess carrier placed in a ordered array of deformable molecules, *i.e.* a molecular crystal (Emin, 1973). It is not intended here to go into the details of polaron theory, but instead to quote the predicted effects of polaron formation on the mobility in organic solids. Further information on the details of polaron theory can be found in Mott and Davis and in Emin's review (Mott and Davis, 1979; Emin, 1973).

Hopping of polarons is activated because in order for the carrier to move it must also transfer the resulting distortion of the lattice. Fig. 4.19 shows a polaron formed on a diatomic molecule and the resulting distortion that must occur to allow the polaron to hop to its nearest neighbour. In this case the molecules are in an ordered 1-D array and are isoenergetic, therefore if the distortion of neighbouring molecules is similar so to will be their overall energies, and thus the polaron can transfer between sites. Note, however that polaron hopping is not restricted to ordered materials, but can also occur in disordered systems as long as energy levels coincide due to molecular vibration.

The rate at which energy coincidences occur can be given by

$$\left[\left(\frac{\omega}{2\pi}\right)\exp\left(\frac{-(\frac{1}{2}\varepsilon_p - J)}{k_B T}\right)\right] \tag{4.63}$$

where ω is a phonon frequency, ε_p the polaron binding energy and J the exchange integral. The polaron hopping frequency (and therefore mobility) is given by the product of the rate of energy coincidence between two neighbouring sites and the probability P, given an energy coincidence that the carrier will hop. The hopping probability is approximately given by

$$P = \left(\frac{J}{\hbar}\Delta t_c\right)^2 \tag{4.64}$$

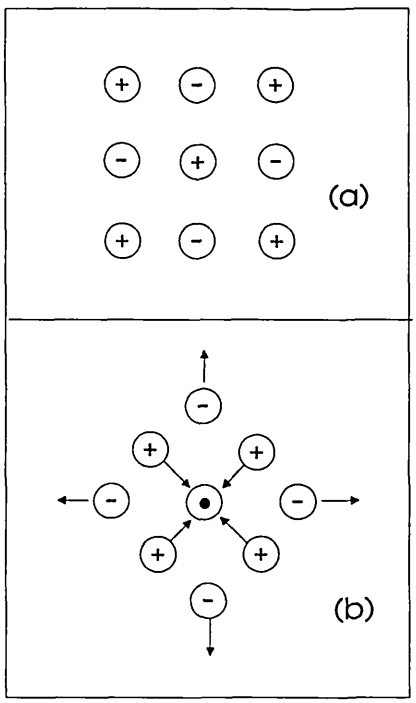

Fig. 4.18 Ionic lattice in the case of (a) no extrinsic charge carrier present, and (b) with an electron added to the central atom. The positive ions are attracted to the electron and the negative ions are repulsed. The resulting charge carrier and distortion produce a *small polaron*.

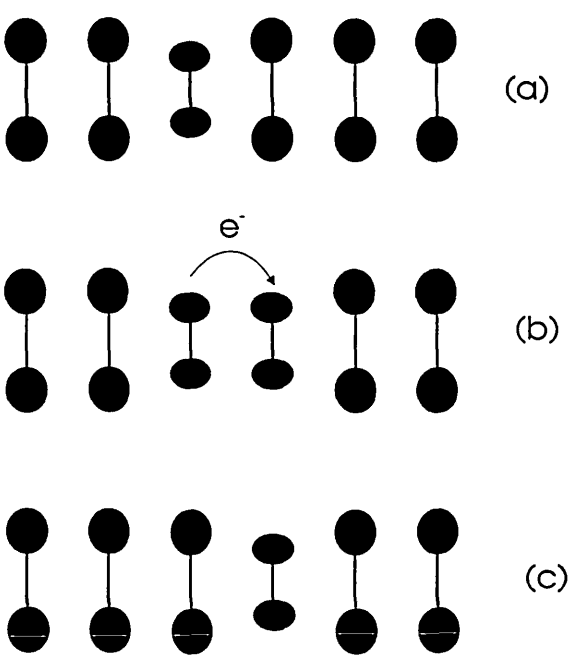

Fig. 4.19 (a) A molecular polaron on a diatomic molecule, (b) the excited state necessary for charge transfer, (c) molecular polaron on new site.

where Δt_c is the "duration" of a coincidence of energy levels. Thus we can write for the polaron hopping rate

$$\upsilon = P\left[\left(\frac{\omega}{2\pi}\right)\exp\left(\frac{-(\frac{1}{2}\varepsilon_p - J)}{k_B T}\right)\right] \tag{4.65}$$

This is the hopping rate in the limit of zero electric field and can be converted to a mobility using the Einstein relation

$$\mu = \left(\frac{ea^2}{k_B T}\right)P\left[\left(\frac{\omega}{2\pi}\right)\exp\left(-\frac{(\frac{1}{2}\varepsilon_p - J(a))}{k_B T}\right)\right] \tag{4.66}$$

where a is the intermolecular separation, note that J has been shown to be a explicit function of a.

Polaron theory predicts two regimes of behaviour for the mobility depending on the probability for charge transfer P. In the *adiabatic* regime the sites are in close proximity and P=1 by definition *i.e.* the mobility is determined entirely by the frequency of energy coincidences: when a coincidence occurs the carrier always hops. Due to the closeness of the hopping sites J is large and can affect the activation energy, as a increases so does the activation energy because J decreases with a. In the *non-adiabatic* regime the intermolecular separations are large (J is small) and thus $P < 1$, which means that in the event of an energy coincidence the carrier may not hop. This is due to the carrier adjusting too slowly to keep up with motion of the lattice. In this regime it is found that $P \propto J^2 \propto \exp(-2\alpha_{loc}a)$, and because J is small the activation energy is essentially constant ($\varepsilon_p/2$).

Polaron theory predicts a field dependence of the mobility of the form

$$\mu \propto \left[\sinh(eEa / 2k_B T)\right] / E \tag{4.67}$$

This has been shown by Schein *et al.* to be inconsistent with experimental mobility data which consistently exhibit an exp ($E^{1/2}$) dependence (Schein *et al.*, 1989).

Schein *et al.* have applied the above ideas to experimental data taken on a range of molecularly doped polymers in the zero field limit (Schein *et al.*, 1990). They write for the mobility

$$\mu = \mu_0 a^2 \exp[-2\alpha_{loc} a] \exp\left[-\Delta\varepsilon_\sigma(a) / k_B T\right] \tag{4.68}$$

where $\exp[-2\alpha_{loc}a]$ is the electron transfer integral, and $\Delta\varepsilon_\sigma(a)$ is the activation energy. At fixed intermolecular spacing, $\Delta\varepsilon_\sigma(a)$ is determined by extrapolating mobility data $\mu(T,E)$, to zero electric field and plotting $\ln \mu(E = 0)$ vs. T^{-1}. The term $\mu_0 \exp\left[-2\alpha_{loc}a\right]$ for each value of intermolecular spacing is then determined by plotting $\ln[(\mu/a^2)\exp(\Delta\varepsilon_\sigma/k_B T)]$ versus a. This technique allows the dependence of $\Delta\varepsilon_\sigma$ on a to be separated from the dependence of $\exp\left[-2\alpha_{loc}a\right]$ on a. The above authors found that for some MDPs $\Delta\varepsilon_\sigma$ was constant with a, whereas the overlap term could be described by $\exp(-2\alpha_{loc}a)$ *e.g.*, DEH:poly(carbonate). However, for others they found that $\Delta\varepsilon_\sigma$ was strongly dependent on a, whereas $\exp\left[-2\alpha_{loc}a\right]$ was independent of a *e.g.*, TPD:poly(carbonate) (Schein and Mack, 1988). This behaviour was ascribed to small polaron hopping in different regimes. In DEH:poly(carbonate) the carriers move by non-adiabatic hopping, in this regime the overlap is small (J is small) and thus the activation energy is approximately constant (see eq. 4.66), here the overlap is given by $\exp(-2\alpha_{loc}a)$. The TPD:poly(carbonate) data suggest adiabatic hopping, where given an energy coincidence the carrier always hops, consequently the overlap does not depend on a. Adiabatic hopping occurs when the overlap is strong, and J may be large enough to affect the activation energy, thus as the intermolecular spacing increases (J decreases) the activation energy should increase, eventually reaching $\varepsilon_p/2$. The reason that adiabatic hopping is observed in TPD and not in DEH was attributed to the greater physical size of the TPD molecule, the highest intersite separation studied was of the order of the length of the TPD molecule and it was argued that there would still be significant overlap between the molecules at these concentrations. Likewise the small physical size of the DEH molecule meant that the overlap was not large enough to observe the adiabatic regime.

In a later paper Schein, Glatz and Scott (1990) used eq. 4.68 to interpret their data on tri-p-tolylamine (TTA). They observed that the activation energy at first increased as the intersite separation increased and then levelled out at a constant value ($\varepsilon_p/2$). The overlap function $\exp[-2\alpha_{loc}a]$ was found to behave in an opposite manner. They attributed these observations to a transition from adiabatic to non-adiabatic small polaron hopping.

Thus the polaron theory relates the intermolecular separation and the temperature dependence of the mobility in MDPs to the material parameters $\varepsilon_p/2$ and J. However it is found that the values for the parameters J and the pre-factor obtained from experimental data are often larger than those predicted by the original polaron theory. It has been suggested that the reason for this is that the original one optical phonon, one dimensional theory needs to be extended into a three dimensional, multiple phonon model also incorporating the effects of disorder to truly be applicable to MDPs. A second major downfall of the polaron theory in describing transport in MDPs is that it cannot account for the experimentally observed electric field dependence. Again further refinement of the original polaron theory may provide an explanation for this, but to the author's knowledge this has not yet been attempted.

4.4.4 Summary

Over the past five years the disorder limited hopping theory has come to the fore and is now generally used as a zero order approach for analysing experimental data on MDPs as well as other organic materials. This is due mainly to the fact that it is able to explain the experimental results much more completely than polaron theory, (for example the mobility field dependence), but it is also due to experimental findings that the contribution of polaron formation to the activation energy is often much smaller than that of diagonal disorder. Site-selective fluorescence spectroscopy yields a Stokes shift which is about an order of magnitude less than the activation energy obtained from the gaussian width σ_g (Mahrt, Yang and Bässler, 1992), and analysis of charge transport in crystalline naphthalene suggests a polaron binding energy of 16 meV only (Kenkre *et al.*, 1989).

Several recent papers have indeed used the DLH theory as a zero order approach, however it has been found that often the existence of disorder in organic samples cannot

fully account for the activation energy. In some cases analysis of $\mu(T)$ data using the DLH theory and of the amount of dispersion in TOF lineshapes yield different values for the gaussian width σ_g; that for the former being greater. Since the degree of diagonal disorder is reflected by the amount of dispersion in the TOF signal disagreement between the values of σ_g derived by the above methods suggests a further activated component contributing to the mobility activation energy (Pautmeier, Richert and Bässler, 1991). In these cases polaron formation has been invoked to provide this component, which is not an unreasonable assumption due to the inevitable difference between the configurations of a neutral transport molecule and a radical cation or anion (Goldie *et al.*, 1993; Hepburn, 1995; Heun *et al.*, 1995). Another possible origin of this extra component could also be the existence of shallow trapping states due to impurities or structural states formed by specific alignments of neighbouring molecules (Zboinski, 1983).

One of the main criticisms of the DLH theory is the use of the Miller-Abrahams jump rate (eq. 4.50) which ignores polaronic effects and yet assumes that the electron-phonon coupling is strong enough to dissipate energy in downward hops. The problems, mentioned above, that the DLH theory has met in explaining some experimental results has led to the suggestion of adding polaronic effects to the DLH model. This could be effected by adding a further Boltzmann factor to the jump rate with an activation energy of $\varepsilon_p/2$ resulting in an activation energy comprised of a disorder component and a polaronic component

$$\Delta\varepsilon_\sigma = \Delta\varepsilon^{pol} + \Delta\varepsilon^{dis} = \frac{\varepsilon_p}{2} + \frac{8}{9}\sigma_g\hat{\sigma} \tag{4.69}$$

where $\Delta\varepsilon^{dis}$ and $\Delta\varepsilon^{pol}$ are the activation energies due to disorder and polaron formation, respectively. Small contributions to the activation energy due to polaron formation are consistent with data analysis by the DLH theory (Bässler, 1993), however the effects of larger contributions, particularly on the mobility field dependence has yet to be investigated. Simulations involving the effects of polaron formation have not yet been attempted.

5. Computer simulation

Many problems involving charge carrier transport in disordered materials (such as organic semiconductors) are either analytically intractable or solvable only when highly artificial assumptions are made. However, in principle, an arbitrary complexity can be introduced into a numerical simulation of transport; in practice limitations of storage space and computing time constrain what can be done.

The increased availability of cheap computing power has led to the widespread development of simulations incorporating a range of transport processes. In this work, two methods have been employed:

1. a Monte Carlo (MC) method, which utilises random numbers to specify the probabilities for transport events.
2. a matrix method, which solves numerically the appropriate rate equations within a discretised density of states.

Each method and its implementation is discussed in detail below. The primary purpose of this work was to give some insight into which transport model (hopping, trap-limited hopping or multiple trapping) most closely approximates the observed experimental behaviour of the oligomer films. Interest in the matrix method grew when it was discovered that run time constraints were beginning to limit the usefulness of the MC method.

5.1 The Monte Carlo method

The Monte Carlo method uses random numbers to specify the outcomes of certain events. The MC method has been used extensively over the past twenty years to simulate both multiple trapping and hopping transport in idealised amorphous systems and these simulation have generally modelled the time of flight experiment in order to examine the temperature and field dependence of the carrier mobility. Hopping in a spatially random array of isoenergetic sites (off-diagonal disorder) was predicted to lead to dispersive transport according to the model of Scher and Montroll (Scher and

Montroll, 1975). This situation was first examined employing the MC method by Marshall, who showed that dispersive transport was restricted to the first few percent of the transit time (Marshall, 1978), although he did observe an anomalously long tail in the transients. This showed that Scher and Montroll's model was over-emphasising the effect of spatially isolated sites; in general the average carrier will avoid these sites because they are as difficult to enter as they are to leave. However the long tail did suggest that the carriers could not totally avoid paths which included difficult jumps.

The corresponding problem of whether diagonal disorder leads to dispersive transport was studied by Schönherr *et al.* who investigated hopping in a gaussian DOS (Schönherr *et al.*, 1981). They found that significant dispersion occurred providing that $\sigma_g/k_BT > 1$ and $eEa/\sigma_g < 1$, where σ_g is the width of the DOS and a is the intersite distance. However if the width of the DOS is small transport becomes gaussian before the transit time and as the temperature is lowered a transition from non-dispersive to dispersive transport occurs. Since the work of Schönherr *et al.* MC simulations have been extensively used to verify the predictions of the disorder limited hopping model (Bässler, 1993), and simulations incorporating both diagonal and off-diagonal disorder have been developed and studied.

The general approach to simulating a TOF experiment using the MC method is discussed below. The program written by the author follows a similar form and is listed in appendix B.

A regular space lattice is set up using three one-dimensional arrays (100,60,60), with each value of x, y and z representing one site. The energy of each of the 360 000 sites is chosen at random using a gaussian random number generator. A carrier is started at a randomly chosen site on the x = 1 plane. The electric field points in the +x direction. The probability that the carrier will hop to a site x_j, y_j, z_j from the starting point x_i, y_i, z_i is

$$P_{ij} = \frac{\upsilon_{ij}}{\sum_{j \neq i} \upsilon_{ij}} \tag{5.1}$$

where

$$\upsilon_{ij} = \upsilon_0 \exp\left(-2\alpha_{loc} a \frac{R_{ij}}{a}\right) \exp\left(-\frac{\varepsilon_j - \varepsilon_i}{k_B T}\right) \exp\left(\frac{eE(x_j - x_i)}{k_B T}\right) \tag{5.2}$$

providing that $\varepsilon_j - \varepsilon_i + eE(x_j - x_i) > 0$. If $\varepsilon_j - \varepsilon_i + eE(x_j - x_i) < 0$, then

$$\upsilon_{ij} = \upsilon_0 \exp\left(-2\alpha_{loc} a \frac{R_{ij}}{a}\right) \tag{5.3}$$

In the above ν_{ij} is the average hop frequency between sites i and j, α_{loc} is the inverse wavefunction decay length. To approximate off-diagonal disorder $2\alpha_{loc}a$ is expressed as the sum of two terms characteristic of the sites i and j separately, *i.e.* $2\alpha_{loc}a = \Gamma_{ij} = \Gamma_i + \Gamma_j$. Both Γ_i and Γ_j vary randomly according to a gaussian distribution. In the computation $\langle\Gamma_{ij}\rangle = 10$, in line with values used by other workers (Pautmeier, Richert and Bässler, 1991). The sum over j in eq. 5.1 includes the nearest 125 sites, this was found to provide a good trade-off between program run time and computational rigour. This approximation is justified by the fact that the wavefunction overlap term in eq. 5.3 is reduced from $4.5 * 10^{-5}$ for a nearest neighbour transition to $1.9 * 10^{-22}$ for a transition of distance 5a.

A random number from a uniform distribution determines the site hopped to which is weighted by its length in random number space according to the value P_{ij}. The time for the jump is given by

$$t_{ij} = \frac{1}{\sum_{j \neq i} \upsilon_{ij}} x_{ei} \tag{5.4}$$

where x_{ei} is taken from an exponential distribution of random numbers. The carrier is now on a new site and the procedure is repeated. The carrier is followed and its position noted as a function of time until it reaches the x = 100 plane. At this point the computation is terminated. This process is repeated for a large number of carriers to obtain the average displacement with time for all the carriers $\langle x(t)\rangle$. The current is calculated using $i(t) = eN(t)\langle x(t)\rangle/Lt$, where N(t) is the number of remaining hopping carriers at time t and L is the sample length. The temporal evolution of the average energy can also be followed. Once all the carriers have been extracted the program finishes.

In the present work we are more interested in the simulation of the transient photocurrent decay experiment. The above Monte Carlo program was thus modified to

allow carriers to continue through the hopping array on arrival at x = 100, rather than being extracted, which was simply achieved by re-injecting them at x = 0 and noting their total displacement in the x-direction. Thus in this modified program the number of hopping carriers is constant and thermalisation of carriers can be observed to arbitrary time intervals after creation. The above situation is similar to TOF in a very thick sample with no recombination, and the temporal evolution of the current directly reflects that of the mobility, $\mu(t)$.

The Monte Carlo simulations agree well with the predictions of the DLH theory, however they suffer from excessive run-time problems, often taking over a day to run, and the results are generally quite noisy. The results could be made less noisy by increasing the number of carrier sent through the array but this greatly increases the run-time.

5.2 Matrix techniques

This simulation method has been used to model multiple trapping transport and is described in Main *et al.* (1991). In this method one starts with a particular DOS distribution which is divided into a number of discrete levels of width $\Delta\varepsilon < k_BT$, resulting in typically 100 discrete DOS levels plus the conduction and valence bands (see fig. 5.1). Rate equations can then be written for the conduction and valence bands and for the localised levels.

For electron multiple trapping the rate equation for free electrons in the conduction band is,

$$\frac{dn}{dt} = -\sum_j nC_{nj}N_{tj} + \sum_j \bar{n}_j C_{n_j} n_{tj} \tag{5.5}$$

where the first sum represents electron capture from the conduction band into the distribution of localised gap states, and the second represents electron release from the gap states to the conduction band. In 5.5 N_{tj} is the density of empty, localised states at level j, C_{nj} is the capture cross-section, n_{tj} is the density of filled electron states at level j and $C_{nj}\bar{n}_j$ is the electron release rate from this level.

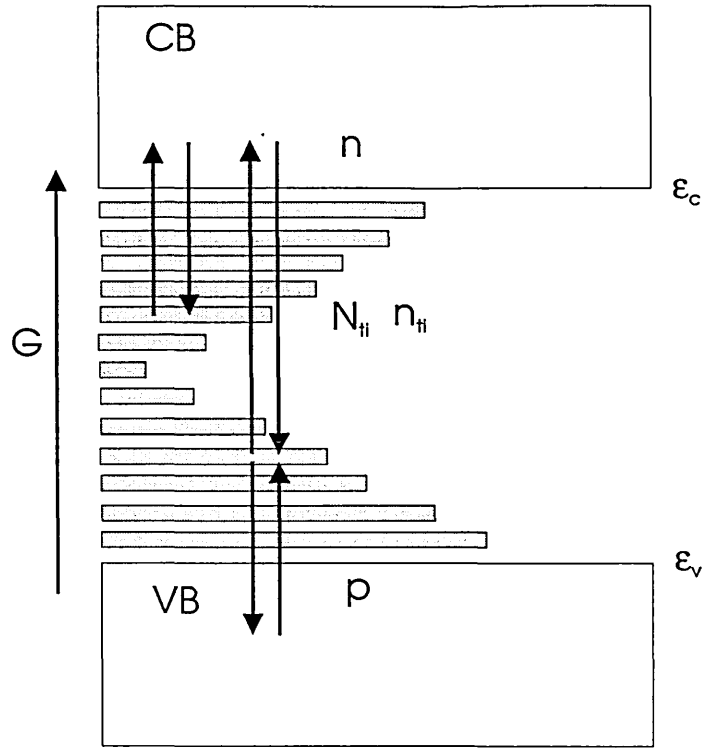

Fig. 5.1 Discretised DOS used in finite difference simulations

The rate of change of the trapped electron density at level j is given by:

$$\frac{dn_{tj}}{dt} = nC_{nj}N_{tj} - \overline{n}_j C_{nj} n_{tj} \tag{5.6}$$

Similar equations can be written for holes.

In the small time step δt, the changes in the free and trapped electron densities δn and δn_t are given by

$$\delta n = -\left[\sum_j nC_{nj}N_{tj} + \sum_j \overline{n}_j C_{n_j} n_{tj}\right]\delta t \tag{5.7}$$

and

$$\delta n_t = \left[nC_{nj}N_{tj} - \overline{n}_j C_{nj} n_{tj}\right]\delta t \tag{5.8}$$

Thus in going from step i to step i+1 we have

$$n^{i+1} = n^i + \delta n \tag{5.9}$$

and

$$n_{ij}^{i+1} = n_{ij}^i + \delta n_{ij} \tag{5.10}$$

The calculation of the evolving electron density can be written for all states in matrix form as

$$[n^{i+1}] = [A][n^i] \tag{5.11}$$

where [A] is the transition matrix, which for electron multiple trapping has the form given in fig 5.2.

$$\begin{bmatrix} A_{11} & A_{12} & A_{1j} & \cdots & \cdots & A_{1N} \\ A_{21} & A_{22} & 0 & 0 & 0 & 0 \\ A_{j1} & 0 & A_{jj} & 0 & 0 & 0 \\ \vdots & 0 & 0 & \ddots & 0 & \vdots \\ \vdots & 0 & 0 & 0 & \ddots & \vdots \\ A_{N1} & 0 & 0 & \cdots & \cdots & A_{NN} \end{bmatrix}$$

Fig. 5.2 The transition matrix for electron multiple trapping.

where,

$$A_{11} = 1 - C_n \sum_j N_{ij} \delta t \tag{5.12}$$

$$A_{1j} = C_n \overline{n}_{ij} \delta t \tag{5.13}$$

$$A_{ji} = C_n N_{ij} \delta t \tag{5.14}$$

$$A_{jj} = 1 - C_n \overline{n}_{ij} \delta t \tag{5.15}$$

It can be seen that in this case only row 1 (electron release) column 1 (electron capture) and the diagonal elements (electron capture and release) are non-zero. The length of the time step can be increased as follows

$$[n^{i+2}] = [A][n^{n+1}] = [A][A][n^i] \tag{5.16}$$

or

$$[n^i] = [A]^i[n^0] \tag{5.17}$$

where $[A]^i$ is the i^{th} power of the transition matrix and $[n^0]$ is the initial condition. The application of eq. 5.17 leads rapidly to the generation of long time steps, the solutions being read from the matrix at the required interval. The form of the transient depends on the matrix $[n^0]$, which defines the kind of excitation. For TPC we use

$$[n^0] = \begin{bmatrix} 1 \\ 0 \\ \vdots \\ 0 \end{bmatrix} \tag{5.18}$$

In order to make the above simulation technique more appropriate for organic materials the basic rate equations for multiple trapping were modified to allow movement between localised levels *i.e.*, hopping transport is incorporated. The rate equation for trapped electrons at level j then takes the form:

rate of change of n_t in level j = e^- capture from CB - e^- release to CB
- hop out to another localised level + hop in from another localised level

which can be written as

$$\begin{aligned} \frac{dn_{tj}}{dt} = nC_{nj}N_{tj} - \overline{n}_j C_{nj} n_{tj} - \sum_i n_{tj}\left(\frac{N_{ti}}{G_T}\right)\upsilon_0 \exp\left[-\frac{\varepsilon_i - \varepsilon_j}{k_B T} - 2\alpha_{loc}R\right] \\ + \sum_i n_{ti}\left(\frac{N_{tj}}{G_T}\right)\upsilon_0 \exp\left[-\frac{\varepsilon_j - \varepsilon_i}{k_B T} - 2\alpha_{loc}R\right] \end{aligned} \tag{5.19}$$

where $G_T = \Sigma N_{tj}$ is the sum density of localised states, υ_0 is the attempt to escape frequency and α is the inverse wavefunction decay length. For a simple cubic lattice with constant hop distance we can simplify the hop terms in eq. 5.19 by introducing the hopping equivalent of the capture coefficient ($C_n = \upsilon_0/N_c$) which is denoted C_h *i.e.*,

$$-C_h n_{tj}\sum_i N_{ti}\exp\left[-\frac{\varepsilon_i-\varepsilon_j}{k_BT}\right]+C_h N_{tj}\sum_i n_{ti}\exp\left[-\frac{\varepsilon_j-\varepsilon_i}{k_BT}\right] \tag{5.20}$$

hop out **hop in**

where

$$C_h=\frac{6\upsilon_0\exp(-2\alpha_{loc}R)}{G_T} \tag{5.21}$$

thus C_n and C_h are related by

$$C_h=C_n\frac{6N_c\exp(-2\alpha_{loc}R)}{G_T} \tag{5.22}$$

The Boltzmann factor for hops up and down in energy is defined to be equal to unity for downward hops as in the MC simulations *i.e.*

$$\exp\left(-\frac{\Delta\varepsilon}{k_BT}\right)=\exp\left(-\frac{\Delta\varepsilon}{k_BT}\right) \qquad \varepsilon>0 \tag{5.23}$$

$$\exp\left(-\frac{\Delta\varepsilon}{k_BT}\right)=1 \qquad \varepsilon\le 0 \tag{5.24}$$

The new set of rate equation for each localised level requires that new terms be added to the transition matrix, we now have

$$A_{ij}=C_h N_{tj}\exp\left(-\frac{\varepsilon_j-\varepsilon_i}{k_BT}\right)\delta t \tag{5.25}$$

$$A_{jj}=1-C_n\bar{n}_{tj}\delta t-C_h\sum_i N_{ti}\exp\left(-\frac{\varepsilon_i-\varepsilon_i}{k_BT}\right)\delta t+C_h N_{tj}\delta t \tag{5.26}$$

The addition of the above terms to the transition matrix allows multiple trapping (between localised levels and the conduction band) and hopping (between localised levels) to occur simultaneously.

This multiple trapping/hopping program can give the electron density in the conduction band and the occupation of the localised state as a function of time, however its main utility in the present context is that it can be used in either MT and/or hopping mode. The hopping terms in the transition matrix (eqs. 5.25 and 5.26) can be zeroed by setting the hopping coefficient C_h to zero, and the program becomes solely a multiple trapping simulation. Alternatively the program can be used in hopping-only mode by displacing the localised states from the conduction band, for example by say 5 eV, ensuring that electrons cannot reach the band and must therefore move by hopping alone. Obviously the ratio of hopping to multiple trapping depends on the density and depth of the localised states and the absolute temperature.

The hopping contribution to the overall conductivity is deduced using the Einstein relation,

$$\mu_j = \frac{e}{k_B T} D_j \tag{5.27}$$

where

$$D_j = \frac{1}{6} \upsilon_j R^2 \tag{5.28}$$

in eq. 5.28 D_j is the diffusion coefficient of level of level j and υ_j is the corresponding hopping frequency. The hopping conductivity of level j can then be written

$$\sigma_j = n_{tj} e \mu_j \tag{5.29}$$

υ_j in eq. 5.28 is equivalent to the probability per second of a carrier jumping out of level j and is given by

$$\upsilon_j = C_h \sum_i N_{ti} \exp\left[-\frac{\varepsilon_i - \varepsilon_j}{k_B T} \right] \tag{5.30}$$

thus the conductivity of level j can be written

$$\sigma_j(t) = n_{ij}(t)e\mu_j = n_{ij}(t)e\left(\frac{e}{6k_BT}\upsilon_j R^2\right) \tag{5.31}$$

but

$$n_{ij}(t) = A_{j1}(t) \tag{5.32}$$

so

$$\sigma_j(t) = A_{j1}(t)e\left(\frac{e}{6k_BT}\upsilon_j R^2\right) \tag{5.33}$$

The total hopping conductivity is the sum over the matrix elements A_{j1} and the hopping rates υ_j

$$\sigma_{hop}(t) = \left(\frac{e^2R^2}{6k_BT}\right)\sum_j A_{j1}(t)\upsilon_j \tag{5.34}$$

The free electron or conduction band contribution to the conductivity is simply given by the density of free electrons multiplied by the CB mobility.

$$\sigma_{free}(t) = n_{ij}(t)e\mu_j \tag{5.35}$$

Here n is given by A_{11}, thus

$$\sigma_{free}(t) = A_{11}(t)e\mu_j \tag{5.36}$$

If multiple trapping and hopping are occurring simultaneously the conductivity is simply the sum of eqs.5.34 and 5.36.

The above described program has been developed and written by the author's second supervisor C. Main and is as yet unpublished. For this work the localised gap states have been given a gaussian distribution to enable the author to compare this new simulation technique with the predictions of the DLH theory and the MC program described in § 5.1. It is not the intention in this chapter to go into a lengthy comparison of the matrix program with the MC simulations, however a few basic points should be

pointed out. Firstly, initial testing of the program by the author has shown that qualitatively, the matrix technique program used in hopping-only mode agrees with the general results obtained from the MC simulations. The hopping current is found to thermalise in a certain time interval to a steady state value, both of which are dependent on the relative degree of (diagonal) disorder σ_g/k_BT; as σ_g/k_BT decreases the relaxation time increases and the steady state conductivity decreases. At present the matrix program yields values for the relaxation time which are several orders of magnitude too small, *i.e.* thermalisation is occurring too quickly. The program can also give the occupation of the localised levels at certain time intervals, in this case the program again gives only qualitatively similar behaviour to that predicted by theory and simulation. Theory and MC simulation predict that the hopping carriers should relax to an average energy given by σ_g^2/k_BT (see eq. 4.52), assuming an occupational density of states of width σ_g. It is found however that the matrix program does not give correct values for this "equilibration energy", the carriers thermalising to an energy closer to the centre of the DOS than predicted. The reason(s) for these discrepancies have not yet been determined. Variation of the adjustable parameters in the command file for the program does not affect the relaxation problems mentioned above. The most likely reason for the relaxation problems is the absence of an applied field in the matrix program. Hopping transport is field dependent (unlike multiple trapping); the application of a field shifting energy levels (in the field direction) into closer coincidence, and therefore providing more possibilities for relaxation. It might be expected that in the absence of field-assisted thermalisation carriers would equilibrate more rapidly, explaining the fast thermalisation and inaccurate equilibration energy.

The matrix program thus promises to be a novel alternative to MC simulations for organic materials, its main advantage being one of computational speed. The MC program took many hours to run necessitating that it be left overnight, and sometimes longer than this if many carriers are averaged to long times Compared to this the matrix technique usually only takes a couple of minutes to run on a PC.

At present there are several important points which the matrix technique cannot deal with:

1. As this technique was initially developed for multiple trapping, a mobility field dependence is not included. This is acceptable for the free carrier mobility but the hopping mobility is likely to be strongly field dependent.

2. It was shown above that the calculation of the hopping conductivity was derived using the Einstein relation, however due to the presence of significant field assisted diffusion in organic materials the Einstein relation is not always valid.
3. Off-diagonal disorder is not accounted for in the hopping process. Variable range hopping could be included but at present only nearest neighbour hopping is considered.

Both simulation methods will be used throughout this work to gain insight into the transport mechanism and the form of the DOS in the studied materials.

6. Experimental methods

This chapter describes the materials preparation and characterisation techniques used in this work. Firstly a description of the materials studied and the two deposition methods employed to prepare the thin films is presented. This is followed by details of the characterisation techniques used to obtain information on carrier transport. This chapter concludes with a discussion of the experimental difficulties encountered in performing measurements on the organic samples studied here.

6.1 Materials studied

The materials studied in this work are oligomers *i.e.* short chain polymers. Oligomers are of particular interest because they can be considered as model systems for polymers, but benefit from being easier to prepare in a pure form because in general polymerisation, which always leaves residual impurities, is not necessary (Barth *et al.*, 1997). The oligomers studied here derive from substituted poly(thienylenevinylene)s and poly(acene). The oligomer deriving from poly(acene), known as pentacene, however is normally not considered as an oligomer but as a small molecule in its own right; this is because poly(acene) has not as yet been synthesised. The chemical structures of pentacene and the thienylenevinylene oligomers (TVTs) are depicted in fig. 6.1.

6.2 Sample preparation

Deposition of the materials used in this work was carried out at the University of Swansea. The oligomers studied have been prepared as thin films via two methods, (i) thermal evaporation (TE); and (ii) pulsed laser deposition (PLD), which are described below.

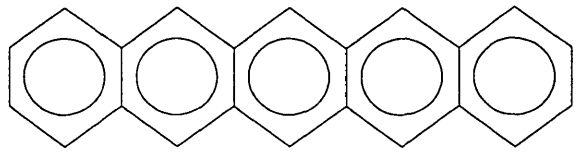

(A) Pentacene

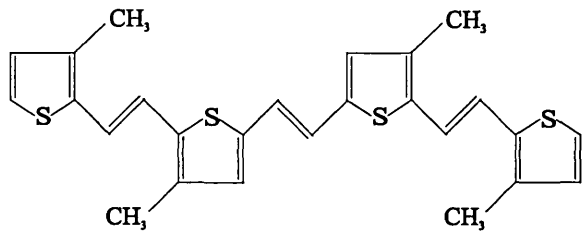

(B) TVD

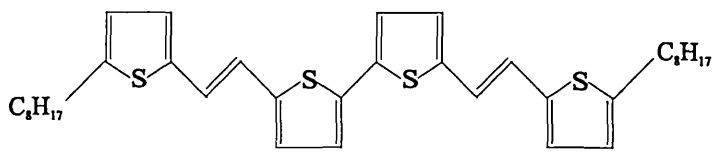

(C) TVB

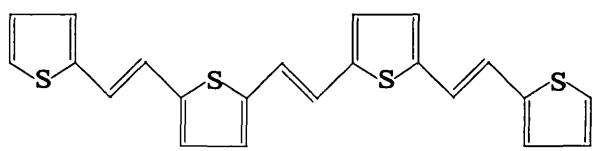

(D) TVC

Fig. 6.1 Chemical structures of oligomers studied in this work.

6.2.1 Thermal evaporation

Thermal evaporation is particularly suited to the deposition of single component organic solids because of their low melting points resulting from the weak intermolecular bonding forces. Thus many different molecular materials can be deposited by evaporation. This is one of the main advantages that organic materials have over electronically-active inorganic amorphous semiconductors which often require complex deposition techniques. Recent work by Väterlein *et al.* has also shown

that thermal evaporation of oligothiophenes stored in air before deposition actually removes absorbed oxygen and thus purifies the material (Väterlein *et al.*, 1996). Subsequent exposure to ambient atmosphere is found to oxygen dope the thin films giving rise to higher levels of conductivity.

Pentacene and the TVT derivatives were deposited by a conventional thermal evaporation technique using an Edwards E306A coating system. The materials were deposited from a heated tungsten boat at a pressure of 10^{-6} torr onto Corning 7059 glass substrates with electrodes already deposited (also using the E306A). Target substrates were mounted on a temperature-controlled holder to allow thin films to be deposited at different temperatures.

6.2.2 Pulsed laser deposition

For a historical overview of the development of pulsed laser deposition and further information the reader is directed to the book by Chrisey and Hubler (Chrisey and Hubler, 1994). Fig. 6.2 shows a schematic experimental set-up of the PLD system used to deposit the pentacene thin films (only pentacene was deposited by PLD). An excimer laser (KrF, Lambda Physik LPX 105) with a wavelength of 248 nm (5 eV) and a beam size of 2.5 cm × 0.7 cm was used to ablate the pentacene. The pentacene sample was held in a glass crucible below the substrate in a vacuum chamber (~10^{-5} torr), the substrate temperature was again controllable. Deposition was achieved by operating the laser at 50 Hz (23 ns pulses) with a power of 6-8 W, 3000-4000 pulses were applied as the laser was scanned across the sample. Samples were deposited at room temperature 160 ^{0}C and 200 ^{0}C and generally had a thickness of 1 μm.

Structural studies of the thin films were not carried out in this work, more information on this can be found in the work of Salih *et al.*, who also compare the properties of thin films deposited by TE and PLD (Salih *et al.*, 1996; Salih, Marshall and Maud, 1997). It has been demonstrated that pentacene films deposited at low temperatures (~20 K) are amorphous, however, on raising such samples to room temperature crystallisation occurs (Eiermann *et al.*, 1983). Salih, Marshall and Maud (1997) performed a SEM study of pentacene thin films deposited by TE and PLD and found that at room temperature both techniques yield crystallites of 0.1-0.2 μm. As the temperature is raised the grain size is found to increase, with the PLD material

developing a more interconnected granular structure. The thin films used in this work are likely to be very similar to those described by Salih *et al.* (1996) as they were prepared in the same labs. No specific structural studies of the thienylene-vinylene oligomers has been carried out, it is expected however, that similar results to those obtained for pentacene are likely to apply.

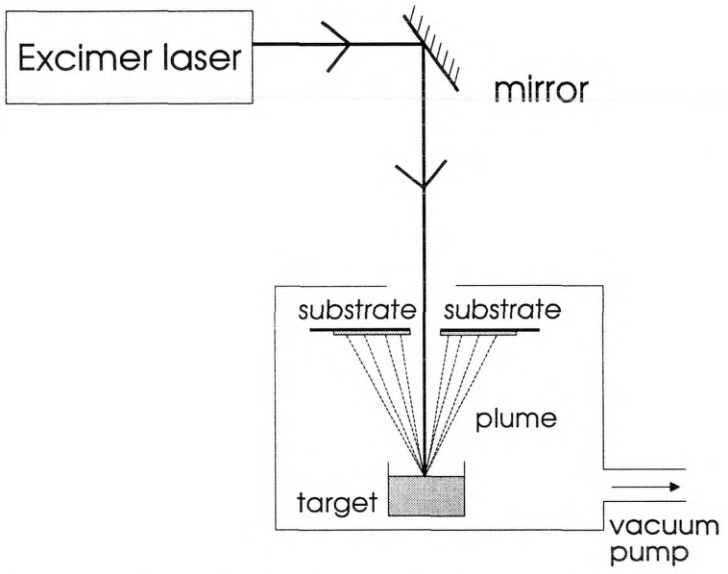

Fig. 6.2 Schematic diagram of the apparatus employed for pulsed laser deposition of pentacene thin films.

6.3 Experimental sample configuration

The electrode configuration of the experimental samples used in this work are of two types, (i) coplanar gap cell, and (ii) sandwich cell. These two types of samples are shown in fig. 6.3. The majority of work has been done with coplanar sample configurations, using either a simple gap cell with two electrodes or an interdigitated Philips mask. The Philips mask corresponds to two electrodes of 8.5 cm length with a 50 μm electrode gap, cf. the simple gap cell where the electrode length is 2.5 cm. The Philips mask is generally preferred over the simple gap cell geometry because the currents achievable at fixed field are higher due to the greater effective conduction cross-section.

The coplanar samples are all approximately 1μm thick whereas the sandwich samples have a thickness of either 2μm or 4μm. The electrodes are aluminium unless

otherwise stated; connections to the external circuit are made by scraping away some of the oligomer and affixing thin aluminium wires using RS silver paint.

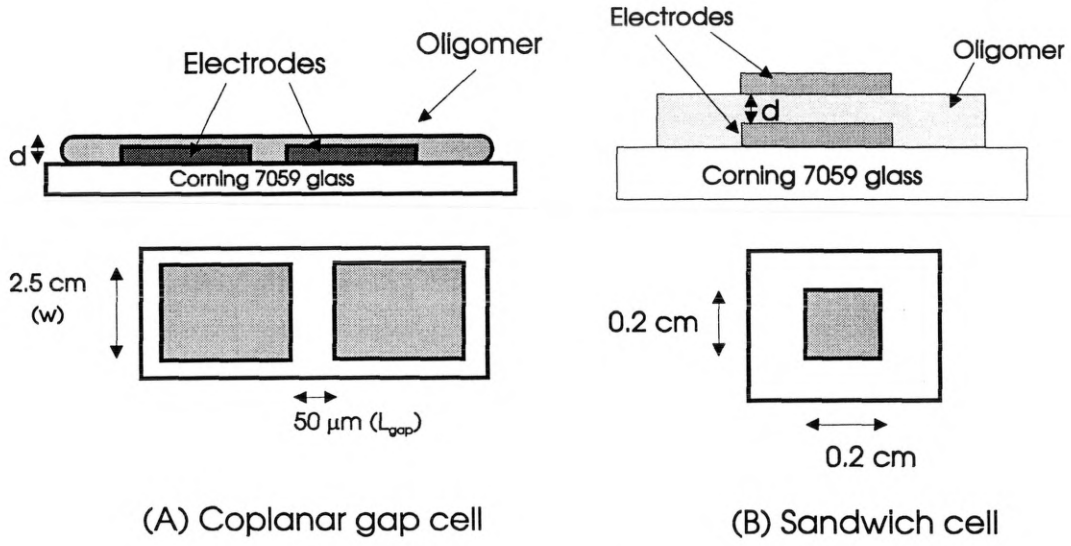

Fig. 6.3 Sample configurations used for characterisation of oligomers

6.4 Sample measurement chamber and sample holder

The sample chamber and holder described here were used for all measurements except the steady state photocarrier grating experiment (SSPG). Fig. 6.4 shows a simplified diagram of the vacuum chamber and the sample holder. All measurements except where stated otherwise were performed with the vacuum chamber evacuated, usually with the rotary pump only, providing a pressure of ~10^{-3} torr. The higher vacuum achievable using the diffusion pump (~10^{-5} torr) was in general found to be unnecessary and this pump was therefore used infrequently due to the extended pumping down time.

The sample was held vertically on the sample stage by silicone grease and was attached to the external circuit via BNC vacuum leadthroughs. Also situated on the sample stage were a temperature sensor, two resistive heaters (one controlled) and a LED holder for performing TPC with optical bias.

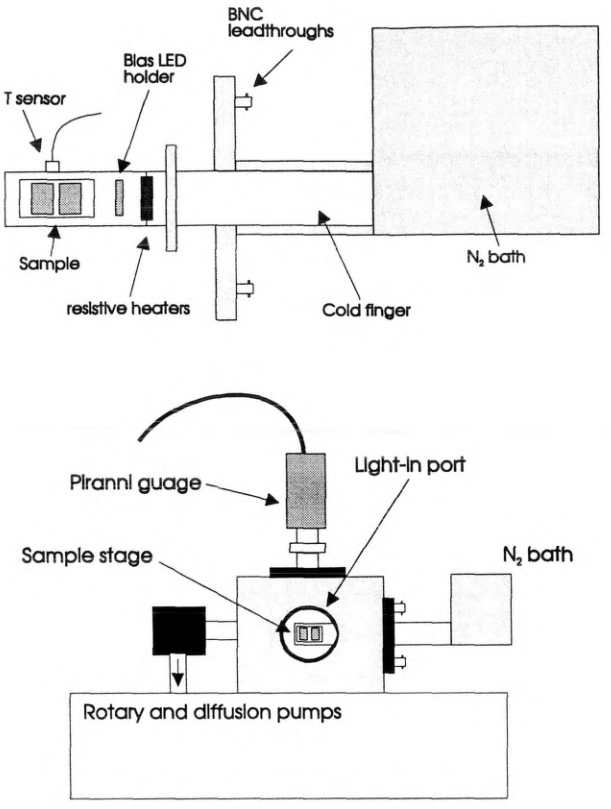

Fig. 6.4 Diagram depicting the sample holder and vacuum chamber used for experimental characterisation.

The sample stage was attached to a cold finger ending in a liquid nitrogen bath. The temperature was controllable to ± 0.1 K by an Oxford instruments digital temperature controller (model DTC-2) which powered one of the resistive heaters on the sample stage. The other heater was used for working against the liquid N_2 when high temperatures were required and was driven by a standard power supply, this heater was only manually controllable. Thus the temperature could be varied accurately from slightly above 77 K to the highest temperature the oligomer can withstand without being damaged.

The sample was illuminated via a port on one side of the vacuum chamber either through a quartz window or a light pipe.

6.5 Steady state techniques

Steady state measurements are those in which the photon flux and thus the carrier generation rate are constant with time, thus the value of the resulting photocurrent is time invariant. The steady state techniques employed in this work include simple photocurrent measurements as a function of temperature, field, excitation intensity and excitation wavelength, and a more complex method, the steady state photocarrier grating technique, SSPG. Measurements of the dark current and its temperature and field dependence were also carried out. Optical absorption, transmission and reflectivity measurements are also defined here as steady state techniques although they do not result from the measurement of dark current or photocurrent.

For simple photocurrent measurements as a function of a given variable a constant, uniform photon flux was directed onto the sample surface via a light pipe arrangement and the total current measured using a Keithley 617 electrometer. The photocurrent was obtained by subtracting the dark current (which is also measured) from the total current. It was often necessary to wait for extended periods of time (5 mins or longer) for the photocurrent to stabilise (see § 6.6.6).

6.5.1 Light sources

All steady state measurements except SSPG and CPM were performed using LEDs of various wavelengths connected to the end of a perspex light pipe (length 12.5 cm and diameter 7 mm) which was used to direct light onto the sample surface. The end of the light pipe was positioned about 10 mm above the sample gap. A Thurlby PL320 power supply was used to drive the LED, and a Fluke 8022-B digital multimeter was used to determine the LED current (see fig. 6.5). The LED output was measured with either a BPX-65 (active area $1mm^2$) or a Hewlett-Packard 5082-4207 (active area $0.8mm^2$) pin photodiode which were already calibrated for sensitivity (*i.e.* photon flux per amp) vs. wavelength (Merazga, 1990).

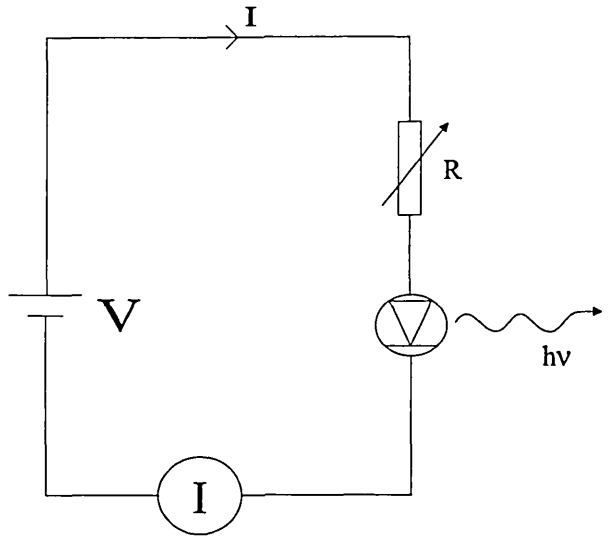

Fig. 6.5 LED drive circuit for steady state illumination.

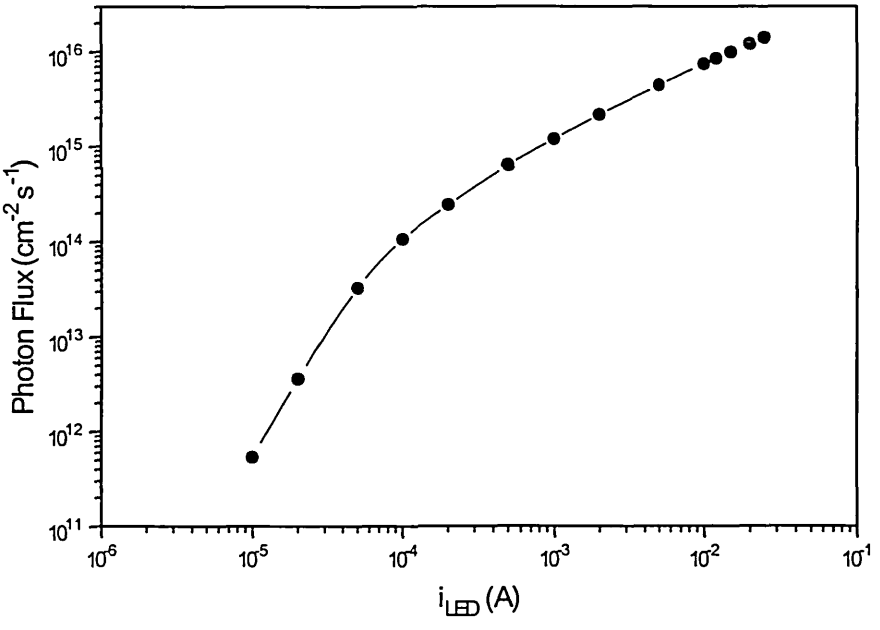

Fig. 6.6 Calibration curve for Marl 110104 high intensity green LED, $\lambda = 525$ nm.

Thus it was possible to obtain calibration graphs of photon flux vs. LED current for each wavelength of LED by measuring the photodiode current induced by a certain LED current and using the photodiode sensitivity reading at that wavelength to convert from photodiode current to incident flux.

When calibrating the LEDs the light pipe was employed and kept at a similar distance from the photodiode as from the sample (z-axis), the photodiode current (measured with the Keithley 617) was then maximised at this distance by manoeuvring the LED in the x-y plane. Figs. 6.6 - 6.8 show the calibration graphs for the LEDs used in this work.

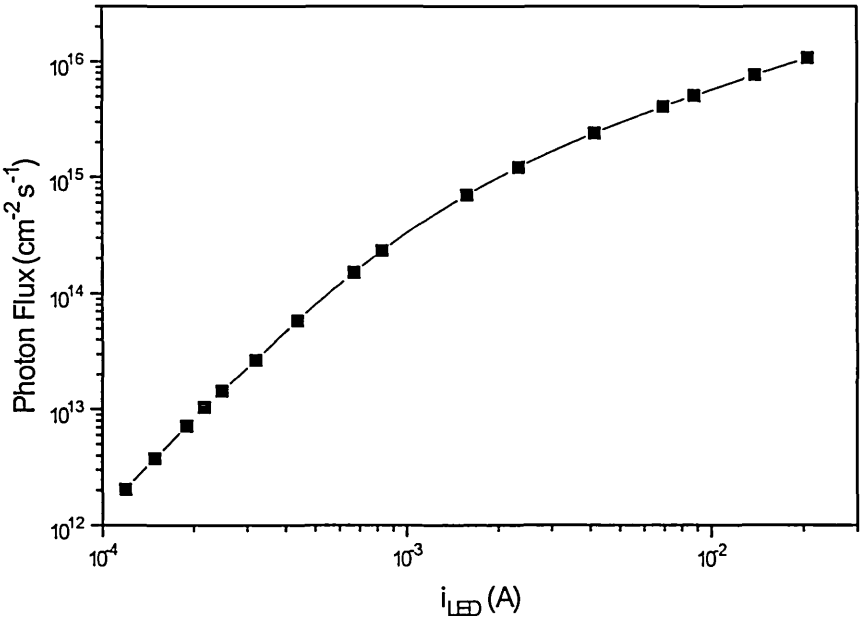

Fig. 6.7 Calibration curve for Hero NLPB 500 blue LED, $\lambda = 450$ nm.

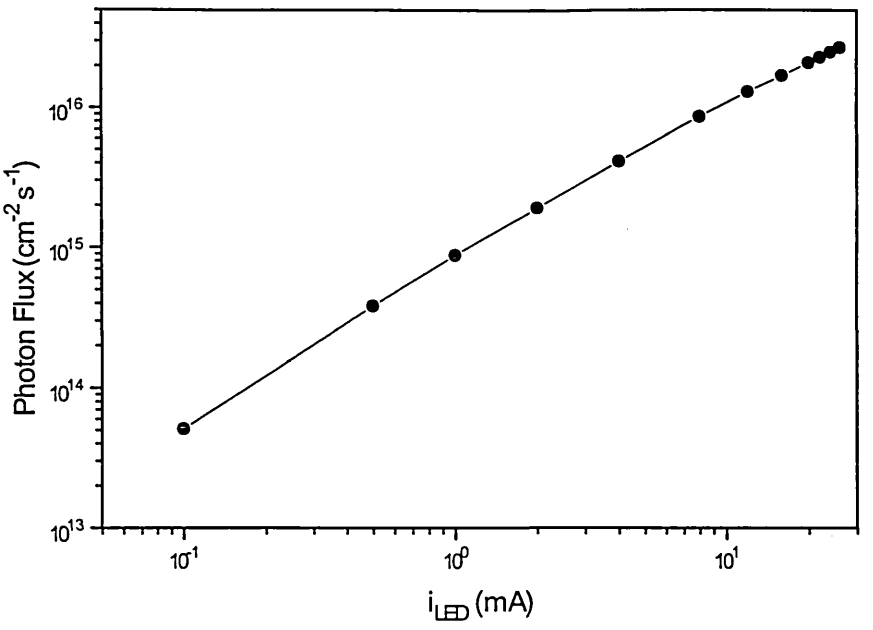

Fig. 6.8 Calibration curve for Stanley HS3000 red LED, λ = 654 nm.

6.5.2 Optical absorption and photocurrent action spectra

The absorbance of all the oligomers vs. photon energy was measured using a Perkin-Elmer Lambda 2, uv/vis spectrophotometer. The absorption plots were recorded using the thin film samples on glass which should be kept in mind when studying the spectra. The spectrophotometer produced data of absorbance vs. wavelength, which has been converted to photon energy in figs. 7.1-7.4. The absorbance is defined as $\ln(I_0/I)$, thus from the absorbance a rough value for the absorption coefficient can be determined using Beer's law. Note however that this does not take account of any reflection and the values so obtained for α should not therefore be considered as accurate.

The photocurrent action spectra were recorded using the experimental set-up depicted in fig. 6.9. The procedure was as follows. The sample/experimental system response due to a fixed photon flux from the bulb is amplified and measured using a lock-in amplifier. The controller computer program then changes the wavelength via a stepper motor connected to the monochromator. At each wavelength the sample current and the detector current are measured, and the sample current is then normalised with respect to the photon flux.

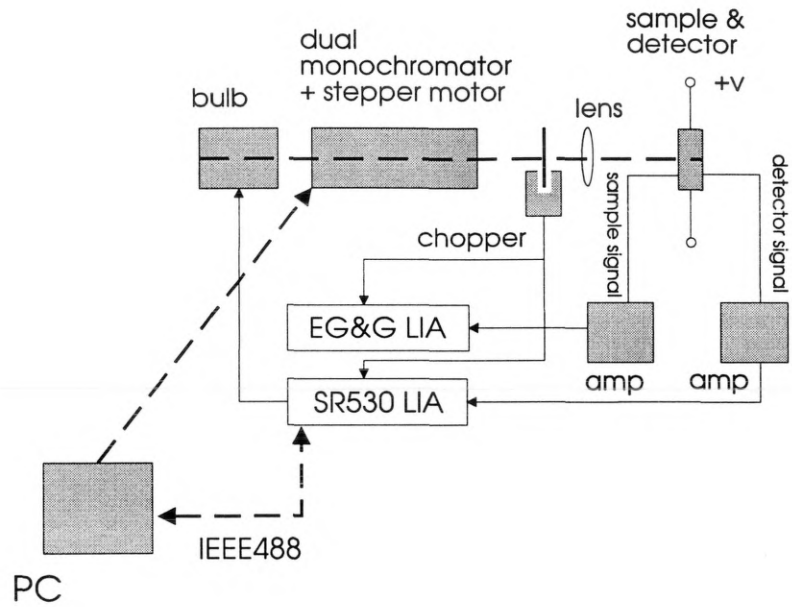

Fig. 6.9 Photocurrent action spectrum measurement system.

6.5.3 The steady state photocarrier grating technique (SSPG)

The steady state photocarrier grating experiment was performed by the author on the oligomeric samples using an experimental system at the Carl V. Ossietsky University in Oldenburg, Germany. Although the SSPG technique has been used extensively on materials such as amorphous silicon and GaAs in order to determine the ambipolar diffusion length, it has not to the author's knowledge been performed on organic materials.

A schematic diagram of the experimental set-up for the SSPG technique is shown in fig. 6.10. A detailed description of the SSPG technique can be found in the papers of Ritter *et al.* (1986, 1987, 1988 and references therein), and only a short description of the technique is given here. In SSPG the sample is illuminated by two coherent light beams of different intensities which interfere and create an interference pattern in the form of a small photocarrier grating superimposed on a large, uniform background carrier density. If the grating period exceeds the carrier diffusion length, a well-defined photocarrier grating is created in the material. However, if the grating period is smaller than the diffusion length the sample will end up being almost uniformly illuminated, resulting in uniform carrier densities. The amplitude of the grating, which depends on the carrier diffusion lengths, can be estimated by measuring

the photocurrent perpendicular to the grating fringes at low applied fields. Since the grating minima have a higher resistivity than the average resistivity when a grating is produced the measured photocurrent is less than that due to uniform illumination. By measuring the photocurrent magnitude as function of grating period, the ambipolar diffusion length can be found.

Experimentally the He-Ne laser beam is split into two with a beam splitter (BS) and each beam is directed on to the sample by mirrors. Beam 2 is attenuated using a neutral density filter (NDF) and chopped. Using a half wave plate ($\lambda/2$) the plane of polarisation of beam 1 can be rotated by 90^0. The lock-in amplifier (LIA) measures the small changes in the photocurrent due to the chopping of I_2 for the case of grating illumination ($\lambda/2$ in the neutral position) and uniform illumination (polarisation of I_1 rotated by 90^0). A bias field of 10^4 V cm^{-1} was applied during measurements.

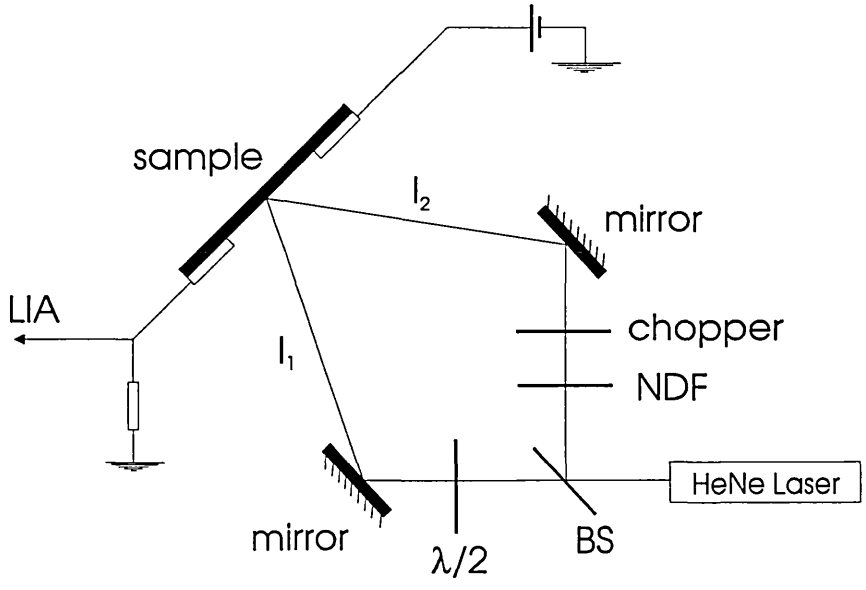

Fig.6.10 Experimental set-up for the steady state photocarrier grating technique.

6.6 Transient techniques

Transient techniques are those in which a light pulse of fixed magnitude and duration is used to excite the sample. The decaying photocurrent is subsequently measured as a function of time until it reaches the thermal equilibrium value (or steady state value if optical bias is present). The transient techniques used in this work have already been mentioned in § 4.2.5, they are the transient photocurrent decay method (TPC) and the time-of-flight technique (TOF). In addition to "straight" TPC this experiment can also be carried out with an additional steady state illumination present, and is then referred to as TPC with optical bias.

Also included in this section are measurements of the photocurrent decay from steady state, which are measured at long times and resemble the persistent photocurrent (PPC) observed in some amorphous semiconductors.

6.6.1 The transient photocurrent decay experiment

The experimental set-up for TPC is shown in fig 6.11. The sample is situated in the vacuum chamber described in § 6.4 (not shown in fig. 6.11), and is illuminated through a quartz window or a light pipe attached to the side of the chamber. A nitrogen pumped dye laser is used to excite the sample. The laser is powered by a 12 V sealed, lead-acid battery, which allows the complete unit to be enclosed in a Faraday cage to reduce interference. The system is partially computer controlled via an IEEE-488 line which is connected to a digital storage oscilloscope (DSO), and a RS232 line which is used to trigger a pulse generator. The pulse generator in turn triggers the laser via a fibre optic link, which is again used to reduce interference with the detected sample signal.

The sample current signal is pre-amplified with a current to voltage amplifier and then displayed on the DSO. The oscilloscope is triggered to capture the signal by a fibre optic cable to which a portion of the laser output has been diverted by an angled glass slide. The captured data set is then sent to the computer (via the IEEE-488 bus) for analysis.

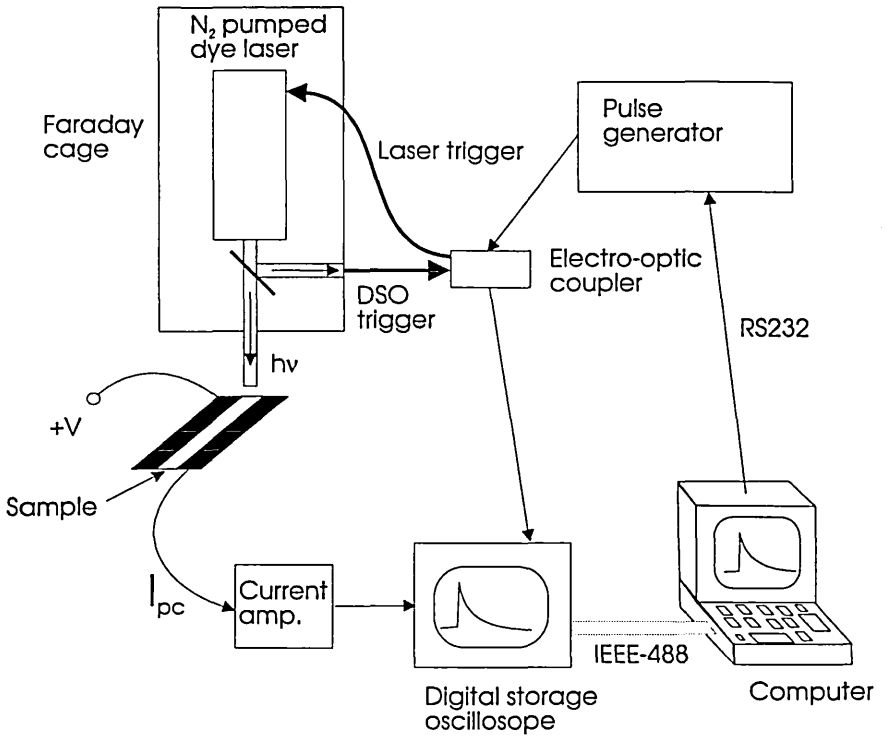

Fig. 6.11 Semi-automated TPC experimental set-up.

For a particular decay time range an appropriate feedback resistor is chosen for the amplifier and the oscilloscope time base and voltage range are adjusted to give an adequate signal. The computer is then instructed to fire the laser a specified number of times and the resulting decays are averaged to minimise the effects of noise. The system can then be reset as described above to obtain data from different time ranges, and a composite decay over many orders of time and current can be built up (typically from ~10^{-9} - 10 s). The major components comprising the system will now be described in more detail.

6.6.2 Dye laser

A nitrogen pumped dye laser (Laser Science inc. VSL 337) was used as a pulsed light source in both the TPC and TOF experiments. The laser was used in most cases with the green dye Coumarin which has an emission peak at approximately 500 nm (2.49 eV), Rhodamin 101, a red dye with an emission peak of 655 nm (1.90 eV) was also used in some cases. The Faraday cage which encloses the laser incorporates in the

beam path a holder for neutral density filters (NDFs), thus the intensity of the laser output may be attenuated by known amounts. The sample was illuminated by the laser via a light pipe arrangement similar to that used for the steady state measurements. The laser was situated 5.5 cm from the end of the light pipe, the end of which was 1 cm above the sample, thus the total laser-sample distance was 19 cm (light pipe length = 12.5cm). The laser position was adjusted at this distance to give the largest signal possible as measured on an oscilloscope.

The laser output was determined using a calibrated pin photodiode (Hewlett-Packard 5082-4207) which replaces the sample in the above set-up, an optical density 4 NDF was needed to reduce the photodiode current to the regime of linear response. The temporal intensity profile was measured with a Gould 4072 digital storage oscilloscope and found to be roughly gaussian in shape. The total charge generated by the laser pulse was determined by using a triangle approximation for the gaussian lineshape (see fig. 5.8). The base of the approximate triangle was measured as 9 ns and the height as 150 mV, the signal was measured across two parallel 50 Ω resistors thus the maximum current was $\Delta i = \Delta V/R = 6$ mA. The approximate charge in the pulse is the area of the triangle and is 2.7×10^{-11} C which corresponds to 2.7×10^{-7} C without the neutral density filter. Multiplying the total charge collected in the photodiode by its sensitivity at the laser wavelength yields the number of photons per square centimetre. The sensitivity at 500 nm is 1.2×10^{21} A^{-1} cm^{-2} s^{-1}, therefore the photon areal density is 3.24×10^{14} cm^{-2}. The accuracy of the estimated laser output depends primarily on the accuracy of the "triangle approximation" used to determine the approximate charge induced by the laser pulse. However, other possible errors can arise due to inaccurate positioning of the laser when performing TPC, although the signal was carefully maximised in all cases to reduce this.

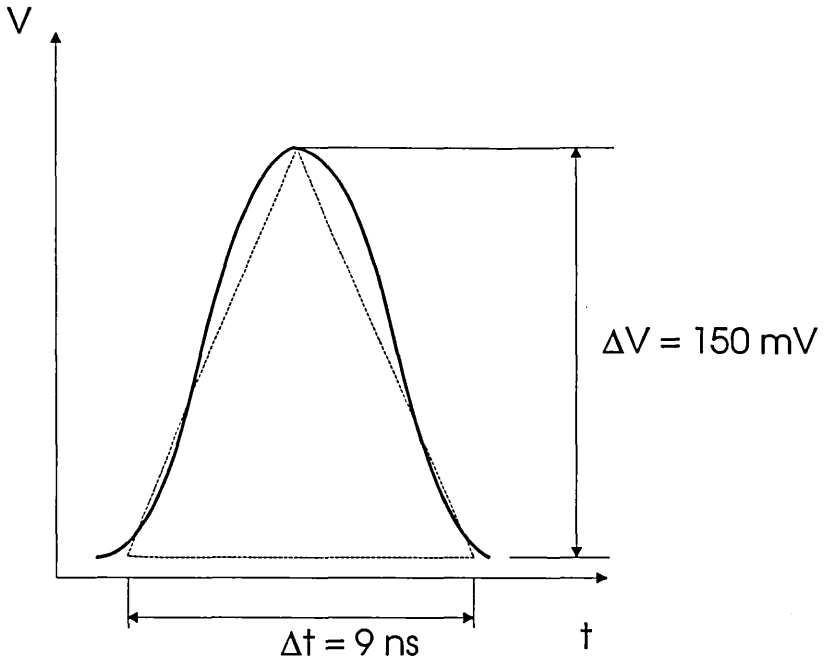

Fig. 6.12 Approximation used for dye laser calibration.

6.6.3 Current pre-amplifier

The sample photocurrent response is a low-level signal and requires amplification. However, the form of the sample signal poses difficulties for amplification due to the fact that the current can be large at short times, but very small at longer times. This means we need an amplifier in which we can vary the gain and bandwidth over a large range. To recover the photocurrent response at short times we require only a small gain but very fast response, whereas for the long time photocurrent response we require a high gain but do not want to overload the amplifier.

The preamplifier system used for all TPC work is based on a Burr-Brown OPA637 DIFET operational amplifier (fig. 6.13). This op-amp offers a useful combination of low current and voltage noise and low offset current, making it ideal for recovery of low-level photocurrents in high-impedance samples. The op-amp also displays good ac performance, with a high slew rate (100 V/μs) and gain-bandwidth product (80 MHz). Particular features of the circuit design include:

- A plug-in resistor network, allowing a variable current gain to be programmed. Values between 10^3 and 10^9 V/A were normally used. A small parallel capacitor was added on the low resistance settings to prevent high-frequency oscillation.

- An adjustable offset current of either polarity in the range 10^{-11} to 10^{-5} A can be combined with the incoming signal. This is useful in cases where the dark current is substantially larger than the photocurrent recorded in a transient photoconductivity measurement, or where a large optical bias is applied. The offset current retains a high stability due to the Zener stabilisation of the current supply.

Fig. 6.14 shows the measured risetimes of the amplifier plotted against the value of feedback resistor, R_f. It can be seen that high gain is achieved at the expense of amplifier response time.

It was found by the present author and by others (see Webb, 1994) that when amplifying steep power law photocurrent decays ($\sim t^{-1}$) the amplifier output signal can overshoot the input signal. Simulations show that for t^{-1} current decays the amplifier output voltage may not follow the input until ten times the rise time (Webb, 1994). Care was exercised during the course of TPC work to identify situations where this overshoot effect was occurring.

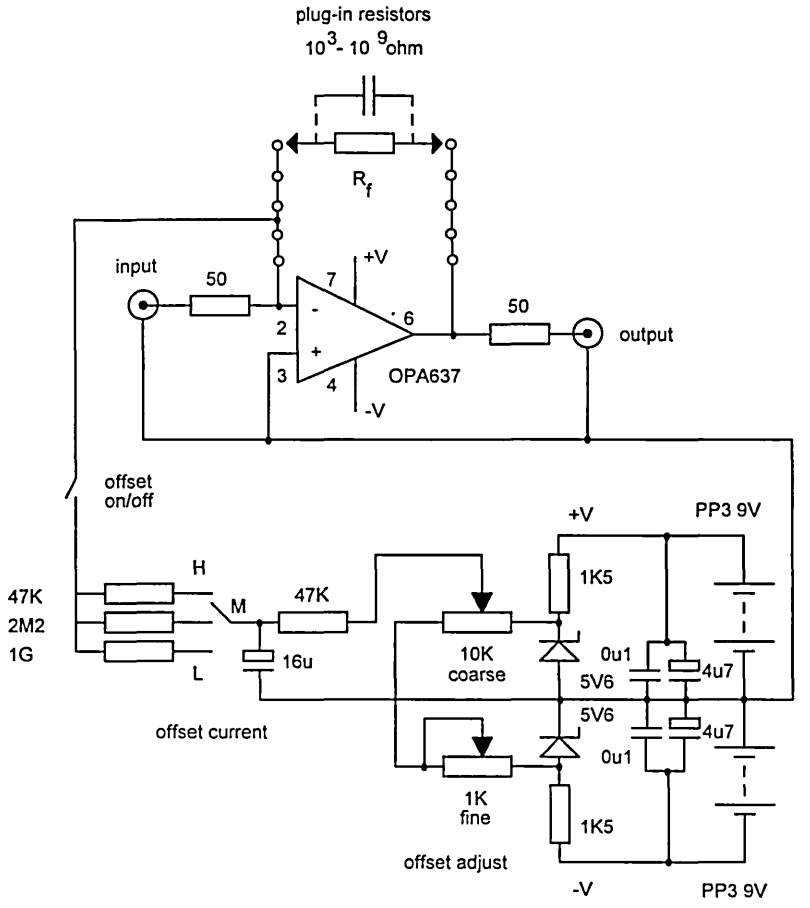

Fig. 6.13 Pre-amplifier circuit diagram.

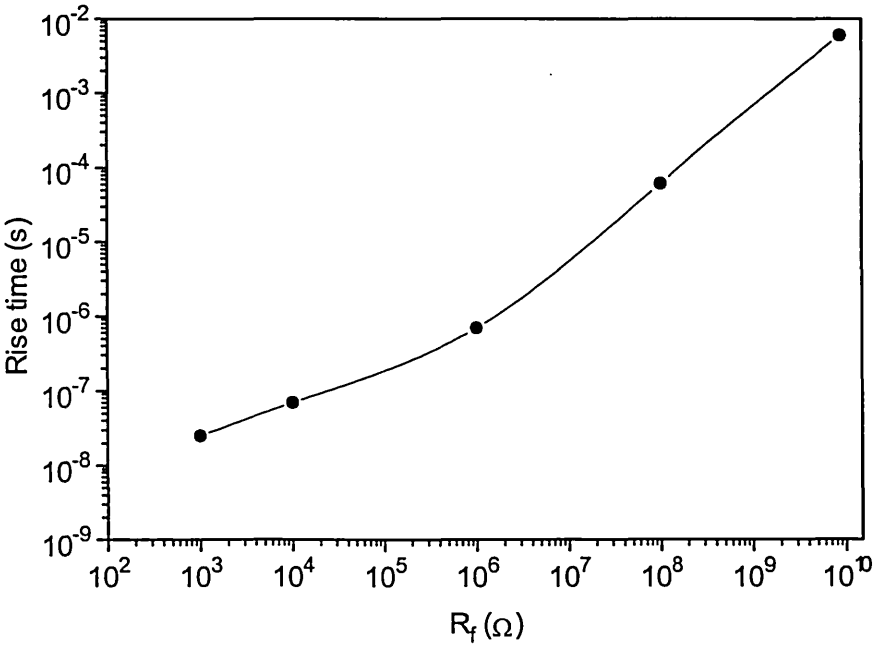

Fig. 6.14 Measured rise times of the pre-amplifier vs. feedback resistance.

6.6.4 Signal capture and processing

The DSO used for TPC was a Gould 4072, which is a two channel, 100 MHz machine and has a sampling range of 5 samples per second to 4×10^8 samples per second. The oscilloscope incorporates an 8-bit ADC and can store 1008 samples per scan on both channels.

For each sampling resistor employed in the pre-amplifier, the DSO voltage sensitivity and time base are set manually to obtain an acceptable signal. The computer is then instructed to fire the laser a specified number of times. After each laser pulse the DSO captures both the sample signal and the signal from the laser, which is used as the DSO trigger. Both channels of data are then transferred to the computer which averages the user-specified number of decays (multi-channel averaging). When the specified number of decays have been averaged the computer interrogates the DSO to determine the voltage sensitivity and the time base and calculates the current and sample time, the value of the sampling resistor and pre-amp gain are supplied by the user. The transient part of the signal is obtained by subtracting the steady state part, which is determined from 150 of the 200 samples recorded before the laser trigger is received. The program interrogates the user to determine the start of the transient decay, and then reduces the number of data points from 808 to 62 for plotting logarithmically by variable bandwidth digital filtering. In this technique all data points in an interval $t - \Delta t$ to $t + \Delta t$ (where $\Delta t \propto t$) are replaced by a single data point at time t, which is the average of the replaced data, this ensures that the smaller currents at long times undergo more averaging.

For the samples used in this work the transient response can be measured from ~ 10^{-8} to 10 s, normally about 30 decays are averaged for each time range setting. At longer times a pause of 100 times the time base setting was introduced between laser pulses to allow the sample to relax. At the longest times a "single shot" method was used because the signal tended to drift off the DSO screen, this could be prevented by using the off-set control on the pre-amp, but necessitated resetting the signal after each laser firing.

6.6.5 Measurements of decay from steady state

It has been found that on the removal of steady state illumination a very slow return to thermal equilibrium is exhibited by all the samples studied in this work. To study this decay more carefully a computer program was written by the author to sample the current at regular intervals after the computer-controlled removal of optical excitation, the program also controls the illuminating LED light source (Appendix C). The experimental set-up consists of a computer-controlled voltage source (Thurlby PL320) which drives the LED and an electrometer (Keithley 617 autoranging electrometer) which measures the sample current. The LED illuminates the sample via the light pipe arrangement described in § 6.5.1. A measurement of the sample dark current must first be made, which is later subtracted from the measured total current. On starting the program the user is prompted for the current sampling interval, in most cases an interval of 3 s is used, the program then asks the user for the illumination period, this was usually about 5 minutes to allow the sample to reach steady state (the current is measured when the LED is on but this is later discarded as only the decay from steady state is being considered). When the LED is turned off the timer resets and the current is sampled at the desired rate until two times the illumination period after which the current is sampled every 30 s; this is just for convenience when the data are plotted logarithmically, it also reduces the size of the data file if the current is sampled to very long times. (N.B. a logarithmically increasing time step was found to be inappropriate because it misses short time data).

PPC decays were measured as a function of temperature, illumination intensity and illumination period. The illumination intensity is changed within the controller computer program by changing the voltage supplied to the LED, which in turn changes the LED current and hence the photon flux.

6.7 Experimental difficulties

The main difficulty with obtaining experimental results on the samples studied in this work was that the currents are very small. The dark currents are typically around the picoamp range or smaller at room temperature which is not dissimilar to say a-Si:H for example. However, unlike a-Si:H which is a relatively good photoconductor in the oligomers studied here the photocurrents are in general not much more than an order of magnitude greater than the dark current. The currents are also found to be quite unstable and noisy, and reproducibility is poor. A partial way around this problem is to take measurements at high fields and temperatures and to use interdigitated samples, however this approach runs into difficulties because in general organic samples have low melting points and glass transition temperatures, and high fields can lead to dielectric breakdown. Thus the experimentally accessible field and temperature range is limited by material properties which means that obtaining representative results can be difficult. Furthermore, due to the relatively poor photoresponse, determination of the photocurrent by direct subtraction of the dark current from the total current can lead to errors.

Other difficulties encountered during the experimental work included the effects of ambient atmosphere and illumination on the measured dark current. Almost all measurements were performed under vacuum to minimise the effects of oxygen absorption by the films. However, when not being studied samples were not stored in an inert atmosphere, so it is very likely that the films contain a considerable amount of absorbed O_2. It was generally found that, after illumination, the current took an extended period of time to relax back to the thermal equilibrium value (persistent photocurrent). This will be discussed further in § 7.2.2, and it will suffice to mention here that raising the sample to elevated temperatures (annealing) increased the relaxation rate and enabled the dark current to be returned to approximately the initial value.

7. Experimental results and discussion

In this chapter the experimental results obtained on the pentacene and TVT samples studied in this work are presented. The results obtained from pentacene and TVT samples are, in the main, quite similar. Therefore, rather than presenting and discussing the data according to material, they are grouped under the generic headings of "steady state" and "transient" results. This approach has the dual advantages of avoiding substantial repetition and highlighting the similarities (and any differences) in behaviour.

Where appropriate, the transport models and numerical simulations introduced in earlier chapters are referred to in discussion of the results.

7.1 Steady state results

One of the characteristic features of these materials is that the time taken to achieve the steady state under given external conditions can be very long, particularly at low temperatures. This will be discussed in more detail in a later section but it should be borne in mind that difficulties in obtaining reproducible and believable results can arise as a consequence. Furthermore the accessible temperature and field range is quite limited, which can lead to inconclusive outcomes when comparing the fit of data to competing theories. These considerations should be kept in mind when studying the results.

7.1.1 Optical absorption and action spectra

Absorbance versus photon energy spectra at room temperature were obtained for all the samples studied. (Absorbance is defined as $\ln (I_0/I_t)$, where I_0 is the incident intensity and I_t is the transmitted intensity). The spectra were recorded using the metallised, thin film samples on glass, thus the resulting graphs will include absorptions due to the metal and glass, as well as the oligomer in which we are interested. Furthermore, reflection is not taken into account in the spectra. This should be taken into account when considering the graphs which should not be regarded as quantitative.

Figures 7.1 to 7.4 plot the absorption coefficient α vs. photon energy. This is to enable us to comment on the penetration depths of various photon energies later in this work. The absorption coefficient is obtained by dividing the absorbance by the sample thickness, *i.e.* $\ln (I_0/I_t) = \alpha d \therefore \alpha = \ln (I_0/I_t)/d$.

Unlike many of the other photoelectronic properties of the four oligomers studied the absorption plots exhibit distinctly different forms from material to material. The pentacene spectrum (fig. 7.1) is perhaps the most distinctive. The vibronic structure of the S_1 electronic state is prominent, with peaks at 1.88 eV, 1.97 eV, 2.14 eV and 2.30 eV, this is in agreement with the observations of other workers (see for example the work on pentacene crystals by Silinsh *et al.*, 1974).

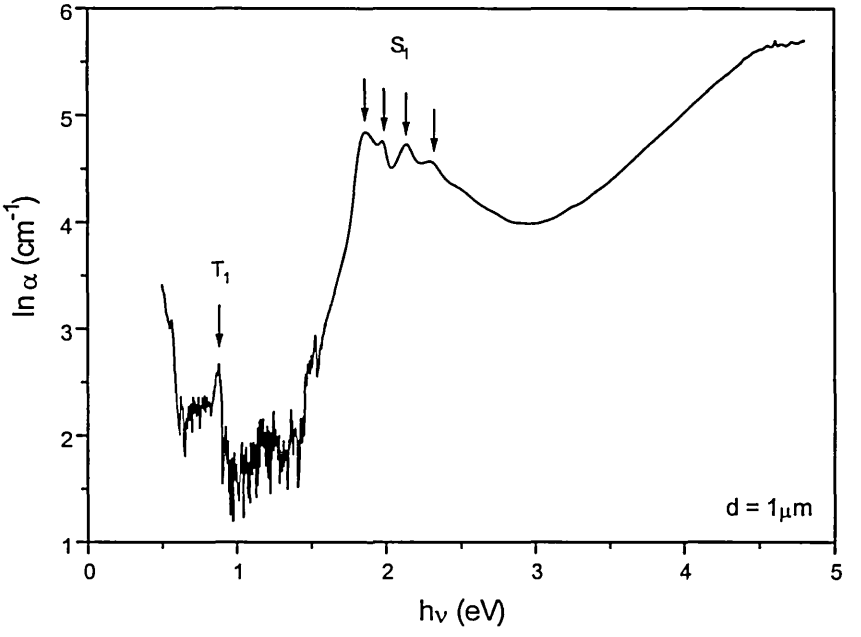

Fig. 7.1 Absorption coefficient vs. photon energy for pentacene thin film.

The first excited triplet state (T_1) for pentacene has been reported as lying at 0.81 eV by Geacintov *et al.* (1971); this is also in line with what we observe in fig. 7.1. The absorption spectra of the two TVT samples TVD and TVC are shown in figs. 7.2 and 7.3 respectively. These two materials have equal conjugation lengths (11 pi bonds) and should thus exhibit absorption edges at roughly the same energy, this is indeed the case as can be seen from the figures. Neither TVD nor TVC show any excitonic absorptions in contrast to pentacene. The flat absorption region in the TVC spectrum has not been

observed subsequently by the author and does not appear in transmission spectra performed on this material.

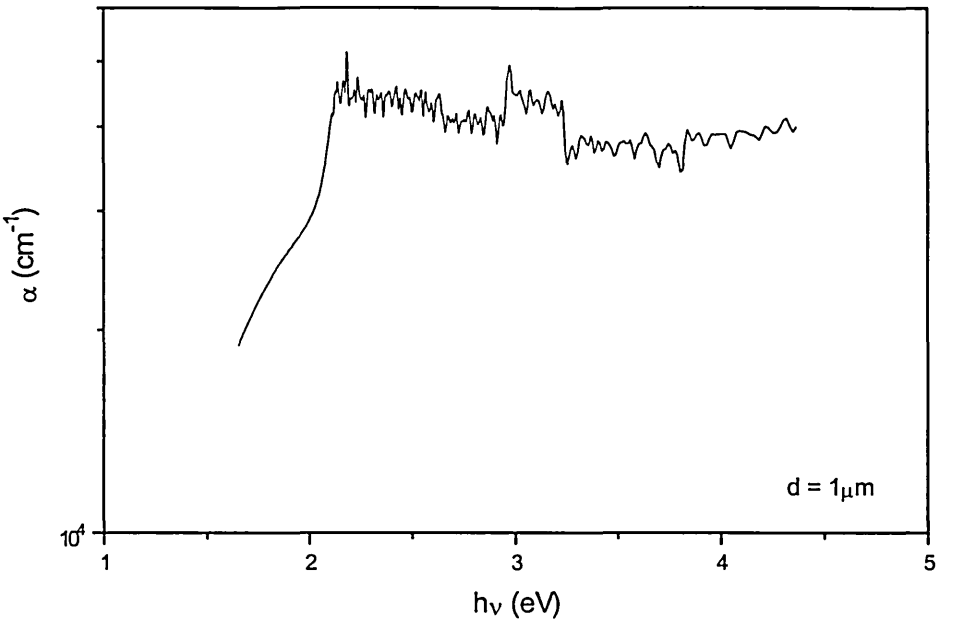

Fig. 7.2 Absorbance spectrum for TVD thin film.

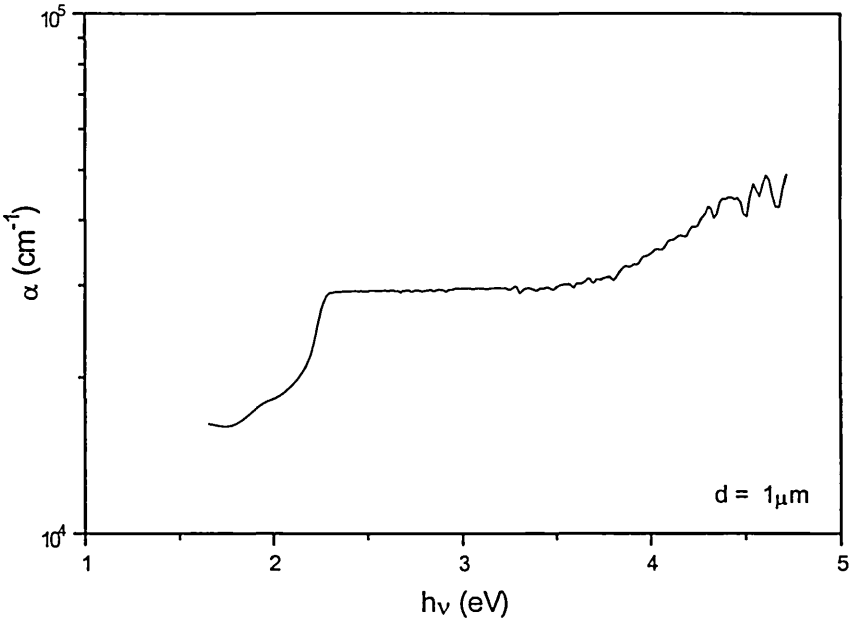

Fig. 7.3 Absorbance spectrum for TVC thin film.

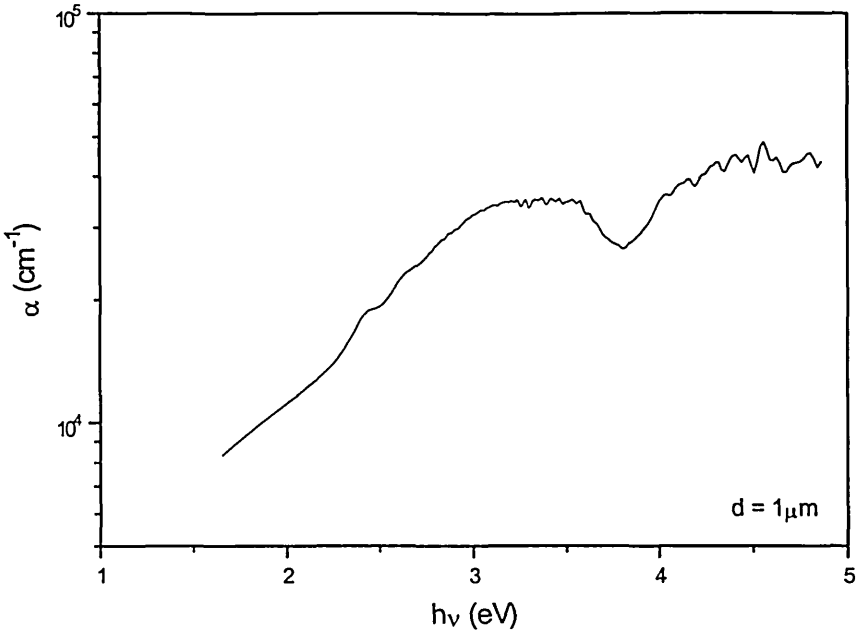

Fig. 7.4 Absorbance spectrum for TVB thin film.

It is therefore suggested that this feature is due to an experimental error of unknown origin and that the true absorption spectrum of TVC should be similar to that of TVD.

The final spectrum, shown in fig. 7.4, is that of TVB. As this material has one less double bond than the other samples its absorption edge should be displaced to higher energies. Absorption begins at about 2 eV, rising to a plateau region at 3 eV, there is then a dip in the absorption between ~3.5 and 4 eV after which the absorbance increases to an approximately constant value as the energy moves into the ultra-violet region.

In order to obtain more insight into the spectral response of the oligomers measurements of photocurrent action spectra (i_{pc} (λ)) were obtained. The utility of this method as compared to optical absorption is that it indicates in which portions of the spectrum absorption is leading to the production of mobile charge carriers. The action spectra for pentacene, TVB and TVC are shown in figs. 7.5-7.7, together with the absorbance plots for comparison. It was not found possible to obtain an action spectrum for TVD due to experimental difficulties arising from the high dark current relative to the photocurrent.

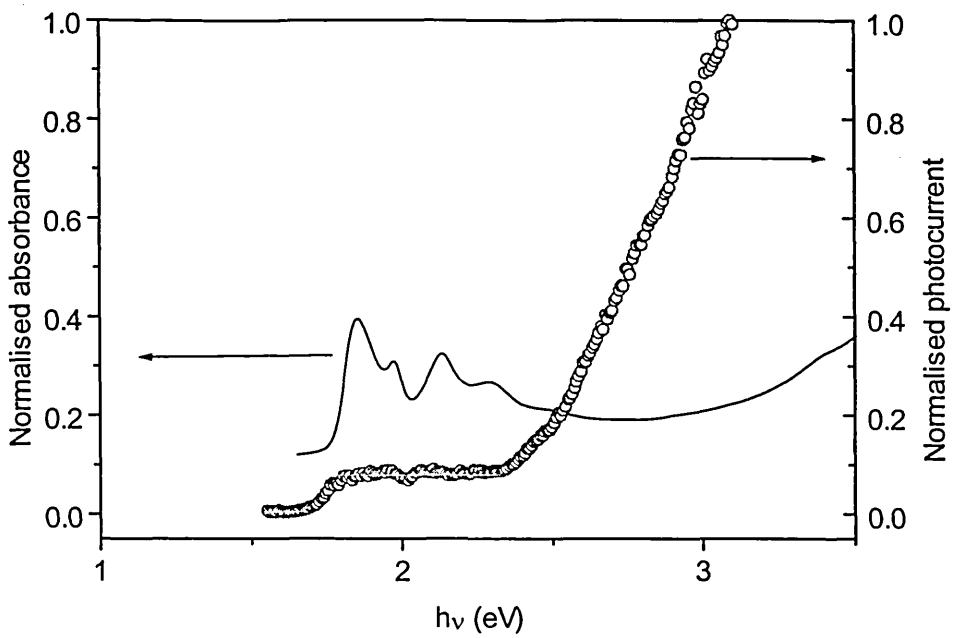

Fig. 7.5 Photocurrent action spectrum for pentacene.

It can be seen from figs. 7.6 and 7.7 that for TVB and TVC the photocurrent edge coincides with the absorption edge, whereas for pentacene (fig. 7.5) the photocurrent increases slightly with the first (singlet) excitonic absorption and is then approximately constant throughout the region of vibronic structure of the S_1 electronic transition. After ~ 2.4 eV the photocurrent rises to relatively high values. This result is again in agreement with the work of Silinsh *et al.* (1974) on crystalline pentacene who showed that in the S_1 absorption band the quantum efficiency is about 10^{-4}, but tends rapidly to unity at energies above ~2.2 eV. Thus the photocurrent rise above ~2.4 eV may be considered as an intrinsic photoconductivity threshold; in this region charge carrier generation is likely to occur by a mechanism similar to that described in § 4.2.2. Below 2.4 eV carrier generation is likely to proceed via the dissociation of triplet excitons (formed by S-T intersystem crossing) either at the sample surface or by interaction with trapped holes.

The TVB and TVC action spectra correlate with the absorption spectra and no excitonic absorptions are observed. It therefore seems likely that free charge carriers are produced at the absorption edge by the mechanism described in § 4.2.2.

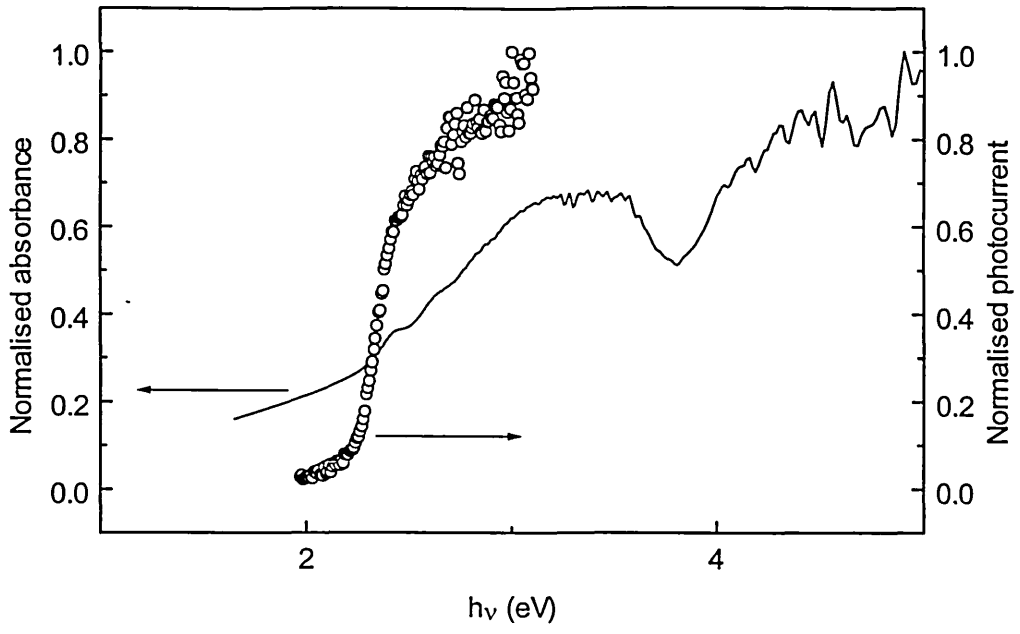

Fig. 7.6 Photocurrent action spectrum for TVB.

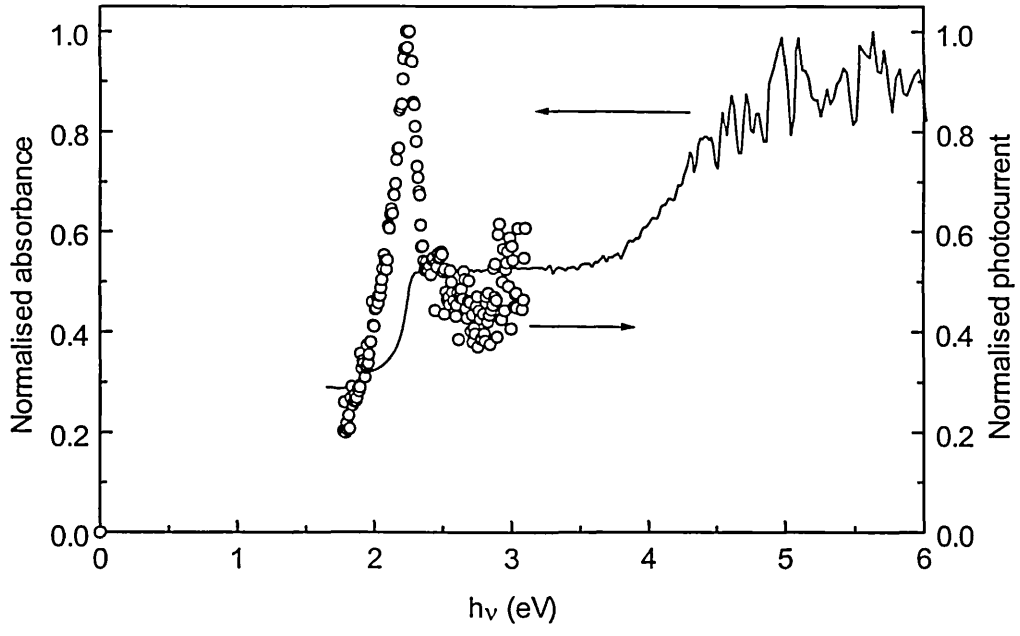

Fig.7.7 Photocurrent action spectrum for TVC.

The TVC action spectrum shows a sharp peak at the absorption edge, which is also observed using the constant photocurrent method (not shown here). A peak just below the absorption maximum has been observed by Lee, Yu and Heeger (1993) in poly(phenylenevinylene), PPV. They use the absorption plot to calculate the theoretical photocurrent response using DeVore's analysis and find a high degree of correlation between theory and experiment (DeVore, 1956). The peak is explained as arising due to enhanced surface recombination near the absorption edge. In the present case a similar situation may be appropriate, although it is unlikely that a conventional, semiconductor band-to-band carrier generation mechanism, assumed by DeVore's model, is appropriate for the oligomers. As has already been discussed, in molecular solids such as these carrier generation is more likely to occur by either exciton dissociation or by the modified autoionisation mechanism discussed in § 4.2.2.. Furthermore, DeVore's model assumes that the carrier diffusion length is large enough to enable carriers created in the bulk to diffuse to the surface. The validity of DeVore's model in these materials will thus also depend on the magnitude of the diffusion length. This may explain why surface recombination should be important in TVC but not in pentacene or TVB. It must be mentioned however, that the TVB action spectrum does not cover a large enough range to determine whether or not it peaks or saturates.

A noticeable absence from the absorption plots and action spectra (also CPM) presented in this section is the appearance of interference fringes. Such fringes are clearly visible in reflectivity data obtained from pentacene, but are not observed in transmission or absorption. The author is unable to explain this apparent anomaly, but would point out that other workers have obtained such interference-free absorption plots and action spectra on thin films (for example, Lee, Yu and Heeger, (1993), on thin films of PPV, although these authors mention interference fringes below the absorption edge which are not shown in their paper).

7.1.2 Functional dependencies of the dark current

The dependence of the dark current on field strength and temperature was measured for all samples under vacuum (10^{-3} torr). The majority of these measurements were performed using coplanar samples and these results will be presented in § 7.1.2.1, results obtained using sandwich samples will be presented for comparison in § 7.1.2.2. The experimental results dealing with the temperature dependence of the dark current are contained in § 7.1.2.2.

7.1.2.1 I-V characteristics of coplanar samples

Figure 7.8 illustrates the effect of annealing on the current-voltage (I-V) characteristic of thermally evaporated pentacene. It can be seen that heating the sample and then returning it to room temperature causes the dark current to decrease and stabilise. This was also found to be the case in the thienylene-vinylene oligomers. This "annealing" process was subsequently performed on all samples before any set of measurements were taken. The lower curve in fig. 7.8 was taken after the sample had been heated at 380 K, under vacuum, for one hour It can be seen that annealing has led to an order of magnitude decrease in the dark current, but without significantly affecting the functional form of the field dependence. In many cases annealing the samples led to an even greater decrease in the dark current (up to 3 orders of magnitude).

The field dependence of the dark current in the unannealed pentacene sample exhibits a linear, ohmic region at low fields which is symmetric about the origin, above about 2×10^4 V cm^{-1} this linear behaviour changes to a quadratic dependence on field, possibly indicative of space-charge limited (SCL) current flow. The field dependence in the annealed state is roughly similar. The low and high field slopes are slightly increased from their unannealed values and the transition region occurs at a slightly higher field.

The I-V characteristics of the thienylene-vinylene samples exhibit strikingly similar behaviour to those of pentacene with all samples showing a low-field approximately linear regime which begins to increase at about 2×10^4 V cm^{-1} to a steeper slope (see fig. 7.9).

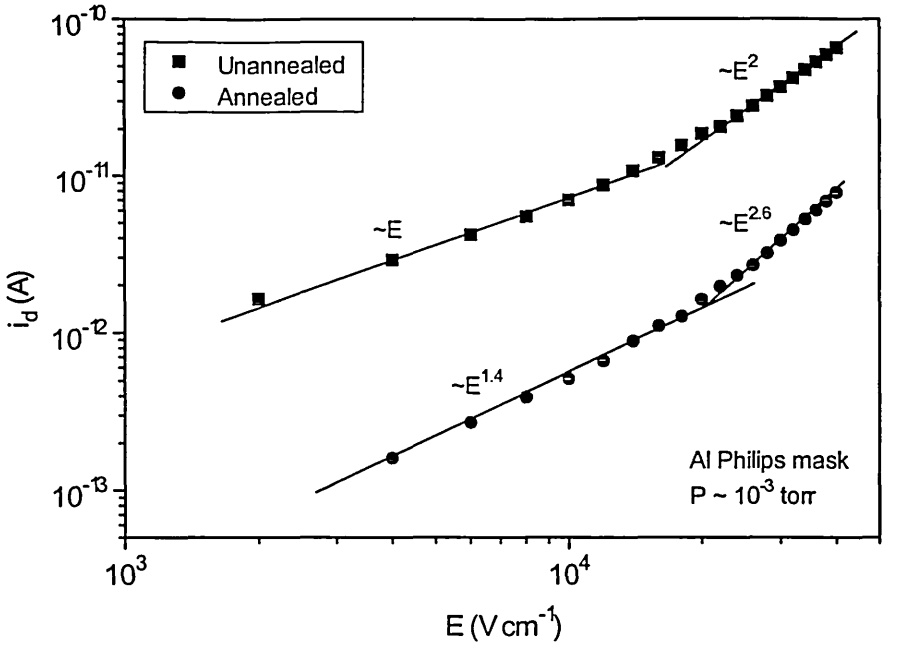

Fig. 7.8 Room temperature current-field plot for pentacene before and after annealing.

It can be seen that the lower the dark current in the ohmic regime the steeper the slope in the SCL regime, which may be an indication that the transition to the true SCL regime is more gradual for samples with a higher dark current. The transition voltage between each regime, V_t, is expected to scale with the dark carrier density, p_0, because the SCL regime begins when the injected carrier density exceeds the thermally generated carrier density (Kao and Hwang, 1981 chap3). Thus for pentacene we can see the SCL regime clearly because p_0 and thus V_t are small, while for TVD it could be argued that the slope is still increasing at the highest fields, *i.e.* the SCL regime has not yet been reached.

The magnitude of the dark current changes significantly between materials. Fig. 7.9 shows the dark currents of pentacene, TVB and TVC, which differ by only about a factor of ten in magnitude at any field, whereas that in TVD is several orders of magnitude higher. As the only difference between the TVC and TVD oligomers is the four methyl groups on TVD this result suggests that these substituents increase the carrier density. It is known that methyl groups are inductively electron donating and can activate aromatic rings (McMurry, 1992), a point to be discussed further in § 7.1.4. In the above discussion we have neglected any difference in mobility between the oligomers and it should be kept in mind that this would also affect the dark current magnitude.

A further point to note from fig. 7.9 is that the choice of electrode metal seems to have little effect on the field dependence of the dark current as can be seen from the TVB data. However, its effect on the dark current magnitude has not been studied for coplanar samples. Not shown in fig. 7.9 is the I-V characteristic for a laser ablated pentacene sample, however there is no significant difference between the I-V for this material and that for the thermally evaporated pentacene.

The magnitude of the dark current in the space-charge limited current regime can be used to estimate the effective carrier mobility via the equation

$$i_{SCL} = \frac{9}{8}\mu_{eff}\varepsilon_r\varepsilon_0 A\frac{V^2}{L_{gap}^{\ 3}} \tag{7.1}$$

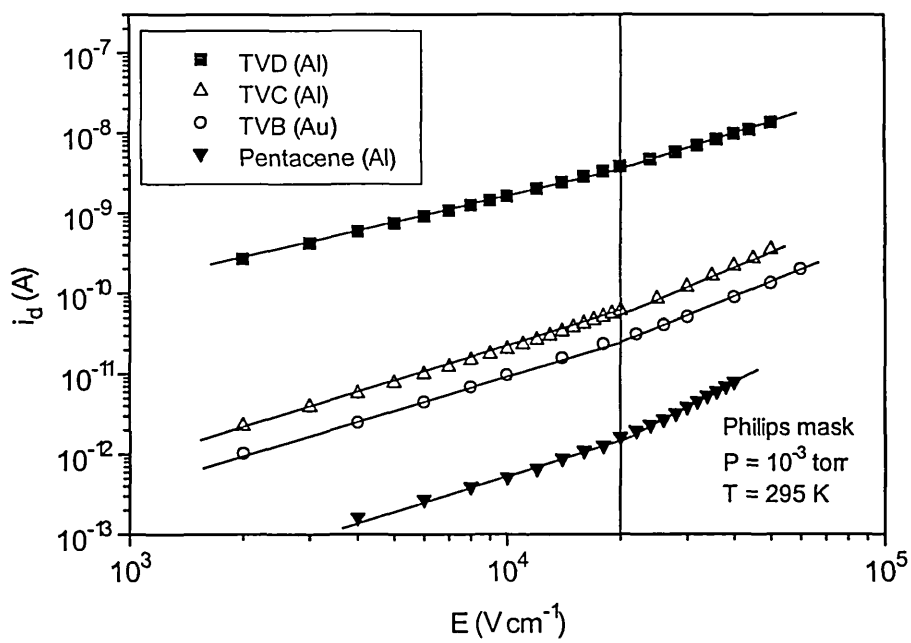

Fig. 7.9 I-V characteristics of all oligomers at room temperature. The vertical line indicates the field above which the current appears to become space-charge limited.

where i_{SCL} is the space-charge limited current, L_{gap} is the electrode gap and A is the conduction cross-section (Kao and Hwang, chap. 3, 1981). The quantity μ_{eff} is an effective mobility and is given by $\mu = \mu_0\,\theta$ in which θ is the ratio of free to trapped charge, given by $N_c/N_t\,\exp(-\varepsilon_t/k_BT)$, where N_t is the density of traps at energy ε_t. This equation is derived from a model with a single discrete trapping level and thus may be

inappropriate for these materials. However a similar equation is obtained in the case of a shallow, gaussian distribution of trapping levels, the difference entering through the effective mobility μ_{eff} (Kao and Hwang, chap. 3, 1981). Applying this equation to the unannealed and annealed pentacene data in fig. 7.8 yields mobilities of 8.1×10^{-7} cm^2 $(Vs)^{-1}$ and 9.6×10^{-8} cm^2 $(Vs)^{-1}$ respectively, using $\varepsilon_r = 3$. Making use of the conductivities the corresponding carrier densities are 1.31×10^{13} cm^{-3} and 1.24×10^{13} cm^{-3} for the unannealed and annealed samples respectively. Thus annealing the sample decreases the mobility by almost an order of magnitude, whereas the change in the carrier density is comparatively small, so the decrease in the conductivity is mainly due to the mobility. The effects of annealing will be discussed further in § 7.1.4.

Fig. 7.10 shows I-V characteristics for TVC parametric in temperature. It is evident that increasing the temperature increases the magnitude of the dark current, but it is not overly clear what effect it has on the slopes of the curves. The ohmic regime seems to be unaffected, but there is a suggestion of a slight decrease of the SCL regime slope with increasing temperature. Unfortunately none of the I-V data obtained on the oligmers is of sufficient quality to verify this. The value of the transition voltage V_t, from the ohmic to the SCL regimes is given by

$$V_t = \frac{8}{9}\frac{ep_0 L_{gap}^{\ 2}}{\theta \varepsilon_r \varepsilon_0} \tag{7.2}$$

where p_0 is the density of thermally generated holes, and θ is defined as in eq. 7.1 (Kao and Hwang, chap. 3, 1981). Changing the temperature does not seem to have a significant effect on the transition voltage, V_t, suggesting that p_0 and θ may have similar temperature dependencies. This might be the case if holes are produced by promotion of electrons to an acceptor level or an empty trapping level, *i.e.* p_0 and θ are both proportional to $\exp(-\varepsilon_t/k_B T)$.

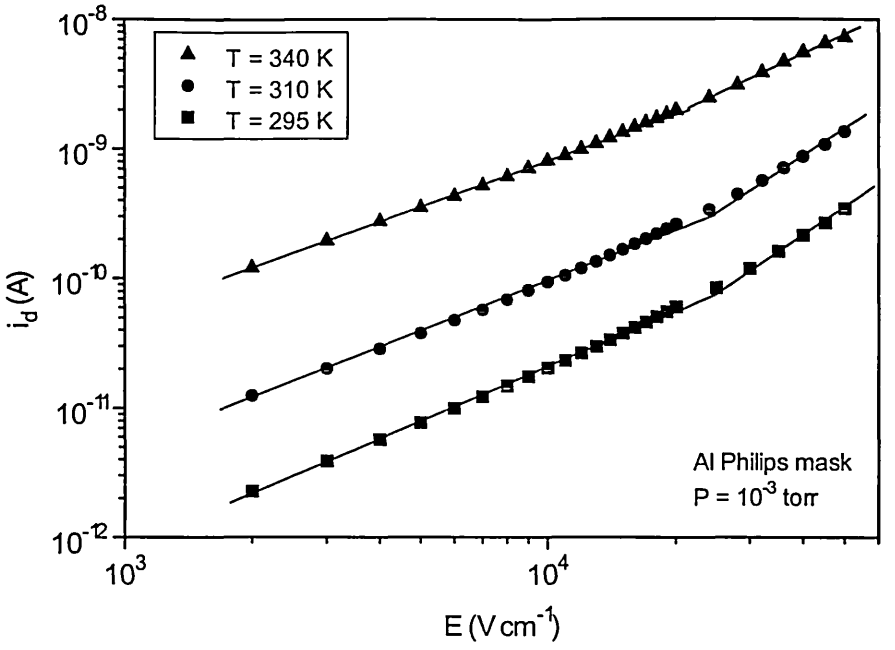

Fig. 7.10 I-V characteristic for TVC parametric in temperature.

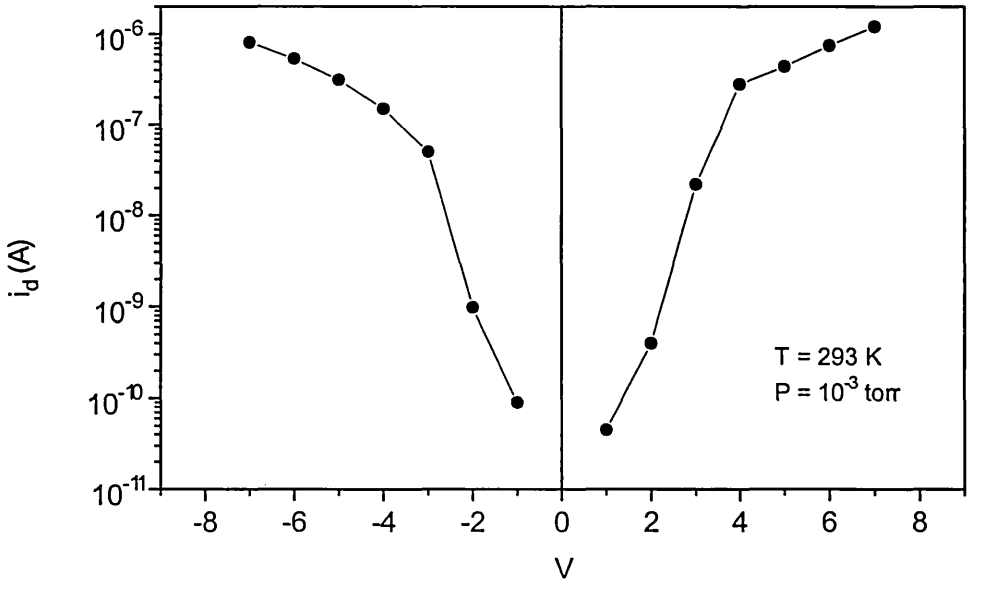

Fig.7.11 Room temperature I-V characteristic for an Al/TVD/Al sandwich sample.

7.1.2.2 I-V characteristics of sandwich samples

The results presented so far were obtained on samples with aluminium and gold coplanar and Philips mask electrodes. It would thus appear that these metals provide an ohmic contact to the oligomers at low fields in a coplanar configuration, however the I-V characteristics of samples in a sandwich configuration are quite different.

Fig. 7.11 shows an I-V characteristic for an Al/TVD/Al sandwich sample, recorded under vacuum. It can be seen that in this configuration the current increases very rapidly with voltage, then begins to level out at about ± 4 V. This suggests that the contacts are important in controlling the current at low fields, and as the voltage is increased beyond 4 V the smaller slope corresponds to the voltage drop across the bulk oligomer. This situation can be appreciated by considering the equivalent circuit of fig. 7.12. At low fields the contacts dominate and the majority of the voltage is dropped across this interface, this corresponds to the voltage drop across the diodes (fig. 7.12) and results in the rapidly increasing portion of the I-V. At higher fields the diodes are strongly conducting and the majority of voltage is dropped across the oligomer, this corresponds to the voltage dropped across the resistor.

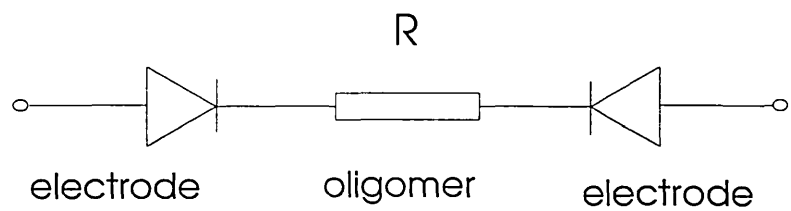

Fig. 7.12 Equivalent circuit for metal/oligomer/metal sandwich sample.

The reduction in slope at high fields is approximately quadratic and begins at ~ 4 V (2×10^4 V cm^{-1}), as in the coplanar samples. As there can be no fundamental difference between the electrode-oligomer interface in both sample configurations the different I-V characteristics obtained for sandwich and coplanar structures must be due to the differing geometries of the samples. It is possible that in the coplanar structures, at low fields, the contact is "blocking" to a certain extent, however, the ratio of the electrode-oligomer contact area to the conduction cross-section is large, providing ample charge carriers. In the sandwich samples, however, the conduction cross-section and contact area are equal which will tend to accentuate the blocking nature of the contact.

The I-V curve in fig. 7.11 is roughly symmetric about the origin, slight differences may be due to the fact that for the bottom electrode the oligomer is deposited onto the metal, whereas the reverse occurs for the top electrode In this sample exposure to oxygen has little effect on the I-V characteristic.

The above characteristic should be compared to that in fig. 7.13 for an Al/TVD/Au sample (Au underneath oligomer). In this case the curve is not symmetric about the origin and exposure to ambient atmosphere has a profound effect on the shape of the curve. In air the forward current (Au +ve) is similar to that in the Al/TVD/Al sample, *i.e.* the current increases very rapidly then tails off (the last three data points are roughly linear). In the reverse direction the current increases much more slowly with field. This I-V characteristic is similar to that of a Schottky barrier exhibiting ohmic effects at high fields (Streetman, 1995). Similar current-voltage characteristics have been observed in PPV sandwich samples with Al and ITO electrodes (Antoniadis *et al.*, 1994), although these workers did not observe the ohmic region at high fields.

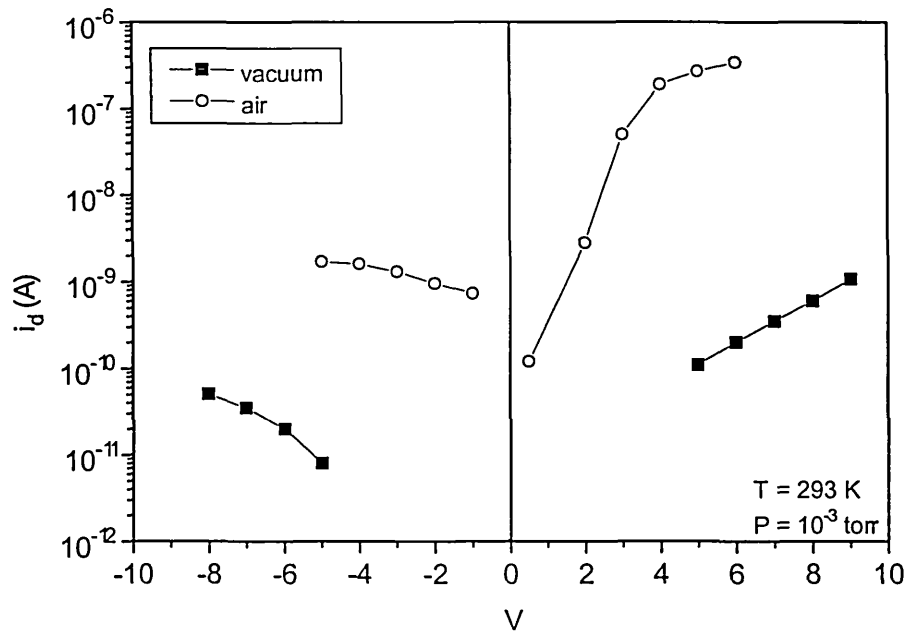

Fig. 7.13 Room temperature I-V characteristic for an Al/TVD/Au sandwich sample measured under vacuum and ambient atmosphere. Forward bias corresponds to Au positive.

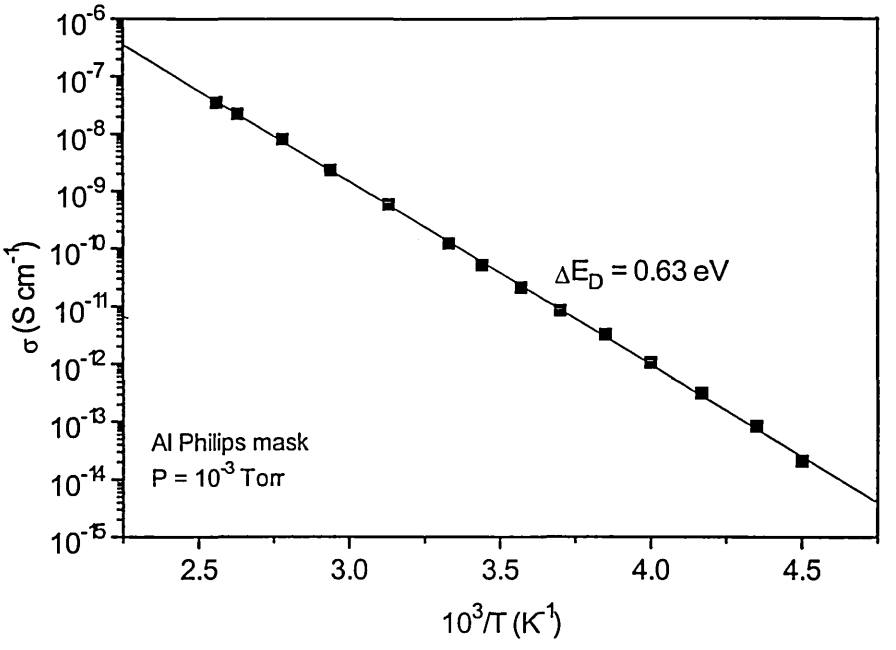

Fig. 7.14 Dark conductivity temperature dependence for a coplanar TVD sample.

Under vacuum the I-V curve again shows rectifying behaviour, but in this case the turnover at high voltages representing the ohmic volt drop across the oligomer is absent. These data suggest that some sort of interfacial effect is occurring when the Al/TVD/Au sample is exposed to air which reduces the barrier to charge injection. An analogous situation to this has been observed by Gailberger *et al.* (1992) who suggested that the accumulation of O_2^- at the electrode-polymer interface in PPV leads to hole injection into the polymer film (see § 7.1.4).

7.2.1.3 Dark current temperature dependence

The dark current is quite strongly thermally activated as can be seen in fig. 7.14 which shows data obtained for a coplanar TVD sample. In general the dark conductivity of most organic semiconductors can be given by the expression

$$\sigma = \sigma_0 \exp\left(-\frac{\Delta\varepsilon_\sigma}{k_B T}\right) \tag{7.3}$$

where σ_0 is the pre-exponential factor, and $\Delta\varepsilon_\sigma$ is the activation energy. The activation energy obtained from the slope of the line is 0.63 eV. Table 7.1 shows the activation energies and the pre-exponential factors σ_0 obtained from Arrhenius plots for the other materials. All values are from samples with a coplanar configuration.

It can be seen that the oligomers all have activation energies close to 0.65 eV, the estimated errors in the values being small. The laser ablated pentacene sample shows a higher activation energy of 0.79 eV. The higher activation energy of the laser ablated pentacene may be due to the fact that this was deposited at 100 ^{0}C, whereas all the other samples were deposited at room temperature. It is also possible that it is an effect of the actual deposition process itself.

The origin of the activation energy in amorphous, inorganic semiconductors has already been discussed in § 4.1. According to this model $\Delta\varepsilon_\sigma$ will have different values over different temperature regions depending on the energy of the dominant transport path relative to the Fermi level. The data in fig. 7.14 show only one value for the activation energy, implying that over this range the transport path does not change. The value of the activation energy is too small to represent the depth of the intrinsic Fermi level (intrinsic band gap > 2 eV for all oligomers).

Oligomer	$\Delta\varepsilon_\sigma$ (eV)	σ_0 (S cm^{-1})
TVB	0.67+/-0.030	0.73
TVC	0.64+/-0.008	0.60
TVD	0.63+/-0.011	5.50
Pentacene (laser ablated)	0.79+/-0.026	0.62
Pentacene (TE)	0.66+/-0.013	0.02

Table 7.1 Dark current activation energies and pre-exponential factors for coplanar samples.

However, if the material is p-type, it may represent the approximate depth of the Fermi level from the (valence band) mobility edge. If carrier generation is due to promotion of electrons to acceptor levels then it is likely that the Arrhenius plots would show a two slope form, with a low temperature shallow slope representing ionisation of acceptor levels, and a high temperature steep slope corresponding to intrinsic band-to-band

carrier generation. No evidence of this is seen in the Arrhenius plots, but again this may be due to the small temperature range over which useful data can be obtained.

Alternatively, it may indicate the transport level for hopping in a band tail. In such a case the conductivity activation energy is the sum of a hopping activation energy at the transport level (W) and a thermal excitation energy, which corresponds to the energy difference between the Fermi level and the transport level, *i.e.* $\Delta\varepsilon_\sigma = (\varepsilon_t - \varepsilon_f + W)$.

In organic semiconductors, and hopping systems in general it is usually found that the mobility is temperature dependent (*e.g.* $\ln \mu \propto T^{-2}$ in the DLH theory, § 4.4.2), and thus the activation energy is likely to depend on $\mu(T)$ and $n(T)$. For the DLH theory, as already discussed, the mobility activation energy is itself temperature dependent which would result in curvature in an Arrhenius plot for the mobility. However, the form of an Arrhenius plot for the conductivity would depend on whether the mobility or the carrier density dominates in the overall temperature dependence of the conductivity. The data in fig. 7.14 do not show any curvature which might suggest a temperature dependence of the mobility, but this may be because the data are restricted to a small temperature range. The DLH theory predicts that after a temperature dependent time interval the hopping carriers will thermalise at an energy given by eq. 4.52, the system is then in steady state and transport proceeds by excitation of carriers to a transport level. This process is known as trap-controlled hopping. At this point the DLH theory predicts a similar sort of transport process to the case of band tail hopping as discussed above. This situation predicts the non-Arrhenius temperature dependence of the mobility, *i.e.* the mobility depends on W. However the conductivity depends on $(\varepsilon_t - \varepsilon_f + W)$ and is likely to be dominated by $(\varepsilon_t - \varepsilon_f)$, thus swamping the mobility field dependence.

The pre-exponential factors given in table 7.1 are too small to represent band transport, in this case they would be expected to be several orders of magnitude higher than those obtained (Mott and Davis, 1979, § 6.4.3). For band tail hopping the pre-exponential factor is given by

$$\sigma_0 = g(\varepsilon_t)\frac{1}{6}e^2 R_{ij}{}^2 \upsilon_0 \exp(-2\alpha_{loc}R_{ij}) \qquad (7.4)$$

thus σ_0 depends only on the density of states at the transport level and on the attempt to escape frequency (R_{ij} depends on $g(\varepsilon_t)^{-1/3}$). The values obtained experimentally are of

the expected order of magnitude for band tail hopping. The activation energies for all the oligomers (excluding LA pentacene) are very similar suggesting that the transport level does not vary significantly between materials. In turn this implies that the variation in the dark conductivities between the oligomers is mainly due to σ_0, and thus the density of states at the transport level.

There are several other possible origins of the activation energy:

1. $\Delta\varepsilon_\sigma$ corresponds to the depth of trapping levels from the band edge, *i.e.* conduction involves band-like transport and is dominated by thermal release of trapped carriers.
2. $\Delta\varepsilon_\sigma$ may correspond to the height of the potential barrier between the electrode and the solid specimen which must be overcome for carrier injection from the electrodes, *i.e.* the effects observed are not bulk phenomena.

Some authors have suggested that the activation energy in a similar type of material, α-sexithiophene gives the depth of trapping levels (Sen *et al.*, 1994, Horowitz *et al.*, 1990). These authors have reported values of 0.73 eV and 0.28 eV respectively, which suggests that the activation energy is dependent on either deposition conditions (which may affect the trap depth and/or density), or the sample configuration (*i.e.* coplanar/sandwich, electrode material, sample thickness, *etc.*). The former authors use finely powdered thin films in a sandwich configuration, whereas Horowitz *et al.* use thermally evaporated films.

Activation energies measured using sandwich electrode structures give values that appear to be dependent on the polarity of the electrode metal. Fig. 7.15 shows Arrhenius plots for an Al/TVD/Au sample with the gold electrode positive and negative. When the Au electrode is positive (hole injecting) a small value for the activation energy is obtained (0.38 +/- 0.03 eV), whereas making the gold electrode negative results in a high activation energy (0.85 +/- 0.03 eV), sadly neither of these values is close to that obtained with a coplanar structure. These different values for the activation energy reflect the asymmetry of the I-V characteristic, with the gold electrode positive hole injection is relatively efficient and the activation energy is low, whereas with the aluminium electrode positive hole injection is relatively inefficient and the activation energy is high.

If, in the case of the sandwich structures, the dark current at a given field is controlled by interfacial effects then the values of the activation energies are likely to

reflect the barrier heights to hole injection at each electrode. The barrier height can be given by

$$\varphi_B = \varepsilon_g - (\varphi_m - A_c) \tag{7.5}$$

where φ_B and φ_m are the barrier height and metal work function respectively, ε_g is the band gap and A_c is the electron affinity (Sze, 1985). Equation 7.5 is valid for p-type semiconductors. The work functions for Al and Au are 4.2 eV and 5.1 eV respectively, ε_g for TVD is ~2.2 eV and we assume that the electron affinity of TVD is similar to that of pentacene for which a value of 2.8 eV has been quoted (Gutmann and Lyons, 1981). Substituting in these values we obtain a barrier height of ~ 0.8 eV for Al which is close to the experimental activation energy. However for Au we obtain a negative barrier for hole injection, this possibly implies that the gold electrode is hole injecting (rather than ohmic or blocking). In the present context eq. 7.5 should in no way be considered quantitative, it is obviously a gross simplification of the real oligomer-metal interface, yet it does appear to demonstrate the rectifying nature of the Al/TVD/Au sample.

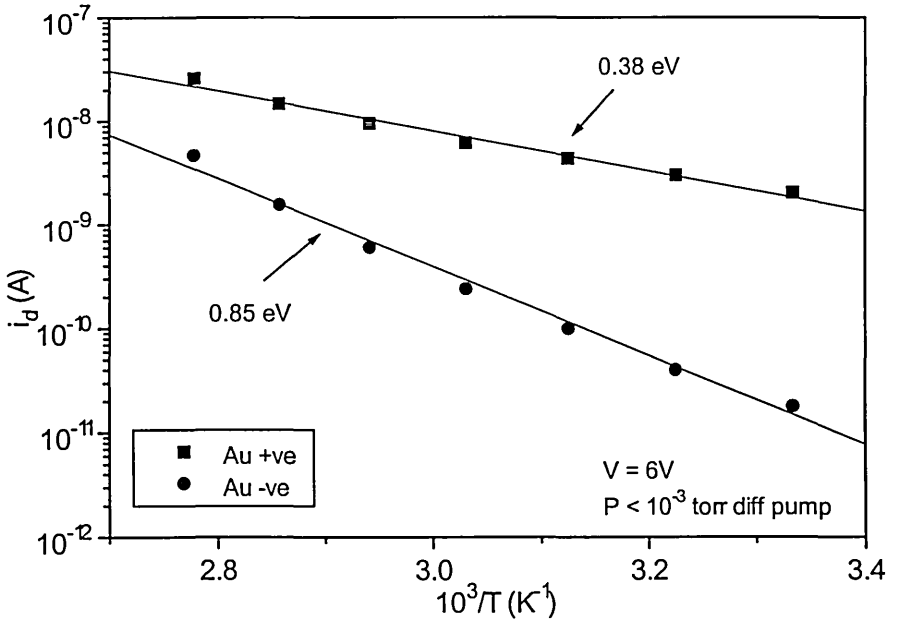

Fig. 7.15 Arrhenius plots for Al/TVD/Au sandwich sample with each electrode +ve.

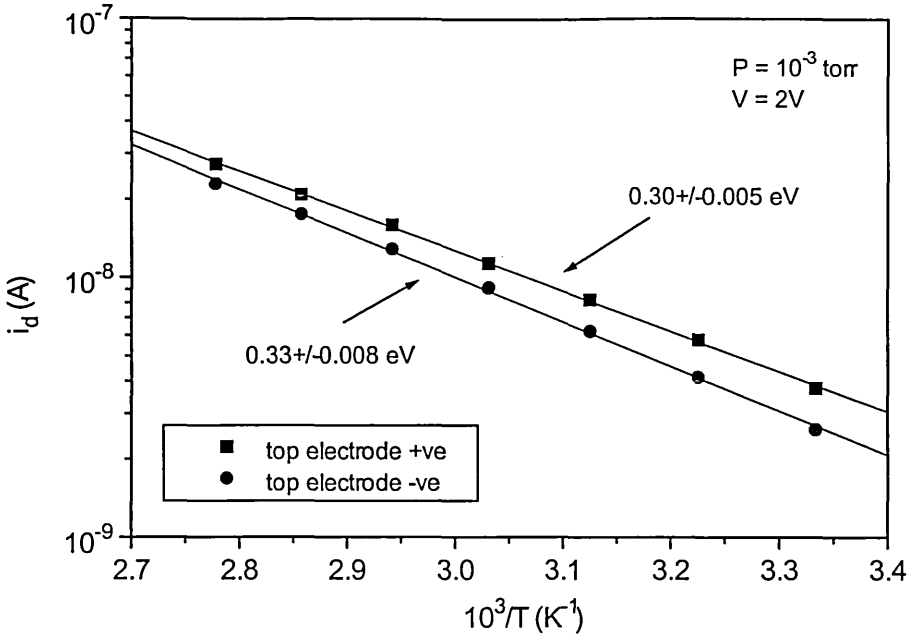

Fig.7.16 Arrhenius plots for Al/TVD/Al sandwich sample with each electrode +ve.

The Al/TVD/Al sample yields an Arrhenius plot in which the activation energy is approximately 0.3 eV at 2V, irrespective of which electrode is positive (fig. 7.16). In this case the similar activation energies reflect the symmetry of the I-V characteristic. If it is assumed that the bulk oligomer activation energy is that obtained with the coplanar samples, then it may be argued that this smaller activation energy is due to a different temperature dependence of the dark current in the electrode limited regime (in which this data was measured). Measurement of the activation energy above ~ 4 V would be expected to yield the temperature dependence of the SCL current regime. However measurement of the activation energy in the voltage range 2-10 V in both directions yielded similar values of around 0.3 eV. It can only be suggested that annealing the sample changes the I-V characteristic in the sandwich configuration: the I-V curve of fig. 7.11 was recorded before the sample was annealed. Indeed later current-voltage measurements on the Al/TVD/Au sample yielded a forward current which did not increase as rapidly at low fields, nor did it show a distinct turnover in the voltage range up to 10 V. Thus annealing perhaps increases the range of electrode-limited behaviour

to higher voltages. This might be expected if annealing removes absorbed oxygen, which was suggested earlier to reduce the range of electrode-limited behaviour.

It was seen earlier in this section that varying the temperature had no noticeable effect on the low field (ohmic) slope of the I-V curves obtained on coplanar samples, and only a slight effect on the SCL regime slope. However changing the field strength does have seem to have a small but noticeable effect on the slope of the σ_d (T) curves as can be seen in the extrapolated Arrhenius plots for TVB shown in fig. 7.17 (note that the high field curve is obtained in the space-charge limited regime). In a simple situation with no mobility field dependence increasing the field would simply be expected to increase the dark current magnitude, thus in the ohmic regime σ_d (T) curves should overlap and in the SCL regime they should scale linearly with field. This is clearly not the case; increasing the field strength decreases the activation energy and causes the extrapolated curves to intercept each other (at ~ 763 K). This phenomenon of a reduction in the activation energy with field is reminiscent of μ_d (T) curves for MDPs which intercept at a characteristic temperature and mobility (§ 4.4.1). In these cases the activation energy decreases because in hopping transport an increased field reduces the average barrier height for energetic uphill jumps. In the present case this result is perhaps a further argument in favour of carrier motion occurring by trap-controlled hopping. Increasing the field is unlikely to affect thermal excitation to the transport level, *i.e.* $(-\varepsilon_f - \varepsilon_t)$ is not dependent on field, but the hopping energy, W, will be reduced by the application of a field and will thus decrease the overall value of the activation energy $(-\varepsilon_f - \varepsilon_t + W)$. (Note that because W is predicted to be much less than $(-\varepsilon_f - \varepsilon_t)$ the change in conductivity activation energy with field will be small, extrapolation of the data as in fig. 7.17 shows much more clearly the change in slope which is not easily observed over the measured range.)

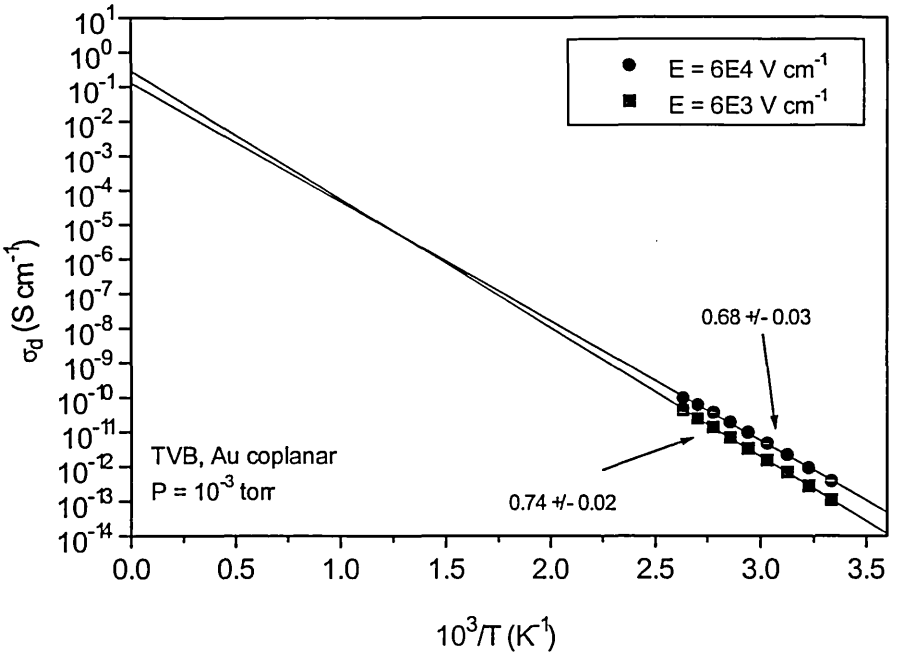

Fig. 7.17 Arrhenius plots for TVB parametric in field, extrapolated to T = ∞.

From the above results it can be seen that only the coplanar samples exhibit an ohmic regime, they also all show a transition to a SCL current regime. Since it is likely that both these currents are attributable to bulk rather than interfacial effects it is suggested that the activation energy measured for these samples is the true bulk activation energy. The activation energies obtained from the sandwich samples are affected by the nature of the metal-oligomer contact. The absolute value of the activation energy appears to be field dependent but is too large to simply be due to hopping motion. Thus it is suggested that carrier motion occurs by trap-controlled hopping, the magnitudes of the mobilities measured using eq. 7.1 in the SCL regime and the pre-exponential factors given in table 7.1 are also indicative of hopping transport.

7.1.3 Functional dependencies of the photocurrent

The steady state photoconductivity of the oligomers studied at room temperature is generally in the range from 10^{-12} to just over 10^{-10} S cm^{-1} (for a flux of 2×10^{15} cm^{-2} s^{-1} at 450 nm), and is larger than the dark current for all samples, except TVD, in which the dark current is relatively large as noted in the last section. The photocurrent is also large in TVD but is swamped by the dark current at ambient temperatures unless the flux is very high. The dark current can become larger than the photocurrent within the experimentally accessible temperature range in some samples as will be seen later. Table 7.2 shows the dark and photoconductivities measured at room temperature for all the oligomers. All data were obtained using coplanar samples of approximately 1 μm thickness.

Oligomer	σ_d (S cm^{-1})	σ_{pc} (S cm^{-1})	σ_{pc}/σ_d
TVB	5.6×10^{-12}	3.5×10^{-11}	6.25
TVC	6.3×10^{-12}	9.1×10^{-12}	1.4
TVD	1.6×10^{-10}	1.2×10^{-10}	0.75
Pentacene (TE)	2.4×10^{-13}	1.1×10^{-10}	458.3

Table 7.2 Room temperature dark and photoconductivities. Photoconductivities measured at a photon flux of 2×10^{15} cm^{-2} s^{-1} at 450 nm.

Using the ratio of photo to dark conductivity as a guide to photosensitivity, from table 7.2 it can be seen that thermally evaporated pentacene is the most photosensitive sample for this set of conditions, whereas TVD is relatively insensitive to illumination. The very low value for σ_{pc}/σ_d obtained for TVD highlights the difficulty encountered when trying to obtain CPM and photocurrent action spectra for this material at room temperature (see § 7.1.1).

The value of the photocurrent in the ohmic regime is given by

$$i_{pc} = eF\alpha\eta\mu\tau_r EA \tag{7.6}$$

where η is the quantum efficiency for carrier generation, α is the absorption coefficient F is the photon flux and τ_r is the carrier lifetime. From eq. 7.6 it can be seen that the

value of the photocurrent does not depend directly on the value of either temperature or wavelength, although in the ohmic regime it is directly proportional to the field strength (cf. eq 7.2 for space charge limited current). The temperature, intensity and wavelength dependencies of the photocurrent are thus due to the dependence of other terms in eq. 7.6 on these variables. Changes in temperature are only likely to affect the quantum efficiency, the mobility and the carrier lifetime; whereas changes in wavelength should only have an effect on the absorption coefficient (which we already know qualitatively), and possibly the quantum efficiency, depending on the mechanism of photogeneration. Changes in illumination intensity affect the overall carrier density and thus the carrier lifetime We can therefore write down the following functional dependencies for the photocurrent,

$$i_{pc}(T) \propto \eta(T)\mu(T)\tau_r(T) \tag{7.7}$$

$$i_{pc}(\lambda) \propto \eta(\lambda)\alpha(\lambda) \tag{7.8}$$

$$i_{pc}(F) \propto \tau_r(F) \tag{7.9}$$

Consideration of relations 7.7, 7.8 and 7.9 reveals further interrelations between variables. For instance, an increase of the quantum efficiency, leading to an increased carrier density, could alter the carrier lifetime; or an increases in α with wavelength could result in surface recombination, again affecting the carrier lifetime.

The field dependence of the photocurrent in all the oligomers is similar to that for the dark current as can be seen in fig. 7.18, which shows data for thermally evaporated pentacene.

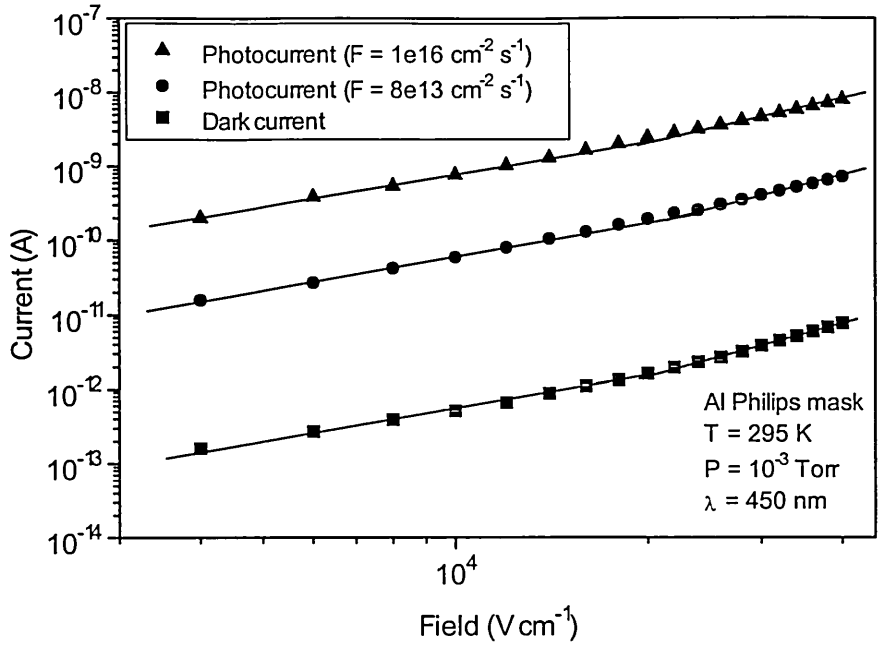

Fig. 7.18 Field dependence of the dark and photocurrents for thermally evaporated pentacene.

The photocurrent retains a two-slope form, similar to the dark current and the transition field between each regime is close to that for the dark current. Increasing the illumination intensity has negligible effect on the field dependence, however the data suggest that it decreases the transition voltage, although the effect is small and the exact shift is difficult to determine from the experimental data. Similar behaviour was observed in all the oligomers. Fig. 7.19 shows data for TVB.

Under illumination the total carrier (hole) density is increased from the dark carrier density p_0 to $(p_0 + \Delta p)$, where Δp is the photogenerated carrier density. Since the space-charge-limited current regime begins when the injected carrier density dominates the conductivity, in the trap-free case ($\theta = 1$) illuminating the material will increase the transition voltage V_t. However, if the material contains traps the situation is more complicated. From eq 7.2 for a single trapping level the transition voltage under illumination will be proportional to the total free carrier density p_{free}, and inversely proportional to the ratio of free to trapped charge θ. The negligible difference between the transition voltage for dark current and photocurrent at various levels of illumination intensity suggests that the ratios $(p_{free}/\theta)_{dark}$ and $(p_{free}/\theta)_{light}$ are equal. Under illumination it is obvious that the total free carrier density is larger, this means that θ must change proportionately.

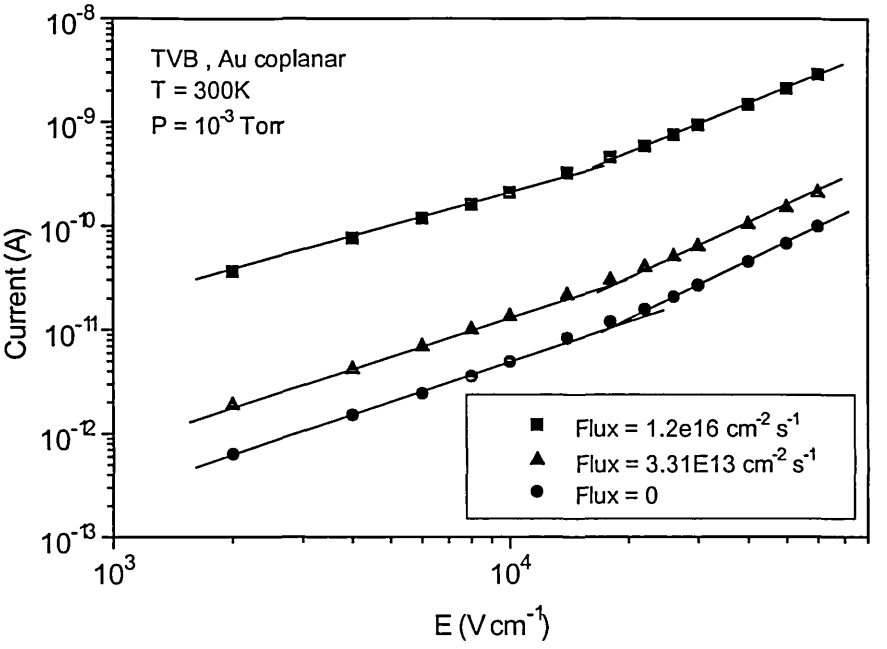

Fig. 7.19 Field dependence of dark and photocurrents for TVB.

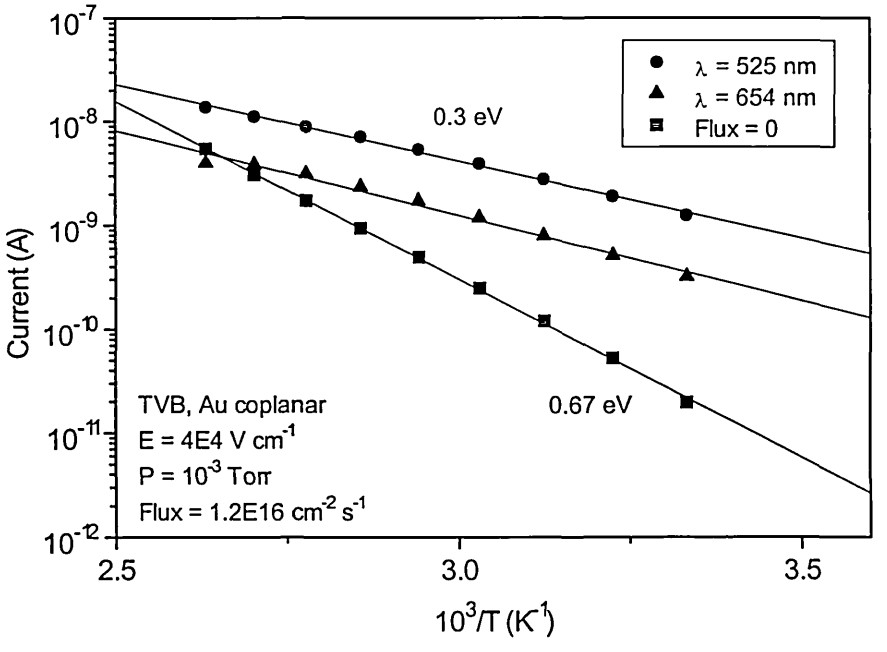

Fig. 7.20 Arrhenius plot for TVB dark and photocurrents.

The photocurrent is thermally activated although to a much smaller degree than the dark current, fig 7.20 shows an Arrhenius plot for the photocurrent in TVB at two different wavelengths at the same flux; the dark current is also shown for comparison.

The activation energy obtained from the slope of the photocurrent lines is 0.3 eV for both wavelengths. The current is slightly higher for green light as would be expected by examination of the photocurrent action spectrum (fig. 7.6). Due to the photocurrent being less temperature activated than the dark current at high temperatures the dark current will eventually become larger than the photocurrent. This can be seen to occur in TVD at around room temperature as already noted (table 7.2). Similarly, as the temperature is lowered the photocurrent decreases less rapidly than the dark current and thus the ratio σ_{pc}/σ_d will become larger. Fig 7.21 shows similar data for a thermally evaporated pentacene sample.

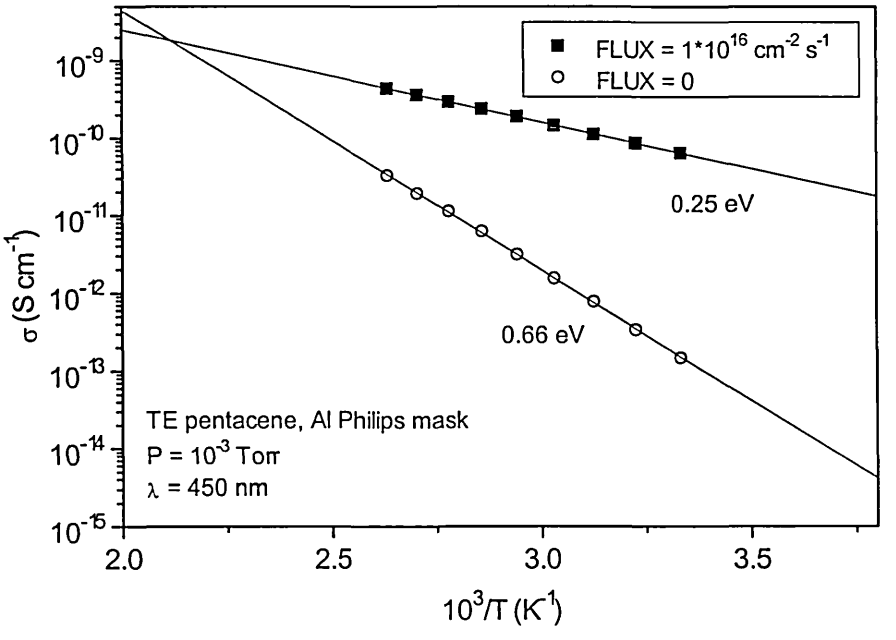

Fig. 7.21 Arrhenius plot for thermally evaporated pentacene dark and photocurrents.

It can be seen that the temperature at which the dark and photocurrents cross in this case (~ 474 K) is much higher in pentacene than in TVB, in keeping with the high σ_{pc}/σ_d ratio in pentacene. The measured photocurrent activation energies for all the oligomers lie within the range 0.25-0.30 eV. These values reflect the temperature dependence of the $\eta\mu\tau_r$ product for each material.

In order to try to separate the temperature dependencies of η, μ and τ_r (all of which are likely to be T-dependent in organic materials), and determine the temperature and field dependencies of the drift mobility the time of flight method was attempted on the oligomers. Only TVD and pentacene were available with sandwich configurations,

on top of this it was only possible to make a reliable electrical contact to the TVD samples. The pentacene samples had very thin electrodes, however it was unclear whether the problem of making an electrical contact was due to this or simply due to the sample batch being faulty. Experimentally it was not found possible to obtain a transit signal for TVD, the photoresponse was very poor, the current decay being almost as fast as the rise. The situation was not helped by a the rather thick top electrode.

An inability to obtain a TOF transit signal in pure, vapour deposited, organic thin films has also been observed by other workers. Goldie *et al.* (1993) found that they could not obtain a transit signal in pure α-3T thin films but a transit signal was, however, observed in molecularly doped samples with less than 55% by weight of oligomer in poly(carbonate). Increasing the concentration beyond this level led to dispersive transit signals. Featureless transient photocurrent decays have been associated with the short lifetime for the oxidised state of short chain oligomers. Fichou *et al.* (1990) suggested that this was the reason for a lack of field-enhanced conduction in thiophene oligomers with less than four thiophene units. In the present case we are dealing with materials that have a high degree of conjugation (TVD has 11 pi bonds), and thus the above argument is not likely to be valid.

Goldie *et al.* further suggested that deep trapping in transport inactive states, followed by recombination may account for the featureless decays observed. It was found that for α-3T samples with oligomer concentrations between 55% and 65% at low fields no extraction feature was obtained, but on increasing the field it could be recovered. Above 65% the decays were completely featureless. The authors suggested that this behaviour was due to carriers being deeply trapped below a critical field such that $\mu_h \tau_r E_{crit} < d$, where d is the film thickness. The loss of an extraction feature above 65% thus suggested that $\mu_h \tau_r$ decreases as the oligomer concentration increases which was attributed to an increase in deep traps with increasing doping. The origin of the deep trapping states is thus related to the average oligomer separation and this in turn may be due to molecular pairing (Zboinski, 1983).

In the pure oligomer films studied here it is very likely that interaction between oligomer molecules results in the generation of trapping levels, but it is unclear whether this is the reason for the unattainability of a transit feature. A rough calculation shows that the lifetime must be approximately 40 ms or less for no extraction (using $E = 10^5$ V cm^{-1}, $d = 4$ μm and assuming $\mu \sim 10^{-7}$ cm^{-2} V^{-1} s^{-1}). For TVD the TPC decays, presented in § 7.2.1, show that recombination may just be beginning at this time, although the

decrease in current is so small that it will probably not affect a TOF transit signal too much.

In the present case it is therefore suggested that the poor TOF response of the sandwich TVD sample is more likely due to problems with the sample configuration than any inherent characteristic of the actual oligomer. It should also be pointed out that the TPC and TOF methods are not directly comparable. In the TOF method the light should be strongly absorbed near to the oligomer-electrode interface which is likely to contain many trapping levels, thus recombination may be higher than in a coplanar sample in which the light is absorbed uniformly. In this case the TOF technique was attempted using a green dye with the laser (λ = 500 nm), as in TPC. The absorption plot for TVD shows that the absorption coefficient at this wavelength is higher than at 337 nm, the operating wavelength of the N_2 laser. Thus the penetration depth in the TOF experiment is the same as for the TPC experiment and is roughly 0.23 μm. Therefore the only difference between the two experiments is due to the film thickness. In the coplanar sample a penetration depth of the size quoted means that the majority of carriers are produced in the top quarter of the sample, whereas in the sandwich sample almost all the carriers are produced within a slice one tenth of the thickness of the sample. It is therefore conceivable that surface recombination *is* a factor contributing to the poor photoresponse of the sandwich sample, but it is unlikely to be the main reason because as we have seen the light is not absorbed uniformly in the coplanar sample either, but we get a considerably better photoresponse from the coplanar samples. As has already been mentioned the top electrode was quite thick which would cut down the absorbed number of photons, and thus photocurrent, considerably. It is shown in § 7.2.1 that there is evidence for early time recombination in the TPC decays, it is a possibility that this early time recombination along with a much reduced photon dose is the cause for the poor response in the TVD sandwich sample which makes the signal too small for the detection circuit to resolve (NB, an amplifier had to be employed to actually observe a sample signal, using a 50 Ω resistor was not enough).

The final functional dependence examined for the steady state photocurrent is the dependence on illumination intensity. For both inorganic and organic semiconductors the photocurrent is related to the intensity by

$$i_{pc} \propto F^{\gamma} \tag{7.10}$$

where F is the photon flux. A double logarithmic plot of i_{pc} vs. F yields a straight line of slope γ. It has already been seen that the value of γ gives information about the recombination mechanism, if $\gamma = 1$ recombination is monomolecular, $\gamma = 0.5$ implies bimolecular recombination. Intermediate values of γ suggest a continuous trap distribution in the gap, the actual value of γ being determined through interaction of trapping and recombination centres (see Rose's model, § 4.2.3).

For the oligomers studied in this work the values obtained for γ from ln i_{pc} vs. ln F plots are generally between 0.5 and 1.0, although some samples yield values below 0.5. Fig. 7.22 shows data for TVC parametric in field, the values for γ are given in the legend (the error in the final decimal place is ~ +/- 0.005).

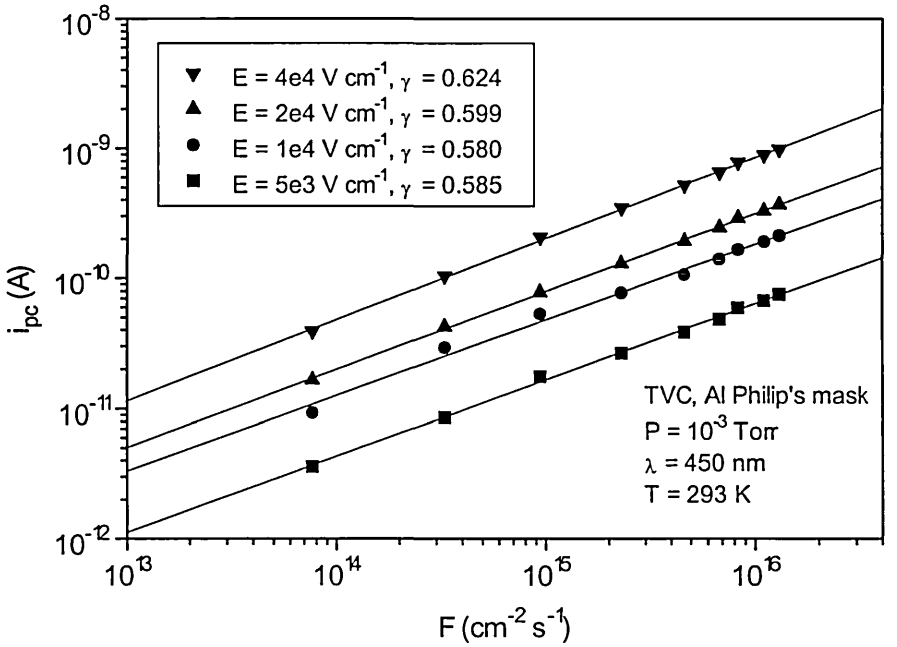

Fig. 7.22 Intensity dependence of photocurrent in TVC at different field strengths.

A value for γ between 0.5 and 1.0 can be accounted for using the Rose model which predicts that $\gamma = T_0/(T + T_0)$, where T_0 is the width of an exponential distribution of traps, thus the value of γ depends only on temperature. However it is unclear whether an exponential DOS is realistic for organic, molecular solids, furthermore the Rose model assumes a multiple trapping transport mechanism whereas transport in these materials is much more likely to occur by hopping or trap-controlled hopping. Fig. 7.22 provides evidence that the Rose model is inappropriate in this case because the value of

γ appears to be field dependent, although the change in γ is small. A field dependence of γ is suggestive of a hopping transport mechanism as in this case increasing the field could lead to an increase in mobility and thus a decrease in carrier lifetime. The data in fig 7.22 show just the opposite however, the recombination rate decreases as the field increases. This may indicate that at higher fields a hopping carrier can more easily escape from the coulombic attraction of a recombination centre.

The variation of γ with temperature in TVC is shown in fig. 7.23, γ values are again given in the legend.

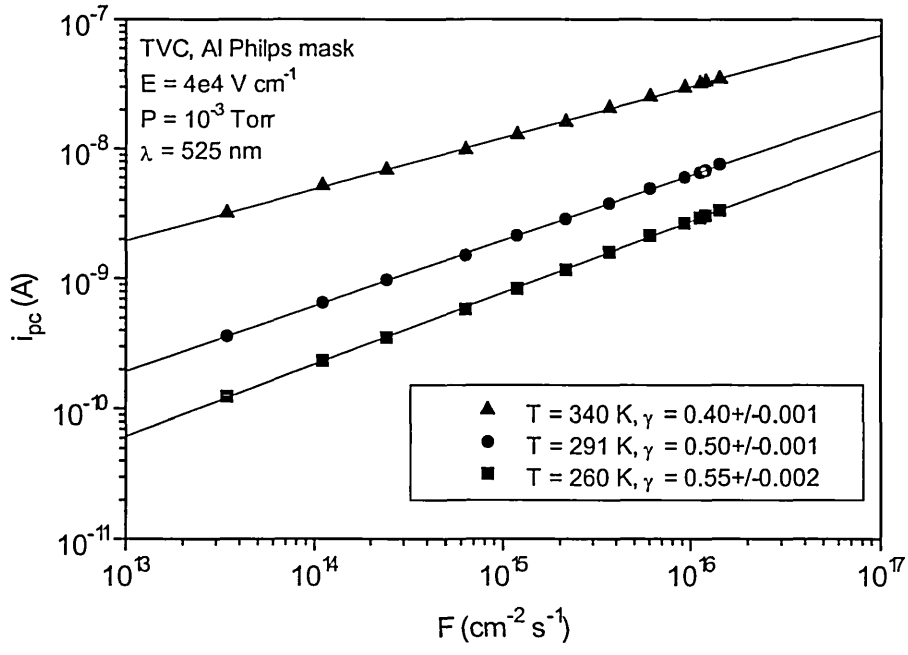

Fig. 7.23 Photocurrent vs. intensity parametric in temperature for TVC.

Note that the high temperature data yields a γ value less than 0.5 which, in terms of the Rose model, means that $T > T_0$. Using $\gamma = T_0/(T + T_0)$ in order to calculate T_0 for each of the data sets in fig. 7.23 does not yield a consistent value, the values for T_0 are 318 K, 293 K and 227 K for T = 340 K, 293 K and 260 K respectively. Thus for the γ (T) dependence the Rose model does not fit the results, although γ does decrease as temperature rises. Qualitatively the decrease in γ with increasing temperature can simply be accounted for by an increase in mobility which should cause photocarriers to encounter recombination centres more rapidly.

Comparison of fig. 7.23 with fig. 7.22 reveals a further dependence of γ on the photon energy, the two similar curves (T = 293 K, E = 4×10^4 V cm^{-1}) are not only

displaced in photocurrent magnitude (see TVC photocurrent action spectra) but the value of γ is higher for higher photon energy. Fig 7.24 illustrates this wavelength dependence of γ for TVB, note that in this case due to the different form of the photocurrent action spectrum the photocurrent magnitude for blue light is higher than that for green (vice versa for TVB), however γ is still found to increase as photon energy increases.

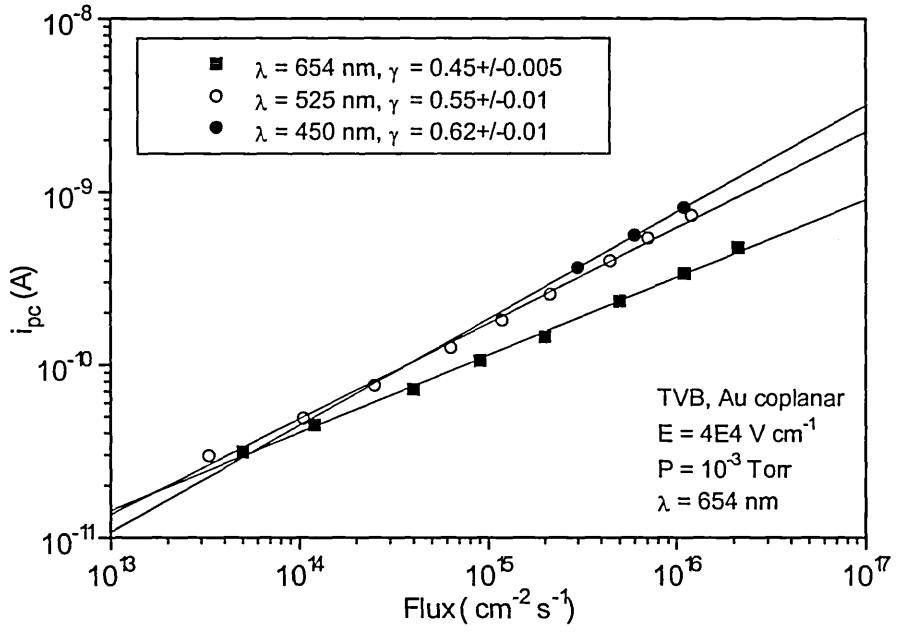

Fig.7.24 Photocurrent vs. intensity parametric in wavelength for TVB.

An increase in γ with increasing photon energy could be due to either a change in the absorption coefficient and thus the penetration depth, or from some change in the generation process. The absorption profiles for the three photon energies used in fig. 7.24 will be different, and using the absorption plots from § 7.1.1 we obtain penetration depths of roughly 1μm, 0.6μm and 0.4μm for red, green and blue light respectively. If surface recombination is important the recombination rate should be highest for blue light and lowest for red light, which is in fact the opposite to what is seen in fig. 7.24. Thus we must assume that in TVB surface recombination is not significant.

An alternative explanation for the change in γ with photon energy is that carriers generated with higher photon energies are "hot", *i.e.* they are excited to high energy/mobility states and have excess kinetic energy (see § 4.2.2), which may enable them to escape from the recombination zone.

A final steady state measurement which was performed on the oligomers was the steady state photocarrier grating (SSPG) technique. The SSPG technique has been used extensively on materials such as a-Si:H to measure the ambipolar diffusion length, but has seemingly not yet been attempted on organic materials. For the present materials a grating effect was not observable *i.e.* the measured photocurrents with the two laser beams coherent (grating on) and non-coherent (uniform illumination) were the same. Although this experiment resulted in a null result (similar to TOF) it allows us to speculate on reasons why this should be.

There are two possible explanations which are able to account for the unattainability of a grating effect in the oligomers. The first is that there is some physical mechanism occurring within the oligomers which prevents a photocarrier grating from forming. The second is that the experimental system was not sensitive enough to resolve the small sinusoidal excitation on top of the uniform background illumination.

The majority of SSPG work carried out on a-Si:H has been performed using the so-called small-signal approach in the lifetime regime (Ritter *et al.*, 1988). In the lifetime regime the dielectric relaxation time τ_{rel} is considerably shorter than the carrier lifetime, which means that charge neutrality prevails everywhere and electrons and holes diffuse together. In this case the diffusion length measured is the ambipolar diffusion length, and if the electron and hole mobilities differ the measured diffusion length is closer to that of the less mobile (minority) carrier. However, for the oligomers studied here rough calculations show that we are not in the lifetime regime, *i.e.* $\tau_{rel} > \tau_r$. The dielectric relaxation time is defined as $\tau_{rel} = \varepsilon_r\varepsilon_0/\sigma_{pc}$, using the σ_{pc} value for pentacene from table 7.2 and $\varepsilon_r = 3.0$, we obtain $\tau_{rel} \sim 0.24$ s. The carrier lifetime can be estimated from the plots of TPC with optical bias in § 7.2.1.3 and for pentacene is of the order of 10 ms. Thus we are clearly in the relaxation regime in which space charge effects are important and electrons and holes can be spatially separated. The amplitude of the photocarrier grating, and thus the change in photocurrent with and without the grating, depends on the ratio of the carrier mobilities μ_p and μ_n. If the mobilities are equal the grating amplitudes for both carriers are equal and the SSPG experiment yields the true ambipolar diffusion length. However, if the mobilities are not equal the grating amplitudes will differ due to faster diffusion of one type of carrier. In this case the measured diffusion length is not the true ambipolar diffusion length, but depends on the ratio of the carrier mobilities and the ratio of lifetime to dielectric relaxation time.

For the oligomers studied here it is likely that conduction is unipolar, holes being the majority carrier type. Electrons are assumed to be effectively immobile, thus $\mu_p >> \mu_n$. In this situation we would expect the hole grating amplitude to be small due to faster diffusion of holes. The resulting decrease in the recombination rate would lead to an increase in the electron grating amplitude. Thus in the oligomers studied we would expect to obtain a photocarrier grating, although the measured diffusion length would not correspond to the true ambipolar diffusion length.

In the above discussion we have so far neglected the effect of an applied field. It has been demonstrated (Ritter *et al.*, 1988) that the application of high fields during a SSPG experiment can lead to a blurring of the photocarrier grating, *i.e.* a reduction in the grating amplitude. The effect is more pronounced the lower the ratio of τ_r/τ_{rel}. In the present materials τ_r/τ_{rel} is roughly 0.05 which is considerably lower than typical values for a-Si:H (τ_r/τ_{rel} is typically about 20), in which the importance of field induced blurring of the photocarrier grating has been demonstrated by the above authors. The SSPG experiment carried out in this work was performed with an applied field of 10^4 V cm^{-1}, this magnitude of field has been shown to affect the grating amplitude in a-Si:H. Thus a high field might be expected to completely blur any photocarrier grating formed in the oligomers studied here. However, if electrons are indeed immobile in these materials we would still expect to observe a grating effect. A high field would reduce the amplitude of the hole grating but would not affect the amplitude of the electron grating.

Using a rough value for the mobility of 10^{-7} cm^2 V^{-1} s^{-1} we can estimate the diffusion coefficient, and thus the carrier diffusion length in pentacene using the carrier lifetime quoted above. From the Einstein relation we obtain a diffusion coefficient of 2.6×10^{-9} cm^2 s^{-1} at 300 K. The diffusion length is given by $L_D = \sqrt{D\tau_r}$ and works out at ~ 50 nm. This magnitude of diffusion length is of the same order of magnitude as that commonly found in amorphous silicon (Webb, 1994). It would thus appear that the lack of a photocarrier grating effect in the oligomers must be due to the experimental system being unable to resolve the small, sinusoidal grating on top of the large uniform background illumination. This is perhaps the most likely explanation, as even in pentacene (which has the best photoresponse of all the oligomers, at room temperature) the ratio of photo- to dark current is poor compared to that in a-Si:H. Experimentally, the pentacene photocurrent was found to be very noisy, which may have swamped the expected photocurrent drop due to grating formation.

7.1.4 Sample annealing and the effects of ambient atmosphere

The majority of results obtained from the oligomers in this study were performed on samples under vacuum, which had been annealed in order to decrease and stabilise the dark current. However, because annealing and exposure to air was found to have such a drastic effect on the dark current in some samples, tentative studies were made of these processes. (It should be pointed out that the effects described above are not strictly within the remit of this project and thus the results presented here are in no way exhaustive, however it was considered useful to obtain some knowledge of how these processes affect the dark and photocurrents).

It has already been shown in § 7.1.2 that annealing the oligomers can lead to very large decreases in the conductivity. Similar changes in conductivity have been observed in other organic materials, *e.g.* in poly(p-phenylenevinylene) by Meyer *et al.* (1995) and in α-sexithiophene by Horowitz *et al.* (1990). Many authors imply that annealing simply removes absorbed (or adsorbed) oxygen which acts as an electron acceptor and dopes the materials; samples are therefore annealed in vacuum with subsequent measurements being performed without exposure to ambient atmosphere (Meyer *et al.*, 1995). However more detailed studies of the annealing process have suggested that simple oxygen diffusion out of the thin films is only one of the processes occuring on heat treatment. Horowitz *et al.* (1990) have shown that annealing α-6T FETs increases the (field-effect) mobility by a factor of 3-4 while at the same time decreasing the conductivity. The increase in the mobility was found to be irreversible, but the initial conductivity could be recovered on exposure to ambient air. Thus in this case annealing increases the mobility and decreases the carrier density, these effects being ascribed to crystallisation of the films. In the case of pentacene annealing leads to an order of magnitude decrease in the mobility (in the SCL current regime), but an insignificant change in the carrier density (see § 7.1.2.1).

The effect of oxygen absorption on thin films of thiophene based polymers has been studied by Abdou *et al.* (1997), and commented upon by Väterlein *et al.* (1997). Horowitz *et al.* also studied this effect in α-6T before and after annealing. It was found in all cases that oxygen absorption led to a reversible increase in conductivity, but there is disagreement on the effect oxygen has on the carrier mobility. Horowitz *et al.* show that the increase in σ is accompanied by a smaller increase in μ, whereas Abdou *et al.* have observed a decrease in mobility on oxygen doping. Both measurements were

performed on FET structures. These results imply that, in general oxygen increases the carrier density. Abdou *et al.* have shown that oxygen forms a charge-transfer complex with poly(thiophene). Dissociation of this complex with electron transfer to the oxygen will result in holes being generated on the thiophene units. Dissociation is presumably temperature and field activated as in the Onsager mechanism (§ 4.2.2). The observation reported in § 7.1.2.1 of a significant difference between the dark currents of TVD and TVC which only differ in chemical structure by four methyl groups may be explained using this model. If the methyl groups inductively donate electrons to the thiophene backbone the resulting complex between a TVD molecule and O_2 may require less energy to dissociate, as electrons delocalised on the TVD molecule are less strongly bound.

The effect of exposure to ambient air of an unannealed, coplanar pentacene sample is presented in fig. 7.25.

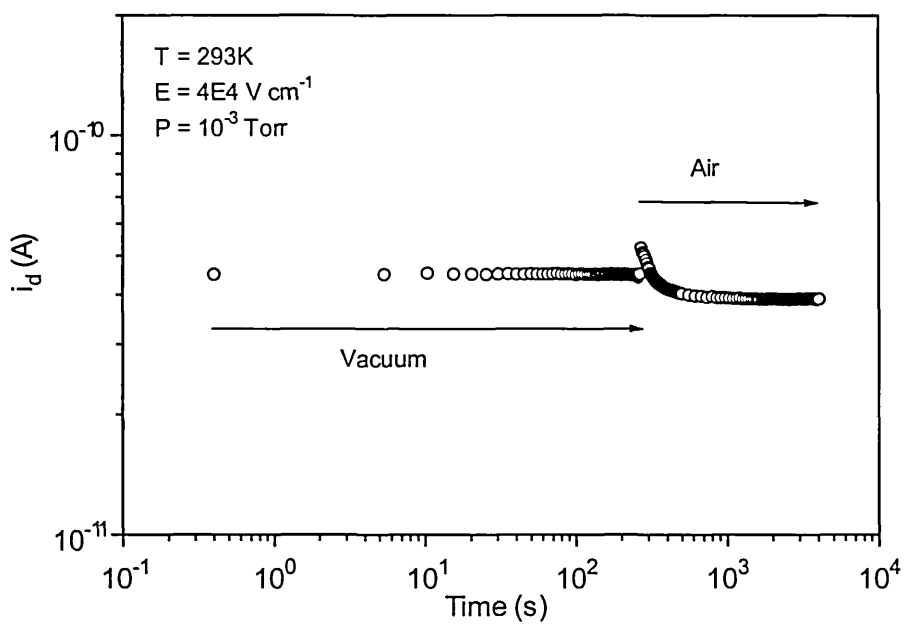

Fig 7.25 Effect of ambient atmosphere on a coplanar pentacene sample.

It can be seen that for this coplanar sample oxygen absorption/adsorption does not lead to an increase in the dark current, in fact the dark current is found to decrease. On exposure to air the current rises rapidly then decreases more slowly to a value slightly below its steady state value under vacuum. This type of response was found to be common for all the oligomers in coplanar configuration. Fig. 7.26 shows similar data for an Al/TVD/Au sandwich sample. In this case (as in the I-V curves) exposure to

ambient air has a profound effect on the dark current and the magnitude of the current increase also appears to depend on the polarity of the electrodes. Under forward bias (Au +ve) the dark current increases by about one order of magnitude on exposure to O_2. There is a rapid initial rise followed by a more slowly increasing region. Under reverse bias the current increases by almost two orders of magnitude. Again there is a fast initial rise followed in this case by a slow decay. In § 7.1.2 it was shown that for this sample the I-V curve exhibited rectifying behaviour and that exposure to oxygen changed this curve so that there was an apparent ohmic loss at high fields under forward bias (fig. 7.13).

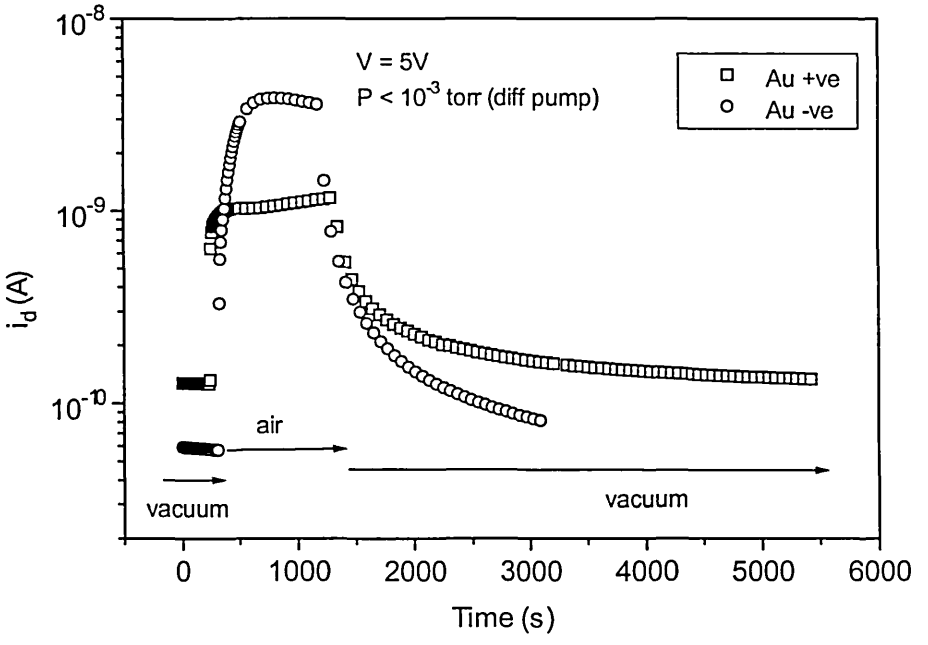

Fig.7.26 Increase of dark current in a Al/TVD/Au sample on exposure to air, with each electrode positive.

The data in fig. 7.26 agree with the I-V under vacuum in that the forward bias current is larger than the reverse current (although the absolute magnitudes do not agree). However upon exposure to O_2 it is found that the forward current becomes less than the reverse current, whereas the I-V suggests that the forward current should be about two orders of magnitude greater. This observation is hard to reconcile with the I-V curve for this sample, which shows that in air and in vacuum the forward current is always larger than the reverse current. However, it can be seen that after the initial fast response the forward current continues to increase while the reverse current slowly decreases, the author can only suggest that given a long enough time interval the respective currents

should reach the values obtained from the I-Vs. It has been observed by Väterlein *et al.* (1997) that the application of high fields across oligothiophene samples increases the dark current. The I-V measurements were performed in both directions by slowly increasing the voltage towards the maximum value and ensuring that the current was stable before tabulation, whereas the data in fig. 7.26 are essentially transient, the sample being exposed to air suddenly with 5V applied. Thus the slowly increasing and decreasing sections in fig. 7.26 may represent the sample recovering from a rapid change in experimental conditions.

The increased effect of oxygen on the sandwich samples as compared to the coplanar samples suggests that the absorption of oxygen is a surface or interfacial effect, at least in the time scales examined in figs. 7.25 and 7.26. If absorbed oxygen does indeed create carriers in the oligomers the coplanar data suggest that this is a very slow process as little change in current is observed within the experimental timescale, thus diffusion into or out of the bulk must be slow (cf. Väterlein *et al.*, 1997). The large effect in the sandwich samples may be due to absorbed oxygen accumulating at the top electrode/oligomer interface and causing carrier injection. A similar explanation was used by Gailberger *et al.* (1992) to explain quantum efficiencies greater than unity in poly(3-dodecylthiophene).

Carrier generation in the thiophene oligomers might thus be pictured as follows. A thiophene unit and an oxygen molecule form a complex. Depending on the temperature and field this complex will dissociate with a certain probability resulting in a hole on the thiophene unit and a electron on the oxygen molecule. The electrons are presumably very strongly localised on the oxygen molecule and are thus rendered essentially immobile. However, the low ionisation energy and large electron affinity of thiophene means that hole motion, which is equivalent to an electron hopping from a neutral thiophene unit to a radical cation, will be energetically favourable at reasonable temperatures and fields (Mort and Pfister, 1985). This explains the observation that current flow in such materials is unipolar. If a situation such as this is valid for the materials studied here it suggests that recombination can be considered to occur between mobile holes and trapped electrons (cf. As_2Se_3, see Orenstein, Kastner and Vaninov, 1982). This will be further discussed in § 7.2.1.

7.2 Transient results

In this section we will discuss the transient photocurrent results obtained using the transient photocurrent decay method which was performed as a function of temperature, field and illumination intensity. The temperature dependence of the TPC decays will be discussed in § 7.2.1.1. Attempts at recovering the density of states from the experimental data will also be included and discussed in this section. The field and illumination intensity dependencies of the TPC decays will be presented in § 7.2.1.2. TPC was also carried out with optical bias to investigate recombination, and these results are contained in § 7.2.1.3. Also included in this section are measurements of the persistent photocurrent which were found to be characteristic of the oligomers.

7.2.1 Functional dependencies of the transient photodecay

The transient photocurrent decay technique was carried out on all oligomers as a function of temperature, intensity and field. The transients so obtained were found to be largely similar from material to material, fig. 7.27 shows room temperature TPC decays for all the oligomers performed using the Philips mask electrode.

Between 10^{-8} and typically 10^{-4} s the decays are quite steep, approximately following a t^{-1} power law. At longer times this changes over to a shallower slope, with no indication, up to about 10 s, of the decays thermalising to a constant current. The straight lines are included as a guide to the eye. Short time (< 10 ns) recombination cannot be ruled out, but there is no indication of significant recombination occurring within the experimentally observed time scale. If this is so, then it may be assumed that the decays simply reflect charge carrier thermalisation within localised states, *i.e.* the form of the decaying photocurrent would reflect changes in the carrier mobility only. Changes in the photocurrent magnitude due to varying the temperature, field or intensity cannot however be solely attributed to the dependence of mobility on these variables as they may also affect the carrier density . In the case of hopping the mobility represents an average over all transport paths, whereas for multiple trapping an effective (drift) mobility, μ_d is obtained which is the band mobility, μ_0 multiplied by the ratio of free to trapped charge, θ.

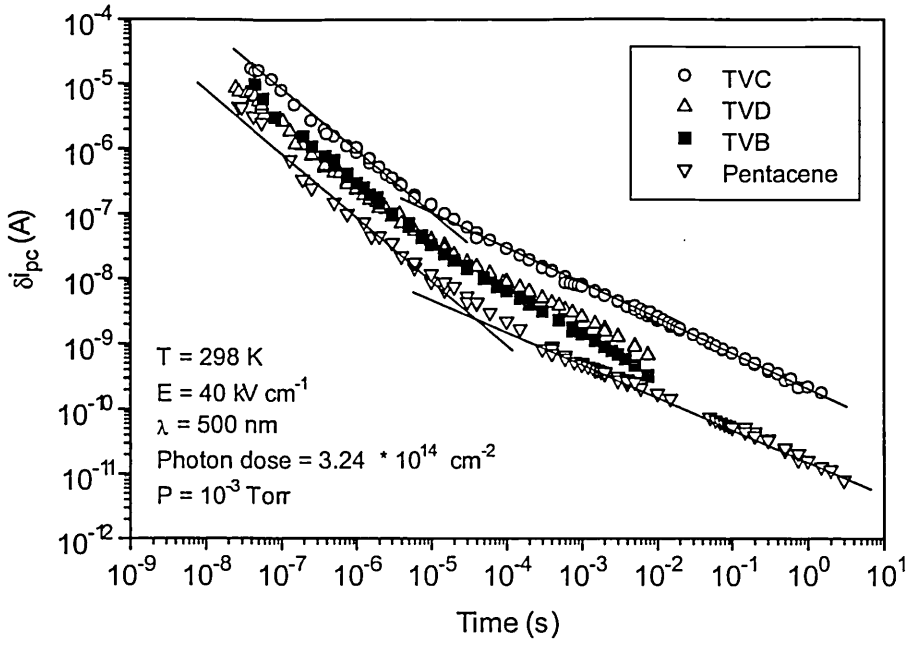

Fig. 7.27 Room temperature TPC decays for all oligomers.

For trap-controlled hopping the situation is similar to multiple trapping although the magnitudes of the transport controlling parameters will differ and field dependencies may occur.

The difference in the magnitude of the photocurrent from oligomer to oligomer does not appear to change appreciably over the time scale examined *i.e.* the curves are eventually parallel. This suggests that a similar thermalisation process is occurring in all materials (the apparent increase in slope at long times in the TVB decay is probably unreproducible as the photocurrent is small compared to the dark current). If the photocurrent is simply a reflection of the carrier mobility then this suggests that the form of the distribution of localised states is largely similar in all the oligomers The relation between the absolute magnitude of the transient photocurrents for the oligomers does not agree with that obtained from steady state measurements (see table 7.2). In the steady state the photocurrents are in the order TVD>pentacene>TVB>TVC, the transient photocurrents however are in the order TVC>TVD/TVB>pentacene, the transient photocurrent magnitudes in TVD and TVB are negligibly different. This different relation between the steady state and transient photocurrent magnitudes is perhaps not surprising as the magnitude of the steady state photocurrent is given by the

$\eta\mu\tau_r$ product, whereas the magnitude of the transient photocurrent should only depend on $\eta\mu(t)$ before recombination.

7.2.1.1 Temperature dependence of TPC and DOS recovery

Fig. 7.28 shows the effect of varying the temperature on the TPC decay in TVC. The overall form of the decay is similar in that it retains a two-slope form. Increasing the temperature can be seen to decrease the index of the long time shallow slope while only increasing the magnitude of the short time ~ t^{-1} region. The time at which the t^{-1} slope changes into the temperature-dependent long time slope is itself essentially independent of temperature, occurring in all cases at about 10 μs. A similar type of temperature dependence has been observed in the other oligomers. Fig.7.29 shows data for thermally evaporated pentacene. Although the transition time between the two slope regions certainly occurs at a shorter time, its precise value cannot be determined from the data.

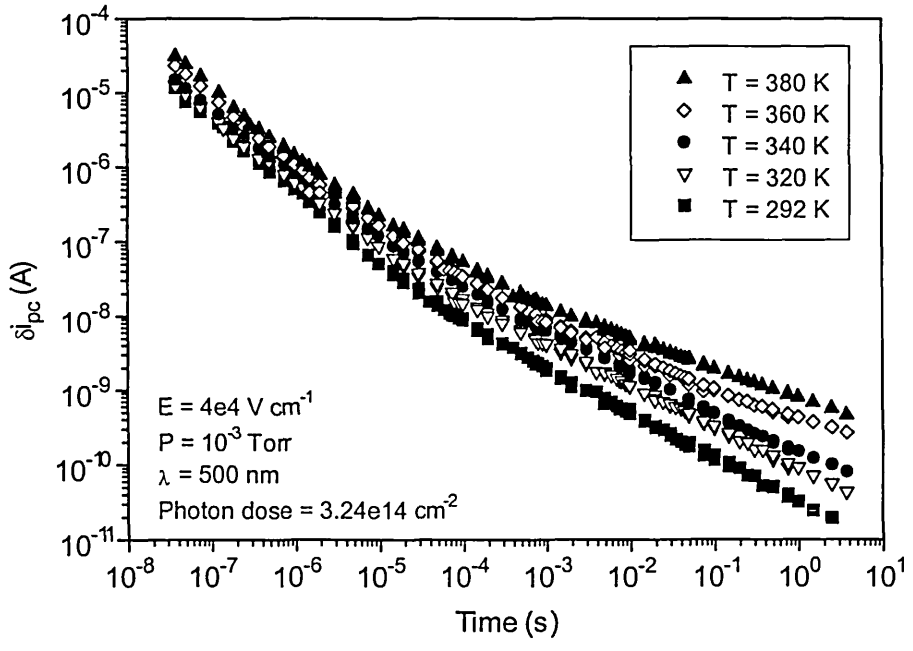

Fig. 7.28 TPC decays for TVC parametric in temperature.

Fig. 7.30 shows TPC decays for TVD parametric in temperature. In this case it can be argued that recombination is altering the form of the three highest temperature decays, and thus it is possible that the form observed in figs. 7.28 and 7.29 would be recovered if no recombination were occurring. Both the bimolecular and monomolecular recombination lifetimes are expected to be temperature dependent.

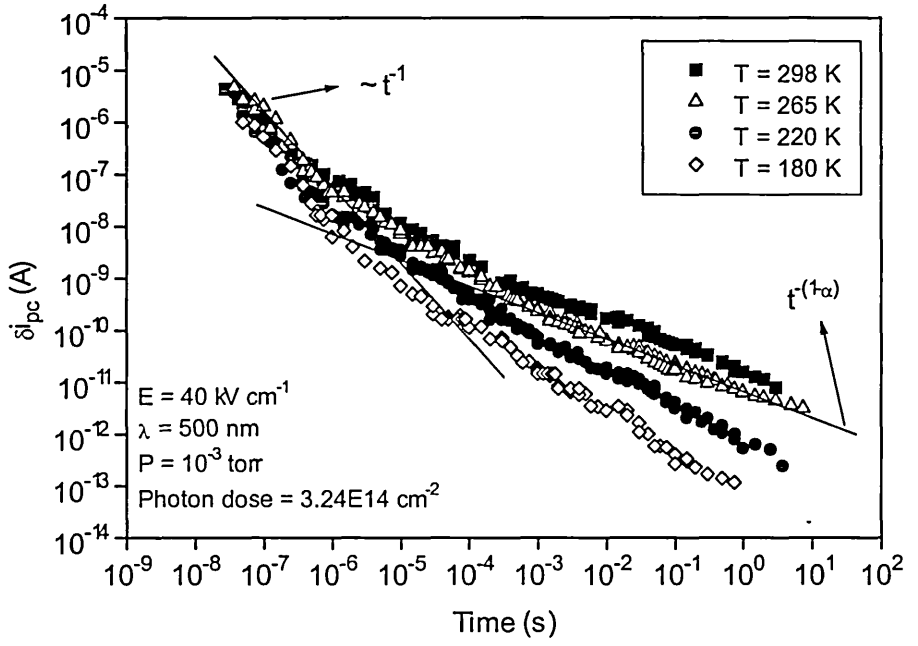

Fig. 7.29 TPC decays for thermally evaporated pentacene parametric in temperature

For monomolecular recombination the temperature dependence of the lifetime depends on the thermally-generated density of recombination centres and $\mu(T)$, whereas the bimolecular recombination lifetime only depends on the latter. It has already been shown that the dark current in TVD is larger than the steady state photocurrent thus it is likely that the recombination occurring in fig. 7.30 is monomolecular. It is clear however that the recombination rate is very low. Note that at the highest temperature recombination has resulted in an erosion of the ~ t^{-1} decay.

Also shown in fig. 7.29 are a t^{-1} slope and a fit to the long-time, temperature dependent slope given a value with an exponent $-(1-\alpha_d)$ as in dispersive TOF signals (Scher and Montroll, 1975). The term α_d is known as the dispersion parameter and can vary between 0 (fully dispersive, $\delta i_{pc} \propto t^{-1}$) and 1 (non-dispersive, δi_{pc} = constant). Thus the short-time t^{-1} slope indicates that transport over this time range is fully dispersive (α_d

= 0), and it can be seen that the slope is temperature independent. It has been shown that for multiple trapping in an exponential DOS that,

$$\alpha_d = T/T_0 \tag{7.11}$$

where T_0 is the width of the distribution of localised states in temperature units (see for example, Pfister and Scher, 1978).

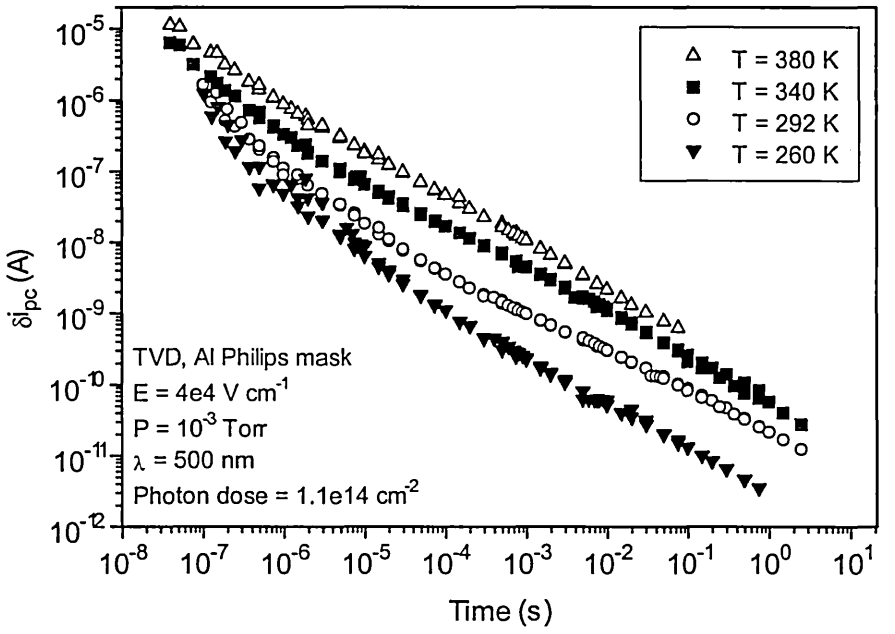

Fig. 7.30 TPC decays for TVD parametric in temperature.

It has also been shown that eq. 7.11 applies to hopping in an exponential DOS (Silver *et al.*, 1982, Monroe, 1985).

For hopping in a gaussian DOS of width σ_g Monte Carlo simulations yield (Schönherr, Bässler and Silver, 1981),

$$\frac{1}{\alpha_d} = \left(\frac{\sigma_g}{4k_B T}\right)^2 + 1 \tag{7.12}$$

In both cases the temperature dependence of the dispersion parameter is due to a spread in the activation energies of the carriers (Mort and Pfister, 1982). Thus from eqs. 7.11

and 7.12 it is possible to estimate T_0 and σ_g using the values of α_d obtained from the slope of the temperature dependent region of the TPC decays at different temperatures. Fig. 7.31 shows values for α_d plotted vs. T. The slope of this graph should yield a value for T_0. From the best-fit straight lines a value for T_0 of 461 K is obtained, which corresponds to an exponential (valence band) tail of width 40 meV. Note that for this fit α_d becomes equal to zero at about 77 K, which implies that (i) below this temperature TPC decays will exhibit a slope of t^{-1}, (ii) above 461 K TPC decays should be non-dispersive, *i.e.* a constant current plateau will be observed.

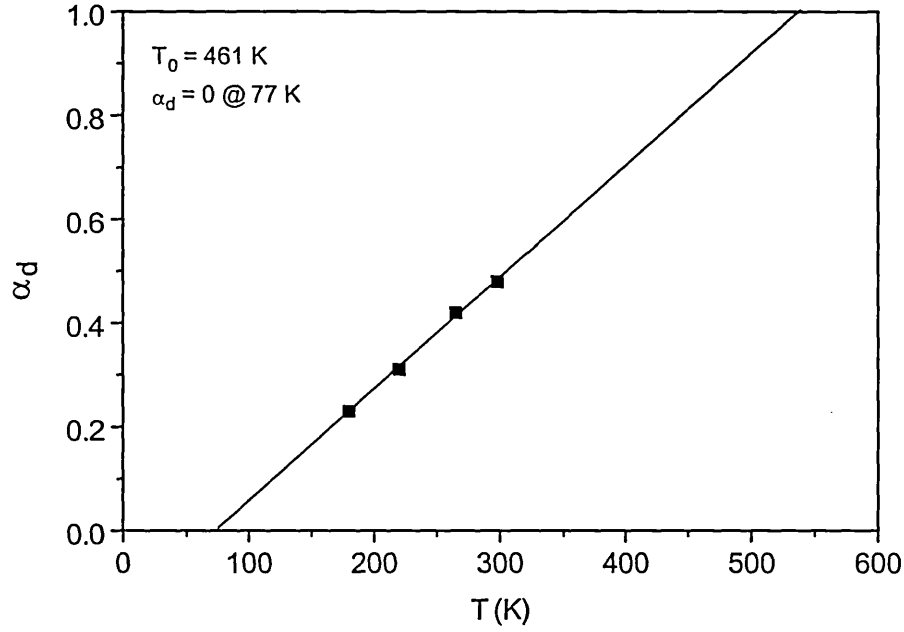

Fig. 7.31 Temperature dependence of the dispersion parameter for pentacene.

Due to temperature limitations however, TPC decays were not obtained at either of these temperatures: 77 K was below the limit of the cryostat, and the photocurrents were too small to measure below approximately 180 K. At the other end of the temperature range it was found that under vacuum raising the temperature above ~ 410 K led to evaporation of the oligomer.

Fig 7.32 shows the same data plotted according to eq. 7.12. The fit to the data of fig. 7.31 results in a width of 0.12 eV for the gaussian DOS, which is typical of the widths obtained experimentally from TOF measurements on molecularly doped polymers (Magin and Borsenberger, 1993). Note that in this case the best-fit line suggests that non-dispersive transport should occur above 733 K. From a consideration

of the intercepts of figs. 7.31 and 7.32 it would appear that the fit to eq. 7.12 is slightly better: the intercept is quite close to unity as predicted, whereas that in fig. 7.31 can be seen to be quite erroneous.

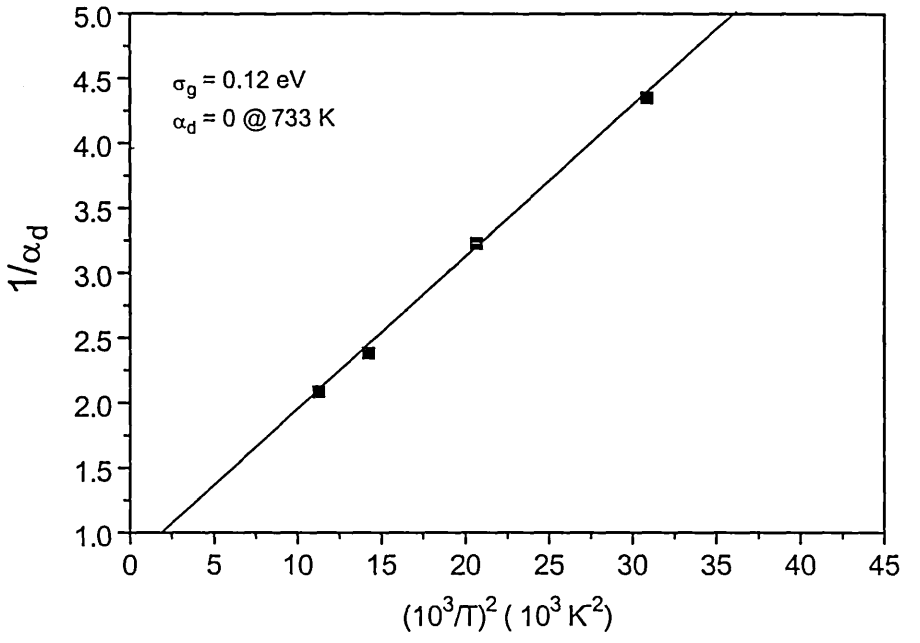

Fig. 7.32 Dispersion parameter for pentacene plotted according to eq. 7.12.

A problem with the above analyses is that each assumes a DOS and then attempts to fit the data to the theory. It would be more desirable to employ an analysis which does not initially assume a distribution for the density of states. We can interpret the form of the DOS qualitatively from the form of the TPC decays. From a multiple trapping viewpoint the t^{-1} current decay at short times would be caused by a flat density of states, whereas the longer time, temperature dependent, decay would be due to an exponential region, presumably of the width predicted by the fit of α_d vs. T in fig. 7.31. Fig. 7.33 shows computer simulated decays (using a program similar to that described in § 5.2) obtained from carriers moving by multiple trapping in a DOS of the form described above, it can be seen that in many ways the decays are similar to those of figs. 7.28 and 7.29, *i.e.* they show a short time ~ t^{-1} decay and a shallower, long time, temperature dependent slope. The main problem with the simulated decays is that the transition time between the two decay regimes is temperature dependent, whereas in the experimental decays the transition occurs at a similar time at all temperatures. This is a reflection of the fact that for multiple trapping the demarcation energy ε_d sinks at a rate

k_BT ln(υt), thus at higher temperatures the demarcation energy will pass into the exponential section of the DOS at an earlier time.

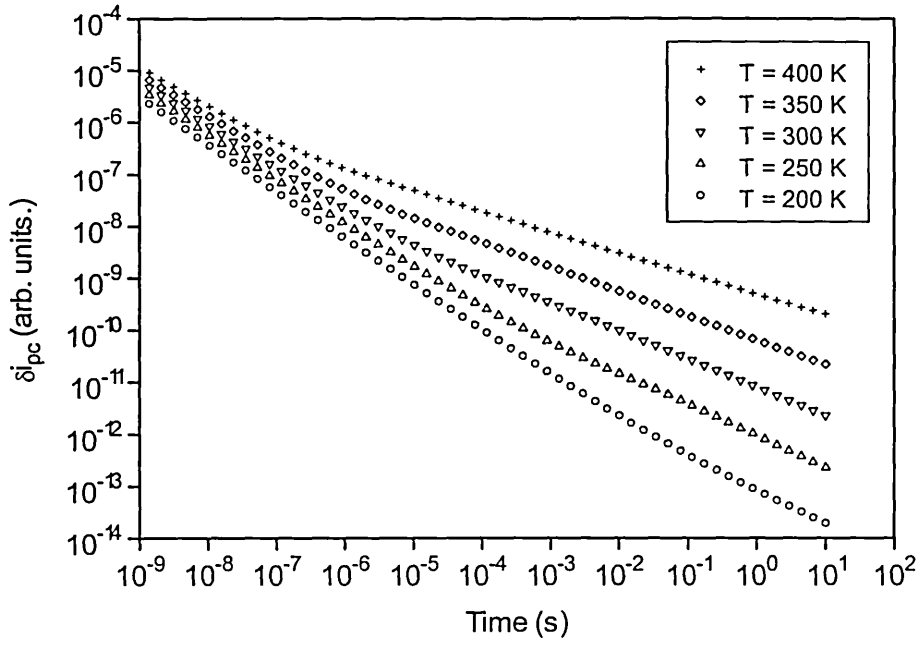

Fig. 7.33 Simulated TPC decays for flat + exponential DOS.

To fully explain the TPC decays we need to arrive at a model which can explain the two-slope form of the decay, and the apparent insensitivity of the transition time to temperature change. It has been shown that hopping in an exponential density of states results in similar transient photodecays to those due to multiple trapping (Silver, Schönherr and Bässler, 1982). Hopping in an exponential DOS can be explained in the following way. Carriers are trapped in the DOS at time t = 0 in a distribution that parallels the density of traps, carriers trapped high in the DOS have high hopping rates due to the high trap density, whereas those trapped deeply have slow hopping rates because the density of states is small. The distribution of trapped carriers can therefore, at any arbitrary time interval after trapping, be separated into those in fast and slow states depending on their energy. Carriers initially situated in shallow states where the trap density is high will move by hopping directly down in energy because the overlap term for the hop rate dominates (eq. 4.51). They will accumulate in deep states, again in line with the trap distribution. Carriers in deep states with slow rates will not have hopped at all and will thus mirror the density of states. Thus shortly after trapping the

majority of carriers will be found at an energy which separates the fast from the slow states, this is known as the demarcation energy, and it is defined as the energy at which the hopping-out rate is equal to the reciprocal of the elapsed time (note the similarity to multiple trapping). Initially the current will be dominated by carriers "hopping down" to lower energy states, in this situation the current decays as t^{-1} and it has been shown that the demarcation energy sinks at a rate given by

$$\varepsilon_d(t) = k_B T_0 \ln\left(\frac{8\alpha_{loc}^{\ 3}}{N_L}\right) - 3k_B T_0 \ln\left[\ln\left(\upsilon_0 t\right)\right] \tag{7.13}$$

where α_{loc} is the inverse localisation length and N_L is the total density of localised states (Monroe, 1985). As ε_d sinks deeper into the DOS the hopping down rate decreases as it becomes increasingly hard for a carrier to find a nearby state to hop to. After a certain time it becomes more favourable for carriers to hop up in energy as this increases the number of states available for thermalisation. Further thermalisation then occurs by trap-controlled hopping, in this case the thermalisation energy sinks at a rate given by $k_BT\ln(\upsilon t)$. In the trap-controlled hopping process carriers trapped deeply in the DOS are excited to a transport energy, ε_t which is given by

$$\varepsilon_t = -3k_B T_0 \ln\frac{3k_B T_0 (4\pi/3)^{1/3}}{2\alpha_{loc} akT} \tag{7.14}$$

For an exponential DOS the hopping down regime is only predicted to occur at low temperatures (< 200K) at any reasonable value of T_0. The hopping down rate is independent of temperature, but is dependent on the form of the density of states, thus hopping in an exponential DOS at room temperature should not show a hopping down regime, and even at low temperatures the transition between the temperature independent and dependent regimes will rely on temperature. Thus hopping in an exponential DOS cannot explain the TPC decays shown in figs. 7.28 and 7.29 because this form of DOS predicts a temperature dependent transition time between the hopping down and trap-controlled hopping regimes, and at room temperature a t^{-1} decay should not be observable.

Thus so far we have concluded that neither hopping nor multiple trapping in an exponential DOS can explain the experimental decays. Furthermore simulation has shown that multiple trapping in a flat + exponential DOS fails to account for the form of the experimental decays. However if we now consider *hopping* transport in a flat + exponential DOS we will see that the experimental decays *can* be explained. If we assume that the carriers are initially produced uniformly in the trap distribution we will have a situation depicted as in fig. 7.34.

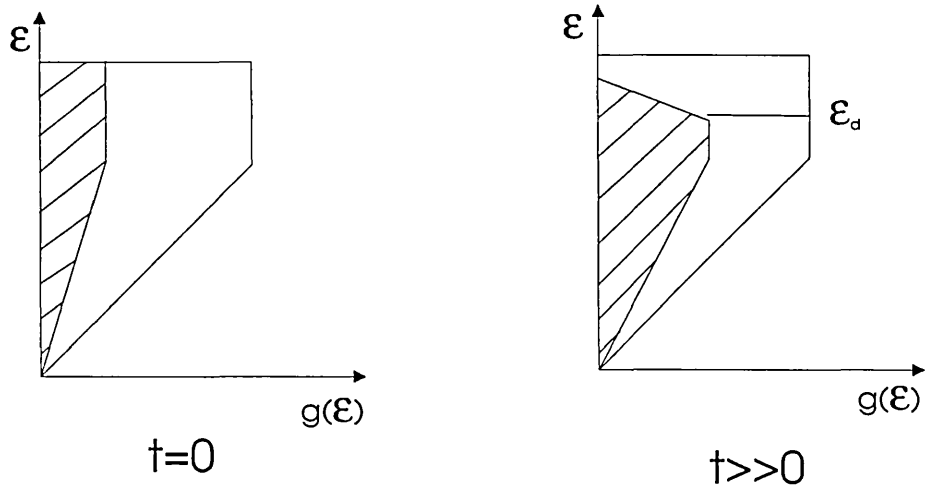

Fig. 7.34 Carrier distribution in flat + exponential DOS at different times.

After a short period of time the carrier distribution will evolve as shown above, again the hopping down rate is independent of temperature but in this case it is also unaffected by the form of the DOS. Thus the demarcation energy should sink at the same rate at all temperatures, and the transition to the trap-controlled hopping regime occurs at the same time for all temperatures.

The form of the density of states predicted above to explain the experimental decays is perhaps not physically realistic, furthermore the initial occupation of the states is very unlikely unless there is a mobility edge from which carriers are uniformly trapped. In a multiple trapping situation, with a well defined mobility edge, such a density of states may be possible, the flat region may not have to be totally flat but may be caused by a very slowly decreasing DOS. However, in a hopping situation in which all the transport states are localised it is hard to argue for such a form for the DOS, which is much more likely to have a roughly gaussian shape.

In order to try to clarify the situation the density of states obtained by processing the experimental TPC data via the Fourier transform program (described in § 4.3.3) was compared with that predicted qualitatively above. (It is pointed out that the FT method for DOS retrieval from TPC data is based on a multiple trapping transport mechanism, it therefore may not be applicable to systems in which transport occurs solely by hopping, however it is likely that it will work for trap-controlled hopping, because in this case the concept of a carrier demarcation energy has been shown to be valid). Fig. 7.35 shows the calculated, unscaled density of states obtained from the TPC decays of pentacene in fig. 7.29 at two different temperatures.

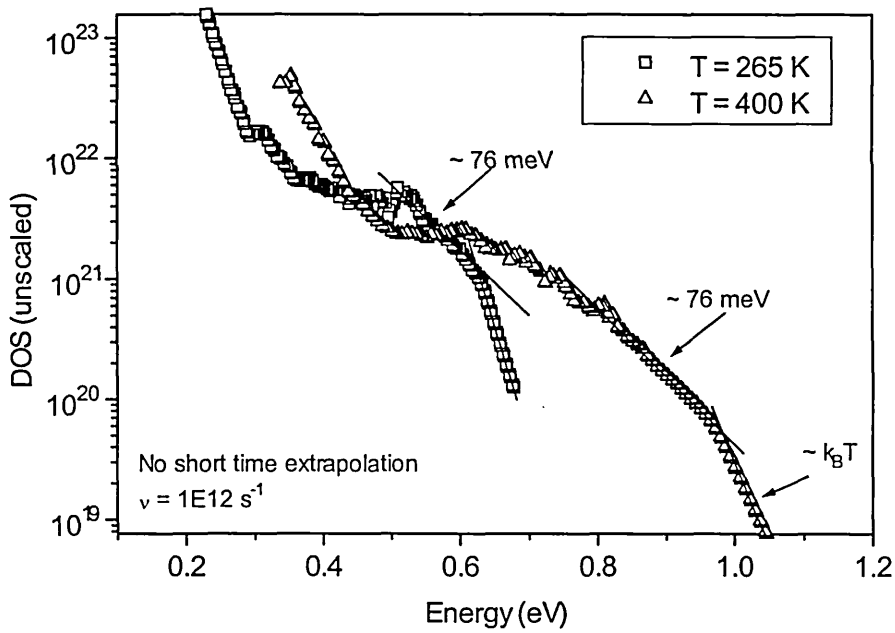

Fig. 7.35 Pentacene density of states obtained by the application of the Fourier transform program to experimental TPC data.

The FT program was run on the raw TPC data with the default parameters and no short time extrapolation of the decay. An attempt to escape frequency of 10^{12} s^{-1} was used to define the energy scale. In the DOS plots of fig. 7.35 the deep energy exponentials at each temperature are of slope ~ k_BT and are an artefact of the FT calculation. The form of the DOS returned by the FT program can be seen to have regions which may explain the form of the TPC decays, after a steep initial tail there is a flat region which gradually evolves into a wide exponential tail of slope ~ 76 meV at deep energies.

Overlapping the density of states distributions obtained from TPC decays at different temperatures builds up a composite picture of the DOS over a wide energy range, however it was found that in order to produce a reasonable fit the attempt to escape frequency had to be decreased. In addition to this the generated carrier density had to be altered *for each temperature* (NB. Although the attempt to escape frequency had to be decreased the same value was used for decays at different temperaures). Fig. 7.36 shows the composite DOS. Note that the value used for the pulsed carrier density at each temperature was simply used to fit the graphs and is not expected to represent the true value, however the fact that it must be altered at different temperatures suggests that carrier generation (quantum efficiency) is temperature dependent.

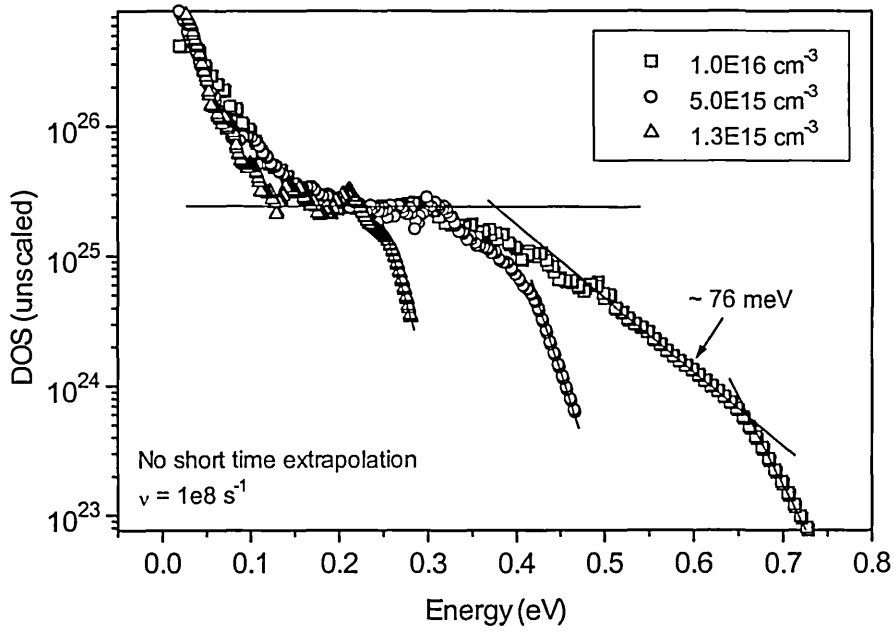

Fig. 7.36 Composite DOS obtained by varying υ and the pulsed carrier density.

It is illustrative to compare the density of states obtained in fig. 7.36 above with that obtained from the simulated TPC decays of fig. 7.33. These decays were produced by multiple trapping in a density of states that is flat at shallow energies and exponential below 0.5 eV ($k_BT_0 \sim 57$ meV). Fig. 7.37 shows the resulting DOS with and without a t^{-1} short time extrapolation of data. It can be seen that without short time current extrapolation the FT program fails to "see" the shallow energy flat region of the DOS, illustrating the importance of short time current data to the calculation of the Fourier integral within the program (see Webb, 1994 for more detailed consideration of this

problem). With the short time current extrapolated back several orders in time the flat region of the DOS is recovered, note that in both cases however the FT program does resolve the exponential region of the DOS. For multiple trapping transport the attempt to escape frequency is usually assumed to be of the order of 10^{12} s^{-1}, using this value with the experimental decays however leads to badly overlapping DOS distributions at different temperatures. It is found that a value of around 10^{8} s^{-1} provides a reasonable fit over the temperature range studied. This observation may indicate that trap-controlled hopping is the transport mechanism, rather than multiple trapping.

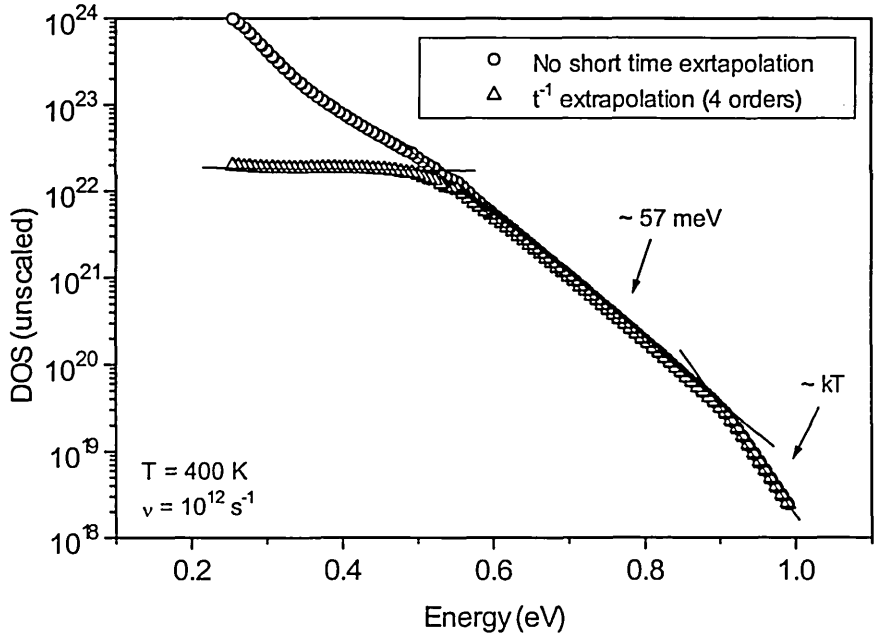

Fig. 7.37 DOS obtained from simulated TPC decays of fig. 7.33, with and without short time current extrapolation.

It is known that for multiple trapping in an exponential DOS, TPC decays obtained at different temperatures can be extrapolated back in time and intercept at a time which is equivalent to the reciprocal of the attempt to escape frequency. It has also been shown that for trap-controlled hopping the same procedure gives the average hopping frequency at the transport level as this is what replaces the band in a multiple trapping model (Monroe, 1985). When the decays of fig. 7.29 are extrapolated back they intercept at approximately 15 ns which corresponds to an attempt to escape frequency of $\sim 0.7 \times 10^{8}$ s^{-1} which is very close to the value used to fit the density of states in fig. 7.36 (10^{8} s^{-1}). The same procedure applied to the TPC decays obtained from TVC yields a

value for υ of 0.3×10^8 s^{-1}. These values for υ are too small for multiple trapping, thus we must assume that for these materials υ represents the average hopping frequency at a transport level in localised states, and that after a certain time interval transport occurs by thermal excitation to this transport level.

A further point to note about the DOS obtained from the FT method is that the exponential slope is not equal to that predicted by plotting the dispersion parameter vs. temperature in fig. 7.31, which is further evidence against the application of eq. 7.11 and a multiple trapping transport mechanism. It can be seen from fig. 7.36 that at higher temperatures more of the exponential region is uncovered, although at least a small section is observed at all temperatures.

From the above discussion it would appear that the FT technique is able to produce a believable density of states if trap-controlled hopping is occurring rather than multiple trapping, however it is less clear whether it can extract a density of states from a TPC decay produced by hopping alone. To investigate this situation TPC decays obtained from a Monte Carlo simulation program of hopping in a gaussian density of states were processed by the FT program. Fig. 7.38 shows TPC decays at different temperatures obtained from the Monte Carlo program (width σ_g = 0.1 eV). It can be seen that, as expected, the current decays to a constant value which is temperature dependent and the time to reach equilibrium is also a function of temperature. During the decay the initially gaussian carrier packet sinks from the centre of the DOS ($\varepsilon = 0$) to the equilibration energy which is given by eq. 4.52, retaining all the time an approximately gaussian shape (Pautmeier, Richert and Bässler, 1989). Once the carriers have assumed their equilibrium occupation transport occurs by trap-controlled hopping at a (T-dependent) transport energy. In this case however, as compared to the exponential DOS, once trap-controlled hopping begins the system is in equilibrium and the current ceases to decrease. The carrier packet ceases to thermalise because of the very rapid decrease in the density of available states in a gaussian distribution. The density of states calculated using the FT program is shown in fig. 7.39. It is obvious that for this situation the FT technique is not returning the actual density of states; firstly the form is not gaussian, and secondly the energy scale is completely inaccurate. Furthermore the attempt to escape frequency used in the program does not result in overlapping DOS plots at different temperatures.

Qualitatively the current decay due to a packet of injected carriers relaxing in an empty gaussian DOS states can be interpreted as follows. The carriers are initially

started, also with a gaussian distribution, at the centre of the DOS. They will begin to relax by directly hopping to lower energy states, only for carriers in deep states will thermal activation to higher energies dominate at early times. This hopping down regime results in the steep power law decay shown in fig. 7.38. As the carriers continue to hop down the rate decreases because the density of available states decreases rapidly with energy, eventually thermal activation begins to dominate and at this point the occupied density of states assumes its asymptotic limit and the carriers cease to thermalise. This process causes the transient current to curve over to a constant value until recombination or carrier extraction begins to decrease the carrier density.

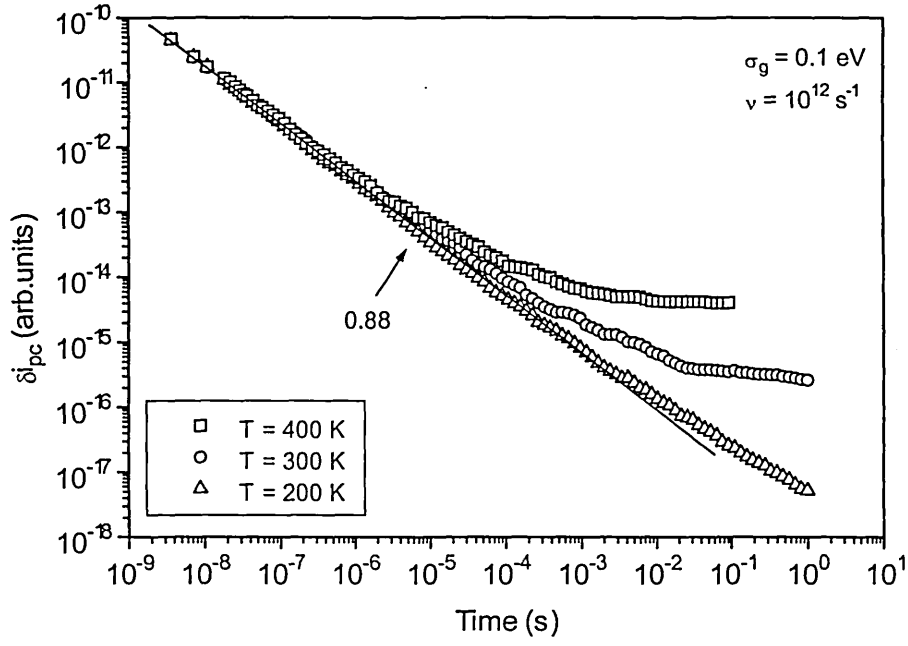

Fig. 7.38 MC simulated TPC decays due to hopping in a gaussian DOS.

This qualitative description of the current decay due to hopping highlights several reasons why the FT technique might not be valid in this case. In the initial hopping down regime the carrier packet sinks at a rate which will be temperature independent, but DOS dependent (similar to eq. 7.14), thus as the density of states decreases the carrier packet will sink more slowly until thermal activation to a higher density of states becomes more favourable. Since the carrier packet is roughly gaussian at all times during the decay the resulting current should reflect the density of states as the majority of carriers are at the peak of the gaussian. However the energy scale in this case will probably not be given by $k_BT\ \ln(\upsilon t)$. Once thermal activation to a transport energy is

occurring thermalisation stops and the current is constant and thus we can no longer obtain DOS information from this region of the TPC decay. Using the program described in § 5.2 current decays due to multiple trapping and hopping in a similar density of states can be directly compared. Fig. 7.40 shows the TPC decays produced by multiple trapping in a gaussian trapping level of width 0.1 eV situated 0.4 eV below the mobility edge.

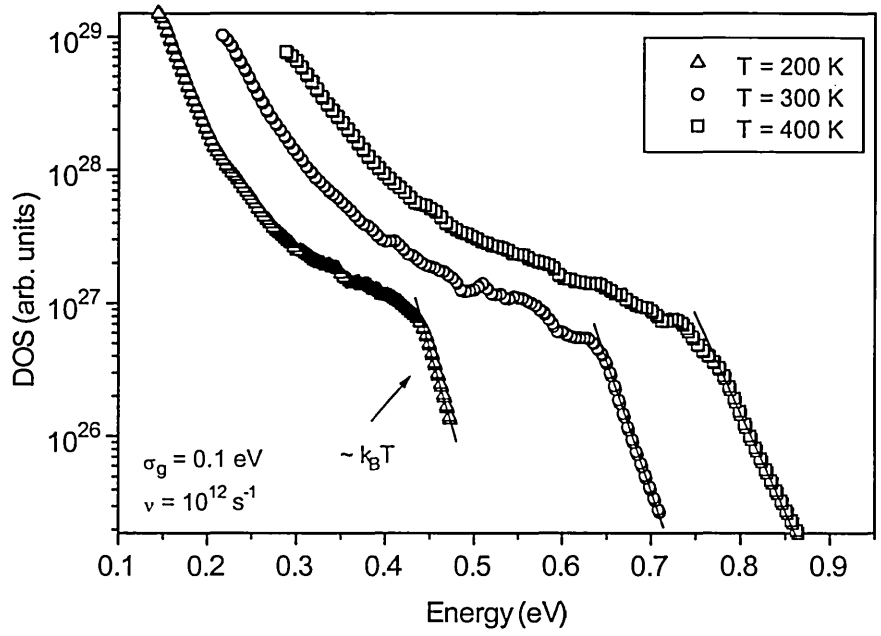

Fig. 7.39 Density of states calculated using MC simulation data of fig. 7.38

Fig. 7.41 shows the resulting DOS returned using the FT technique with no short time extrapolation of the data. It is clear that for multiple trapping the FT technique recovers the true density of states, in fig. 7.41 the position and peak density of the DOS is correct. However the form of the TPC decays and the resulting DOS distributions due to hopping are quite different as can be seen in figs. 7.42 and 7.43. In this case the DOS is again 0.1 eV wide, but it is displaced from the mobility edge by 4 eV so that multiple trapping cannot occur. Note also that in this simulation (as mentioned in § 5.2) the relaxation time is incorrect, it is several orders of magnitude too fast at 300 K, however the general form of the decays at different temperatures is similar to those produced by the Monte Carlo program. The density of states distribution obtained from the decays of fig. 7.42 are unusual due to the problem mentioned above concerning the

relaxation time of the carriers, however it can be seen that the form of the DOS is similar to that obtained from the MC decays although the scaling is altered.

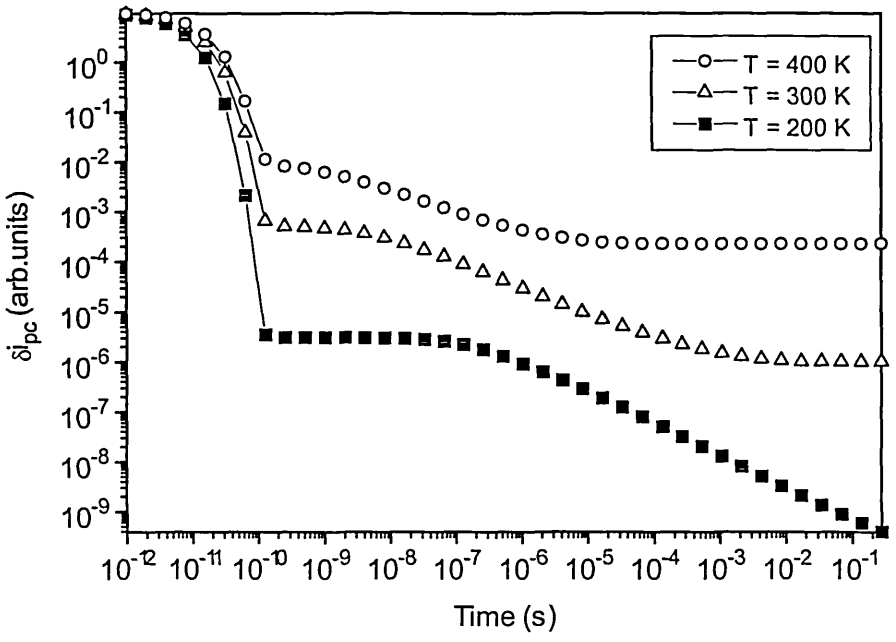

Fig. 7.40 TPC decays produced by multiple trapping in a gaussian trap distribution.

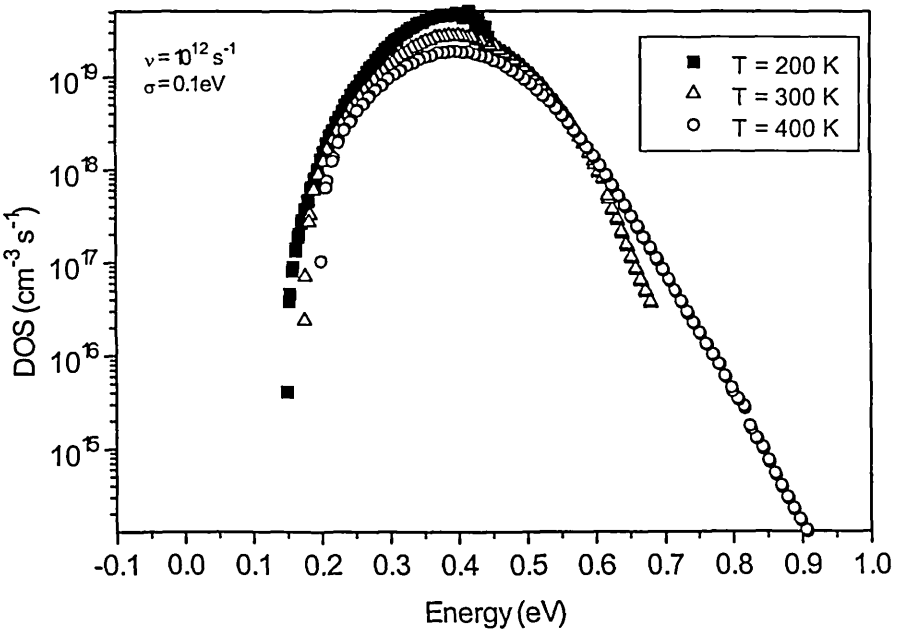

Fig. 7.41 DOS obtained from TPC decays of fig. 7.40.

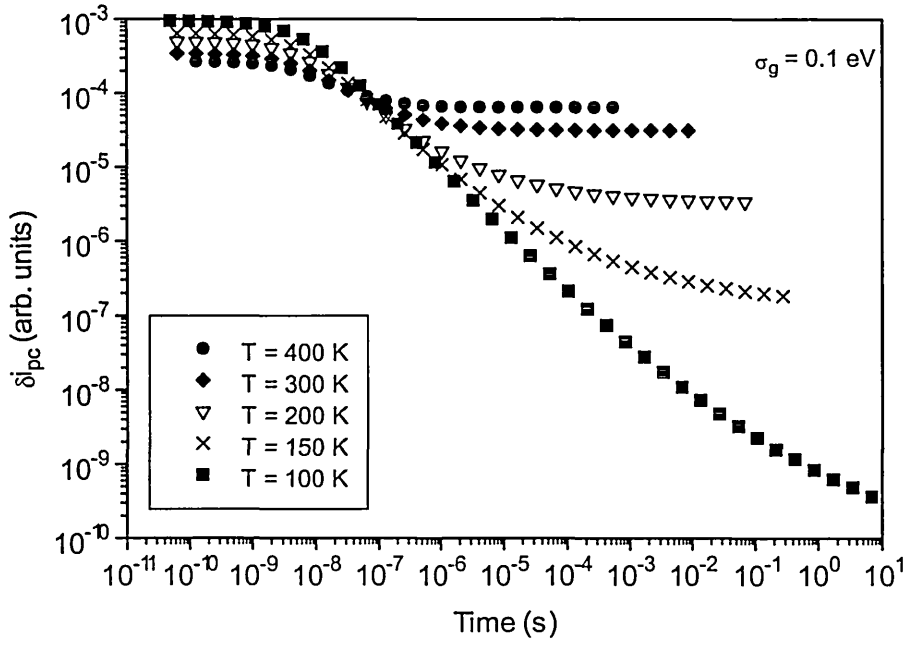

Fig. 7.42 Matrix technique simulated TPC decays for hopping in a gaussian DOS.

From the preceding discussions it must be concluded that the FT technique does not provide a full spectroscopy for a gaussian density of states if carriers move by hopping. Mulller-Horsche *et al.* (1987) applied a Laplace transform technique to poly(vinylcarbazole) and obtained trapping rate distributions. They found that the distribution of trapping rates was flat over the experimentally accessible range, which is at least partially in line with what has been observed with the oligomers studied here. Meyer *et al.* (1995) applied the FT technique to a derivative of poly(p-phenylenevinylene) and observed an exponential DOS of width 40 meV over an energy range of about 0.125 eV. In this case a conventional semiconductor band picture with localised band tails is more likely to be valid than in the oligomers, however the authors go on to suggest that delocalised band transport does not occur to any great extent and that transport occurs by hopping. In the case of an exponential density of states trap-controlled hopping will lead to a density of states from the FT technique. However, if a delocalised band does not exist an exponential distribution of localised states is perhaps unrealistic, a gaussian DOS would be much more likely. This is similar to the situation

in the present work in which it is unclear whether a genuine mobility edge exists, or whether transport occurs by multiple trapping or trap-controlled hopping.

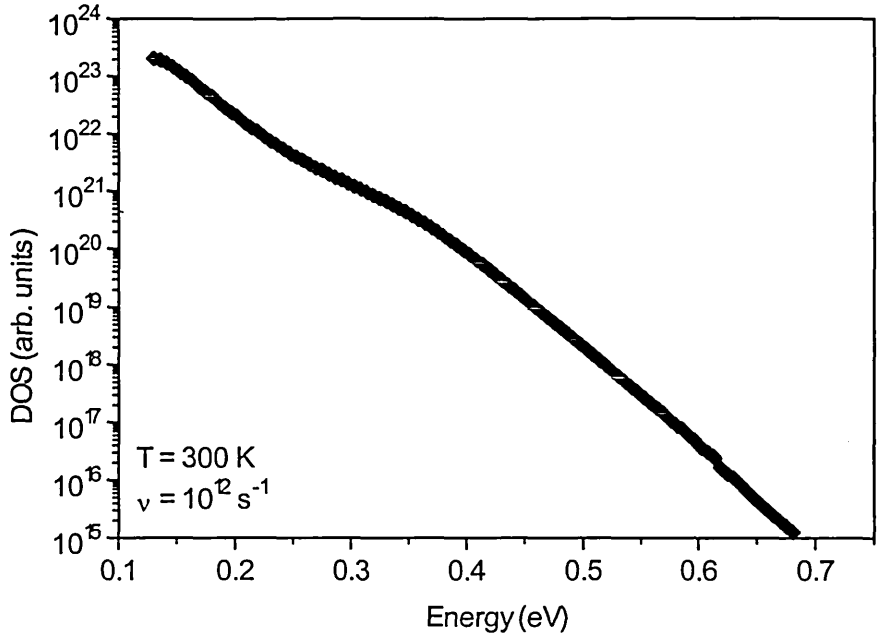

Fig.7.43 DOS obtained from 300 K TPC decay of fig. 7.42.

7.2.1.2 Field and intensity dependence of TPC decays

Varying the field strength was found to have no functional effect on the $\delta i_{pc}(t)$ curves, the effect of field was simply to increase the magnitude of the transient photocurrent (fig. 7.44). (Note, however that the investigated field range is small).

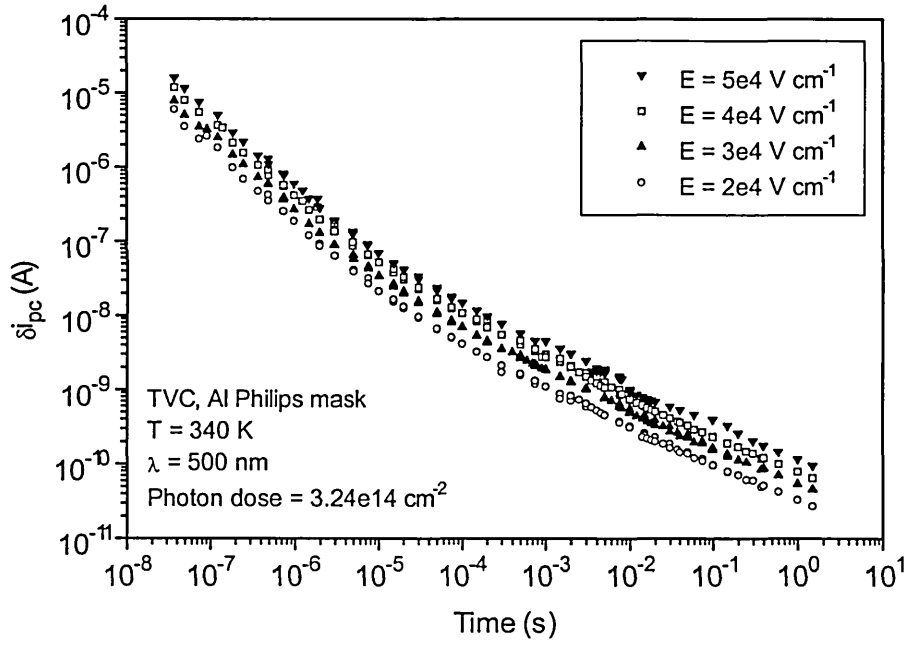

Fig. 7.44 TPC decays for TVC at different field strengths.

If we assume that the carrier density is constant within the TPC decay timescale then the magnitude of δi_{pc} in fig. 7.44 can be due to either the linear increase of δi_{pc} with field (quadratic increase in SCL regime) and/or changes in either the mobility or the quantum efficiency with field. If carriers move by multiple trapping the instantaneous transient photocurrent depends on the density of carriers in the band which is controlled by trapping and release from localised gap states, leading to a drift mobility. The free carrier mobility, μ_0 is generally assumed to be constant with field. The trapping and release equations do not contain field terms and thus changing the field should not alter the form of the δi_{pc} curves *i.e.* the effective mobility is independent of field, this is seen to be the case in fig.7.44. However altering the field should change the magnitude of δi_{pc} because E appears in the (ohmic) photocurrent equation, thus δi_{pc} should vary linearly with field, similarly in the SCL regime δi_{pc} should vary quadratically with field.

If the quantum efficiency is field dependent, as might be the case if carriers are produced by the model suggested in § 4.2.2, then the increase in the magnitude of δi_{pc} may also contain a component due to this. The result of plotting the instantaneous transient photoconductivity against the field strength is shown in fig. 7.45

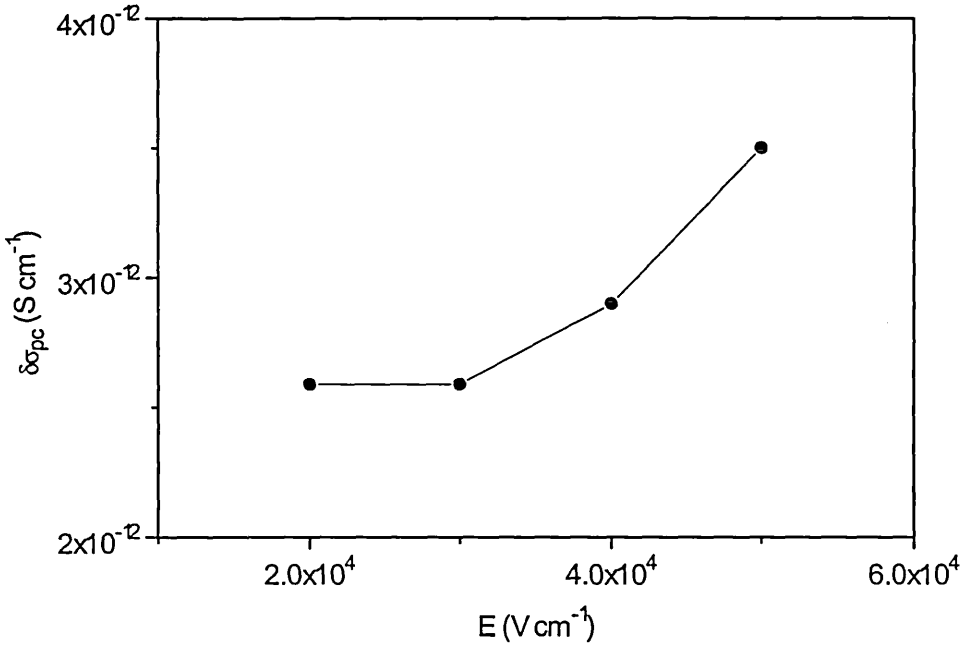

Fig. 7.45 Transient photoconductivity measured at 0.6 s vs. field strength.

In the linear regime the photoconductivity should be independent of field as is seen to be the case. The two data points at higher fields suggest that in this range the photoconductivity is in the SCL regime, this is in line with the photo-I-V curves which show a transition at around this field strength.

If carrier motion proceeds by hopping the main difference from the multiple trapping case is that the mobility should be field dependent. Unlike multiple trapping, in which a trapping/release cycle involves no spatial displacement and is therefore not affected by field, on hopping a carrier actually alters its position and is thus affected by the field strength and direction. Fig.7.46 shows MC simulated TPC decays of carriers hopping in a gaussian DOS of width 0.1 eV, parametric in field. In the simulation the injected carrier density is constant and there is no recombination, thus in this case the curves directly reflect the temporal variation of the mean carrier velocity in the x direction, δv_x (t) which is proportional to the mobility.

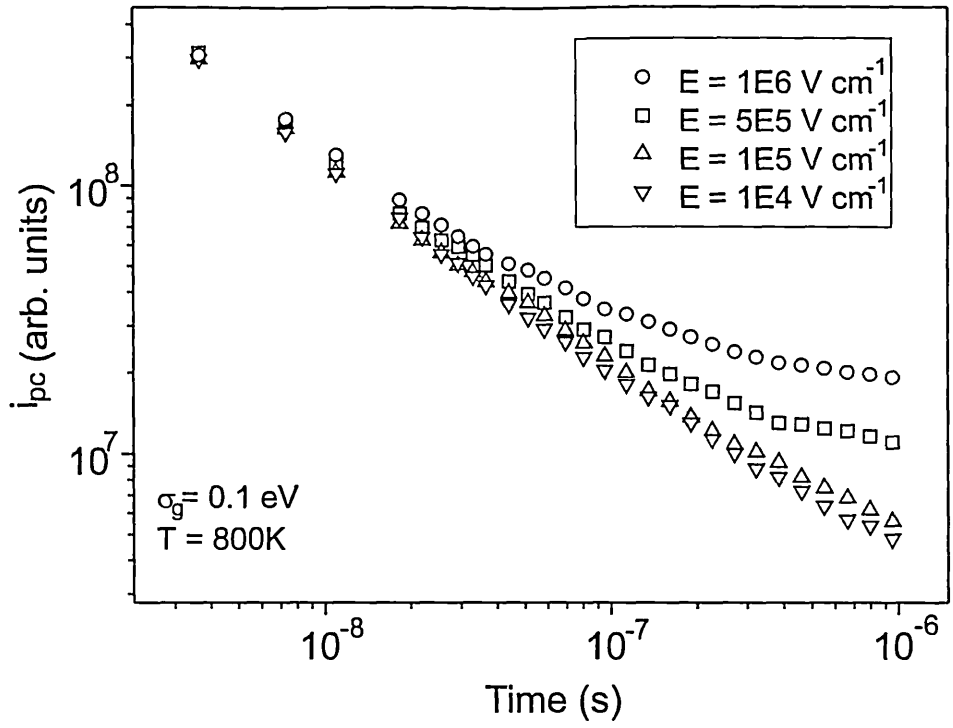

Fig. 7.46 MC simulated TPC decays parametric in field for hopping carriers in a gaussian DOS.

The simulation decays represent a physically unlikely situation, *i.e.* data obtained at 800 K, the simulation was run at this temperature simply because it decreases computation time. However, the result clearly shows that the field strength does affect the form of the $\delta v(t)$ curves. It can be seen that at the shortest times the currents are similar for all fields, but as time increases the effect of the field gradually begins to alter the form of the $\delta v(t)$ curves. The currents are similar at the start of the decay because the magnitude of the field is not explicitly included in the expression for determining the current, this means that the currents are effectively normalised at the shortest times because a fixed density of carriers are started from the x = 0 plane and will thus have similar initial velocities. A more realistic TPC simulation would start the injected carriers in an exponential distribution from the x = 0 plane as carriers are not generally strongly absorbed in the TPC technique, however this was not incorporated in the simulation. Note also that the MC simulation technique takes no account of a field (or temperature) dependence of carrier generation, which could alter the initial currents.

As the field is increased the $\mu(E)$ curves thermalise more rapidly to a constant current, steady state situation, this is in line with the DLH theory which predicts a field-induced narrowing of the DOS (Bässler, 1993). To obtain $v(E)$ (and thus $\mu(E)$) from the decays we would have to measure the change in δv with field when the decays have

decays we would have to measure the change in δv with field when the decays have thermalised to a constant velocity; in the simulation case this represents v(E) and therefore μ(E) directly, in a real sample however μ(E) would need to be corrected for the linear increase of δi_{pc} with field (quadratic in the SCL regime). The DLH theory predicts an $E^{1/2}$ field dependence of the mobility at high fields whereas at low fields the mobility is shown to be relatively field independent. The data in fig. 7.44 do not show any change in form with field which suggests that the mobility has a negligible field dependence in this range. This implies that the field strengths are in the field independent range of the mobility if the DLH model is to be valid. The field independent regime of the mobility generally lies below about 10^5 V cm^{-1} (Bässler, 1993) thus we are very likely to be in this regime as fields above 10^5 V cm^{-1} were not applied to the oligomers studied in this work.

Fig. 7.47 shows the effect of changing the illumination intensity on the TPC decays.

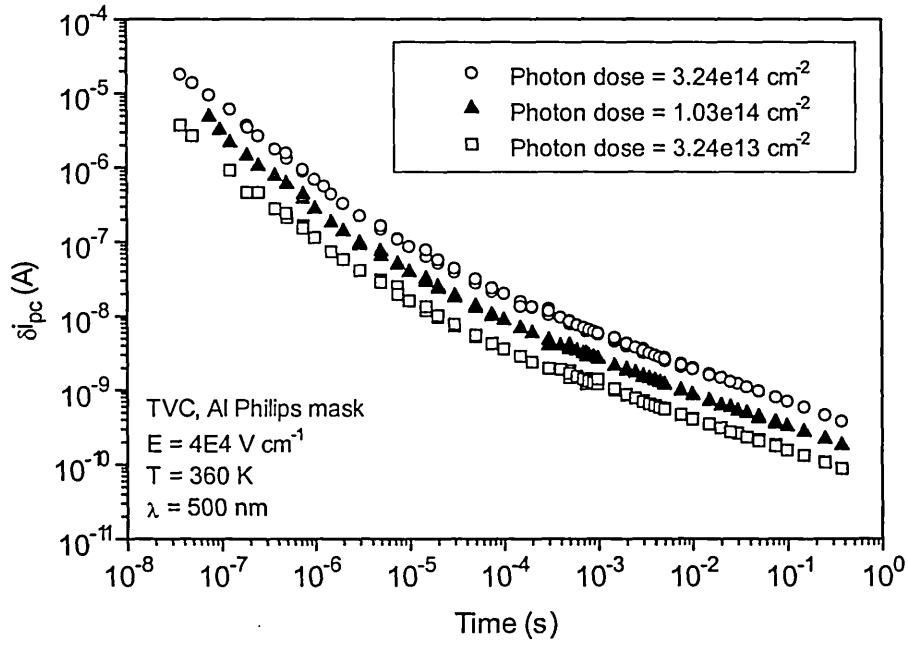

Fig.7.47 TPC decays for TVC at 360 K, parametric in pulse intensity.

Increasing the intensity will be expected to linearly increase the magnitude of the transient photocurrent before recombination begins as more charge carriers will be present, if recombination occurs within the experimental timeframe the functional form of the decays will be altered. The transient photocurrents measured at 0.4 s for the

decays in fig.7.47 are shown vs. intensity in fig.7.48. From this plot it can be seen that the TPC response is sublinear, exhibiting a slope of 0.63, although this value cannot be regarded as accurate due to the lack of data points.

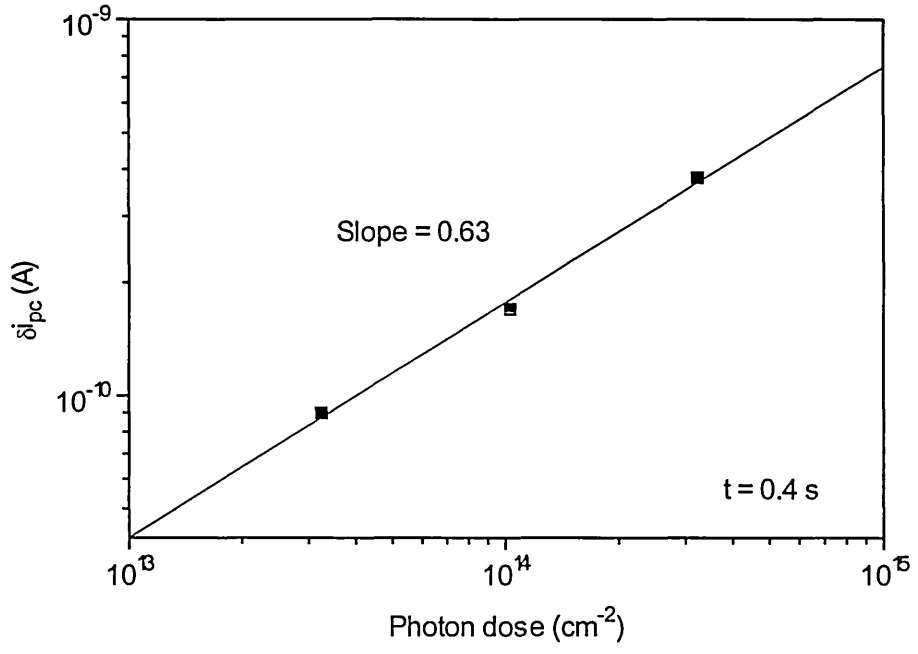

Fig. 7.48 Transient photocurrent measured at 0.4 s vs. photon dose.

The decays at different intensities do not change functionally in the experimental timescale, so it must be assumed that no recombination is occurring at these times, however a sublinear dependence of TPC with intensity suggests that recombination may have occurred at short times, *i.e.* before ~ 10 ns. Similar sublinear behaviour of the TPC magnitude on intensity has been observed in the other oligomers. Fig. 7.49 shows data for pentacene measured at 380 K. For this sample the TPC response is again sub-linear suggesting early recombination, however for this sample there appears to be a recombination feature at long times, although the decrease in current is not particularly clear from the data. The temperature is relatively high and the turnover to the steeper slope does not seem to be dependent on intensity which suggests that the recombination is monomolecular, again however the change in slope is quite small which means that the recombination rate is slow.

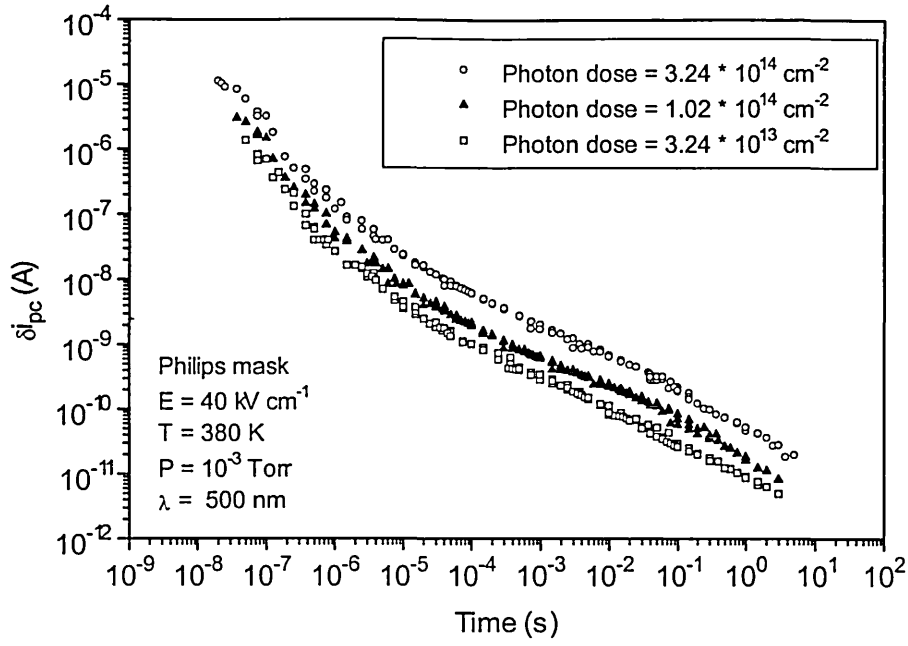

Fig. 7.49 TPC decays for thermally evaporated pentacene at 380 K, parametric in pulse intensity.

7.2.1.3 TPC with optical bias

In order to find out more about recombination in the oligomers TPC was carried out with optical bias applied. This technique is in effect a method of carrying out transient and steady state photoconductivity simultaneously. Performing TPC with optical bias enables us to probe the steady state situation, recombination features in optical bias decays yield information about the bias created carriers. Fig. 7.50 shows TPC decays for pentacene at room temperature with four levels of optical bias. It can be seen that optical bias results in a recombination feature entering the experimental time window, in this case the carrier lifetime (given approximately by the turnover in the TPC data) decreases with increasing optical bias intensity. When optical bias is applied it appears to increase the total number of recombination centres, thus decreasing the lifetime of the pulse generated carriers. If we assume that holes are the predominant charge carriers and recombination occurs between free holes and trapped electrons then we can denote the total density of recombination centres under bias as $n_{tr} + \Delta n_r$, where n_{tr} is the thermally-generated density and Δn_r is the bias-generated density. In general if $n_{tr} >> \Delta n_r$ then the hole lifetime should be bias independent but should decrease as temperature increases (monomolecular regime), however if $n_{tr} << \Delta n_r$ then the lifetime

should decrease with increasing photon flux and temperature although the latter effect is likely to be much smaller than the former (bimolecular regime). For the data in fig. 7.50 the bias intensities employed have been shown to result in a steady state photocurrent that varies sub-linearly with photon flux (see § 7.1.3), so increasing the photon flux results in a decrease in the carrier lifetime as can be seen. Also shown in fig. 7.50 are the slopes of the pre- and post-recombination slopes, the post-recombination slope is approximately constant with intensity. Using the slopes from fig. 7.50 the values obtained for the dispersion parameter are 0.46 for α_1 and 1.03 for α_2. This is in agreement with values from TOF decays (Schönherr, Bässler and Silver, 1981) in which the values of the dispersion parameter before and after extraction are not equal, and do not add to 2, as predicted by the theory of Scher and Montroll (1975).

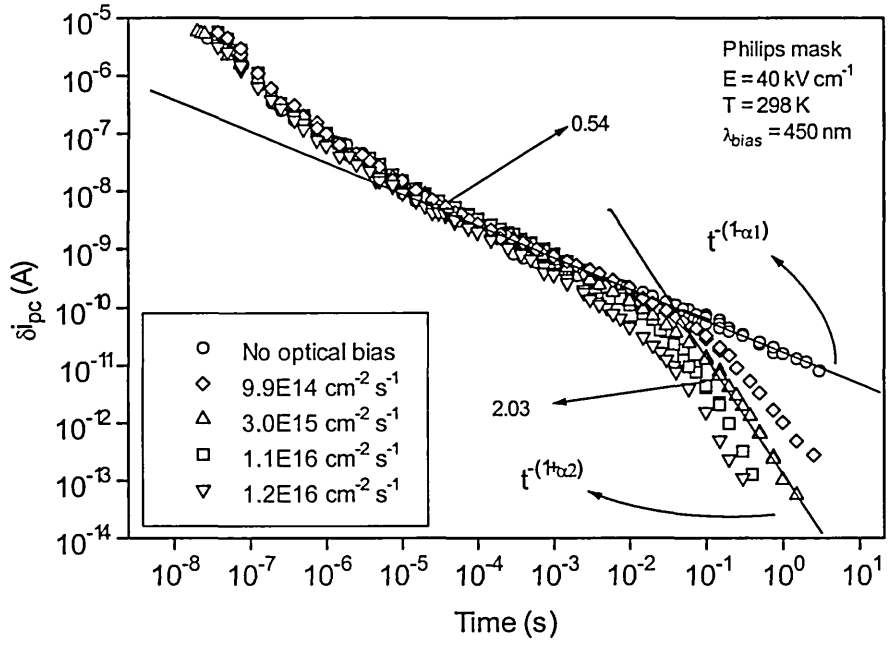

Fig. 7.50 TPC decays for pentacene at room temperature with different levels of optical bias.

From the decays in fig. 7.50 we can see that the carriers have not thermalised prior to recombination. Using the terminology of Pandya and Schiff (1985) this corresponds to the B-trapping case (in the A-trapping case the carriers thermalise *before* recombination occurs). However the recombination time is intensity dependent implying recombination is bimolecular. For multiple trapping in an exponential DOS as treated by the above authors the resulting decay form should then depend on the ratio C_t/C_R where C_t and C_R are the trapping and recombination coefficients respectively. If $C_t/C_R >$

1 then complete thermalisation occurs before recombination, corresponding to the A-trapping case, if $C_t/C_R < 1$ then recombination begins before the carriers have thermalised, in this B-trapping case a sign reversal is expected in the TPC decay, this situation has been observed experimentally in a-Si:H by Webb (1994). In the transitional case of $C_t = C_R$ neither thermalisation nor a sign reversal is expected. In the present context the work of Pandya and Schiff is unlikely to be applicable because it employs a multiple trapping transport mechanism, however it does give insight into the form of the decays under optical bias and how to interpret them. To the author's knowledge a similar analysis for hopping carriers has not been carried out. The decays in fig. 7.50 thus correspond to bimolecular recombination, however thermalisation obviously has not occurred, there is also no evidence of a sign reversal in the decays, therefore using the above model we must assume that $C_t = C_R$.

The decays in this case may also be interpreted more simply if we consider what the pulse-generated carriers "see" once they are created. In thermal equilibrium the density of recombination centres is low thus pulse generated carriers encounter very few recombination centres, increasing the temperature will increase n_{tr} but in the experimentally probed range n_{tr} does not become large enough to shift recombination features into the experimental time window. When optical bias is applied so that $\Delta n_r >> n_{tr}$ the pulse-generated carriers "see" a large density of bias-created recombination centres (equivalent to raising the temperature) and thus their lifetime is reduced. In this case it is obvious that increasing the bias flux increases Δn_r and thus decreases the carrier lifetime.

Fig. 7.51 shows TPC decays for TVC at 340 K with three different levels of optical bias. For this oligomer the bias intensity does not have as large an effect on the carrier lifetime. The decays do not follow a common decay once recombination has begun, but it is hard to tell from the data the exact time at which the turnover occurs. The functional form of the post-recombination decay is also unclear. The difference in the form of the decays in TVC and pentacene is most likely to be due the different measurement temperatures. As we saw in § 7.1.3 the ratio of the photoconductivity to dark conductivity was quite different for each oligomer at room temperature, pentacene showed the highest value of ~ 458 whereas TVC showed a value of only 1.4. For TVC the photocurrent should cross the dark current at ~ 360 K at a flux of ~ 10^{16} cm^{-2} s^{-1}. At high temperatures therefore, the density of thermally generated recombination centres may exceed those created by illumination, resulting in monomolecular recombination.

In this situation optical bias should have negligible effect on the TPC decay. The data in fig. 7.51 are definitely changed by the optical bias: recombination occurs within the experimental time window whereas TPC decays without optical bias do not exhibit recombination, even at 380 K.

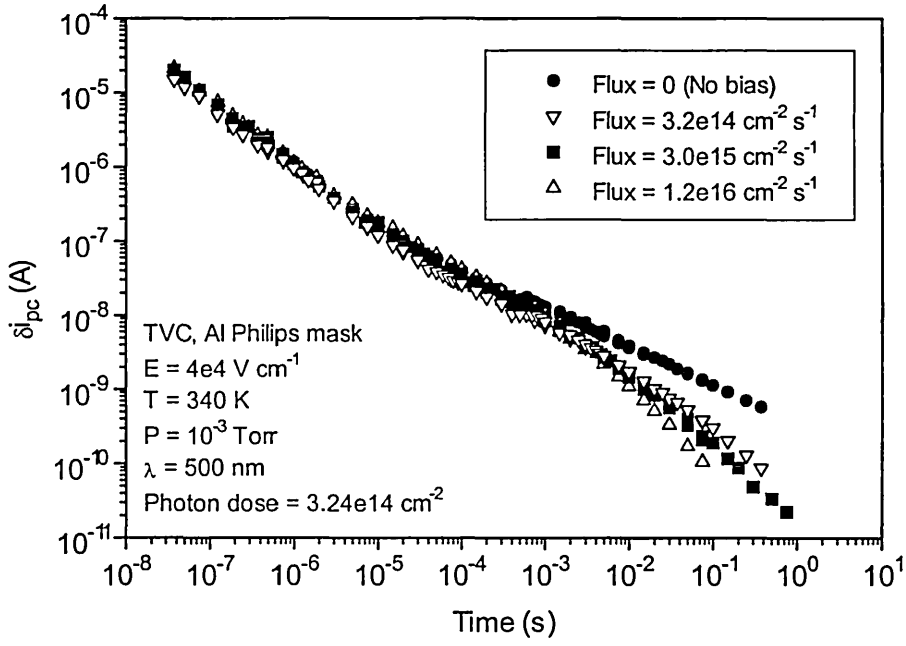

Fig. 7.51 TPC decays in TVC at 340 K with varying levels of optical bias.

Therefore it must be assumed that the bias-generated recombination centres are dominant in this situation, the absence of a significant shift in the recombination time may be because for TVC at this temperature the decays represent a transition situation in passing from bimolecular to monomolecular recombination regimes.

Fig. 7.52 shows data for TVD in which the optical bias intensity is adjusted to give equal steady state photocurrents at each wavelength. It can be seen that the bias wavelength has a quite significant effect on the recombination, for lower wavelength the current decreases much more rapidly after the recombination time. As was shown earlier recombination can already be seen to be affecting the TPC decay even with no bias applied. The photocurrents at fixed flux are different due to changes in the absorption coefficient and/or the quantum efficiency with wavelength. If the photocurrents are equalised then the carrier density and thus lifetime must also be equal

at each wavelength, however the absorption profiles may be different for each wavelength which means that the carrier density will vary with depth into the sample.

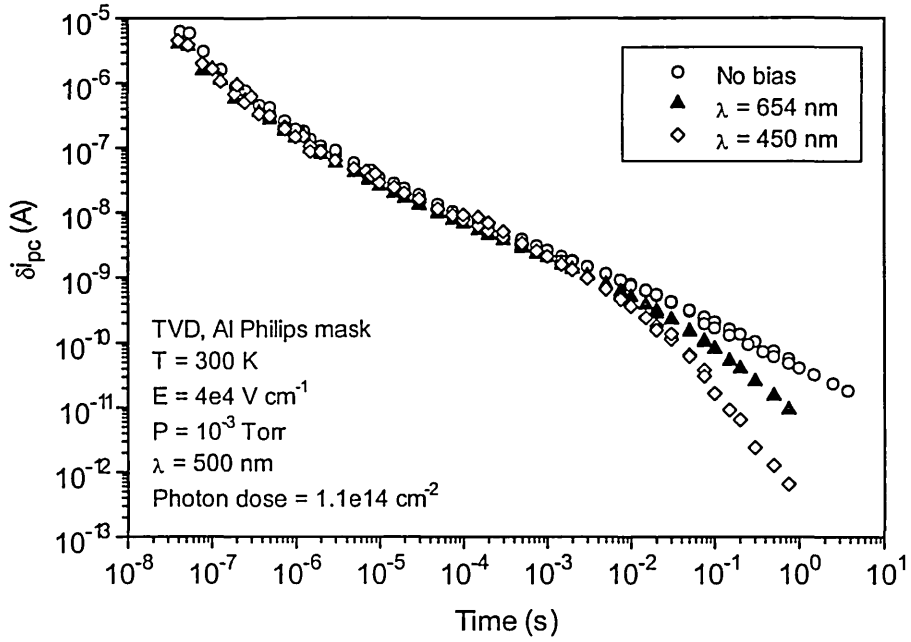

Fig. 7.52 TPC decays for TVD at 300 K with different optical bias wavelengths.

The decays in fig. 7.52 can be explained as long as the absorption coefficient for blue and red bias light are different, if the absorption coefficient is larger for blue light the carrier density near the sample surface will be higher than for red bias. If the pulsed carriers are also absorbed in the surface region they will therefore see a higher carrier density if blue bias is employed, and will thus recombine more rapidly. Examination of fig. 7.2 confirms this reasoning. From this spectrum the penetration depths of red, blue and green light are roughly 0.37 μm, 0.25 μm and 0.23 μm respectively.

7.2.2 Persistent photocurrent measurements

It was generally found with the oligomers studied that on removal of steady state illumination the return to the thermal equilibrium condition was very slow. Consequently experiments in which it was desired to measure photocurrents and dark currents became impractical, as after illumination it was often necessary to wait for very long time periods until the initial dark current was recovered. However, it was found that the dark current could be recovered more rapidly by increasing the temperature (cf. dark current reduction by annealing), and thus this was generally performed after the sample had been light soaked. This phenomenon of very slow relaxation after illumination, commonly referred to as persistent photocurrent (PPC), has been observed in other organic solids, as previously discussed in § 4.2.4. As in the case of sample annealing and exposure to ambient atmosphere, persistent photocurrent effects were found to be a common characteristic of all the oligomers and therefore tentative investigations of this important phenomenon were carried out.

Fig. 7.53 shows the decay from steady state for laser ablated pentacene at different temperatures, plotted in log-lin form. The sample was illuminated for five minutes with green light (λ = 525 nm) before removal of excitation. It can be seen that there is a fast initial decay followed by a slow, approximately exponential, decay. For the three lowest temperatures the decay is exponential up to the longest times measured, with a slope that appears to be independent of temperature, however the decays at higher temperatures are not similar. At 380 K there is again an exponential region but at this temperature the slope is steeper and at the longest times the current decreases very rapidly. At 400 K the situation is similar but more pronounced, an exponential region can only be fitted over a small range in this decay which is steeper than the one obtained at 380 K. After about 2500 s the decay begins to fall off more rapidly. Note that for the 360 K decay a transition to a more rapid decay is not observed, even at 10000 s suggesting that at low temperatures the relaxation time to thermal equilibrium after illumination is very long.

Fig 7.54 shows the data of fig. 7.53 plotted in log-log form for comparison, which shows more clearly the similar form of the decays at short times and the temperature-dependent turnover at the highest temperatures.

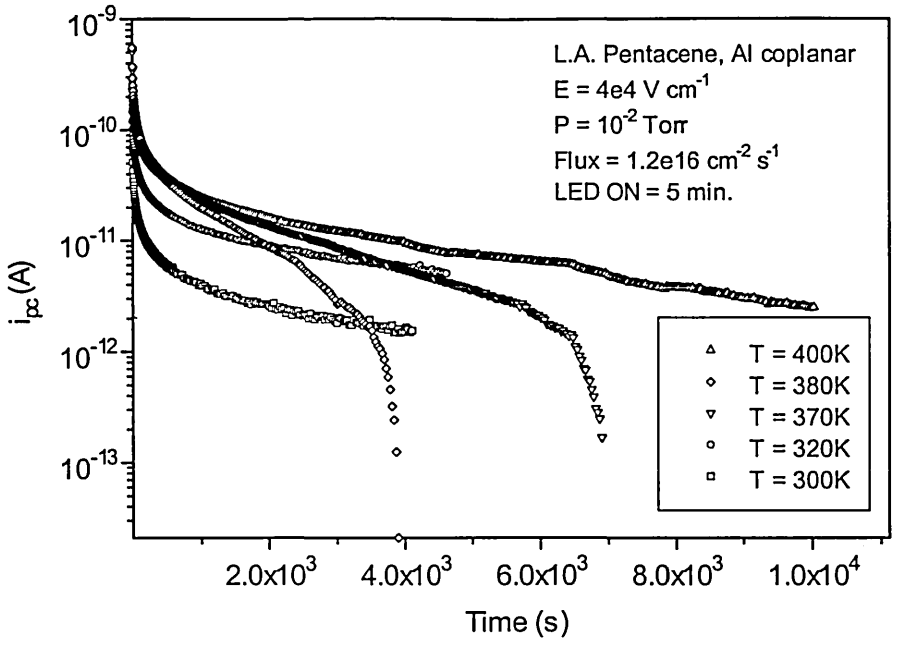

Fig. 7.53 Relaxation from steady state for laser ablated pentacene.

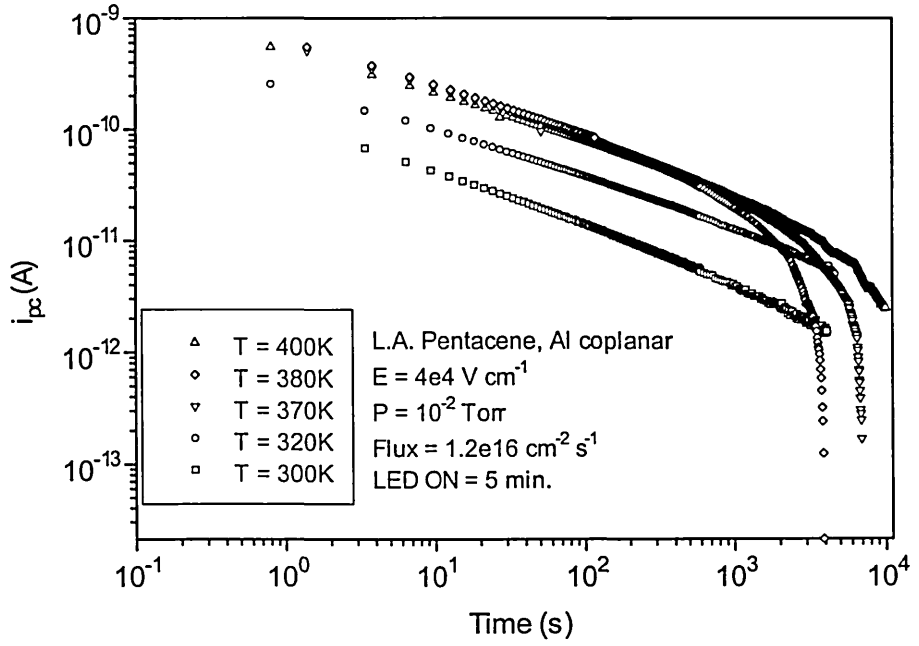

Fig. 7.54 PPC decays of fig. 7.52 plotted in log-log format.

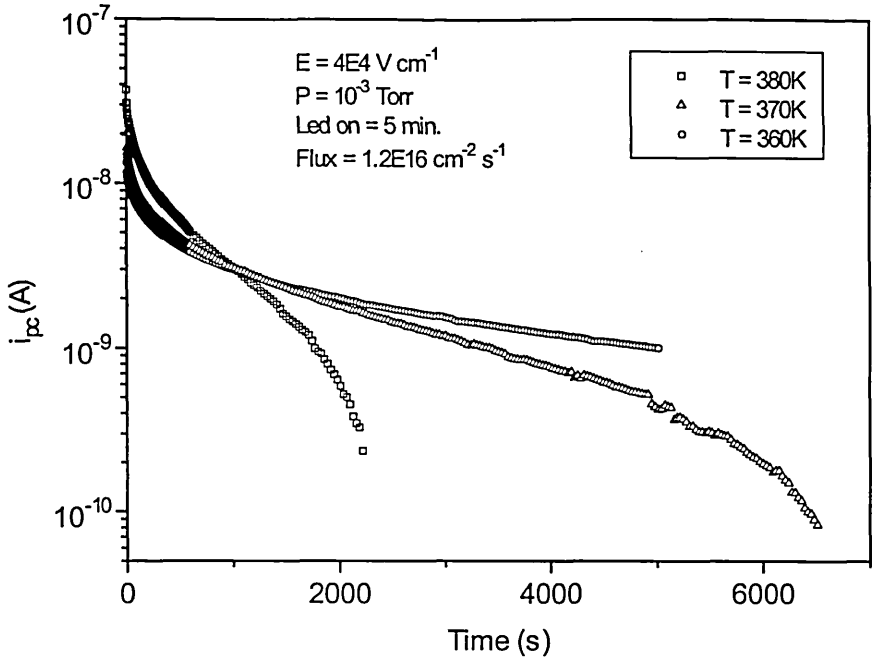

Fig. 7.55 PPC decays for TVC at different temperatures.

Fig. 7.55. shows experimental data for TVC, the general from of the decays is similar although the relaxation rate at a certain temperature is faster for this sample than for pentacene. The decays of figs. 7.53 7.54 and 7.55 demonstrate that increasing the temperature increases the relaxation rate. This explains why annealing the samples after exposure to light resulted in a faster return to thermal equilibrium.

The effect of varying the steady state illumination intensity on the form of the PPC decays is presented in fig.7.56, increasing the intensity tends to increase the decay rate at short times and the decays for the three highest photon fluxes can be seen to merge at longer times. At the highest illumination intensity the decay can be fit reasonably accurately by a power law of slope ~ 0.5. Also investigated was the effect of increasing the length of steady state illumination on the PPC decays, but no significant difference was observed with the exposure time varied between 1-10 minutes.

The extremely long relaxation time exhibited by the oligomers can be attributed to either very slow recombination, which may be caused by a barrier to the recombination event or due to charge being stored, for example in deep traps. What is clear is that there must be a very wide range of individual carrier lifetimes to produce such extended decays.

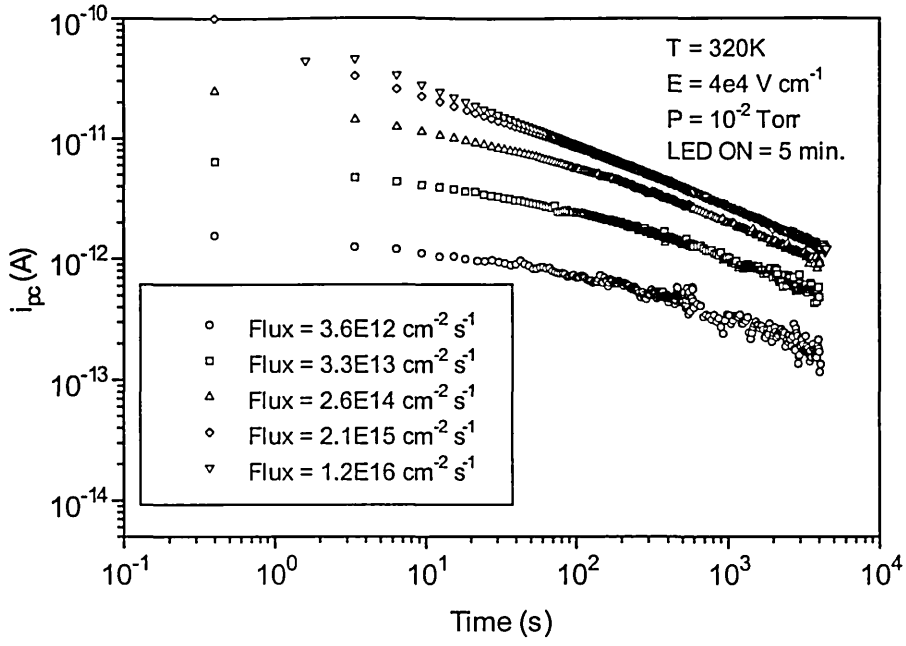

Fig. 7.56 PPC decays for laser ablated pentacene with different steady state illumination intensities.

From fig. 7.56 it is clear that higher steady state illumination levels result in a faster initial decay, *i.e.* higher recombination rate, due to the higher carrier density. It can be seen that due to this the top three decays tend to merge into a common decay at long times. It is possible that given enough time even the low intensity decays will eventually collapse on to this common decay. The decays at different temperatures in fig. 7.54 are parallel over most of the experimental time range, suggesting that higher temperatures do not affect the recombination rate until the long time, temperature dependent, turnover. The magnitude of the persistent photocurrent is temperature dependent however. This change in magnitude with temperature may be due to a temperature dependence of the mobility or the carrier density, but the fact that in fig. 7.54 the PPC decays are parallel whereas in fig. 7.56 the slope is dependent on intensity, and therefore carrier density, suggests that the temperature dependence of the persistent photocurrent is mainly due to the mobility.

The present experimental results do not appear to fit well with the persistent photocurrent models described in § 4.2.4. The model of Akashi *et al.* (1994) is obviously not valid in this case because we are dealing with undoped materials. However, as noted in § 7.1.4 the films may be unintentionally doped with O_2, although the extent of this doping is unclear. Transfer of an electron from the oligomer to O_2

may result in the generation of a mobile hole and a trapped electron, however it is unclear why the ultimate recombination of the electron and hole is inhibited. It is unlikely that a similar mechanism to that described by the above authors is possible. In fact reduction of oxygen to form O_2^- causes the O-O bond length to increase, which might be expected to increase the overlap between the electron and hole, and facilitate recombination. This is just the opposite situation to that which occurs in the model of Akashi *et al.*, in which the charge redistributes on the C_{60} dopant and reduces electron-hole overlap.

The model of Lee *et al.* predicts a stretched exponential form for the persistent photocurrent decay (Lee, Yu and Heeger, 1993). The PPC decay observed in the oligomers studied do not appear to be of this form as can be seen in figs. 7.53-7.56. In TVC a peak is observed at the absorption edge which would fit in with the idea of increased surface recombination according to DeVore's theory. Lee *et al.* use this as a key piece of evidence to support their model of slow bipolaron diffusion to the surface, and subsequent recombination. However, for the oligomers studied here the validity of DeVore's theory is uncertain, as it assumes a conventional semiconductor band to band transition which is unlikely for materials such as this. Furthermore the presence of a peak at the absorption edge is not necessary for the production of a persistent photocurrent in these materials. This can be appreciated by comparing the PPC decays of TVC and pentacene which are functionally similar, then comparing the action and absorption spectra of both oligomers which differ considerably. Thus it would appear that the above models are too material specific to explain the persistent photocurrent effects observed in these oligomers.

As mentioned above deep trapping of holes could account for the extremely slow recombination, in a qualitative manner at least. Thermal emission from a discrete trapping level would account for the temperature activated, long time recombination feature. The slow, almost power law decay observed over most of the experimental timescale is functionally unaffected by temperature and could possibly be due to tunneling of trapped holes to recombination centres.

7.3 Interpretation of results - a synthesis

In this final section an attempt is made to pull together the steady state and transient results presented in the previous sections and thereby to obtain an overall picture of the transport mechanism and density of states of the oligomers studied. There are three transport mechanisms which have been considered in this work and we shall take each in turn and discuss the validity of the model for the oligomers. We shall start by discussing the multiple trapping model, then move on to look at hopping and trap-controlled hopping.

It is useful to begin by noting that the majority of the results initially appear to be consistent with a multiple trapping transport mechanism. However, as has been mentioned several times, the multiple trapping model is usually not considered applicable to molecular materials. Transport models for organic, molecular solids have been discussed in § 4.4 and are invariably based around hopping as the basic transport mechanism. There are several results which support this and do not fit with multiple trapping. Among the most important of these are the magnitudes obtained for the mobilities and the conductivity pre-exponential factors. These are several orders of magnitude smaller than values typically observed in multiple trapping systems. The magnitude of the dark current activation energy is also too small for multiple trapping. A further experimental observation which does not agree with the multiple trapping model is the apparent field dependence of the photocurrent and the dark current. The activation energy of the dark current, and the magnitude of the photoconductivity index γ were found to display field dependent behaviour.

The above mentioned experimental results are strong evidence against a multiple trapping transport mechanism, however these type of results *are* expected for hopping carrier motion. Unfortunately on closer examination of the experimental results we must conclude that hopping transport, as described by the DLH model, is also unable to fully account for the experimental results. The DLH theory for hopping in a gaussian density of states predicts that hopping carriers thermalise at long times, with transport then proceeding by trap-controlled hopping at the transport energy. This would result in TPC decays which become time invariant after a specified time interval. This is not observed experimentally. In addition, even if the main transport band is a localised gaussian DOS the materials studied here are certain to have trapping levels outwith this band. These trapping states could be caused by interaction between oligomers or be due to crystalline grain boundaries. The existence of traps below the main transport band

would lead to trap-controlled hopping, purely hopping transport would only be expected at very low temperatures.

It has been suggested at several points in this work that trap-controlled hopping may be an appropriate transport mechanism. Trap-controlled hopping is in effect a hybrid of pure hopping and multiple trapping and would thus be expected to exhibit some characteristics of both. There are several results which suggest that trap-controlled hopping may be occurring. For example, in § 7.1.2 it is suggested that band tail hopping is responsible for the dark current activation energy, as this is too small to represent the depth of the intrinsic Fermi level. This conjecture is backed up by the apparent field dependence of the Arrhenius plots which would not be expected for multiple trapping with a delocalised valence band. Further evidence in favour of trap-controlled hopping comes from the TPC decays and the density of states obtained from the FT technique. Extrapolating back in time from the TPC decays yields a value for the attempt to escape frequency that is too small for multiple trapping, but reasonable for trap-controlled hopping. It is also found that using this value of the attempt to escape frequency to fit the DOS plots at different temperatures results in overlapping data and thus a good agreement. Thus it would appear that a trap-controlled hopping mechanism is the only case which can adequately explain the experimental results in the temperature range studied.

The form of the density of states will, in general, determine the transport mechanism that occurs at a specified temperature. The majority of information concerning the form of the density of states in the oligomers comes from the transient results, however the steady state results suggest that there is a continuous distribution of trapping states in the band gap. The photocurrent vs. intensity graphs yield values for γ which are in general between 0.5 and 1.0, which is strong evidence for a continuous trap distribution, at least over the energy range by which the quasi Fermi level is shifted by illumination (see Rose, 1978).

In § 7.2.1 the form of the density of states for the oligomers was inferred by working back from the TPC decays using qualitative and quantitative methods. It was decided that the TPC decays could only result from trap-controlled hopping motion in a DOS consisting of a flat region at high energies and an exponential at deeper energies. However, Monte Carlo simulations of hopping in a DOS such as this were not carried out. On the other hand, it has been demonstrated that multiple trapping in such a DOS does not account for all the features of the TPC decays. Applying the FT method to the TPC decays resulted in a density of states which was roughly consistent with that

predicted qualitatively, however in the flat region of the DOS, where carriers would thermalise by hopping down, the rate at which the demarcation energy sinks is not given by $k_BT\ \ln(\upsilon t)$ as in multiple trapping. It has been shown by Monroe (1985) that for an exponential DOS the rate at which the demarcation energy sinks in the hopping down regime is temperature independent but is dependent on the form of the DOS. Thus in this case the rate decreases as the demarcation energy sinks deeper into the DOS. In a flat DOS, however, the rate is likely to depend only on the magnitude of the density of states. Therefore the energy scale of the DOS obtained from the TPC decays cannot be relied upon.

Simulated TPC decays for hopping in a gaussian density of states, as assumed in the DLH theory, yield DOS distributions which look quite similar to those obtained from experiment. However, in this case an exponential form at deep energies is not observed. Furthermore the experimental TPC decays do not show features consistent with carrier thermalisation within the experimental time window at any temperature, which is very solid evidence against the idea of a single, gaussian DOS of localised states. Silver *et al.* (1981) have performed MC simulations of hopping in a gaussian DOS with a single trapping level below the main transport band. The resulting transients are in no way similar to those obtained on the oligomers in this work, which supports the idea of a continuous trap distribution.

The similarities between the TPC decays for all materials studied implies that the density of states distribution in all the oligomers is of a similar form. If this is the case it explains the largely similar experimental results obtained on all the materials. Note, however, that it was pointed out in § 7.2.1.3 that the magnitude of the density of states at the transport level does apparently vary from oligomer to oligomer, as deduced from the variations in the pre-exponential factors, σ_0. The reason that the DOS is similar for all the oligomers may be a result of the similar size and shape of the molecules resulting in a similar thin film structure. If each molecule can be considered as a potential state for a charge carrier then it is not unreasonable that such similarly structured materials will exhibit a similar density of states distribution. However, it is still possible that the specific *chemical* structure of the transport molecule will affect the magnitude of transport relevant parameters. Thus carrier generation, and therefore the free carrier density, is likely to be determined by the type of chemical groups attached to the oligomer backbone (cf. the increase in the dark current in TVD due to methyl group electron injection).

8. Summary and conclusions

The primary aim of this thesis was to form an general picture of the electronic properties of several oligomer thin films, and specifically to elucidate the charge transport mechanism. Furthermore it was endeavoured to determine how the chemical structure of the oligomers affects the electronic properties, such as the density of states and parameters relevant to charge transport. It was hoped that such information would make possible an assessment of such materials for device applications.

Possibly the unifying theme amongst the materials studied here is the almost identical behaviour observed in all experiments performed. This immediately suggest that all the oligomers have a similar density of states, and thus transport mechanism. However, there were some notable differences between the materials. The most obvious amongst these was perhaps the fact that all four oligomers were different colours, which is reflected in the absorption and photocurrent action spectra which vary considerably from oligomer to oligomer. The reason for this is that both these measurements highlight properties of the individual oligomer molecule and not the solid as a whole. The fact that the electronic properties of the materials varied little is more likely a reflection of the similar *structure* of the thin films for all oligomers. The only situation in which a direct comparison was valid was between TVD and TVC. Here it was found that the addition of the four methyl groups on TVD resulted in a large increase in the dark current, but a less significant increase in the photocurrent, resulting in a photocurrent smaller than the dark current at room temperature. This was attributed to electron injection from the methyl groups facilitating carrier generation.

The experimental results have been interpreted using current transport models, in particular the multiple trapping and disorder-limited hopping models. It is found that neither of these models fully explains the experimental data. The multiple trapping model is found to explain superficially most of the transient and steady state data. However more detailed investigations showed that in most cases the magnitudes of important transport parameters, such as the mobility, were inconsistent with multiple trapping. These findings lead to the conclusion that transport, in the temperature range studied, must be occurring by trap-controlled hopping. This naturally accounts for the observation of characteristics consistent with both hopping and multiple trapping.

A large part of the thesis has been devoted to extracting the density of states from the TPC decays. It was found that the DOS implied qualitatively from the form of

the TPC decays agreed satisfactorily with those obtained by processing the experimental data using the Fourier transform method. However the validity of the resulting DOS is still unresolved. The FT method is valid for a multiple trapping transport mechanism and it has been suggested in § 7.2.1.1 that it may also be valid for trap-controlled hopping. If transport proceeds by trap-controlled hopping though, it is unlikely that the energy scale can be defined using eq. 4.36, unless the attempt to escape frequency is modified. Certainly in the hopping down regime predicted in the flat region of the DOS this equation is not valid. It has further been shown that the FT method does *not* provide a DOS spectroscopy in a purely hopping situation such as that described by the DLH theory. Thus in oligomeric materials such as those studied here the FT method, in its present form, is at best a qualitative tool for obtaining information on the *form* of the DOS. It cannot be relied upon to give an accurate density of states magnitude at a specific energy.

Other experimental measurements which seem to be a characteristic of these materials are the effect of ambient atmosphere on the conductivity and the persistent photocurrent effect. It has already been shown that poly(thiophene) is doped by oxygen, leading to carrier generation (Abdou, 1997). In the oligomers studied here a similar process is likely, although the results suggest that it is only important in sandwich samples, where oxygen absorbed at the electrode-oligomer interface leads to carrier injection into the oligomer.

The persistent photocurrent observed in these materials does not appear to fit to either of the models described in § 4.2.4 for polymeric samples. It is possible that an entirely different mechanism is occurring in oligomeric materials. In the present context these effects can only be considered as detrimental to the applications potential of the studied oligomers.

Pentacene thin films deposited using the methods of thermal evaporation (TE) and pulsed laser ablation (PLD) were briefly compared during the course of the work. Unfortunately the present author found very little difference in the electronic properties between samples deposited using each technique. It is a possibility that the higher mobilities reported in the laser ablated thin films (as compared to similar thermally evaporated films) are due to the measurement being performed in the more ordered surface layer observed in the laser ablated thin films, whereas the present measurements reflect the bulk oligomer which is similar in both PLD and TE films (see Salih *et al.*, 1997).

Two notable failures within this work were the unsuccessful attempts at the time of flight and steady state photocarrier grating techniques. In both cases the lack of success was attributed to experimental difficulties.

Looking at the experimental results in general, it becomes apparent that the oligomers investigated here are not well suited for the majority of current device applications for organics. The major reason for this is that the carrier mobility is very low ($\sim 10^{-7}$ cm^2 V^{-1} s^{-1}) making them unsuitable for use in, for example, field-effect transistors. A further drawback is the poor photoresponse exhibited by all the materials. In pentacene and TVB at room temperature the photocurrent is only between a factor of ten to one hundred higher than the dark current, in TVC they are approximately equal, whereas in TVD the photocurrent is less than the dark current. This makes these materials unsuitable for applications in which a high photocurrent/dark current ratio is important. A further problem with the oligomers which is detrimental for device applications is the instability of the dark and photocurrents, and the poor reproducibility of results which were found to be a common problem throughout the course of the work. This problem is intimately linked with the atmospheric and persistent photocurrent effects mentioned above.

8.1 Directions for future work

There are several aspects of the present work which merit further investigation. Firstly, it is clear that the results obtained in this study are not sufficient to determine the exact nature of the charge transport mechanism in these materials. Considerably more data on basic material properties is necessary before this could be attempted.

The two experiments which were unsuccessful, *i.e.* TOF and SSPG both deserve more study as it was decided that only experimental difficulties were responsible for the null result obtained from both. The TOF technique may be realisable if the oligomers were dispersed in an inert binder, as in molecularly doped polymers (Goldie *et al.*, 1993) If the experiment was successful in this case it would allow us to determine whether the behaviour of the mobility in these oligomers agree with the predictions of the disorder limited hopping model in a more direct manner. It would further be insightful to perform TPC on such materials, and process the resulting decays with the FT technique. The SSPG experiment certainly merits continued investigation, simply

because a method for determining the diffusion length of photocarriers in organic materials would be extremely useful for assessing material quality. It is possible that performing this experiment on pentacene using blue light instead of red would result in a better photoresponse, and using a lower field may also result in a grating of larger amplitude which might prove easier to detect.

Further studies of the persistent photocurrents and the effects of ambient atmosphere would be advantageous. A knowledge of how and why these processes occur would allow us to assess their importance. In particular a clear understanding of how oxygen interacts with the oligomers is necessary as this would allow us to determine whether charge transfer from the oligomers to oxygen is important for carrier generation.

Continued assessment and development of the matrix simulation technique is necessary. It has been shown to yield qualitatively correct results for hopping in a gaussian density of states, but does not agree quantitatively with similar Monte Carlo programs. It should also be applied to different DOS distributions, *e.g.* exponential tail with multiple trapping and hopping. It would also be advantageous if the effect of a bias field could be included. This is important for hopping carriers, although it is usually not considered in multiple trapping models.

Thermally evaporated and laser ablated thin films of pentacene have been studied in this work, however no direct comparisons between their electronic properties have been carried out. From the results presented in the text however there appears to be little difference in the films deposited by each technique, in contrast to results presented by other workers. The improved surface smoothness, and resulting higher mobilities, of laser ablated films have been demonstrated; however it is possible that this is indeed just a surface effect (Salih *et al.*, 1997). Detailed investigations of mobilities in the surface layer and in the bulk of laser ablated pentacene films are needed to resolve this problem.

Finally, it was stated in the introduction that we wished to determine what effect adding different substituents to the oligomer chain had on the electronic properties. Unfortunately, the set of oligomers studied showed little difference in their electronic properties, and additional materials were not available. A comprehensive study of the effect of a larger range of substituents, including highly polar groups, would be insightful; as would a study of the effect of varying the chain length.

Appendices

(A) Matrix multiple trapping/hopping simulation program

This is the code for the program hop6gb.for described in § 5.2.

```
$NOFLOATCALLS
$STORAGE:2
C    TRANSIENT PC SIMULATION INC. HOPPING
C    MATRIX METHOD
     PARAMETER (INL=101,JNL=200)
     DOUBLE PRECISION A(INL,INL),B(INL,INL),C(INL,INL),N1(INL)
    1,T,AH,SA(INL),DT,DE,ED,CN,S,E1,S2,KT,E1R,EX(JNL),CH,BH
    2,FL(JNL),MU(INL),NC,TC,ALPHA,Nt(inl)
    3,TTC,TCT,NUO,RO,NO,En(inl),Eb,Ew,Gb,ei
     REAL X(2000),Y(2000)
     INTEGER TS,NL,NM,NN,M1,M2,STNO(10)
     INTEGER IDNO(20)
     CHARACTER*3 OPT,OPT2,optip,EOPT

     COMMON X,Y,IDNO

1040  DO 667 I=1,20
     IDNO(I)=0
667   CONTINUE
1050       SIGMA=0.0D0

*          GEc density of states at Ec /cc/eV

     GEc = 4.0d21
*     NC=1.0D20
     NO=1.0D15
*     ALPHA=1.0D7
*     NUO=1.0D12

     WRITE(*,*)' The simulation defaults to a density'
     WRITE(*,*)'of states at the mobility edge of GEc=4.D21/cc/eV'
     WRITE(*,*)' '
     WRITE(*,*)'Input NL, the number of levels the DOS is divided into'
     write(*,*)' NL to be ODD, if Gaussian option'
     READ(*,*)NL
1020  WRITE(*,*)'Input TS, the number of timesteps to take'
     WRITE(*,*)' '
     WRITE(*,*)'Please note that if you choose the trapped carrier'
     WRITE(*,*)'distribution option,the distribution will be stored'
     WRITE(*,*)'at 10 equally spaced time intervals - so in this case,'
     WRITE(*,*)'ensure that TS is a multiple of 10 (& >=20)'
     WRITE(*,*)'OK input TS now  '
     READ(*,*)TS
     WRITE(*,*)' '
     WRITE(*,*)' input att-to-esc freq Nuo- e.g. 1.0D12 Hz'
     read(*,*)Nuo
     write(*,*)' '
     WRITE(*,*)'Input DT, the length of the initial step'
     WRITE(*,*)' in seconds - e.g. 1.d-14 '
     READ(*,*)DT


*    EXP TAIL SECTION
```

```
*    skips exp tail for now
     go to 987
     WRITE(*,*)'Input ED, the total depth of the distribution (eV)'
     READ(*,*)ED
     WRITE(*,*)'Input E1, the characteristic energy of'
     WRITE(*,*)'      the distribution(eV)'
     READ(*,*)E1
987  continue
*         just to keep it going
          E1=0.05
*    I'll fix this later - honest


*         Gaussian option

          write(*,*)'input Eb, the energy of the peak (eV)'
          write(*,*)'relative to the band edge'
          read(*,*)Eb
          write(*,*)'input Ew, the characteristic width eV'
          read(*,*)Ew
          write(*,*)'input Ed, the overall width to be included (eV)'
          read(*,*)Ed

          write(*,*)'input Gb, the peak density, /cc/eV'
          read(*,*)Gb



666  WRITE(*,*)'Input T, the temperature'
     READ(*,*)T
     WRITE(*,*)'Input alpha the overlap factor (1/cm)'
     READ(*,*)alpha
     WRITE(*,*)'Multiple trapping (Y/N  default=Y)'
     READ(*,212)OPT
     IF (OPT.EQ.'n') OPT='N'
     IF (OPT.NE.'N') OPT='Y'
212  FORMAT(A)
     WRITE(*,*)'Hopping (Y/N default=Y)'
     READ(*,212)OPT2
     IF (OPT2.EQ.'n') OPT2='N'
     IF (OPT2.NE.'N') OPT2='Y'

     WRITE(*,*)' Do you wish to plot '
     WRITE(*,*)'       A) Effective mobilities vs time'
     WRITE(*,*)'             OR'
     WRITE(*,*)'       B) Energy distributions of trapped electrons'
     WRITE(*,*)'  '
     WRITE(*,*)' Key in your choice- <A>  or  <B>,  please'
     READ(*,212)EOPT
     IF(EOPT.EQ.'a') EOPT='A'
     IF(EOPT.EQ.'b') EOPT='B'


     IF(EOPT.EQ.'B')THEN
       IF(FLOAT(TS)/10.0.NE.FLOAT(TS/10)) GOTO 1020
       DO 1010 JSTP=1,10
            STNO(JSTP)=JSTP*TS/10
1010    CONTINUE
       JSTP=1
     ENDIF
```

```
*           some constants can now be set
      NM=NL+1
      NN=2*NL
      TC=E1/8.625D-5
      dEGEc = dE*GEc
      KT=8.625D-5*T
      Nc=kT*GEc
      Cn=Nuo/Nc

*     or  Cn=1.0d-8 ?


C     FLOAT FUNCTION ARRAY FOR I
      DO 65 I=1,INL
65      FL(I)=FLOAT(I)



*     EXP TAIL SECTION - skip
      Go to 72
C     DENSITIES - exp tail
      dE =Ed/NL
      e1r=e1

      S=0.0
      DO 70 I=1,NL
            Nt(I)=dEGEc*EXP(-FL(I)*DE/E1R)
            S=S+Nt(I)
            En(i)=dE*FL(i)
            N1(I)=Nc*EXP(-En(i)/kT)
70    CONTINUE


72    continue

*     Gaussian option densities

*     DE - width of each level
      dE=ED/NL
*     check - or is it nl-1 ?

      GbdE=Gb*dE
      S=0.0

      do 71 i=1,nl

            ei=(de*(i-(nl+1)/2))

            Nt(i)=GbdE*exp(-((ei/ew)**2))

            En(i)=eb+ei

            n1(i)=Nc*exp(-En(i)/kT)

            s=s+Nt(i)

71          continue


*           Nt(I) - density of i'th states /cc =dE*g(i)
*           S - sum density of loc states
```

```
C    CAPTURE COEFFICIENTS
*    CN=1.0D0/S
*    Cn=Nuo/Nc


C          CALCULATE BH FROM INPUT PARAMETERS
           TCT=TC/T
           TTC=T/TC

     write(*,*)' total loc state density(/cc) = ',S

          RO=S**(-1.0D0/3.0D0)

     write(*,*)' av. site separation RO = ',RO


     WRITE(*,*)'2*alpha*RO = ',2.0*alpha*ro



*     this condition - no hopping
     BH=1.0d0
     IF (OPT2.EQ.'N') BH=0.0D0

*    ??? CHECK ??
*    CH=BH*CN
*    should be ?
*         CH=BH/s

*         *** assume nearest neighbor hops for now ***
*     *** assume cubic lattice - 6 neighbors at distance ro
           CH=BH*6.d0*(Nuo/s)*exp(-2.0d0*alpha*ro)


*     this condition - no MultiTrapping
     IF (OPT.EQ.'N') CN=0.0D0

*    hopping conduction prefactor PREF

     PREF=(1.6D-19*RO*RO)/(6.0D0*KT)


     WRITE(*,*)'hopping prefactor = ',PREF
     DO 300 I=1,NL
          EX(I)=1.0D0
300  CONTINUE
     DO 310 I=NM,NN
          EX(I)=EXP(dE*FLOAT(NL-I)/kT)
310  CONTINUE
     DO 75 I=1,NM
     DO 75 J=1,NM
          A(I,J)=0.0
          C(I,J)=0.0
          C(I,J)=0.0
75   CONTINUE



     if (Cn*S*dT.gt.0.11d0)then
           write(*,*)'time step dT is too long'
           write(*,*)'It has been reduced to ensure stability'
```

```
          dT= 0.1d0/(Cn*S)
          write(*,*)'new dT = ',dT
      end if

      write(*,*)'read in a number (just to pause)'
      read(*,*)dummy



C     TRANSITION MATRIX A(I,J)
      A(1,1)=1.0D0-Cn*S*dT
      write(*,*)'A(1,1)=  ',A(1,1)


      DO 110 I=2,NM
          A(1,I)=n1(I-1)*Cn*DT
          A(I,1)=Nt(I-1)*Cn*DT
          A(I,I)=1.0D0-A(1,I)
110   CONTINUE

C     add in HOP TERMS to transition matrix
      DO 330 I=2,NM
          S2=0.0
          DO 340 J=2,NM
            M2=I-J+NL
            M1=J-I+NL
            A(I,J)=A(I,J)+Ch*Nt(I-1)*EX(M1)*DT
            AH=Ch*Nt(J-1)*EX(M2)*DT
            S2=S2+AH
340     CONTINUE
          SA(I)=S2

C         MU()=PROBABILITY OF HOPPING FROM LEVEL I
          MU(I)=SA(I)/DT
          A(I,I)=A(I,I)-S2
330   CONTINUE

C     DUMMY MATRIX B(I,J)
      DO 120 I=1,NM
      DO 120 J=1,NM
120     B(I,J)=A(I,J)
C       STORE VALUES IN Y()


C     MATRIX MULTIPLICATION
      DO 140 L=2,TS
          DO 155 I=1,NM
          DO 155 J=1,NM
          DO 155 K=1,NM
            C(I,J)=C(I,J)+B(I,K)*B(K,J)
155   CONTINUE


*     ***** ENERGY DISTRIBUTION OPTION *****

      IF(EOPT.EQ.'B')THEN
        IF(L.EQ.STNO(JSTP))THEN
          WRITE(*,*)' '
              WRITE(*,*)L,DT*2.0D0**(L-1)
          DO 1000 I=1,NL
```

```
        IF(OPT.EQ.'N')THEN
c        assumes all carriers start at highest localised state
              X(I+(JSTP-1)*NL)=C(I+1,2)
            ELSE
c        assumes all carriers start free
          X(I+(JSTP-1)*NL)=C(I+1,1)
        ENDIF
              Y(I+(JSTP-1)*NL)=-SNGL(En(i))
1000      CONTINUE
        IDNO(JSTP)=NL
        JSTP=JSTP+1
      ENDIF
    ELSE

*     ******** END OF ENERGY DISTRIBUTION OPTION **********



C    STORE VALUES IN Y()
    DO 370 I=1,NL
C          C()*MU()=RELATIVE RATE OF HOPPING AWAY
    IF (OPT.EQ.'N') THEN
          SIGMA=SIGMA+(C(I+1,2)*MU(I+1))
          ELSE
          SIGMA=SIGMA+(C(I+1,1)*MU(I+1))
          ENDIF
370   CONTINUE
    Y(L-1)=PREF*SIGMA*NO/(NO*1.6D-19)
    X(L-1)=DT*2.0D0**(L-1)
    X(L-2+TS)=DT*2.0D0**(L-1)
    IF (OPT.EQ.'N') THEN
          Y(TS-2+L)=10.D0*1.6D-19*C(1,2)*NO/(NO*1.6D-19)
          ELSE
          Y(TS-2+L)=10.0D0*1.6D-19*C(1,1)*NO/(NO*1.6D-19)
          ENDIF
          WRITE(*,*)X(L-1),Y(L-1),Y(TS-2+L)
          SIGMA=0.0D0
360   CONTINUE
    IDNO(1)=TS-1
    IDNO(2)=TS-1

    ENDIF


C    UPDATE B ZERO C
    DO 170 I=1,NM
    DO 170 J=1,NM
    B(I,J)=C(I,J)
170   C(I,J)=0.0
140   CONTINUE



                WRITE (*,*) 'Do you wish to write a data file?'
                WRITE (*,*) 'Input <Y/N>'
                READ (*,687) GF
687           FORMAT (A)
                IF (GF.EQ.'Y'.OR.GF.EQ.'y') THEN
                 CALL SAVDAT(X,Y,IDNO)
                END IF
```

```
c     WRITE(*,*)'Create data file ? input <Y/N>'
c     READ(*,213)DF
c     IF(DF.EQ.'y') DF='Y'
c     IF(DF.EQ.'Y') THEN
c          CALL graph(x,y,idno)
c     ENDIF

      DO 1070 I=1,20
      IDNO(I)=0
1070  CONTINUE

      WRITE(*,*)'Re-run programme '
      WRITE(*,*)' with same basic parameters - input <A>'
      WRITE(*,*)' with new set of parameters - input <B>'
      WRITE(*,*)' EXIT programme - input <E>'
      READ(*,213)optip
213   FORMAT(A)
      if (optip.eq.'a') optip='A'
      if (optip.eq.'b') optip='B'
      if (optip.eq.'e') optip='E'
      IF (optip.eq.'A') goto 666
      IF (optip.eq.'B') goto 1050
      IF (optip.eq.'E') goto 1060

1060  STOP
      END



c
c
      SUBROUTINE savdat(X,Y,ind)
      dimension x(*),y(*),ind(*)
      character*30 title,xaxis,yaxis,xopt*3,yopt*3
      character*20 fname
20    format(a)
c     call gmode(3)
      write(*,*)
      write(*,*)'Input Save File Name, including .dat extension'
      write(*,*)
      read(*,20)fname
      write(*,*)
      write(*,*)'Input graph title'
      write(*,*)
      read(*,20)title
      write(*,*)
      write(*,*)'Input x axis label'
      write(*,*)
      read(*,20)xaxis
      write(*,*)
      write(*,*)'Input y axis label'
      write(*,*)
      read(*,20)yaxis
      write(*,*)
      write(*,*)'x axis log/lin (default log)?'
      write(*,*)
      read(*,20)xopt
      write(*,*)
      write(*,*)'y axis log/lin (default log)?'
      write(*,*)
      read(*,20)yopt
```

```
      if ((xopt.eq.'lin').or.(xopt.eq.'LIN')) then
           xopt = 'LIN'
      else
           xopt = 'LOG'
      end if
      if ((yopt.eq.'lin').or.(yopt.eq.'LIN')) then
           yopt = 'LIN'
      else
           yopt = 'LOG'
      end if

c     call addext(fname,'DAT')
      OPEN(1,FILE=FNAME,STATUS='unknown')
      WRITE(1,20)TITLE
      WRITE(1,20)XAXIS
      WRITE(1,20)YAXIS
      WRITE(1,20)XOPT
      WRITE(1,20)YOPT
      INUM=0
      JSTA=1
      JEND=0
      i=1
10    inum=inum+1
      i=i+1
      if (ind(i).ne.0) goto 10
      write(1,*)inum
      DO 150 I=1,INUM
        WRITE(1,*)I
        WRITE(1,*)ind(I)
        JEND=JEND+ind(I)
        DO 160 J=JSTA,JEND
          WRITE(1,*)X(J),Y(J)
160     CONTINUE
        JSTA=JEND+1
150   CONTINUE
      CLOSE(1)
      RETURN
      END
```

(B) Monte Carlo hopping simulation program

This is the code for the Monte Carlo hopping program gaustpc.for discussed in § 5.1.

```
C     PROGRAM GAUSTPC.FOR

C     TPC SIMULATION FOR A GAUSSIAN DOS WITH DIAGONAL
C      AND OFF-DIAGONAL DISORDER AND OPTIONAL TRAPS


      INTEGER MX,MY,MZ,MM,N1,MT,ST,ELTRN,HOPS,DHX
      INTEGER PSTNX,PSTNY,PSTNZ,X(100),Y(40),Z(40)
      INTEGER SITEX(124),SITEY(124),SITEZ(124),FD
      INTEGER POS(1000),RE,TOE,TOEL,XDIST(200,1000)
      INTEGER XTARGET,YTARGET,ZTARGET,TPOINTS,FLAG,NTRAP

      REAL K,TOT,PROB,TSUM,GAMMA(160000),ETIME(200,1000)
      REAL CRNT(1000),TAV,ALPHA,DD,EAV,TIMER(1000),STD(1000)
      REAL dX,dY,dZ,SSQR,RND,DIS,DISAV,TIME,ESTD(1000),CTRAP
      REAL MOBIL,Field,ENERGY(160000),XAV(1000),EMEAN(1000)
```

```
      REAL ACC(124),NORM(124),HOPTIME(1000),TAU(124),EXPO
      REAL XSUM,ESUM,TEMP,timeS,TOTAL,NU(124),DIFFCOEFF(1000)

      PARAMETER(Vh=1E12,ELTRN=50,AVR=1E-9,TEMP=300)
      PARAMETER(timeS=3.67E-9,K=8.6E-5,Field=1E6,CTRAP=0.0)
      PARAMETER(DD=0.1,EAV=0.0,DIS=0.0,DISAV=5.0,RUNTIME=1e-1)


C               SETS UP A REGULAR 3-D LATTICE

      idum = -8


      OI = 1
      DO 1 B = 1,100
        X(B) = B
        DO 2 C = 1,40
          Y(C) = C
          DO 3 D = 1,40
              Z(D) = D
 3    CONTINUE
 2    CONTINUE
 1    CONTINUE



C                   SET UP DISORDER
C                   SPATIAL

      DO 4 ERG = 1,160000
          GAMMA(ERG) = GASDEV(idum,DIS,DISAV)
 4    CONTINUE

C                   ENERGETIC

      DO 5 GRE = 1,160000
          ENERGY(GRE) = gasdev(idum,dd,eav)
*         WRITE(6,*) ENERGY(gre)
 5    CONTINUE

C                   ADDS SPECIFIED DENSITY OF DEEP TRAPS

          NTRAP = CTRAP*160000

      DO 30 REG = 1,NTRAP
          GER = INT(160000*RAN3(idum))
          ENERGY(GER) = gasdev(idum,0.2,0.4)
 30   CONTINUE



C       DETERMINES TRANSITION RATES TO 125 NEAREST
C           NEIGHBOURS OF OCCUPIED SITE


      TPOINTS = 0
      TSUM = 0.0
      HOPS = 0
      CHANGE = 20

C                   CARRIER LOOP
```

```
      DO 6 RE = 1,ELTRN
      WRITE(6,*) RE

      FLAG=0
      N1=1
      DHX=5
      FD=1

      XTARGET = 1
*  7  EXPO = -LOG(RAN3(idum))
*       IF(EXPO.GE.1.OR.EXPO.EQ.0)GO TO 7
*     XTARGET = INT(EXPO*100)
   8  YTARGET = INT(RAN3(idum)*40)
       IF(YTARGET.EQ.0)GO TO 8
   9  ZTARGET = INT(RAN3(idum)*40)
       IF(ZTARGET.EQ.0)GO TO 9



C                              HOP LOOP

  21  MX = XTARGET
      MY = YTARGET
      MZ = ZTARGET

        HOPS = HOPS+1

      IF(RE.EQ.CHANGE)THEN

  15    DO 10 GRE = 1,160000
            ENERGY(GRE) = gasdev(idum,dd,eav)
  10    CONTINUE

          DO 31 RGE = 1,NTRAP
            GER = INT(160000*RAN3(IDUM))
            ENERGY(GER) = gasdev(idum,0.2,0.4)
  31    CONTINUE

                    CHANGE = CHANGE+20

      ENDIF


      S = 1

      DO 11 N = 1,100
               dX = (X(N) - X(MX))
         IF(dX.GT.2.0.OR.dX.LT.-2.0)GO TO 11
      DO 12 LM = 1,40
               dY = (Y(LM) - Y(MY))
         IF(dY.GT.2.0.OR.dY.LT.-2.0)GO TO 12
      DO 13 ML = 1,40
               dZ = (Z(ML) - Z(MZ))
         IF(dZ.GT.2.0.OR.dZ.LT.-2.0)GO TO 13

         IF(MX.EQ.N.AND.MY.EQ.LM.AND.MZ.EQ.ML)GO TO 13


        SSQR = SQRT((((dX)*(dX)) + ((dY)*(dY)) + ((dZ)*(dZ))))

         SITEX(S) = X(N)
         SITEY(S) = Y(LM)
```

```
        SITEZ(S) = Z(ML)

          MT = ((MX-1)*1600)+((MY-1)*40)+MZ
          ST = ((SITEX(S)-1)*1600)+((SITEY(S)-1)*40)+SITEZ(S)

          ALPHA = GAMMA(MT)+GAMMA(ST)
       EDIFF = ENERGY(ST)-ENERGY(MT)-(Field*(SITEX(S)-MX)*AVR)

          IF(EDIFF.LE.0.0)THEN

        NU(S) = Vh * EXP(-ALPHA*SSQR)

          ELSE

           NU(S) = Vh * EXP(-ALPHA*SSQR) * EXP(-(EDIFF/(K*TEMP)))

       ENDIF

        S = S + 1

  13  CONTINUE
  12  CONTINUE
  11  CONTINUE


C            NORMALISES TRANSITION RATES IN RANGE 0-1 AND FINDS
C                                HOP TIME


     PROB = 0
     DO 14 U = 1,S-1
          TOT = NU(U) + PROB
          PROB = TOT
  14  CONTINUE

*     IF(PROB.LT.5000)GO TO 15

     DO 16 SCR = 1,S-1
          NORM(SCR) = NU(SCR)/PROB
  35      RAND = RAN3(idum)
          IF(RAND.EQ.0.0)GO TO 35
          TAU(SCR) = (-LOG(RAND))/(PROB)
  16  CONTINUE


C              ACCUMULATES PROBABILITIES

     TOTAL = 0
     DO 17 NI = 1,S-1
          ACC(NI) = NORM(NI) + TOTAL
       TOTAL = ACC(NI)
  17  CONTINUE



C              DETERMINES SITE HOPPED TO AND TIME TAKEN

     RND = RAN3(idum)
     DO 18 OH = S-1, 1, -1
      IF(RND .LE. ACC(OH) .AND. RND .GT. ACC(OH-1))THEN
        PSTNX = SITEX(OH)
        PSTNY = SITEY(OH)
```

```
          PSTNZ = SITEZ(OH)
          HOPT = TAU(OH)
          RATE = NU(OH)
       ELSEIF(RND .LE. ACC(1) .AND. RND .GE. 0.0)THEN
          PSTNX = SITEX(OH)
        PSTNY = SITEY(OH)
        PSTNZ = SITEZ(OH)
          HOPT = TAU(OH)
          RATE = NU(OH)
        ELSE
          GO TO 18
        ENDIF
 18  CONTINUE

    HOPTIME(RE) = HOPTIME(RE)+HOPT


C       STORES POSITION OF ALL CARRIERS AT CERTAIN TIME


 20       TIME = TIMES*N1

          IF(TIME.GT.RUNTIME)GO TO 6

C       SAMPLE=TIMES*10000

C         IF(TIME.EQ.SAMPLE)THEN

C           DO 19 YI = 1,100
C                 IF(MX.EQ.YI)THEN
C                   POS(YI) = POS(YI)+1
C                 ENDIF
C  19     CONTINUE
C         ENDIF


C           DETERMINES X-DISPLACEMENT OF CARRIER FOR
C              TIME N1 FOR ALL CARRIERS


      IF(HOPTIME(RE).GT.TIME)THEN


         IF(N1.LT.4)THEN

          IF(FLAG.EQ.0)THEN
           XDIST(FD,RE) = MX
          ELSE
           XDIST(FD,RE) = MX+(FLAG*100)
          ENDIF

           TIMER(FD) = TIME
           ETIME(FD,RE) = ENERGY(MT)
           FD=FD+1

         ELSEIF(N1.EQ.DHX)THEN

          IF(FLAG.EQ.0)THEN
           XDIST(FD,RE) = MX
          ELSE
           XDIST(FD,RE) = MX+(FLAG*100)
          ENDIF
```

```
            TIMER(FD) = TIME
            ETIME(FD,RE) = ENERGY(MT)
            FD=FD+1
            DHX = INT(DHX*1.2)

          ENDIF

            N1 = N1+1

            GO TO 20

        ELSE

            XTARGET = PSTNX
            YTARGET = PSTNY
            ZTARGET = PSTNZ

            IF (XTARGET.EQ.100)THEN
                XTARGET=1
                FLAG=FLAG+1
            ENDIF

            GO TO 21

        ENDIF

 6  CONTINUE



C         CALCULATES AVERAGE NO. OF HOPS

      HOPS = HOPS/ELTRN


C          CALCULATES AVERAGE DISPLACEMENT AND ENERGY
C            OF ALL CARRIERS AFTER N1 TIME STEPS


      DO 23 YOP = 1,FD-1

          XSUM=0.0
          ESUM=0.0

          DO 24 POY = 1,ELTRN

         XSUM = XDIST(YOP,POY)+XSUM
            ESUM = ETIME(YOP,POY)+ESUM

 24  CONTINUE

            XAV(YOP)=XSUM/ELTRN
            EMEAN(YOP)=ESUM/ELTRN

 23  CONTINUE


C         CALCULATES ENERGETIC AND POSITIOAL VARIANCE AND
C    POSITIONAL DIFFUSION COEFFICIENT AFTER N1 TIME STEPS
```

```
C     DO 25 T=1,FD-1
C        DO 26 S = 1,ELTRN

C          VAR = (((XDIST(T,S)-XAV(T))**2)+VAR)/ELTRN
C          EVAR = (((ETIME(T,S)-EMEAN(T))**2)+EVAR)/ELTRN
C  26  CONTINUE

C        STD(T) = VAR
C        DIFFCOEFF(T) = VAR/(2*TIMER(T))
C        ESTD(T) = EVAR
C  25  CONTINUE


C                  CALCULATES CURRENT AT EACH TIME STEP


     DO 27 JH = 1,FD-1
       CRNT(JH) = (XAV(JH)*1.602E-19)/TIMER(JH)
  27  CONTINUE


C          WRITES FILE OF CURRENT(or mean energy) vs. TIME


     OPEN(1,FILE='GAUSTPC.DAT',STATUS='NEW')


     DO 28 QW =1,FD-1

          WRITE(1,*) TIMER(QW),Emean(QW)

  28  CONTINUE
     ENDFILE(1)
     CLOSE(1)


C        WRITES FILE OF NO. OF CARRIERS vs. DISPLACEMENT


C    OPEN(2,FILE='POS.DAT',STATUS='NEW')

C    DO 29 WQ = 1,100
C       WRITE(2,*) WQ,POS(WQ)
C  29  CONTINUE
C    ENDFILE(2)
C    CLOSE(2)


     STOP
     END




     FUNCTION GASDEV(idum,STD,MEAN)

     REAL MEAN
```

```
      DATA ISET/0/
      IF(ISET.EQ.0)THEN
1        V1=2.*RAN3(idum)-1
         V2=2.*RAN3(idum)-1
         RSQ=V1**2+V2**2
         IF(RSQ.GE.1.)GO TO 1
         FAC=SQRT(-2.*LOG(RSQ)/RSQ)
         GSET=V1*FAC
         GASDEV=V2*FAC
         ISET=1
      ELSE
         GASDEV=GSET
         ISET=0
      ENDIF
         GASDEV=(STD*GASDEV)+MEAN
      RETURN
      END



      FUNCTION RAN3(IDUM)

      PARAMETER (MBIG=1000000000,MSEED=161803398,MZ=0,FAC=1.E-9)
      DIMENSION MA(55)
      DATA IFF /0/
      IF(IDUM.LT.0.OR.IFF.EQ.0)THEN
       IFF=1
       MJ=MSEED-IABS(IDUM)
       MJ=MOD(MJ,MBIG)
       MA(55)=MJ
       MK=1
       DO 11 I=1,54
        II=MOD(21*I,55)
        MA(II)=MK
        MK=MJ-MK
        IF(MK.LT.MZ)MK=MK+MBIG
        MJ=MA(II)
11     CONTINUE
       DO 13 K=1,4
        DO 12 I=1,55
         MA(I)=MA(I)-MA(1+MOD(I+30,55))
         IF(MA(I).LT.MZ)MA(I)=MA(I)+MBIG
12      CONTINUE
13     CONTINUE
       INEXT=0
       INEXTP=31
       IDUM=1
      ENDIF
      INEXT=INEXT+1
      IF(INEXT.EQ.56)INEXT=1
      INEXTP=INEXTP+1
      IF(INEXTP.EQ.56)INEXTP=1
      MJ=MA(INEXT)-MA(INEXTP)
      IF(MJ.LT.MZ)MJ=MJ+MBIG
      MA(INEXT)=MJ
      RAN3=MJ*FAC
      RETURN
      END
```

(C) Controller program for automated PPC measurements

This is the code for the PPC measurements described in § 6.6.6

```
'Controller program for automated PPC measurements

'Establish communication with personal488

OPEN "\DEV\IEEEOUT" FOR OUTPUT AS #1

'reset personal488
IOCTL#1,"BREAK"
PRINT#1,"RESET"

'open file to read responses from personal488
OPEN "\DEV\IEEEIN" FOR INPUT AS #2
PRINT#1,"FILL ERROR"

'SET TIME

TIME$ = "00:00:00"

IPC=0.0
CPI=0.0

FLAG=0

PRINT "Enter led ON duration in mins"
INPUT ONLED
ONLED=(ONLED*60)+100
ONLEDB=ONLED+1

PRINT "Press esc to quit"
10

S$=INKEY$
IF S$=CHR$(27) THEN GOTO 100

ON TIMER(10) GOSUB READCURRENT

IF TIMER>100 AND TIMER<101 THEN GOSUB LEDON
IF TIMER>ONLED AND TIMER<ONLEDB THEN GOSUB LEDOFF

100
END


READCURRENT:
'READS AMPS ON AUTORANGING FROM KEITHLY 617 (IEEE488 ADDRESS: 27)

PRINT#1,"OUTPUT 27;F1R0X"
PRINT#1,"ENTER 27"
INPUT#2, R$
N$=MID$(R$,5)
N=VAL(N$)


IF N>IPC OR N<CPI THEN

  IPC=N+(N/2)
  CPI=N-(N/2)
```

```
  PRINT TIMER   N

  FLAG=FLAG+1

    IF FLAG=1 THEN
          OPEN "PPC.DAT" FOR OUTPUT AS #3
    ELSE
          OPEN "PPC.DAT" FOR APPEND AS #3
    END IF

  WRITE #3, TIMER ,  N

  CLOSE 3
ELSE

  GOTO 10

END IF

  GOTO 10
RETURN


LEDON:
'Switches on LED

 PRINT#1,"OUTPUT 07;X10.73V30MA"
 GOTO 10

RETURN

LEDOFF:
'Switches off LED

 PRINT#1,"OUTPUT 07;X0V30MA"
 GOTO 10

RETURN
```

References

Abdou, M.S.A. Orfino, F.P. Son, Y. Holdcroft, S. (1997) Interaction of Oxygen with Conjugated Polymers: Charge Transfer Complex Formation with Poly(3-alkylthiophenes), *Journal of the American Chemical Society*, **119**: 4518-4524

Abkowitz, M.A. Knier, F.E. Yuh, H.-J. Weagley, R.J. Stolka, M. (1987) Electronic Transport in Amorphous Silicon Backbone Polymers, *Solid State Communications*, **62**: 547-550

Abkowitz, M.A. Bässler, H. Stolka, M. (1991) Common features in the transport behaviour of diverse glassy solids: exploring the role of disorder, *Philosophical Magazine B*, **63**: 201-220

Abkowitz, M.A. Stolka, M. Weagley, R.J. McGrane, K.M. Knier, F.E. (1990) Electronic Transport in Polysilylenes, *Advances in Chemistry Series*, **224**: 467-503

Abkowitz, M.A. Stolka, M. (1988) Common features in the electronic transport behaviour of divers glassy solids, *Philosophical Magazine Letters*, 58: 239-245

Akashi, T. Morita, S. Zakhidov, A.A. Yoshino, K. (1995) New features of photoconductivity in fullerene doped conducting polymer, *Synthetic Metals*, **70**: 1363-1364

Anderson, P.W. (1958) Absence of diffusion in certain random lattices, *Physical Review*, **109**: 1492-1505

Antoniadis, H. Hsieh, B.R. Abkowitz, M.A. Jenekhe, S.A. Stolka, M. (1994) Photovoltaic and photoconductive properties of aluminium/poly(p-phenylenenvinylene) interfaces, *Synthetic Metals*, **62**: 265-271

Arkhipov, V.I. Rudenko, A.I. (1978) Kinetics of the photoinjection current in semiconductors, *Journal of Non-Crystalline Solids*, **30**: 163

Bagley, B.G. (1970) The field dependent mobility of localised electron carriers, *Solid State Communications*, **8**: 345-348

Baranovskii, S.D. Thomas, P. Adriaenssens, G.J. (1995) The concept of transport energy and its application to steady state photoconductivity in amorphous silicon, *Journal of Non-Crystalline Solids*, **190**: 283-287

Barth, S. Bässler, H. Wehrmeister, T. Müllen, K. (1997) Photoconduction in oligo-para-phenylenevinylene films, *Journal of Chemical Physics*, **106**: 321-327

Bässler, H. (1981) Localised states and electronic transport in single component organic solids with diagonal disorder, *Physica Status Solidi B*, **107**: 9-53

Bässler, H. (1984) Charge transport in molecularly doped polymers, *Philosophical Magazine B*, **50**: 347-362

Bässler, H. (1993) Charge transport in disordered organic photoconductors, *Physica Status Solidi B*, **175**: 15-56

Batt, R.H. Braun, C.L. Hornig, J.F. (1968) Electric-field and temperature dependence of photoconductivity, *Journal of Chemical Physics*, **49**: 1967-1968

Borsenberger, P.M. Pautmeier,L. Bässler, H. (1991) Charge transport in disordered molecular solids, *Journal of Chemical Physics*, **94**: 5447-5454

Borsenberger, P.M. Bässler, H. (1991) Concerning the role of dipolar disorder on charge transport in molecularly doped polymers, *Journal of Chemical Physics*, **95**: 5327-5331

Borsenberger, P.M. Magin, E.H. Shi, J. (1996) Charge transport in vapor deposited molecular glasses, *Physica B*, **217**: 212-220

Brüggemann, R. Main, C. Berkin, J. Reynolds, S. (1990) An evaluation of phase-shift analysis of modulated photocurrents *Philosphical Magazine B*, **62**: 29-45

Burns,G. (1985) *Solid State Physics* (London: Academic Press Inc)

Burroughs, J.H. Jones, C.A. Friend, R.H. (1988) New semiconductor device physics in polymer diodes and transistors, *Nature*, **335**: 137-141

Burroughs, J.H. Bradley, D.D.C. Brown, A.R. Marks, R.N. Mackay, K. Friend, R.H. Burns, P.L. Holmes, A.B. (1990)) Light-emitting diodes based on conjugated polymers, *Nature*, **347**: 539-541

Chance, R.R. Braun, C.L. (1976) Temperature dependence of intrinsic carrier generation in anthracene single crystals, *The Journal of Chemical Physics*, **64**: 3573-3581

Chance, R.R. Baughman, R.H. (1976) Photoconduction in polydiacetylene single crystals, *The Journal of Chemical Physics*, **64**: 3889-3890

Chiang, C.K. Fincher, C.R. Park, Y.W. Heeger, A.J. Shirakawa, H. Louis, E.J. Gau, S.C. MacDiarmid, A.J. (1977) Electrical conductivity in doped polyacetylene, *Physical Review Letters*, **39**: 1098-1101

Chrisey, D.B. Hubler, G.K. (1994) *Pulsed Laser Deposition of Thin Films* (Wiley)

DeVore, H.B. (1956) Spectral distribution of photoconductivity, *Physical Review*, **102**: 86-91

Eiermann, R. Parkinson, G.M. Bässler, H. Thomas, J.M. (1983) Structural

investigations of amorphous tetracene and pentacene by low-temperature electron diffraction, *Journal of Physical Chemistry*, **87**: 544-551

Emin, D. (1972). In: *Electronic and Structural Properties of Amorphous Semiconductors*, edited by P.G. Le Comber and J. Mort, (London: Academic Press)

Facci, J.S. Stolka, M. (1986) Redox mogration mechanism of charge transport in molecularly doped polymers, *Philosophical Magazine B*, **54**: 1-18

Fichou, D. Horowitz, G. Xu, B. Garnier, F. (1990) Stoichiometric control of the successive generation of the radical cation and dication of extended α-conjugated oligothiophenes: a quantitative model for doped polythiophene, *Synthetic Metals*, **39**: 243-259

Fincher, C.R. Chen, C.E. Heeger, A.J. MacDiarmid, A.G. Hastings, J.B. (1982) Structural determination of the symmetry-breaking parameter in *trans*-$(CH)_x$, *Physical Review Letters*, **48**: 100-104

Fujino, M. Kanazawa, Y. Mikawa, H. Kusabayashi, S. Yokoyama, M. (1984) Glass transition in charge transport phenomena of amorphous photoconductive polymers, *Solid State Communications*, **49**: 575-577

Gailberger, M. Thanh, B.N. Bässler, H. (1992) Photoconduction in conjugated polymers, *Molecular Crystals and Liquid Crystals*, **217**: 217-221

Gailberger, M. Bässler, H. (1991) dc and transient photoconductivity of poly(2-phenyl-1,4-phenylenevinylene), *Physical Review B*, **44**: 8643-8651

Geacintov, N. Pope, M. (1967) Generation of charge carriers in anthracene with polarised light, *Journal of Chemical Physics*, **47**: 1194-1195

Geacintov, N. Burgos, J. Pope, M. Strom, C. (1971) Heterofission of pentacene excited singlets in pentacene-doped tetracene crystals, *Chemical Physics Letters*, **11**: 504-508

Gill, W.D. (1972) Drift mobilities in amorphous charge-transfer complexes of trinitrofluorenone and poly-n-vinylcarbazole, *Journal of Applied Physics*, **43**: 5033-5040

Goldie, D.M. Hepburn, A.R. Maud, J.M. Marshall, J.M. (1993) The influence of inter-oligomer separation distance on observed hopping mobilities in terthiophene-doped polycarbonate, *Philosophical Magazine B*, **68**: 753-766

Grünewald, M. Pohlmann, B. Movaghar, B Würtz, D. (1984) Theory of non-equilibrium diffusive transport in disordered materials, *Philosophical Magazine B*, **49**: 341-356

Gutmann, F. Lyons, L.E. (1981) *Organic Semiconductors*, (Florida: Robert E. Krieger Publishing Company), parts A and B

Hagler, T.W. Pakbaz, K. Voss, K.F. Heeger, A.J. (1991) Enhanced order and electronic delocalisation in conjugated polymers oriented by gel processing in polyethylene, *Physical Review B*, **44**: 8652-8666

Hartenstein, B. Bässler, H. (1995) Transport energy for a gaussian density of states distribution, *Journal of Non-Crystalline Solids*, **190**: 112116

Heeger, A.J. (1993) In: *Conjugated Polymers and Related Materials*, edited by W.R. Salaneck, I. Lundström and B. Ranby (Oxford University Press)

Hepburn, A.R. (1995) Study of charge transport in poly[3-(carbazolyl-9-yl)propyl]methylsiloxanes, *Philosophical Magazine B*, **72**: 19-34

Hesse, R. Bässler, H. (1980) Short-time carrier transport in amorphous pentacene, *Physica Status Solidi*, **101**: 481-487

Heun, S. Bässler, H. Borsenberger, P. (1995) The spectral assessment of the origin of the polaronic contribution to charge transport in a highly conjugated triarylamine donor molecule, *Chemical Physics*, **200**: 265-270

Hirsch, J. (1979) Hopping transport in disordered aromatic solids: a re-interpretation of mobility measurements on PVK and TNF, *Journal of Physics C: Solid State Physics*, **12**: 321-335

Horowitz, G. Peng, X. Fichou, D. Garnier, J. (1990) The oligothiophene-based field-effect transistor: how it works and how to improve it, *Journal of Applied Physics*, **67**: 528-532

Inokuchi, H (1954) Photoconductivity of the condensed polynuclear aromatic compounds, *Bulletin of the Chemical Society of Japan*, **27**: 22-27

Ito, T. Shirakawa, H. Ikeda, S. (1974) *Journal of Polymer Science and Chemistry*, **12**: 11

Jankowiak, R. Rockwitz, K.D. Bässler, H. (1983) Absorption spectroscopy of amorphous tetracene, *Journal of Physical Chemistry*, **87**: 552-557

Kakalios, J. Street, R.A. Jackson, W.B. (1987) Stretched-exponential relaxation arising from dispersive diffusion of hydrogen in amorphous silicon, *Physical Review Letters*, **59**: 1037-1040

Kao, K.C. Hwang, W. (1981) *Electrical Transport in Solids*, (Oxford: Pergamon Press)

Kato, K. Braun, C.L. (1980) The photoconduction threshold in anthracene single crystals, *Journal of Chemical Physics*, **72**: 172-176

Kenkre, V.M. Anderson, J.D. Dunlap, D.H. Duke, C.B. (1989) Unified theory of mobilities of photoinjected electrons in naphthalene, *Physical Review Letters*, **62**: 1165-1168

Kepler, R.G. (1960) Charge carrier production and mobility in anthracene crystals, *Physical Review*, **119**: 1226-1229

Kiess, H. (1992) *Conjugated Conducting Polymers*, (Berlin: Springer Verlag)

LeBlanc, O.H. (1960) Hole and electron drift mobilities in anthracene, *Journal of Chemical Physics*, **33**: 626-628

Lee, C.H. Yu, G. Heeger, A.J. (1993) Persistent photoconductivity in poly(p-phenylenevinylene): Spectral response and slow relaxation, *Physical Review B*, **47**: 15453-15553

Mack, J.X. Schein, L.B. Peled, A. (1989) Hole mobilities in hydrazone-polycarbonate dispersions, *Physical Review B*, **39**: 7500-7508

Magin, E.H. Borsenberger, P.M. (1993) Electron transport in N,N'-bis(2-phenethyl)-perylene-3,4:9,10-bis(dicarboximide), *Journal of Applied Physics*, **73**: 787-791

Mahrt, R.F. Yang, J. Bässler, H. (1992) Spectroscopic assessment of the role of disorder and polaron formation on electronic transport in molecularly doped polymers, *Chemical Physics Letters*, **192**: 576-580

Main, C. Berkin, J. Merazga, A. (1991) In: *New Physical Problems in Electronic Materials*, edited by P.G. LeComber and J. Mort (London: Academic Press)

Main, C. Brüggemann, R. Webb, D.P. Reynolds, S. (1992) Determination of gap-state distribution in amorphous semiconductors from transient photocurrents using a Fourier-transform technique, *Solid State Communications*, **83**: 401-405

Main, C. Brüggemann, R. Webb, D.P. Reynolds, S. (1993) Time and frequency domain studies of photoconductivity in amorphous semiconductors, *Journal of Non-Crystalline Solids*, **164-166**: 481-484

Marshall, J.M. (1978) Simulation of hopping transport for a random spatial distribution of localised sites, *Philosophical Magazine B*, **38**: 335-348

Marshall, J.M. Main, C. (1983) Transient photoconductivity and thermalisation in amorphous semiconductors, *Philosophical Magazine B*, **47**: 471-480

Marshall, J.M. Berkin, J. Main, C. (1987) Calculation of localised-state energy distributions from transient-photoresponse data, *Philosophical Magazine B*, **56**: 641-652

Marshall, J.M. (1989) In:*Amorphous Silicon and Related Materials*, edited by H, Fritzsche (Singapore: World Scientific)

Maruyama, Y. Bässler, H. (1981) Mobility and recombination coefficient of charge carriers in disordered pentacene, *Physica Status Solidi*, **103**: 263-268

McMurray, J. (1992) *Organic Chemistry*, 3rd Edition (Brooks/Cole Publishing Company)

Merazga, A. (1990) Ph.D. thesis, University of Abertay Dundee

Meyer, H. Haarer, D. Naarmann, H. Hörhold, H.H. (1995) Trap distribution for charge carriers in poly(paraphenylenevinylene) (PPV) and its substituted derivative DPOP-PPV, *Physical Review B*, **52**: 2587-2598

Michiel, H. Marshall, J.M , Adriaenssens, G.J. (1983) Determination of localised state distributions from anomalously dispersive transport data, *Philosophical Magazine B*, **48**: 187-202

Michiel, H. Adriaenssens, G.J. (1985) Analysis of dispersive transport in amorphous semiconductors by discretisation of a continuous distribution of localised states *Philosophical Magazine B*, **51**: 27-38

Monroe, D. (1985) Hopping in exponential band tails, *Physical Review Letters*, **54**: 146-149

Mort, J. Pfister, G. (1982) In: *Electronic Properties of Polymers*, edited by J. Mort and G. Pfister (New York: Wiley)

Mott, N.F. Davis, E.A. (1979) *Electronic Processes in Non-Crystalline Materials*, 2nd Edition (Oxford: Clarendon press)

Movaghar, B. Grünewald, M. Ries, B. Bässler, H. Würtz, D. (1986) Diffusion and relaxation of energy in disordered organic and inorganic materials, *Physical Review B*, **33**: 5545-5553

Muller-Horsche, E. Haarer, D. Scher, H. (1987) Transition from dispersive to non-dispersive transport: Photoconduction of polyvinylcarbazole *Physical Review B*, **35**: 1273-1280

Natta, G. Mazzanti, G. Corrandini, P. (1958*) Att. Acad. Naz. Lincei. A. Sci. Fis. Mat.*

Nat. Rend., **25**: 2. Quoted in Monkman, A.P. (1995) In: *Inroduction to Conducting Polymers*, edited by M.C. Petty, M.R. Bryce and D. Bloor, (London: Edward Arnold)

Oheda, H. (1981) Phase-shift analysis of modulated photocurrent - its application to the determination of the energetic distribution of gap states, *Journal of Applied Physics*, **52**: 6693-6700

Onsager, L. (1938) Initial recombination of ions, *Physical Review*, **54**: 554-557

Orenstein, J. Kastner, M.A. Vaninov, V. (1982) Transient photoconductivity and photo-induced optical absorption in amorphous semiconductors, *Philosophical Magazine B*, **46**: 2362

Pandya, R. Schiff, E.A. (1985) A multiple trapping model with optical bias, *Philosophical Magazine B*, **52**: 1075-1095

Pautmeier, L. Ries, B. Richert, R. Bässler, H. (1988) Disorder-enhanced triplet exciton diffusion in condensed aromatic systems, *Chemical Physics Letters*, **143**: 459-462

Pautmeier, L. Richert, R. Bässler, H. (1989) Hopping in a gaussian distribution of energy states: transition from dispersive to non-dispersive transport, *Philosophical Magazine Letters*, **59**: 325-331

Pautmeier, L. Richert, R. Bässler, H. (1990) Poole-Frenkel behaviour of charge transport in organic solids with off-diagonal disorder studied by Monte Carlo simulation, *Synthetic Metals*, **37**: 271-281

Pautmeier, L. Richert, R. Bässler, H. (1991) Anomalous time-independent diffusion of charge carriers in random potential under a bias field, *Philosophical Magazine B*, **63**: 587-601

Peled, A. Schein, L.B. (1988) Hole mobilities that decrease with increasing electric fields in a molecularly doped polymer, *Chemical Physics Letters*, **153**: 422-424

Peled, A. Schein, L.B. Glatz, D. (1990) Hole mobilities in films of a pyrazoline:polycarbonate molecularly doped polymer, *Physical Review B*, **41**: 10835-10844

Pfister, G. (1977) Hopping transport in a molecularly doped polymer, *Physical Review B*, **16**: 3676-3687

Pfister, G. Scher, H. (1978) Dispersive (non-gaussian) transient transport in disordered solids, *Advances in Physics*, **27**: 747-798

Ries, B. Bässler, H. Grünewald, M. Movaghar, B. (1988) Monte Carlo study of relaxation and diffusion in glassy systems, *Physical Review B*, **37**: 5508-5517

Ritter, D. Zeldov, E. Weiser, K. (1986) Steady state photocarrier grating technique for diffusion length measurement in photoconductive insulators, *Applied Physics Letters*, **49**: 791-793

Ritter, D. Weiser, K. Zeldov, E. (1987) Steady state photocarrier grating technique for diffusion-length measurements in semiconductors: Theory and experimental results for amorphous silicon and semi-insulating GaAs, *Journal of Applied Physics*, **62**: 4563-4570

Ritter, D. Zeldov, E. Weiser, K. (1988) Ambipolar transport in amorphous semiconductors in the lifetime and relaxation-time regimes investigated by the steady state photocarrier grating technique, *Physical Review B*, **38**: 8296-8304

Rose, A. (1978) *Concepts in Photoconductivity and Allied Problems* (revised edition). (New York: Krieger)

Rudenko, A.I. Arkhipov, V.I. (1982) Drift and diffusion in materials with traps 1. Quasi- equilibrium transport regime, *Philosophical Magazine B*, **45**: 177-187

Salih, A.J. Lau, S.P. Marshall, J.M. Maud, J.M. Bowen, W.R. Hilal, N. Lovitt, R.W. Williams, P.M. (1996) Improved thin films of pentacene via pulsed laser deposition at elevated substrate temperatures, *Applied Physics Letters*, **69**: 2230

Salih, A.J. Marshall, J.M. Maud, J.M. (1997) High-mobility low-threshold-voltage pentacene thin-film transistors prepared at rapid growth rates by pulsed-laser deposition, *Philosophical Magazine Letters*, **75**: 169-177

Santos Lemus, S.J. Hirsch, J. (1986) Hole transport in isopropyl carbazole-polycarbonate mixtures, *Philosophical Magazine B*, **53**: 25-39

Schein, L.B. Rosenberg, A. Rice, S.L. (1986) Hole transport in a molecularly doped polymer: p-diethylaminbenzaldehyde-diphenyl hydrazone in polycarbonate, *Journal of Applied Physics*, **60**: 4287-4292

Schein, L.B. Mack, J.X. (1988) Adiabatic and non-adiabatic small polaron hopping in molecularly doped polymers, *Chemical Physics Letters*, **149**: 109-112

Schein, L.B. Peled, A. Glatz, D. (1989) The electric field dependence of the mobility in molecularly doped polymers, *Journal of Applied Physics*, **66**: 686-692

Schein, L.B. Glatz, D. Scott, J.C. (1990) Observation of the transition from adiabatic to non-adiabatic small polaron hopping in a molecularly doped polymer, *Physical Review Letters*, **65**: 472-475

Schein, L.B. (1992) Comparison of charge transport models in molecularly doped polymers, *Philosophical Magazine B*, **65**: 795-810

Scher, H. Montroll, E.W. (1975) Anomalous transit-time dispersion in amorphous solids, *Physical Review B*, **12**: 2455-2477

Schmidlin, F.W. (1977) Theory of trap-controlled transient photoconduction, *Physical Review B*, **16**: 2362-2385

Schönherr, G. Bässler, H. Silver, M. (1981) Dispersive hopping transport via sites having a gaussian distribution of energies, *Philosophical Magazine B*, **44**: 47-61

Sen, S. Pal, P. Rossini, S. Misra, T.N. (1994) Photo- and semiconductive properties of α-sexithienyl, *Journal of Physics and Chemistry of Solids*, **55**: 17-21

Shockley, W. Read, W.T. (1952) Statistics of the recombination of holes and electrons, *Physical Review*, **87**: 835

Silinsh, E.A. (1970) On the physical nature of traps in molecular crystals, *Physica Status Solidi*, **3**: 817-828

Silinsh, E.A. (1974) Photoelectrical properties, energy level spectra, and photogeneration mechanisms of pentacene, *Physica Status Solidi*, **25**: 339-347

Silinsh, E.A. Kolesnikov, V.A. Muzikante, I.J. Balode, D.R. (1982) On charge carrier photogeneration mechanisms in organic molecular crystals, *Physica Status Solidi*, **113**: 379-390

Silinsh, E.A. Inokuchi, H. (1991)) On charge carrier photogeneration mechanisms in organic molecular crystals *Chemical Physics*, **149**: 373-383

Silver, M. Schönherr, G. Bässler, H. (1981) Trap-controlled hopping in a system with a gaussian distribution of the energy of hopping sites, *Philosophical Magazine B*, **43**: 943-947

Silver, M. Schönherr, G. Bässler, H. (1982) Dispersive hopping transport from an exponential energy distribution of sites, *Physical Review Letters*, **48**: 352-355

Skotheim, T.A. (1986) *Handbook of Conducting Polymers* (New York and Basel: Marcel Dekker Inc.)

Streetman, B.G. (1995) *Solid State Electronic Devices*, 4th Edition (Prentce Hall International)

Su, W.P. Schrieffer, J.R. Heeger, A.J. (1979) Solitons in polyacetylene, *Physical Review Letters*, **42**: 1698-1701

Su, W.P. Schrieffer, J.R. (1980) *Proceedings of the National Academy of Science USA*, **77**: 5626

Sze, S.M. (1985) *Semiconductor Devices Physics and Technology*, (New York: John Wiley & Sons)

Taylor, G.W. Simmons, J.G. (1972) Basic equations for statistics, recombination processes, and photoconductivity in amorphous insulators and semiconductors, *Journal of Non-Crystalline Solids*, **8-10**: 940-945

Tiedje, T. Rose, A. (1980) A physical interpretation of dispersive transport in disordered semiconductors, *Solid State Communications*, **37**: 49-52

Väterlein, C. Ziegler, B. Gebauer, W. Neureiter, H. Stoldt, M. Weaver, M.S. Bäuerle, P. Sokolowski, M. Bradley, D.D.C. Umbach, E. (1996) Electrical conductivity and oxygen doping of vapour-deposited oligothiophene films, *Synthetic Metals*, **76**: 133-136

Webb, D.P. (1994) Ph.D. thesis, University of Abertay Dundee

Yannoni, C.S. Clarke, T.C. (1983) Molecular geometry of *cis*- and *trans*-polyacetylene by nutation NMR spectroscopy, *Physical Review Letters*, **51**: 1191-1193

Yoshino, K. Akashi, T. Yoshimoto, K. Yoshida, M. Morita, S. Zakhidov, A.A. (1994) Novel optical properties of fullerene doped conducting polymers, *Molecular Crystals and Liquid Crystals*, **256**: 343-357

Young, R.H. (1995) Dipolar lattice model of disorder in random media: Analytical evaluation of the gaussian disorder model, *Philosophical Magazine B*, **72**: 435-457

Yuh, H.J. Stolka, M. (1988) The origin of dispersion of transiting charge carriers in molecularly doped polymers, *Philosophical Magazine B*, **58**: 539-549

Zboinski, Z. (1983) Are new chemical species in anthracene crystals formed as a result of charge-carrier trapping at physical defects?, *Chemical Physics*, **75**: 297-304